UNIVERSITA' DEGLI STUDI DI NAPOLI

"FEDERICO II"

DOTTORATO DI RICERCA IN

BIOLOGIA APPLICATA

XXVI CICLO

(*2011-2014*)

Proteasome and Acylpeptide hydrolase system: exploring an alternative strategy in cancer therapy

PhD student:
Dr. Marta Gogliettino

Tutor:
Dr. Gianna Palmieri

Coordinator:
Prof. Ezio Ricca

INDEX

Chapter 1

1. Introduction **2**

1.1 The Nightmare of Cancer: when good cells go bad

1.2 Ubiquitin-Proteasome pathway: destruction for the sake of construction
1.2.1 Ubiquitin Is Linked to Substrates through an Enzymatic Cascade
1.2.2 The Proteasome

1.3 Proteasome Inhibitors and Cancer Therapy
1.3.1 Mechanism of action of proteasome inhibitors

1.4 Ubiquitin-proteasome pathway and oxidative stress

1.5 Acylpeptide hydrolase

1.5.1 Role of Acylpeptide hydrolase in human diseases

2. Results and Discussion **25**

2.1 Peptide design and characterization

2.2 Mammalian APEHs are specifically and efficiently inhibited by SsCEI peptides

2.3 SsCEI 4 is a selective and non-covalent APEH inhibitor

2.4 SsCEI 4 downregulates APEH and proteasome activities in adenocarcinoma cell lines

2.5 SsCEI 4 increases the level of UPS substrates in Caco-2

2.6 CF3-lmph is a selective inhibitor of APEH having an uncommon mechanism of inhibition and a stable bant conformation

2.7 APEH and proteasome expression at both mRNA and protein level correlates with their enzyme activity in cancer cell lines

2.8 SsCEI 4 inhibits proliferation and decreases APEH/proteasome activity in U2OS osteosarcoma cell lines

2.9 U2OS exposure to high SsCEI 4 doses increases the level of UPS substrates in association with APEH-proteasome downregulation

2.10 SsCEI 4 induces cell death and G0/G1 phase cell cycle arrest in osteosarcoma cell lines through inhibition of Nf-κB signaling

2.11 Proteasomal degradation of the cystic fibrosis transmembrane conductance regulator (CFTR) mutated protein is prevented by SsCEI 4

3. Conclusions **57**

4. References **60**

Chapter 2

5. Introduction **69**

5.1 Conjugated linoleic acid

5.2 Biological activities of CLA

6. Results **76**
6.1 t10,c12-, t9,t11- and c9,t11-CLA isomers differentially inhibit APEH and proteasome
6.2 Cancer cell proliferation is significantly inhibited and associates with caspase 3 activation in melanoma cells exposed to t10,c12-CLA
6.3 t10,c12-CLA decreases glutathione level and APEH/proteasome activity in A375 cells triggering apoptosis in a dose-dependent fashion
6.4 A375 exposure to high t10,c12-CLA doses increases ROS production in association with apoptotic events and APEH-proteasome downregulation in time-dependent fashion
6.5 Putative APEH binding site for t10,cis12-CLA isomer

7. Discussion **91**

8. References **96**

9. Materials and Methods **102**
9.1 Reagents
9.2 Peptide design, synthesis and characterization
9.3 Gel filtration analysis of synthetic peptides
9.4 Circular dichroism spectroscopy
9.5 Enzyme assays
9.6 Enzyme inhibitory assays
9.7 Cells, culture conditions and treatments
9.8 Antibodies
9.9 Protein extraction and Western blotting analysis
9.10 MTT-based cytotoxicity assay
9.11 Apoptosis assays
9.12 Cytotoxicity assay
9.13 ROS detection
9.14 Cell cycle analysis
9.15 Intracellular redox status and cell viability assessment
9.16 Small interfering RNA transfection
9.17 RNA isolation and quantitative real-time PCR analysis
9.18 Statistical analysis

Publications

Chapter 1

1. Introduction

1.1. The Nightmare of Cancer: when good cells go bad

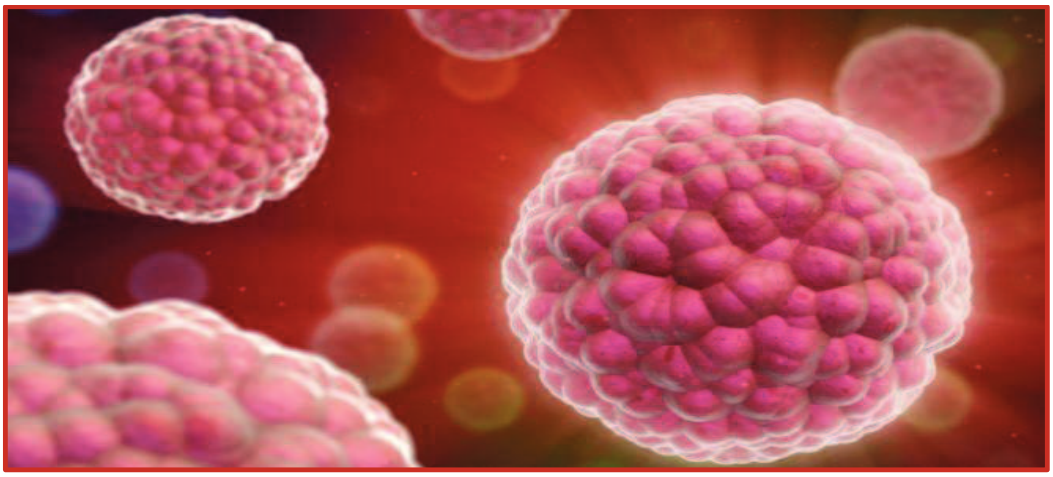

Cancer continues to be a worldwide killer, despite the enormous amount of research investments and rapid developments seen during the past decade. According to recent statistics, cancer is the second most common cause of death after heart disease but, if the latter can benefit from increasingly effective pharmacological and surgical therapies, cancer continues to be a disease with few alternative therapies. Because every type of cancer is unique, a treatment that works wonders for a leukemia patient, for example, might do little or nothing for a woman with breast cancer. Even patients with the same kind of cancer will have different responses to the same therapy, because the way the cancer arises and plays out depends on unique cellular events and the patient's individual genome. Cancer isn't just a single condition; it's actually a complex collection of diseases that can arise in almost any tissue in the body. The remarkable thing about cancer is that, although in many ways the disease acts like a foreign invading body, it is actually our own cells that have started to misbehave. When we look at how cancer cells operate they can seem crafty, clever and at times downright evil. Of course they're not. They're cells – unable to think or have any emotion-like behavior. Although cancer comprises at least 100 different diseases, all cancer cells share one important characteristic: they are abnormal cells in which the processes regulating normal cell division are disrupted. These changes are often the result of inherited mutations or are induced by environmental factors such as UV light, X-rays, chemicals, tobacco products, and viruses. All evidence suggests that most cancers are not the result of one single event or factor. A multicellular organism can thrive only when all its cells function in accordance with the rules that govern cell growth and reproduction. Why does a normal

cell suddenly become a “rebel”, breaking the rules, dividing recklessly, invading other tissues and in some cases eventually killing the body in which it lives? Cancer cells differ from the normal cells of the body in their ability to divide indefinitely and evade programmed cell death. The cells are constantly in the process of making decisions about what they want to do next and the decision to grow is one such major choice. Most cells in our body behave the way they should. When they get signals from the tissue surrounding telling them to multiply they will divide into two new cells; when they get old or damaged they will kill themselves in a cell-suicide process called apoptosis. Cells are very altruistic in this way. Cancer cells are not altruistic. What characterizes cancer cells is that they’ve become decidedly anti-social, carrying on their activities without regard to the other cells and tissues around them. While normal cells function solely to benefit the organism as a whole, cancer cells have their own agenda and that is to stay alive and to keep dividing. Cancer is frequently considered to be a disease of the cell cycle. As such, it is not surprising that the deregulation of the cell cycle is one of the most frequent alterations during tumor development. The abnormal behaviors demonstrated by cancer cells are the result of a series of mutations in key regulatory genes (tumor suppressors and proto-oncogenes). Normal cells grow and divide in an orderly fashion, in accordance with the cell cycle. In cancer this regulatory process malfunctions, resulting in uncontrolled cell proliferation. The cells become progressively more abnormal as more genes become damaged.. The normal speed of a car can be maintained by controlled use of both the accelerator and the brake. Similarly, controlled cell growth is maintained by regulation of proto-oncogenes, which accelerate growth, and tumor suppressor genes, which slow cell growth. Potential cancer cells become really dangerous when they not only divide in an uncontrolled way but also fail to recognize when they need to commit suicide. Normally the cell will detect a mistake and either rectify it or if that’s not possible commit suicide. Therefore, the rates of new cell growth and old cell death are kept in balance. In cancer this balance is disrupted and, when these processes break down, cancer begins to form and a mass of abnormal cells that grows out of control. Abnormal cells can also grow out of control and invade other tissues something that normal cells cannot do. Even though every cancer is different, there’s a shared set of behaviors that characterizes all cancer cells (**Figure 1**).

Figure 1. *Acquired functional capabilities of cancer cells.*

Researchers are working on identifying drugs that target, destroy or stop division of cancer cells. During the last 30 years, investigation of the transcriptional and translational mechanisms of gene expression has been a major focus of molecular cancer biology. More recently, it has become evident that cancer-related mutations can also affect post-translational processing of cellular proteins controlling vital processes. In this context, one of the post-translational mechanisms that is receiving considerable attention, is the protein turnover regulated by the Ubiquitin-Proteasome pathway (UPS), whose diverse components represent potential anti-cancer targets.

1.2 Ubiquitin-Proteasome pathway: destruction for the sake of construction

"Every minute of every day a scene straight out of an Indiana Jones movie plays out in all our cells. One second a hapless protein is tooling along just trying to do its job. The next instant it is branded for destruction and gets sucked into a dark tunnel, where it is quickly cut to pieces. Unlike Indiana Jones, for the protein there is no escape. Inside the chamber of doom, the protein is stretched out like a medieval prisoner on the rack and fed through a series of enzymatic knives that deliver the Death of a Thousand Cuts. A few seconds later the remnants

emerge from the tunnel, only to be pounced on and chewed up further by simpler enzymes" (The cellular chamber of Doom by A.L. Goldberg, S.J.Elledge and J. Wade Harper-2001).

Many diseases are manifestations of homeostatic imbalances like cancer. The number of cells in a healthy adult organism must be kept relatively constant. This is accomplished by balancing the processes of cell proliferation and programmed cell death (apoptosis). Therefore, one of the common strategies for cancer therapy is the targeting of cell homeostasis leading to dysfunction of cell processes necessary for survival. Cancer occurs when the balance between cell proliferation and apoptosis is altered and cells proliferate faster than they die.

In eukaryotic cells, the ubiquitin-proteasome pathway (UPS) is the central non-lysosomal pathway for protein degradation. It is estimated that more than 80% of intracellular proteins can be degraded by this system. One major function of the UPS is to protect the cell against misfolded, oxidized or otherwise damaged-and potentially toxic-proteins. Therefore, the UPS constitutes a kind of the cell's quality control system. Additionally, it also regulates the half-life of many proteins involved in important biological processes such as transcription, cell cycle regulation, oncogenesis, differentiation and apoptosis. For this reason, the UPS system plays a critical role in preserving cellular homeostasis, particularly in cancerous cells. In order to sustain their higher levels of metabolic activity, cancer cells rely more heavily upon the proper function of the UPS as compared to their normal counterpart. Therefore, tumoral cells are more sensitive to the proapoptotic effects of proteasome inhibition than normal cells, making the proteasome a rational therapeutic target in oncology. Its inhibition disturbs the critical intracellular balance between proapoptotic and antiapoptotic signals shifting it towards tumor growth inhibition, apoptosis, and decreased metastasis.

1.2.1 Ubiquitin Is Linked to Substrates through an Enzymatic Cascade

In the UPS pathway, which is present ubiquitously in both the nucleus and the cytosol, most substrates are first marked for degradation by covalent linkage to multiple ubiquitin molecules. In fact, polyubiquitination, an enzymatic, post-translational modification process, is the triggering signal that leads to degradation of the protein in the proteasome. It is polyubiquitination that constitutes the "kiss of death" for the protein.

Ubiquitin, an evolutionary highly conserved 76 amino acid protein that acts as a death warrant, is covalently linked to proteins in a multistep process involving E1 (ubiquitin-activating enzyme), E2 (ubiquitin-conjugating enzyme) and E3 (ubiquitin ligase) enzymes (**Figure 2**). Polyubiquitin chains are assembled *via* an isopeptide linkage between the carboxylic acid group of the last ubiquitin's glycine (glycine 76) and the epsilon amino group of the substrate's lysine. The process of ubiquitination is balanced by the process of de-ubiquitination, which is mediated by a number of enzymes. The polyubiquitin chain is removed from the substrate prior to entering the proteolytic core of proteasome, and is recycled to free ubiquitin by the action of a deubiquitinating enzyme (DUB).

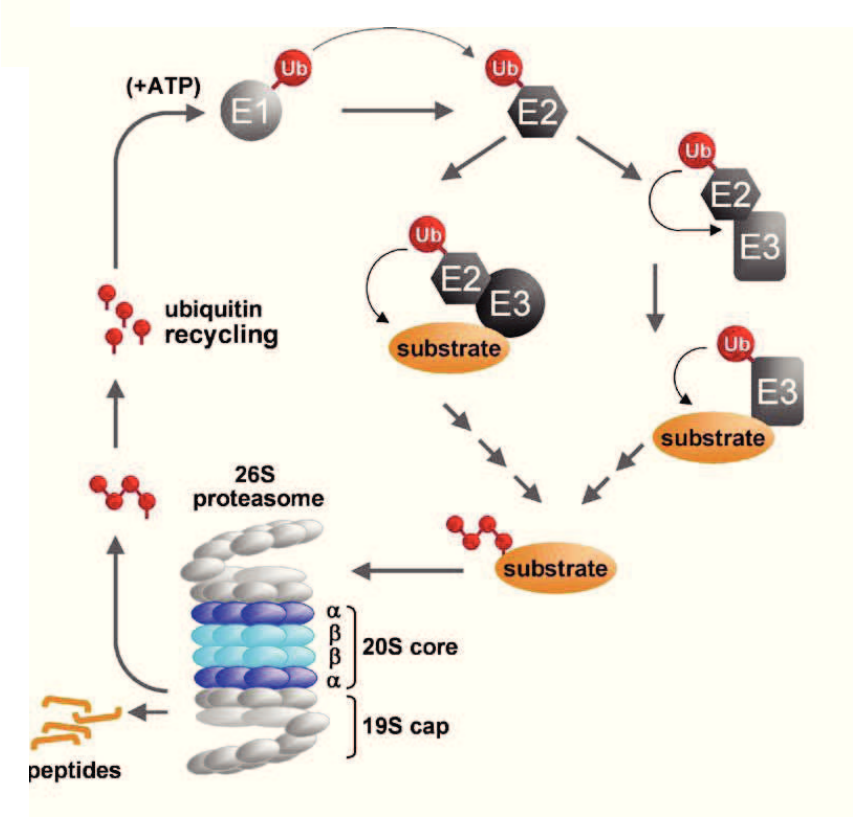

Figure 2. *The conjugation of ubiquitin (Ub) to substrates usually involves three steps: an initial activation step catalyzed by E1; an intermediate step in which the ubiquitin is covalently linked to a conjugating enzyme, E2; and a final step in which the ubiquitin reaches its ultimate destination of the substrate amino group. The last step is facilitated by the E3 ligase enzyme family.*

1.2.2 The Proteasome

The rapid degradation of ubiquitinated proteins is catalyzed by the 26S proteasome which can be defined as the cell's garbage shredder. This complex is found in the nucleus and the cytosol of all cells and constitutes approximately 1 to 2% of cell mass [**1**]. It's absolutely essential for survival. The 26S particle is composed of approximately 60 subunits and therefore is approximately 50 to 100 times larger (1500–2000 kDa) than the typical proteases that function in the extracellular environment and differs in critical ways. The most fundamental difference is that it is a proteolytic machine in which protein degradation is linked to ATP hydrolysis. The 26S complex is composed of a central barrel-shaped 20S proteasome with a 19S regulatory particle at either or both of its ends (**Figure 3**). The 20S proteasome is a hollow cylinder that contains the mechanisms for protein digestion. It is composed of four stacked, hollow rings, each containing seven distinct but related subunits [**1**]. The two outer α rings are identical, as are the two inner β rings. Three of the subunits in the β rings contain the proteolytic active sites that are positioned on the interior face of the cylinder: chymotrypsin-like (CT-L), trypsin-like (T-L) and caspase-like (C-L) activities which are associated with β5, β2 and β1 subunits, respectively. All three of these proteolytic activities regulate one another to coordinate their actions on a substrate protein [**2**]. When the chymotrypsin-like activity is turned on, the caspase-like and trypsin-like activities are off. This system for concerted and cooperative interactions between the proteasome activities is termed the ‘‘bite/chew’’ model, because the chymotrypsin-like activity bites a chunk out of the substrate protein, and the other two activities chew it into smaller pieces. The active sites in the proteasome cleave peptide bonds by a unique mechanism: peptide bonds are cleaved by the hydroxyl group on a critical threonine residue [**3**]. Therefore, proteasomes are a novel type of threonine proteases. The outer α subunits of the 20S particle surround a narrow, central, and gated pore through which substrates enter and products exit [**4**]. Substrate entry is a complex process that is catalyzed by the 19S particle. This complex architecture evolved to isolate proteolysis within a nano-sized compartment and to prevent the nonspecific destruction of cell proteins. One can view protein ubiquitination and the functioning of the 19S particle as mechanisms that ensure proteolysis as an exquisitely selective process; only certain molecules get degraded within the 20S proteasome [**5**]. The 19S regulatory particles at the ends of the 20S proteasome are composed of at least 18 subunits [**6**]. Its base contains six homologous ATPases in a ring and adjoins the outer ring of the 20S particle. These ATPases bind the proteins to be degraded and use ATP

hydrolysis to unfold and translocate the protein into the 20S particle [**7**]. The 19S's outer lid contains subunits that bind the polyubiquitin chains plus two deubiquitinating enzymes (also called isopeptidases) that disassemble the Ub chain so that the Ub can be reused in the degradation of other proteins [**6**]. There is growing evidence that additional factors associate with the 19S particle and actually help to deliver ubiquitinated proteins into the particle [**8**].

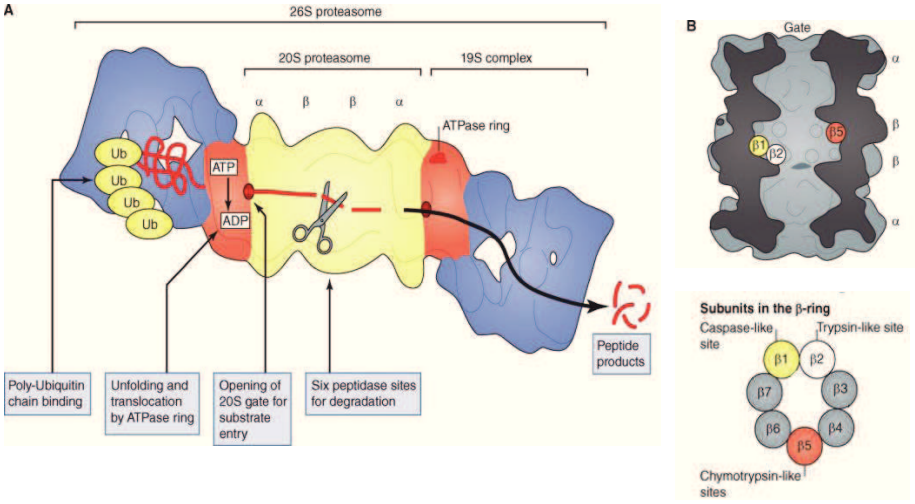

Figure 3. *Structure and function of the 26S proteasome. (**A**) Structure and components of the 26S proteasome. (**B**) Location of active sites in the 20S proteasome core. There are three types of proteolytic sites in the 20S proteasome's central chamber, and each β ring contains three active sites.*

Much has been learned about the mechanisms by which a ubiquitinated protein is degraded. After it binds to the 19S component, the polyubiquitin chain is cleaved off the substrate and disassembled. The protein is unfolded somehow by the six ATPases in the base of the particle [**7**]. Linearization of the folded protein is essential for it to be translocated through the gated entry channel into the 20S particle because this pore, even in its open state, is too narrow for globular proteins (i.e., most cell proteins) to enter [**4**]. The ATPases also act as a "key in a lock" to cause opening of the gated, substrate entry channel of the 20S outer ring and into its central degradative chamber [**9**]. After the substrate enters the 20S's central chamber, the polypeptide is cleaved by its six proteolytic sites on the inner face of the changer, forming small peptides that range from three to 25 residues in length [**10**]. Unlike traditional proteases, which cut a protein once and release the fragments, the proteasome digests the substrates all the way to small peptides that exit the particle. Peptides that are released by the proteasome

only exist in the cell for seconds, because they are quickly digested into amino acids by the abundant cytosolic endopeptidases and aminopeptidases. The amino acids can be reutilized to synthesize new proteins or metabolized, yielding energy [**11**].

1.3 Proteasome Inhibitors and Cancer Therapy

"This is an exciting time for cancer therapeutics. The identification of promising molecular targets has led to the development of many exciting new drugs for which an antitumor mechanism of action has been clearly delineated. Given the recent major advances in our understanding of the biology of cancer cells, one might surmise that an era of truly rational therapeutics has arrived. Nevertheless, we continue to find new therapeutic agents that target unforeseen molecular pathways" (The proteasome-an emercing therapeutic target in cancer by B.S.Mitchell).

The UPS pathway is responsible for degradation of the majority of regulatory proteins in eukaryotic cells, including proteins that control apoptosis, cell-cycle progression and DNA repair, and for that reason plays a critical role in preserving normal cellular homeostasis. Inhibition of the proteasome leads to stabilization and accumulation of its substrates, resulting in a concomitant activation of pro- and anti-proliferative signals, disruption of cell-cycle regulation, and, ultimately, activation of apoptotic pathways and cell death [**12, 13**]. Neoplastic cells usually have higher levels of proteasome activity compared with normal cells and, in addition, are more sensitive to the proapoptotic effects of proteasome inhibition than normal cells for reasons that are not entirely understood. This is in part due to the high replication rate of malignant cells, which implies rapid protein synthesis and turnover, but also because of the genetic changes that accompany transformation that disable diverse protective checkpoint mechanisms. Accordingly, the proteasome has emerged as an attractive target for cancer therapy [**12, 14**].

Based on promising preclinical results, proteasome inhibition has been widely explored as a therapeutic strategy and proteasome inhibitors (PIs) now form a keystone of anticancer treatment. On a cellular level, blocking the proteasome generally stresses cancer cells by jamming them with proteins. Therefore, cancer cells may be selectively vulnerable to PIs because they can't handle the stress of the protein buildup as easily as normal cells can. This stress causes "*catastrophic signaling events, which drive the tumor cell to die. A normal,*

untransformed cell can withstand the stress response, at least for short periods of time" (cit. Julian Adams).

Clinical validation of the proteasome as a cancer therapeutic target was established by Bortezomib (Velcade; Millennium Pharmaceuticals/Takeda Pharmaceuticals), the first PI approved by the US Food and Drug Administration for the treatment of relapsed multiple myeloma (MM) [**15**]. Bortezomib-induced cell death is related with induction of endoplasmic reticulum stress and activation of the unfolded protein response, inhibition of the nuclear factor kappa B (NF-κB) inflammatory pathway, activation of caspase-8 and apoptosis, and augmented generation of reactive oxygen species [**16**]. Bortezomib, a boronic acid dipeptide, inhibits the proteasome pathway rapidly and in a reversible manner primarily acting on the CT-L activity of the proteasome and blocking its enzymatic activity.

Proteasomal chymotrypsin-like activity is considered the most important because associated with the survival of tumor cells, and then considered the first important target for the development of anticancer drugs. Even if the approval of Bortezomib has modified treatment of MM, there are restrictions to the use of this drug including toxicity, limited activity in solid tumors and resistance. A large amount of patients fail to respond to Bortezomib therapy, and almost all patients relapse from this drug, either when it is used alone or as combination therapies. This prompted the development of a new generation of structurally distinct proteasome inhibitors with diverse mechanisms of action, in an effort to overcome resistance to Bortezomib and its toxicity. These additional PIs include drugs that bind either reversibly or irreversibly to the active sites of the proteasome (mainly β5 subunit) , as well as molecules (es. Chloroquine and 5AHQ) that allosterically inhibit the function of the proteasome by binding the complex outside (α ring) of the active site (**Figure 4**) [**17**]. The "second generation" PIs, representing distinct structural classes (peptidyl epoxyketones, beta-lactones, peptidylboronic acids, and salinosporamides), with diverse mechanisms of action and affinities for the catalytic sites within the proteasome core, have now entered clinical development.

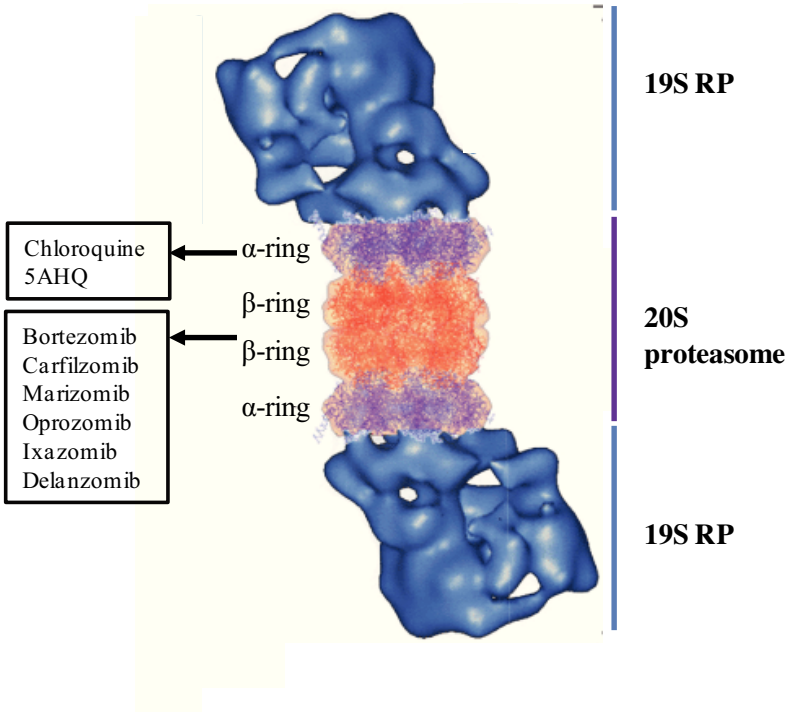

Figure 4. *Sites of action of proteasome inhibitors. 5AHQ and chloroquine act at the interface between the alpha and the beta subunits outside of the active site of the proteasome. Bortezomib, Carfilzomib, Marizomib, Oprozomib, Ixazomib and Delazomib bind the active site of the proteasome at the β5 subunits of the 20S core particle.*

1.3.1 Mechanism of action of proteasome inhibitors

The UPS pathway is the principal mechanism of degradation for several short-lived cellular regulatory proteins, including p53, cyclins and the cyclin-dependent kinase (CDK) inhibitors p21 and p27 and the inhibitor (IκB) of nuclear transcription factor kappa B (NF-κB). Some of these mechanisms are summarized below.

- **Nf-κB pathway: from innocent bystander to major culprit**

A primary rationale for the therapeutic use of PIs in oncology relies on their ability to inhibit the nuclear transcription factor kappa B (NF-κB) activity through stabilization of its inhibitor IκB. According to Hanahan and Weinberg, tumorigenesis requires six essential alterations to normal cell physiology: self-sufficiency in growth signals; insensitivity to growth inhibition; evasion of apoptosis; immortalization; sustained angiogenesis; and tissue invasion and metastasis [**18**]. NF-κB is able to induce several of these cellular alterations and it is

constitutively active in a large proportion of advanced cancers [**19]** playing a role in resistance to chemotherapeutic agents.

NF-κB regulates various immune and inflammatory responses and it is also involved in tumorigenesis by inducing angiogenesis, proliferation, migration and suppression of apoptosis. Inactive NF-κB is sequestered in the cytoplasm bound to its inhibitory regulator IκB. Following activation of NF-κB by various stresses stimuli, IκB is degradated by UPS and NF-κB translocates to the nucleus inducing the expression of a variety of genes encoding several growth and antiapoptotic factors, which promote the survival of cancer cells and actually propagate the tumor [**20**]. Inhibition of proteasome activity prevents degradation of IκB and subsequent activation and translocation of NF-κB to the nucleus (**Figure 5**).

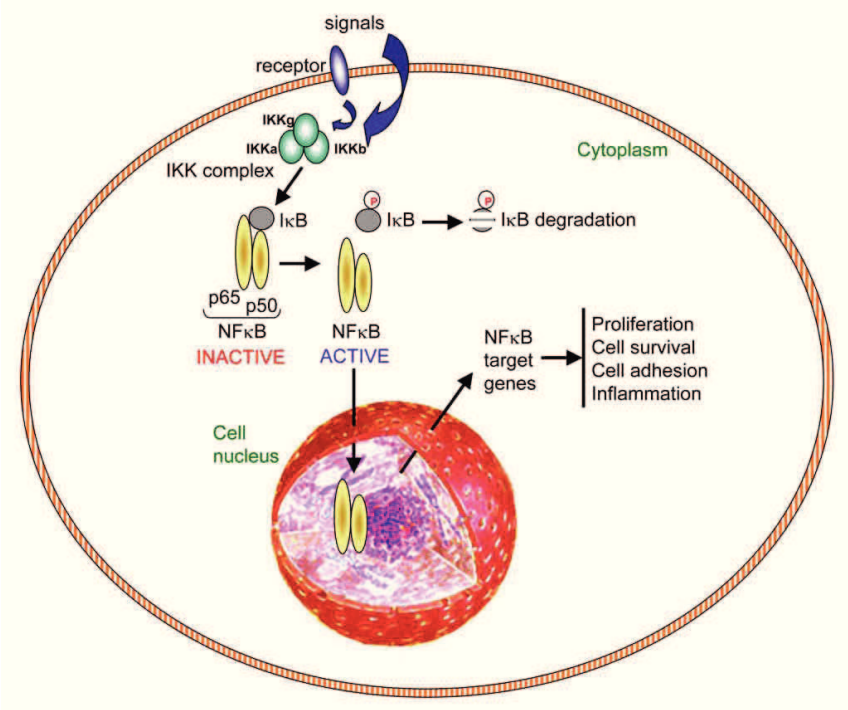

Figure 5. *Bortezomib and nuclear factor-kappa B (NF-κB) inhibition. Bortezomib prevents the degradation of I-κB and, thereby, inhibits NF-κB activation.*

- **Cell cycle**

The principal, immediate consequence of proteasome inhibition is a decrease of overall rates of protein breakdown in cells [**21, 22**]. Various proteins involved in the processes of carcinogenesis and cancer survival have been identified as targets of the UPS, including the proteins related to cell cycle process like cyclins A, B, D and E [**21, 23**], tumor suppressor

protein p53 [**24**], pro-apoptotic factor Bax [**25**], cyclin-dependent kinase inhibitor (CKI) p27 [**26, 27**], and the inhibitor of NF-κB, IκB-α [**28**]. Progression of cell cycle occurs through tightly controlled interplay between cyclins and cyclin dependent kinases (CDKs) [**29**]. Loss of cell cycle control is a critical step in oncogenesis. In fact, cyclin proteins are found to be highly upregulated (particularly cyclins D and E) in cases of aberrant cell division in cancer cells, [**30, 31**]. Cyclin D binds to CDK 4/6 in the initial phase of G1 , where it performs two major functions, hypophosphorylation of retinoblastoma protein (Rb) [**32**] and protection of cyclin E/ CDK2 complex from inhibitory effect of p21 and p27 [**30**] (**Figure 6**).

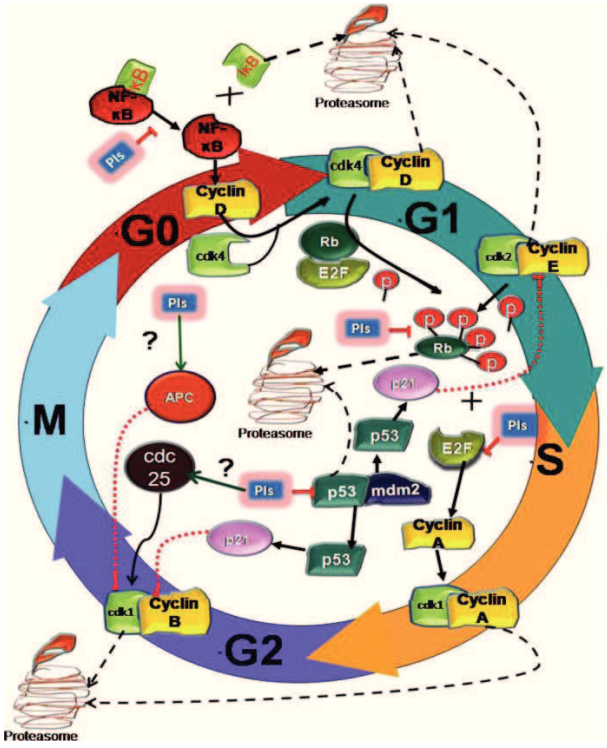

Figure 6. *Regulation of* NF-κB*, E2F/Rb and p53/p21 pathways of cell cycle arrest by PIs*.

The upregulation of cyclins is further supported by the down regulation of another class of CDK regulatory proteins, the CKIs, which bind, inactivate and degrade the cyclin/CDK complex. Rapid proteasomal degradation of CKIs in subsequent cell cycle phases contribute to the uncontrolled cell division in cancer cells.

There are a number of ways in which proteasome inhibitors may induce cell cycle arrest by interfering with the degradation of cyclins and cell cycle regulatory proteins in malignant cells. CKIs, p21 and p27 are known to be suppressed in several cancer types and are attributed to cancer progression [**33, 34**]. Bortezomib, along with other PIs has been reported to significantly increase the expression of p21 and p27 proteins in many cancers thereby causing cell cycle arrest [**35-37**]. On the other side, proteasome inhibition also causes accumulation of the tumor suppressor p53, which is a crucial component of cell cycle regulation, abrogating its degradation and reactivating its function in G1/S and G2/M arrest [**38**]. Proteasomal inhibition allows accumulation of p53 and its nuclear export in cancer cells and thereby increases the expression of its transcriptional target gene p21, a potent CDK inhibitor, which binds and inactivate cyclin E and the CDK2 complex. This complex is essential for late G1 phase mediating entry in the S phase of cell cycle. However, activation of p53 and p21 proteins leads to G0/G1 cell cycle arrest. For this reason, p53/p21 pathway blocks the doorstep of cell cycle entry. Finally, administration of PIs mediates retinoblastoma (Rb) protein escape from proteasomal degradation. Rb acts as a tumor suppressor protein playing a crucial role in cell cycle regulation, DNA replication, DNA damage repair and many other cellular processes. Another key component of PI mediated growth arrest, is the inhibition of NF-κB signaling and its downstream target proteins mainly cyclin D, responsible for G1/S transition and commitment to DNA synthesis.

- **Regulation of apoptosis**

Programmed cell death, or apoptosis, is necessary to the survival of all multicellular organisms playing an important role in normal growth and development. The discovery that a family of proteases, the caspases, mediates the execution of apoptosis, generated interest in a possible involvement of the proteasome in this process. Apoptosis is regulated by the opposing activities of pro-apoptotic and anti-apoptotic molecules. Cancer cells often have disregulated apoptotic signaling pathways which give malignant cells a survival advantage and can confer resistance to chemotherapeutic agents. The proteasome is involved in the control of apoptosis by modulating the levels of pro- and anti-apoptotic factors. Specifically, inhibition of proteasome activity results in an upregulation of pro-apoptotic factors such as p53 and Bax while reducing levels of anti-apoptotic proteins such as Bcl-2 [**39**]. The Bcl-2 family is the best characterized protein family involved in the regulation of apoptotic cell death. Bcl-2 protein prevents apoptosis either by sequestering proforms of death-driving

cysteine proteases called caspases (a complex called the apoptosome) or by preventing the release of mitochondrial apoptogenic factors such as cytochrome c into the cytoplasm. After entering the cytoplasm, cytochrome c directly activates caspases that cleave a set of cellular proteins to cause apoptotic changes. In contrast, pro-apoptotic members of this family, such as Bax, induce the release of mitochondrial apoptogenic factors into the cytoplasm thereby leading to caspase activation. Thus, the Bcl-2 family of proteins acts as a critical life–death decision point within the common pathway of apoptosis. Moreover, p53 is a transcription factor capable of binding DNA in a sequence-specific fashion and directly activate the transcription of genes known to promote apoptosis [**40-43**]. Specifically, the most intuitive link between p53-mediated transactivation and apoptosis comes from its ability to control transcription of pro-apoptotic members of the Bcl-2 family, such as Bax, Noxa [**44**] and Bid [**45**] (**Figure 7**).

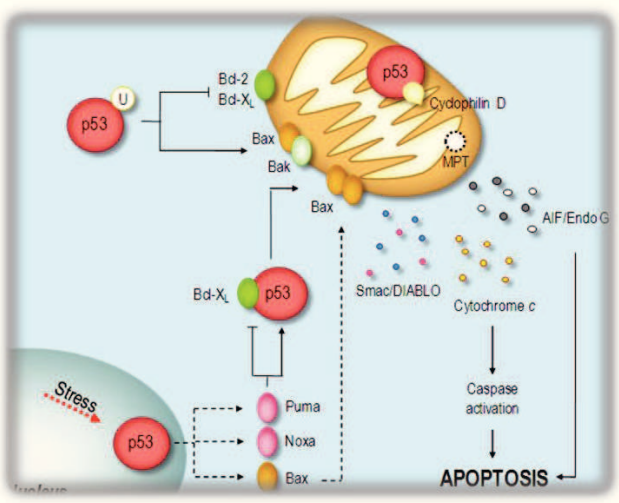

Figure 7. *Cytosolic and mitochondrial p53 apoptotic pathways*.

1.4 Ubiquitin-proteasome pathway and oxidative stress

The past decade has seen an exponential increase in the number of cancer therapies with defined molecular targets. Interestingly, many of these new agents are also documented to raise levels of intracellular reactive oxygen species (ROS) in addition to inhibiting a biochemical target. The first report that proteasome inhibitors cause oxidative stress came from a study examining Bortezomib action in lung cancer cell lines [**46**]. In support of a

strong role for redox modulation by proteasome inhibitors, there are numerous observations that other classes of proteasome inhibitors also induce an oxidative stress [**47**].

Oxidative stress is a complex and dynamic situation characterized by an imbalance between the productions of so called ROS (reactive oxygen species)- and the availability and action of antioxidants. Oxygen is one of the greatest blessings and perhaps curses to complex life, this is what is often referred to as the 'Oxygen Paradox' [**48**]. Higher eukaryotic aerobic organisms cannot exist without oxygen; nevertheless oxygen is fundamentally dangerous to their existence. This 'disadvantage' of oxygen relates to the fact, that molecular oxygen has two unpaired electrons in its outer electron shell. This electronic structure makes oxygen reactive. Besides molecular oxygen, a number of even more reactive species, the ROS, are derived from molecular oxygen. ROS refer to oxygen-containing breakdown products of molecular oxygen that are highly reactive and are able to damage lipid membranes, proteins, and DNA when present in high amounts, thus leading to aberrant molecular activities and resulting in dysfunction of bioprocesses [**49-51**]. The main endogenous source of ROS production is the mitochondrial metabolism. Other sources are the cytochrome P450 metabolism, different environmental influences and inflammation processes (**Figure 8**).

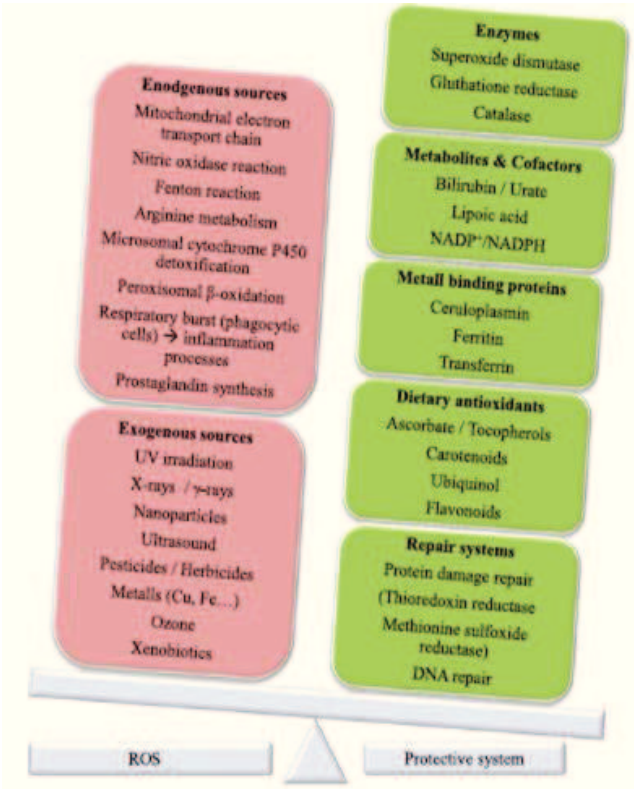

Figure 8. *The occurrence of oxidative stress depends on the interaction between the cellular antioxidative system and the formation of ROS*.

Because proteins are most abundant in cells, it is not surprising that they are the major targets for oxidative modifications. ROS can attack proteins in different ways: directly at the protein backbone, amino acid residue side chains or they can lead to the formation of protein carbonyls. As a result of this damage, the affected proteins lose their biochemical functionality, protein expression is altered and finally aggregate formation occurs, resulting in different consequences for the cells. Therefore, to maintain cell viability and normal homeostasis, aerobic organisms have evolved multistep defense mechanisms for reducing the deleterious effects of oxidative stress. The first step is the direct scavenging and detoxification of reactive chemicals by antioxidants (e.g. glutathione) and cytoplasmic antioxidative enzymes (e.g. superoxide dismutase SOD, catalase, and glutathione peroxide) (Phase 1). The second step is the restoring of reversibly denatured proteins by chaperones (Phase 2). The final step is the elimination of irreversibly denatured proteins (Phase 3), catalyzed by several cytoplasmic proteases. One of those is the proteasomal system that is essential for cells to cope with oxidative stress [**52**] and prevent cytotoxicity. Therefore, inhibition of proteasomal

function can lead to an accumulation of damaged (e.g., oxidized) proteins which produce oxidative stress-dependent toxicity and contribute to induction of cell death. Specifically, ROS have been suggested as regulating the process involved in the initiation of apoptotic signaling [**53**]. For these reasons, redox status may be an element to consider in trying to maximize the utility of the proteasome inhibitors and oxidative stress can be a relevant and requisite outcome of many new cancer therapies.

Finally, inhibition of NFκB activity, altered degradation of cell cycle related proteins, pro-apoptotic and anti-apoptotic protein unbalance and inhibition of DNA repair, have all been reported to contribute to the apoptotic effects of proteasome inhibitors in tumor cells. These mechanisms are summarized in **Figure 9**.

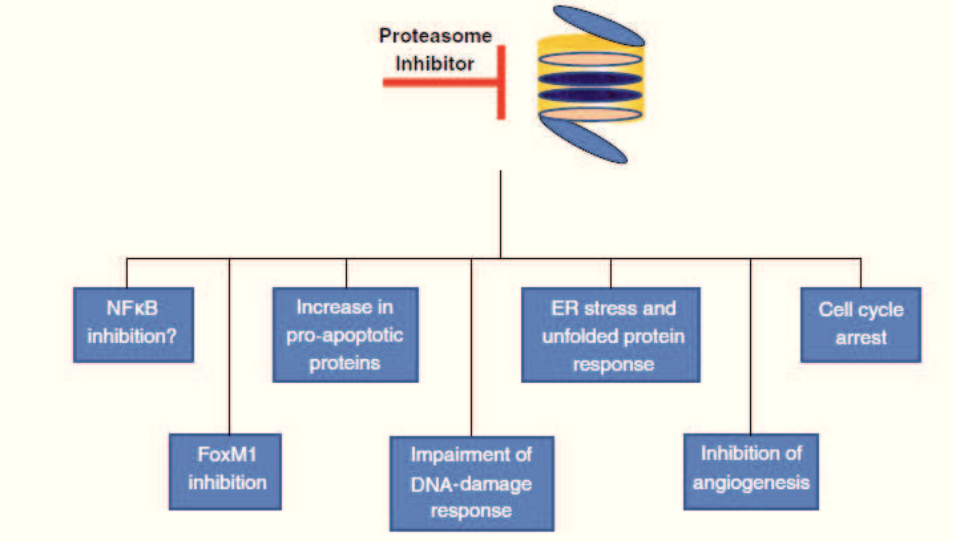

Figure 9. *Critical targets for proteasome inhibitors in malignant cells*

Much emphasis has been placed on the identification of specific and targeted molecular therapy for the treatment of many cancer types. To establish a new targeted therapy, at least two criteria have to be met: a validated therapeutic target, and a highly specific inhibitor (or activator) towards that target. In the UPS, few targets have been well-established and validated, including proteasomal β1, β2 and β5 subunits. One should keep in mind that although the UPS is ubiquitously present in all cell types, the identification of a novel therapeutic target within this system could still prove to be tumor type-specific or at least superior in one tumor type over another. For example, the current clinical application of

proteasome inhibitors is still limited to multiple myeloma and lymphomas with limited success in solid tumors. Moreover, in spite of all its successes, the proteasome inhibitors currently in use often have severe disadvantages. As a result of their high reactivity they attack other proteins, thereby damaging not only cancer cells but also other healthy cells. For these reasons, several studies have suggested that the targeting of functionally related, up-stream or down-stream proteasome effectors [**54**], can be an alternative and a safer way to recover proteasome dysfunction associated with pathological conditions. Specifically, one of this target could be identified in a specific serine-pepdidase, the Acylpeptide hydrolase (APEH), which has been hypothesized acting in coordination with proteasome in the protein turnover processes, opening new important and challenging perspectives for the development of novel strategies in cancer therapy.

1.5 Acylpeptide hydrolase

Acylpeptide hydrolase (APEH), also referred as oxidized protein hydrolase (OPH) or acylaminoacyl peptidase, is a member of a novel class of serine-type peptidases namely the prolyl oligopeptidase (POP, clan SC, family S9) [**55**], unique in the family for its substrate preference. It is a cytoplasmic exopeptidase that catalyzes the removal of N-acylated amino acids from blocked peptides, producing an acylamino acid and a peptide with a free N-terminus shortened by one amino acid residue [**56**]. In eukaryotes, N-acetylation is one of the most common protein modifications occurring on approximately 85% of proteins, both co- and post-translationally [**57**]. The acetylation of proteins and peptides serves to protect the aminopeptidases present in eukaryotic cells from proteolytic degradation, and thus increases their half-life. Therefore, APEH has a broad role in regulating the basal N-terminal acetylation states of many proteins in the proteome but its cellular functions have been still unclear and the mechanism underlying the intracellular catabolism of N-acetylated proteins has not yet been elucidated. It is assumed that the intracellular catabolism of N-acetylated proteins is regulated by the cooperative action of the ubiquitin-proteasome system and APEH. Therefore, this enzyme has been postulated to be important in the endpoint of the ubiquitin system and thus in the breakdown of proteins into free amino acids (**Figure 10**) [**58**].

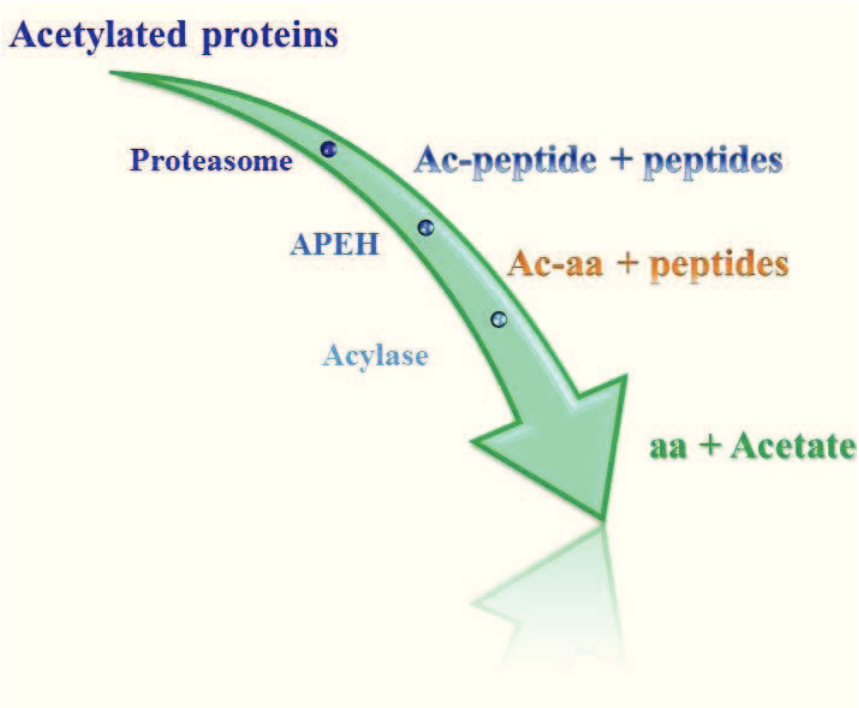

Figure 10. Proposed scheme of the intracellular catabolism of α-NH_2-acetylated protein. aa: amino acid, Ac-: acetyl-

APEH is an ubiquitous enzyme but few members of this family have been characterized to date; specifically, these enzymes have been studied in a number of eukaryal organisms [**59**], in some Archaea [**60**, **61**], in a bacteria [**62**] and, more recently, also in plant [**63**].

APEH displays a broad spectrum of specificity with respect to the blocking group, (acetyl, chloroacetyl, formyl, and carbamoyl moieties) and the most notable property is its selectivity, which is restricted to oligopeptides comprising not more than about 30 amino acid residues

Mammalian APEH is composed of four identical subunits and, like all members of the POP family, contains a catalytic site identical to that of serine peptidases, but it hydrolyzes short peptides only. From a structural point of view, this enzyme has the expected domain architecture of the POP family: a C-terminal catalytic domain with an α/β hydrolase fold and its catalytic triad (Ser, Asp and His) is covered by the central tunnel of an unusual seven-bladed β-propeller at the N- terminal that hides the active site. This domain makes the enzyme an oligopeptidase by excluding large, structured peptides from the active site. In this way, the propeller operates as a gating filter and protects large peptides and proteins from proteolysis in the cytosol. Indeed, unlike POP members, this entrance has a diameter wide enough to

allow passage of a peptide substrate in a random coil conformation. There is a second smaller opening located between blades 1 and 2, suggesting the possibility of separate substrate entry and product exit sites for APEH. The only 3D structure available to date is that of the hyperthermophilic enzyme from the archaebacterium *Aeropyrum pernix* K1 (ApAAP) [**61**]. This crystal structure allowed to obtain the enzyme model of an APEH from *Sulfolobus solfataricus* ($APEH_{Ss}$) which shares a significant sequence identity (34%) with ApAAP [**64**]. $APEH_{Ss}$, unlike the tetramer mammalian enzymes, is a symmetrical homodimer with each subunit made up of a seven-bladed β-propeller domain and α-peptidase domain, which are characteristic of this enzyme family (**Figure 10**).

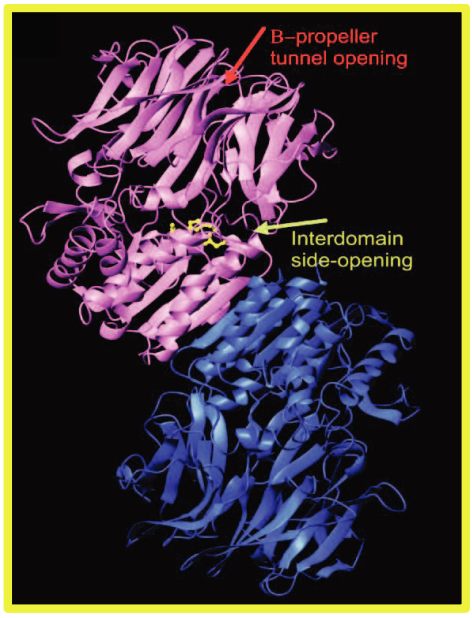

Figure 10. APEHSs dimer model. *The two monomeric subunits are displayed in different colors as cartoon. For only one of the two subunits the catalytic triad residues (Ser425, Asp505, His537) are shown in yellow (ball-and-stick mode); the red and green arrows indicate the β-propeller tunnel opening and the interdomain side-opening, respectively.*

1.5.1 Role of Acylpeptide hydrolase in human diseases

Like the other members of the POP family, APEHs are believed to be important targets for drug design, being involved in the development of several diseases such as neurodegenerative disorders and cancer. Despite the broad distribution of APEH in animal tissues including blood, brain and liver, its physiological functions have not been well understood other than its involvement in the degradation of N-acylated proteins.

- Recently, it has been suggested that APEH may play an important role in inflammatory diseases providing the first line of defense against unwanted inflammatory responses at tissue sites that are in continuous contact with commensal bacteria (e.g., intestines) [**65, 66**]. Mammalian large intestine is constantly exposed to bioactive and immunoreactive N-formyl peptides, a potent chemoattractants for phagocytes, derived from proteolytic degradation/processing of bacterial and mitochondrial proteins [**67, 68**]. Thus, to prevent unwanted immune response to commensal bacteria, mammals must possess enzymes that can effectively degrade the N-formyl peptides such as APEH.
- Shimizu *et al*. demonstrated that APEH [**69**] may contribute to the elimination of the oxidized proteins, acting as secondary antioxidant defense systems in coordination with proteasome [**70**]. Strongly oxidized proteins are known to be poor substrates for the proteasome, since they easily form covalent cross-links and aggregates [**71**]. Therefore, APEH may play a homeostatic role in sustaining the cytoplasmic antioxidative system and in the clearance of such oxidized proteins [**63**], against which it has been biochemically demonstrated to have endopeptidase activity [**72, 73**]. As a fact, APEH may represent a promising therapeutic target for a wide array of human diseases in which oxidative stress increases such as diabetes mellitus. Specifically, it has been hypothesized that APEH might have a preventive or at least delaying role in the development and progression of diabetes mellitus, due to its ability to preferentially degrade oxidized and glycated proteins [**74**]. In this context, it is important to emphasize that glycated proteins, which increase in diabetes, are not readily degraded by 20S proteasome [**75**] and that the proteasome activity decreases in diabetes while a concomitant increase in APEH activity has been observed [**76**]. These events suggest that APEH takes part in a biological defense mechanism against oxidative stress and could represent a potential therapeutic target for the treatment of these type of pathologies.
- There are many evidences indicating an involvement of APEH in the development of several human cancers. Human APEH is encoded by the DNF15S2 *locus* on the short arm of chromosome 3 at region 21 [**77**], which suffers deletions in small cell lung carcinomas and renal carcinomas, resulting in deficiency in the expression of the enzyme [**78-80**]. In addition, it has been demonstrated that downregulation of the

enzyme induces apoptosis in human monoblastic U937 cells suggesting that APEH may play a vital role for the survival of eukaryotic cells [**81**], although its involvement in the malignant state of these cell lines has not yet been established.

- A lot of interest was aimed at the role of APEH in neurodegenerative diseases such as Alzheimer's. It has been reported that porcine brain APEH is implicated in synaptic plasticity processes that are responsible for mediating the organophosphorous-induced cognitive effects. Therefore, this enzyme has been proposed as alternative non-cholinergic target in the treatment of neurodegenerative diseases [**82**].

For these reasons, modulation of APEH activity appears to be an important event in controlling the UPS dysfunction associated with a wide array of human diseases, opening new important and challenging perspectives for the development of novel strategies in the therapeutic field. Moreover, the discovery of small bioactive molecules able to specifically and efficiently inhibit APEH may represent a valuable starting point to study the biological function by ‘‘knocking-out” its activity.

2. Results and Discussion

2.1 Peptide design and characterization

As previously described, APEH inhibition could represent a novel strategy to regulate proteasome activity, with potential applications in biomedical fields. Therefore, the knowledge of the enzyme–inhibitor binding sites at the molecular level could be pivotal for our understanding of the underlying mechanisms, as well as for the design of novel and more efficient inhibitors.

The identification and characterization of an endogenous inhibitor protein of APEH from *S. solfataricus,* named SsCEI (*Sulfolobus solfataricus* chymotrypsin-elastase inhibitor) [**64, 83**], was the starting point for the present study. SsCEI, obtained in recombinant form, belongs to phosphatidylethanolamine-binding protein (PEBP) family. SsCEI is a monomer protein with a molecular mass of 19.0 kDa and a pI of 6.7, which is able to inhibit the serine proteases α-chymotrypsin and elastase but not trypsin, a distinct feature of all the members belonging to the family PEBP. In addition, *in vitro* inhibition studies showed that the isolated SsCEI was the first protein inhibitor able to efficiently interact and inhibit the APEHs from different sources. Homology modeling and site-specific mutagenesis techniques of the gene codifying SsCEI (*sso0767*) allowed the identification of the "*reactive site loop*" (*RSL*) of the inhibitor, located on the surface at the C-terminal region of SsCEI and responsible for the interaction with the protease targets. Such site shows an amino acid sequence never found in any protease inhibitor so far characterized. On the basis of the *RSL* of SsCEI, a set of four peptides, differing in size and nature at their P1 site, were designed and synthesized. Peptides SsCEI 1 and SsCEI 2 correspond to residues 119–134 and 123–134 of the SsCEI protein, respectively, and include the P1-P'1 (L126-E127) binding site which is reportedly involved in protease inhibition (**Figure 1**).

Figure 1 Amino acid sequence of SsCEI protein. *The sequence of SsCEI 1 and SsCEI 2 are indicated in red and blue boxes, respectively (**A**). Model of RSL of SsCEI (**B**).*

The shorter variant (SsCEI 2), starting with the N-terminus of *RSL*, was designed to minimize peptide length while maintaining intact the *RSL* binding site. Two further peptides were projected, SsCEI 3 and SsCEI 4, to replace the P1 residue Leu with Ala, which is the preferred amino acid in the substrates of mammalian APEHs. The sequences of these peptides are reported in **Table 1.**

Peptide	Theoretical mass value (Da)	Measured mass value (Da±SD)	P1P'1
SsCEI 1	1818.12	n.d.	YAIDTILLEIKNINAD
SsCEI 2	1355.61	1961±265	TILLEIKNINAD
SsCEI 3	1766.04	2012±150	YAIDTILAEIKNINAD
SsCEI 4	1313.53	1986±28	TILAEIKNINAD

Table 1. Synthetic peptides designed. *Peptides were synthesized with a free amino group at the N terminus and an amidic group at the C terminus. The apparent MWs of SsCEI peptides were determined by gel filtration chromatography. Data reported are the result of three independent determinations.*

Amidation at the C-terminal end was introduced to mimic the amino acid stretch within the protein backbone, whereas the amino termini of peptides were not acetylated to prevent substrate-like effects when in contact with APEH. Peptide structures within SsCEI protein inhibitor are predicted to be random/extended, as they have to be free in adopting the best conformation needed to dock the target proteases. Circular dichroism (CD) spectroscopy analyses were carried out to obtain information on the secondary structures of peptides outside the context of the native protein. Interestingly, the CD spectra measured between the 190 nm and 250 nm demonstrated that, except for SsCEI 4, which was largely unstructured (**Figure 2**), these peptides have well defined secondary structures in aqueous solution. Specifically, CD spectra of SsCEI 2 and SsCEI 4 at 37 °C, despite the single mutation, showed markedly different profiles, suggesting that the Leu→Ala substitution at the P1 site induces significant conformational alterations. CD spectra of SsCEI 2 featured canonical 'α-helix' curves with surprising fidelity (**Figure 2**). These data are in agreement with the role that the *RSL* has in the native inhibitor protein, and suggest a strong tendency of these peptides to adopt different conformations following even minimal sequence modifications. CD spectra were also recorded in the temperature range between 37 °C and 77 °C, with increasing temperature steps of 10 °C. Under these conditions, SsCEI 2 and SsCEI 3 showed considerable structural stability, as seen by the poor influence of temperature on their conformations (**Figure 2**). SsCEI 1 was not examined due to its poor stability in aqueous solution at the concentrations required for these analyses. These findings indicate that, in our model, the backbone architecture of the inhibitory loop is imposed by its specific amino acid sequence, and that the protein scaffold does not constrain the conformation of the *RSL*. Given the relevant contents of β-sheet structures observed in SsCEI 2 and SsCEI 3, we next investigated the oligomerization properties of these peptides to exclude the occurrence of macroscopic aggregates. For this purpose, 100 μM solutions of peptides SsCEI 2, SsCEI 3 and SsCEI 4 were analyzed by size-exclusion chromatography, and their apparent molecular masses were extrapolated from a calibration curve. As shown in **Table 1**, SsCEI 2, SsCEI 3 and SsCEI 4 were essentially monomers, suggesting that the secondary structures detected by CD were not a result of non-specific self-association, but seemed to be an intrinsic property of the peptides.

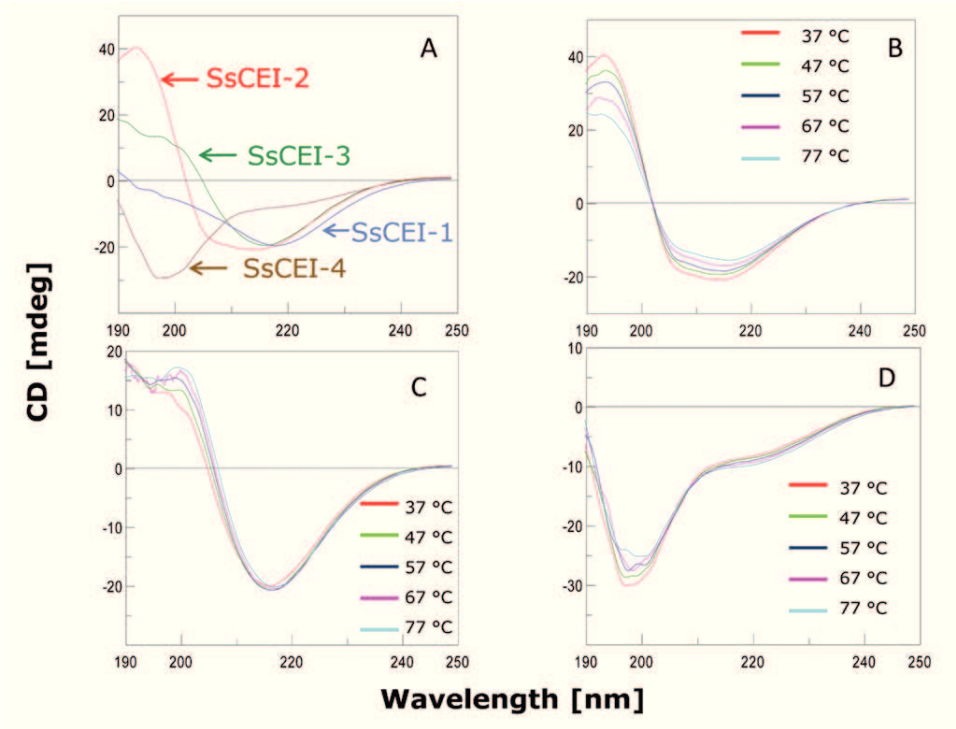

Figure 2*. *Far-UV CD spectra of the SsCEI peptides at different temperatures. *SsCEI 1-4 at 37°C (**A**), SsCEI 2 (**B**), SsCEI 3 (**C**), SsCEI 4 (**D**), in the temperature range of 37 °C to77 °C (as indicated). All the spectra were taken in aqueous solution*.

2.2 Mammalian APEHs are specifically and efficiently inhibited by SsCEI peptides.

The inhibition activity of SsCEI peptides was assessed using mammalian APEH purified from porcine liver (hereafter $APEH_{pl}$), which shares more than 90% sequence identity with the human APEH, as calculated by the ClustalW algorithm (http://www.ebi.ac.uk/Tools/msa/clustalw2/). Ac-Ala–pNA was used as the preferential substrate for the mammalian APEH. Inhibition analyses were performed by pre-incubating the enzyme with increasing amounts of these compounds and their half-maximal inhibitory concentrations (IC50) were determined. As shown in **Figure 3A**, both SsCEI 2 and SsCEI 4 dose-dependently decreased porcine APEH activity, although to different extents (IC50 values were 142±30 µM and 84±16 µM, respectively). Notably, APEH activity followed a Michaelis–Menten kinetic, both in the absence and in the presence of SsCEI 4 but only the Michaelis constant (Km) was affected by increasing concentrations of substrate, suggesting that SsCEI 4 behaved as a typical competitive inhibitor. It was confirmed by plotting the data according to the Lineweaver–Burk equation (**Figure 3B**). The straight lines obtained at

different inhibitor concentrations, all intersecting in one point corresponding to 1/Vmax, indicate a typical competitive mechanism. Therefore, these results demonstrated that an increase in substrate concentration induced a displacement of SsCEI bound to the APEH resulting in Enzyme-Inhibitor (EI) dissociation. In fact, competitive inhibition is a mechanism where binding of the inhibitor to the active site of the enzyme prevents binding of the substrate and *vice versa* in a dynamic equilibrium-like process. Analysis of the data obtained yielded a dissociation constant (Ki) value of 4.0±0.8 μM for the SsCEI 4–APEH complex. The greater efficacy of SsCEI 4 over SsCEI 2, can be ascribed to the preference for an Ala residue, with respect to leucine, at the P1 site, assuming that the SsCEI 4–APEH association occurs in a substrate-like manner. Data also suggested that the additional N-terminal residues in SsCEI 3 (**Table 1**), negatively affected the inhibition capacity towards mammalian APEH (**Figure 3A**).

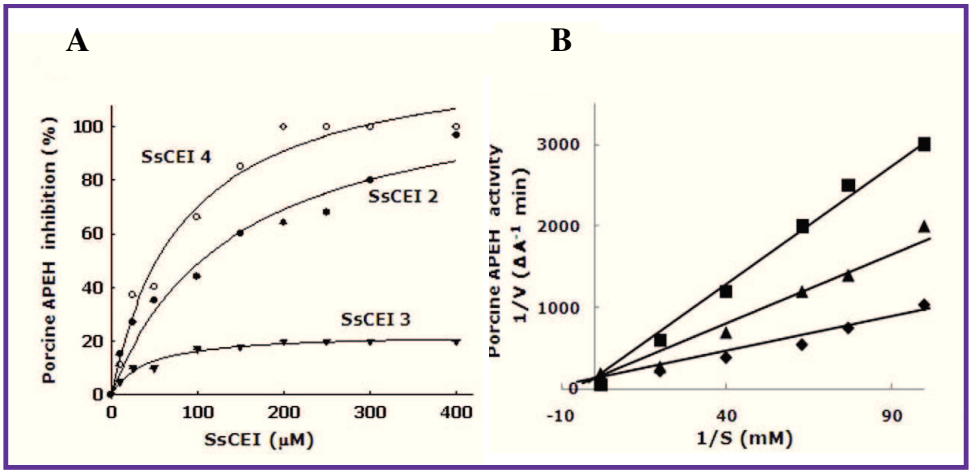

Figure 3. ***Kinetic analysis of SsCEIs***. *Binding of SsCEI peptides towards porcine APEH using Ac-Ala-pNA as substrate (**A**). The hyperbolic curves indicate the best fits for the data obtained, with IC50 values calculated from the graphs. Inhibition kinetics analyses with porcine APEH (0.5 nM) at increasing SsCEI 4 concentrations: 100 μM (triangles) and 150 μM (squares). Enzyme incubated without inhibitors were used as control (diamonds) (**B**). The inhibition constants, Ki, were determined by the Lineweaver–Burk equation for competitive inhibition*.

2.3 SsCEI 4 is a selective and non-covalent APEH inhibitor

In order to confirm the specificity of SsCEI 4 towards APEH, a panel of eukaryotic serine proteases comprising trypsin, α-chymotrypsin, elastase, carboxypeptidase Y, subtilisin and proteinase K, was analyzed in biochemical assays. Results showed that SsCEI 4 has no

detectable effects on the proteases tested. Moreover, to further examine the SsCEI 4 selectivity, its inhibition activity was determined in a reaction mixture containing the entire set of proteases reported above including $APEH_{pl}$. Under these conditions, the inhibition efficiency and the Ki of SsCEI 4 towards $APEH_{pl}$ were comparable to those measured in the presence of the $APEH_{pl}$ alone (data not shown). Moreover, to exclude the formation of adducts or degradation products between SsCEI 4 and its protease target $APEH_{pl}$, we investigated the incubation mixtures by reverse-phase HPLC chromatography. The lack of new peaks in the HPLC chromatogram and invariability of peak area corresponding to SsCEI 4, suggested that neither peptide degradation nor covalent binding with $APEH_{pl}$ occurred under the assay conditions (**Figure 4**). Data thus demonstrated that SsCEI 4 is a highly selective, and non-covalent inhibitor of APEH.

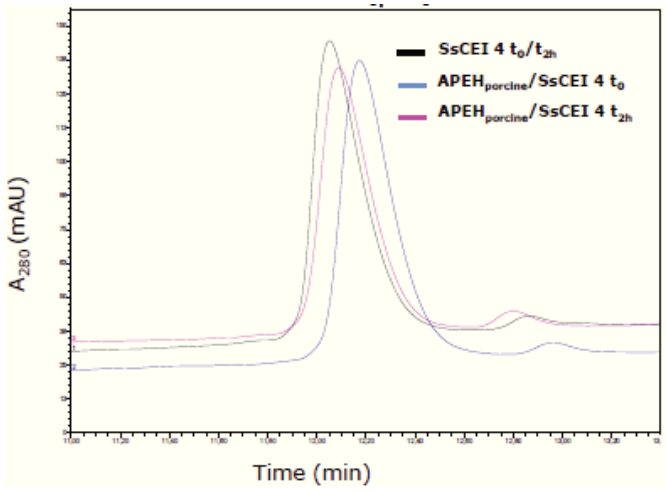

Figure 4. ***Representative chromatogram from RP C18 column analysis of SsCEI 4*** *incubated with or without porcine APEH for different times as indicated*.

2.4 SsCEI 4 downregulates APEH and proteasome activities in adenocarcinoma cell lines

Proteasome inhibition represents a validated, although challenging, anticancer approach. However, to prevent the adverse effects deriving from indiscriminate cell death, inhibition of the proteasome needs to be tightly controlled or selectively induced in cancer tissues. Therefore, the concept that proteasome activity could be decreased *via* APEH inhibition was investigated in a cancer cell line to confirm the inhibitory activity of SsCEI 4 in a more complex assay system. To this end, differentiated human colon carcinoma Caco-2 cells have

been used as preliminary model system. The parental cell line, originally obtained from a human colon adenocarcinoma, undergoes in culture a process of spontaneous differentiation that leads to the formation of a monolayer of cells, expressing several morphological and functional characteristics of the mature enterocyte. For these reasons, Caco-2 cell line has been extensively used over the last twenty years as a model of the intestinal barrier. The choice of using such model system was given to us by the data reported in the literature [**65**]. Indeed, among the top-ranked proteases associated with inflammatory bowel disease, one of the most important is APEH, which is highly expressed in the intestinal mucosa where it is able to cleave N-formyl peptides derived from bacteria, a potent pro-inflammatory chemo-attractant for phagocytes [**66**].

Therefore, Caco-2 cells were treated with SsCEI 4 or with a specific proteasome inhibitor (PI) MG132 for 48 h. As shown in **Figure 5A**, the peptide markedly reduced APEH activity in a dose-dependent manner, reaching their maximum effect at 200 μM, where enzyme activity was decreased by 70%. Under the same conditions MG132 treatment had no detectable effects. We next examined the inhibitory effects of SsCEI 4 on the chymotrypsin-like proteasomal (CT-like) activity in Caco-2 cells and in *cell-free* assays. In these latter experiments, partially purified proteasome fractions from Caco-2 cells were used instead of the commercially available 20S proteasome. Indeed, it has been reported that in neoplastic cell lines the CT-like activity, as well as the sensitivity to different PIs, is greatly influenced by the highly variable proteasome subunit composition [**84**]. Therefore, cell exposure to SsCEI 4, produced a dose-dependent decrease (up to 45% of the residual activity) of the CT-like activity with respect to the untreated cultures, whereas partially purified proteasome was not affected by these compounds (**Figure 5B**), thus confirming that it is not directly targeted by these inhibitors.

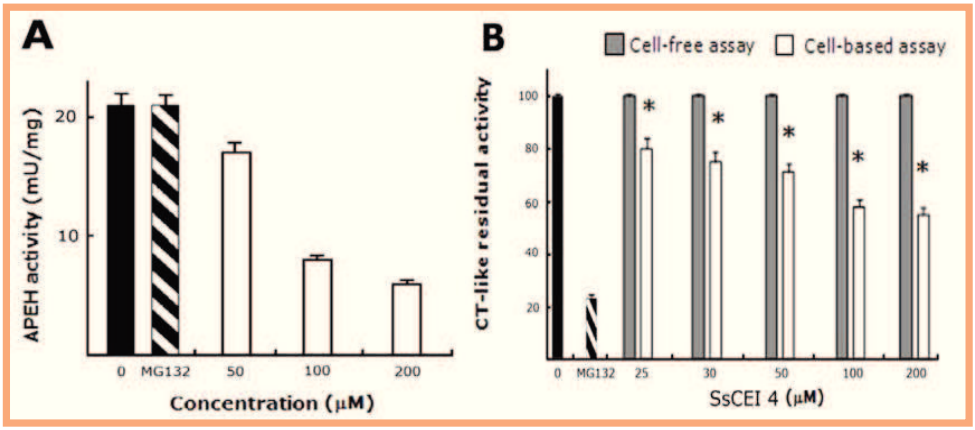

Figure 5. Downregulation of the proteasome/APEH enzymes by SsCEI 4 in Caco-2 cells. *APEH activity was measured in Caco-2 cells incubated with 50 µM, 100 µM and 200 µM SsCEI 4 (white bars) for 48 h (**A**). CT-like activity was measured in cell-free system (a partially purified proteasome fraction from differentiated Caco-2 cells, gray bars) and in Caco-2 cells (white bars) treated with increasing concentrations of SsCEI 4 (**B**). Cell-free protein mixtures, or Caco-2 cell cultures, treated with DMSO alone (black bars) or with MG132 (10 µM) (striped black bars) were used as positive controls. The data are expressed as means±SD. *Significantly different (P<0.005) from respective controls.*

Next, we evaluated the effects of SsCEI 4 treatment on the activation of caspases. As shown in **Figure 6A**, caspase-3 activity, a key effector of apoptosis, was improved at increasing doses of SsCEI 4. These data are in agreement with the well-established association between proteasomal inhibition and apoptosis induction. Moreover, this was not associated with any cytotoxic effect even at the highest concentration (200 µM), as indicated by the lactate dehydrogenase (LDH) activity levels in culture broth, which remained comparable to those of controls (**Figure 6B**). The toxicity resulting from the APEH-mediated inhibition of proteasome activity, as indicated by the treatment with SsCEI 4, was significantly lower than that observed in cultures incubated with MG132.

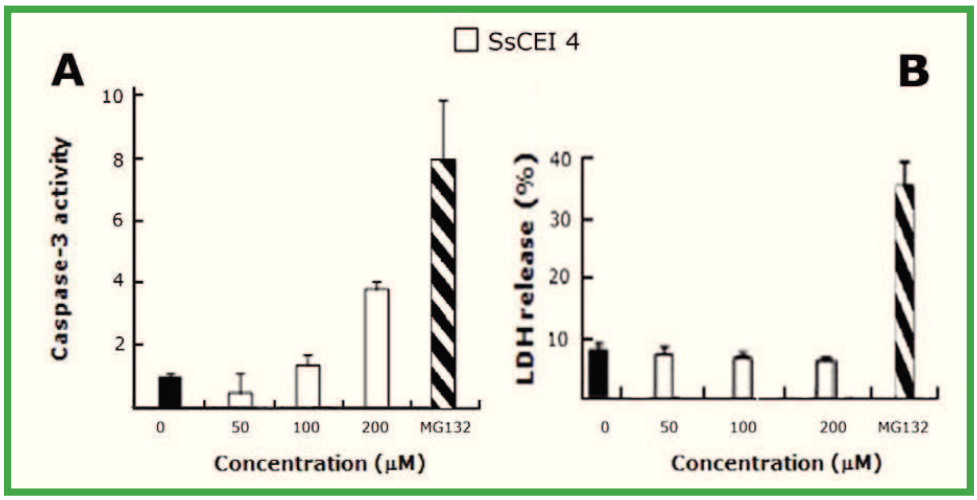

Figure 6. Treatment with SsCEI 4 triggers apoptosis in Caco-2 cells without any cytotoxicity. *Caspase-3 activities and LDH release were measured upon 48 h incubations of Caco-2 cells with increasing concentrations of SsCEI 4 (white bars) (**A**). The cytotoxic effect of the different treatments was evaluated by measuring the LDH release in the culture media (**B**). Cell-free protein mixtures, or Caco-2 cell cultures, treated with DMSO alone (black bars) or with MG132 (10 µM) (striped black bars) were used as positive controls. The data are expressed as means±SD. *Significantly different (P<0.005) from respective controls.*

Therefore, our results, consistently with the reporting coordinated functions of proteasome and APEH in protein turnover [**70**], add the relevant information that proteasome modulation could occurs *via* a complex pathway which has APEH like an important and regulative factor. Moreover, since APEH activity is not influenced by cell treatment with the specific PI MG132 (**Figure 5A**), proteasome modulation should be hierarchically down-stream of APEH inhibition. This view is also corroborated by the observation that APEH and proteasome seem to have no direct interactions, as they are distinctly eluted from gel filtration columns loaded with protein extracts obtained from SsCEI 4-treated or untreated Caco-2 cells.

2.5 SsCEI 4 increases the level of UPS substrates in Caco-2 cells

To finally confirm the reliability of the APEH-mediated strategy to affect the ubiquitin-proteasome system (UPS), several readouts were evaluated in differentiated Caco-2 cells treated with SsCEI 4 (200 µM) for 48 h. The commercially inhibitor of APEH (ebelactone) or the PI MG132, were used as positive controls. The immunoblot analysis showed that the levels of APEH in cells were not affected by any of these treatments while a significant increase of well-known proteasome substrates (p21Waf1 and NF-κB, two-fold or four-fold,

respectively; **Figure 7A, B**) was revealed. These findings are consistent with the idea that the relationship between apoptosis and the accumulation of damaged or short-lived regulatory proteins has a prominent role in controlling the homeostasis of cancer cells [**85**]. Cytoplasmic increase of NF-κB levels is indeed regarded as a major hallmark of different cell death mechanisms including apoptotis, since NF-κB nuclear translocation, following IκB degradation by UPS and gene transcription, is a well-established signal of cell growth. Proteasome inhibition in cancer cells leads to a reduced rate of IκB degradation, and to a longer persistence of NF-κB in the cytoplasm [**86**]. In the same way, accumulation of p21Waf1, a negative regulator of the cell division cycle, is a direct evidence of increased apoptosis and of reduced proteasome function, since it has been reported that its degradation occurs through N-terminal as well as internal lysine ubiquitinylation [**87**]. Polyubiquitinylated proteins are normally degraded by UPS, and downregulation of proteasome activity has been shown to substantially suppress bulk intracellular protein turnover [**55**]. As evidenced in **Figure 7C**, following incubation with SsCEI 4, ebelactone or MG132, we detected in cell extract the presence of high-molecular mass immunoreactive species (66 kDa to 160 kDa) which were absent in untreated cultures. These signals are indicative of polyubiquitin conjugates in the treated cells, confirming that the three tested compounds deregulate UPS in cancer cells. As a whole, our *in vitro* results demonstrate that APEH inhibition by SsCEI 4 treatment is associated with increased levels of the typical markers of proteasome inhibition without any cytotoxic effect.

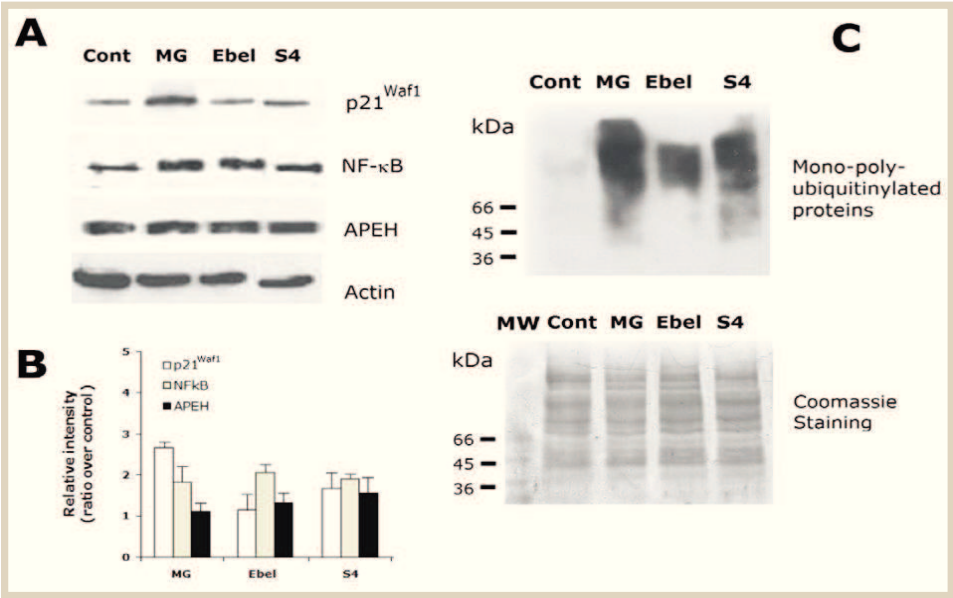

Figure 7. Evaluation of proteasome inhibition markers in Caco-2 cells incubated with SsCEI 4. *Representative immunoblots of the expression of p21Waf1, NF-kB, and APEH in Caco-2 cell exposed for 48 h to 10 µM MG132 (MG), 100 µM ebelactone (Ebel) or 200 µM SsCEI 4 (S4) (**A**). Data on Western blot analysis are expressed as the density ratio of target to control (β-actin) in arbitrary units. The values were expressed as average relative intensity as compared to untreated cultures and expressed as means±SD of measurements performed in triplicate (**B**). Protein ubiquitinylation in Caco-2 cell exposed for 48 h to MG, Ebel or S4 (**C**, upper panel). Upon the immunodetection, the membrane was stained with Coomassie blue. The lane loaded with molecular mass markers [MW kDa] was shown (**C**, lower panel).*

In this study we showed for the first time that, by using APEH inhibitors, proteasome activity can be regulated through an APEH-mediated mechanism which represents a novel strategy to control UPS functions. Beside these findings, we demonstrated that the stable, a selective and non-toxic inhibitor of APEH (the peptide SsCEI 4) is able to produce a noticeable downregulation of UPS in tumor cells. Moreover, this molecule represents an attractive template for the design of more potent inhibitors, with potential applications as anticancer and anti-inflammatory agents.

2.6 CF3-lmph is a selective inhibitor of APEH having an uncommon mechanism of inhibition and a stable bent conformation

With the aim of developing new compounds able to modulate APEH activity and to further investigate the role played by APEH in cell viability, we have undertaken the screening of a complex library of short synthetic peptides modified on the N terminus by a set of diverse

chemical groups; this to prevent undesired substrate-like behaviors of the peptides exposed to the enzyme. After five iterative rounds of screening and resynthesis needed to elucidate the whole peptide structure, we identified in the N-terminally modified tetrapeptide of sequence TFA-D-Leu-D-Met-D-Pro-D-His-NH2 (hereafter termed CF3-lmph), the one best molecule able to inhibit the $APEH_{pl}$ activity, in a dose-dependent manner (**Figure 8A)** with an IC50 value of 98.0±6.4 μM. The selectivity of CF3-lmph was initially evaluated in biochemical assays using a panel of eukaryotic proteases (trypsin, α-chymotrypsin, elastase, carboxypeptidase Y, subtilisin and proteinase K). Results showed that the best protein target for CF3-lmph was APEH with a maximum of 72% inhibition reached at 150 μM. This inhibition did not increase even using the peptide at 1 mM. Moreover, in the presence of increasing amounts of CF3-lmph, both the Vmax of $APEH_{pl}$ that Km were affected, indicating a uncompetitive inhibition mechanism, with a Ki value of 24.0 ± 0.8 μM. This mechanism was confirmed by the Lineweaver−Burk plot, that reveals a series of parallel lines, which is the hallmark of uncompetitive inhibition (**Figure 8B**). This very uncommon type of inhibition takes place when an enzyme inhibitor binds only the complex formed between the enzyme and the substrate (the E-S complex). This reduction in the effective concentration of the E-S complex increases the enzyme's apparent affinity for the substrate (Km is lowered) and decreases the maximum enzyme activity (Vmax), as it takes longer for the substrate or product to leave the active site.

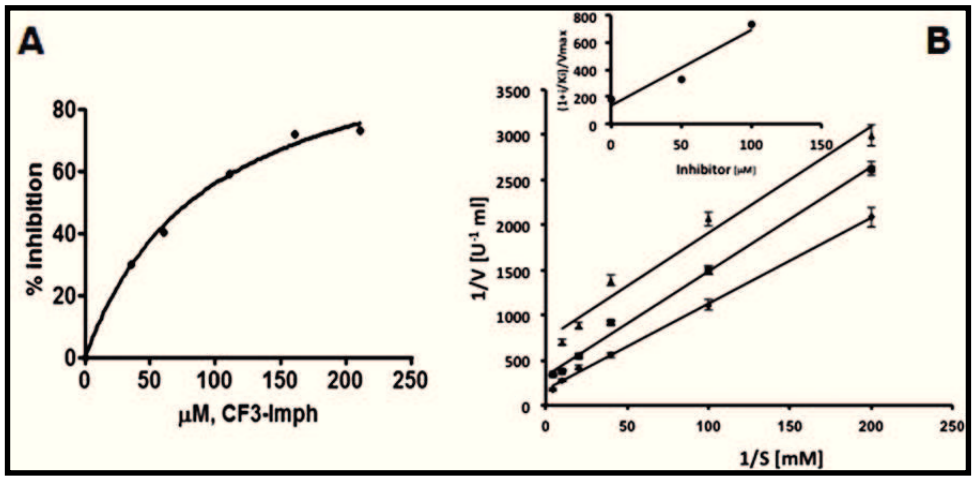

Figure 8. Kinetic analysis of CF3-lmph towards APEH. *Binding of CF3-lmph to porcine liver APEH ($APEH_{pl}$) using Acetyl-Ala-pNA as substrate (**A**). The hyperbolic curve indicates the best fit for the percentage inhibition data obtained, and the IC50 value was calculated*

*from the graph. Double-reciprocal plots of the velocity against substrate (Ac-Ala-pNA) concentration at three different CF3-lmph concentrations (no inhibitor ◆, 50 μM ■, and 100 μM ▲) (**B**). The velocity of the reaction is expressed as μmol of p-nitroaniline released/min/mL of enzyme on incubation at 37 °C. Ki value was determined from the equation of the uncompetitive inhibition (see insert for a plot of [(1 +i/Ki)/Vmax] vs inhibitor concentration).*

Also the activity of the acetylated and nonacetylated variants was tested against $APEH_{pl}$ to assess the role of the N-terminal trifluoroacetyl group. The presence of this moiety confers a high specificity to peptide activity, because no enzyme inhibition was seen with the acetylated and the NH2-free peptides. Finally, a structural analysis of the peptide, carried out by circular dichroism (CD) and NMR spectroscopy, revealed that the molecule in solution adopts a well-organized and stable (twisted or bent) conformation induced by the presence of a D-proline on position 3. The molecular model obtained by restrained molecular dynamics simulations showed a good agreement with experimental NMR data and were chosen as representative of peptide structures (**Figure 9**).

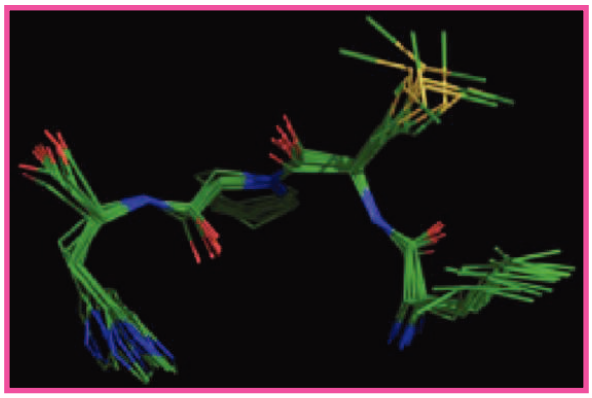

***Figure 9. Backbone superposition** of ten molecular frames collected during the last 2 ns of restrained molecular dynamics for CF3- lmph.*

2.7 APEH and proteasome expression at both mRNA and protein level correlates with their enzyme activity in cancer cell lines.

To deepening the ability of the two peptides under investigation to reduce cell proliferation, we decided to test the molecules on a collection of tumoral cell lines.

Initially, we decided to examine the basal expression/activity levels of these enzymes in fourteen cancer cell lines and in normal human fibroblasts (at their pre-confluent stage),

among those most commonly used in laboratory practice, to select the best cellular candidate for further investigations. The pre-confluent stage was chosen for practical considerations altought, in some cases, it do not provide suitable cell models for drug testing.

As shown in **Figure 10**, when basal specific APEH activity was plotted against the corresponding proteasomal chymotrypsin-like (CT-like) activity, a significant positive correlation was found (r^2=0.81, P=<0.01), supporting the idea of a functional relationship between these two enzymes which could act in cooperation for degradation of damaged proteins [**70, 88**].

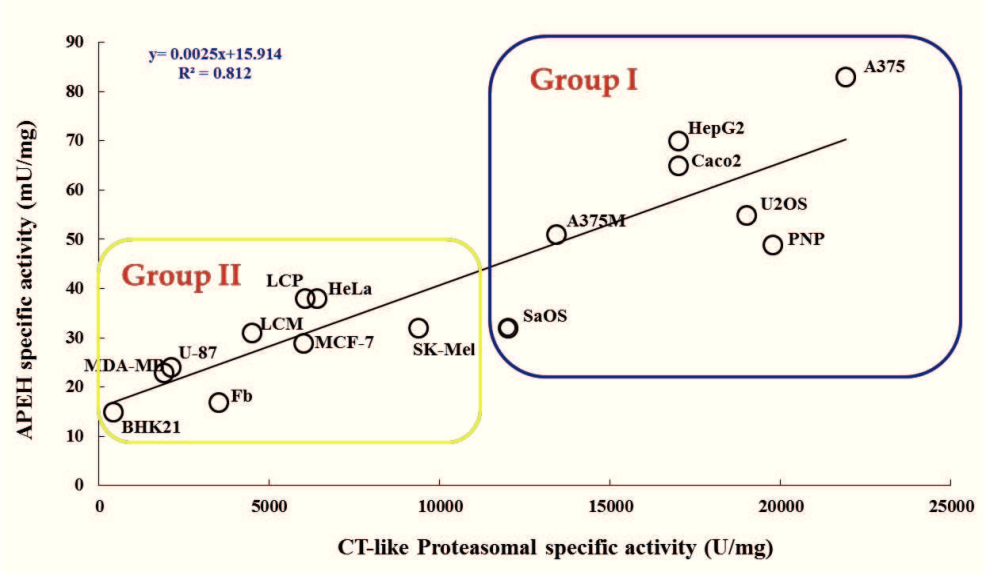

Figure 10. *Human cancer cell lines may be grouped according to the basal enzyme activities of APEH and proteasome. Cells from fourteen human cancer lines and non-cancerous cells (BHk21, fibroblasts) were harvested at the pre-confluent stage. Basal APEH and proteasomal CT-like activities were measured in cytoplasmic extracts. Results are presented as the mean values ±SD of triplicate analyses from at least three different experiments.*

On the basis of the basal levels, we identified two groups of cells displaying high (**Group I**) or low (**Group II**) APEH and proteasome activity values. The analysis of gene expression and intracellular protein levels of APEH and proteasome (β-5) in the different cell lines confirmed the existence of the two groups (**Figure 11A-B**). In light of results obtained, we decided to undergo to further investigations the cells of Group I, in good accordance with the hypothesis that cells exhibiting high activity and expression levels of APEH and proteasome

could be highly dependent on these enzyme functions and therefore more sensitive to their specific downregulation.

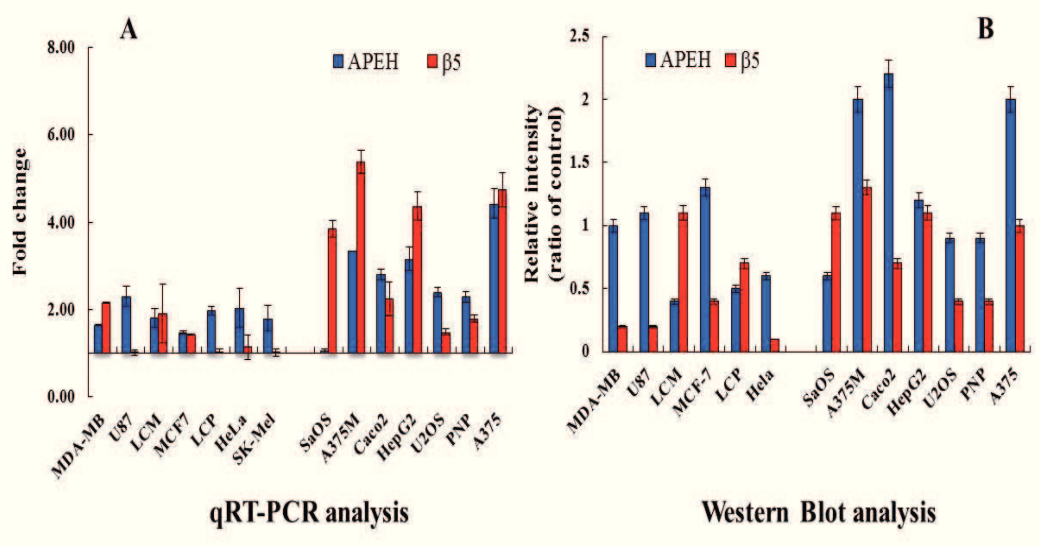

Figure 11. ***Expression and protein levels of APEH and proteasome***. *Cells from fourteen human cancer lines were harvested at the pre-confluent stage and used for cytoplasmic or mRNA extract preparation. The mRNA levels of APEH and β-5 subunit were evaluated by qRT-PCR and expressed as fold change in comparison to expressed levels in human fibroblast (**A**). Intracellular levels of β-5 and APEH were detected by immunoblotting (B). Data from three different analyses were normalized to the density of control protein (β-actin) and expressed as ratio over control (**B**). Results are presented as the mean values ±SD of triplicate analyses from at least three different experiments*.

2.8 SsCEI 4 inhibits proliferation and decreases APEH-proteasome activity in U2OS osteosarcoma cell lines

The susceptibility of cell lines belonging to Group I to the growth inhibitory effects of SsCEI 4 and CF3-lmph was estimated up to 48 h exposure at two different concentrations (50 and 100 μM).

As shown in **Figure 12**, the treatment of cells with SsCEI 4 caused a marked dose and time-dependent reduction in cell viability of osteosarcoma cell lines (U2OS and SaOS) respect to untreated cells, reaching a maximum reduction of viability of 63% and 40%, respectively to the highest concentration used (100 μM) and at 48 h. In addition, exposure of cells to the

peptide CF3-lmph resulted in a significant dose-dependent anti-proliferative effect only on the osteosarcoma cell lines SaOS at 48 h, reaching a maximum inhibition of 40% .

It is worth to note that, in these experimental conditions, Caco-2 cells were unaffected by SsCEI 4 treatment, possibly because the differentiation stage could be a necessary requisite for the susceptibility of these cells to the SsCEI 4 anti-proliferative effects.

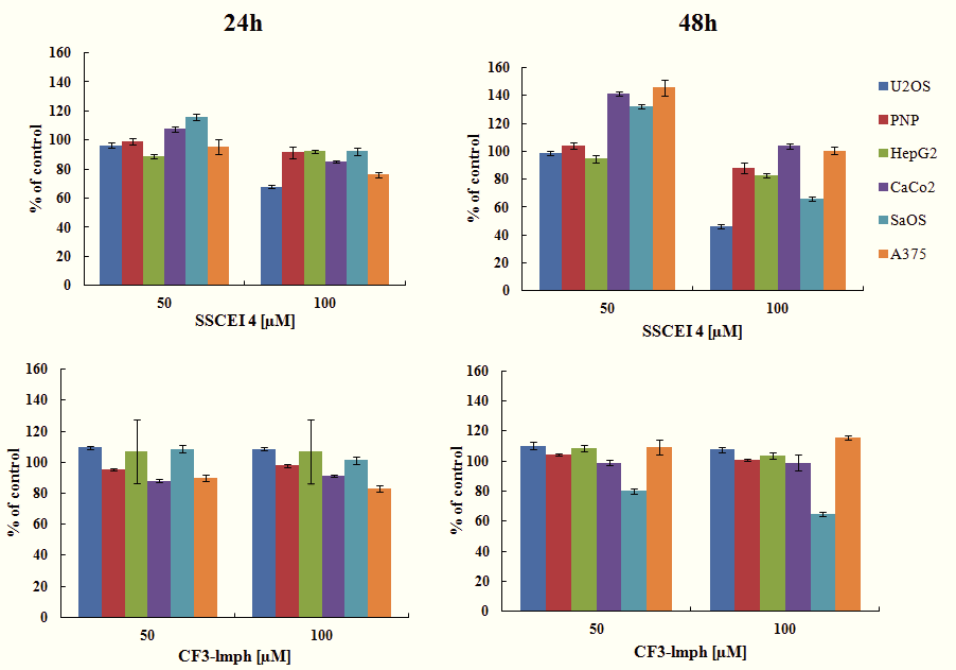

Figure 12. ***Human cancer cells exhibit differential sensitivity to the anti-proliferative activity of peptides SsCEI 4 and CF3-lmph*** . *The effects of peptides on cell viability were assessed in six cancer cell lines exposed for 24 and 48 h to increasing concentrations of SsCEI 4 or CF3-lmph. Data are expressed as means ±SD values of triplicate data from three independent experiments*.

These results suggest that the high basal levels of proteasome and APEH may be a necessary but not sufficient condition to identify cancer cells sensitive to APEH inhibition. Moreover, the ability of the two peptide molecules to induce a marked anti-proliferative effect on osteosarcoma cell lines could indicate the existence of a tumor target specificity linked to diversity of response and physiology of these cell lines.

On the basis of the proliferation assay (**Figure 12**), we selected SsCEI 4 and U2OS osteosarcoma cell line as model system for investigation on the role played by APEH in the multiple cancer cell anti-proliferative pathways. In order to define the dose accountable for 50% decrease of cell viability (IC50), U2OS cells were incubated for different time (24, 48

and 72 h) with increasing concentrations of SsCEI 4 (ranging from 100 nM to 200 µM), using human fibroblasts as control and the viable cell number was determined using an MTT assay. The resulting isobolograms (**Figure 13**) revealed that SsCEI 4 reduced the cell viability of U2OS in a concentration- and time-dependent manner with an IC50 value of 50.0±1.0 µM. Moreover, proliferation data obtained from fibroblasts, even at higher concentration of SsCEI 4, supported the lack of toxic effects (data not shown). As the maximal effect of cell viability inhibition was observed at 72 h, this time was chosen to set up our further experiments.

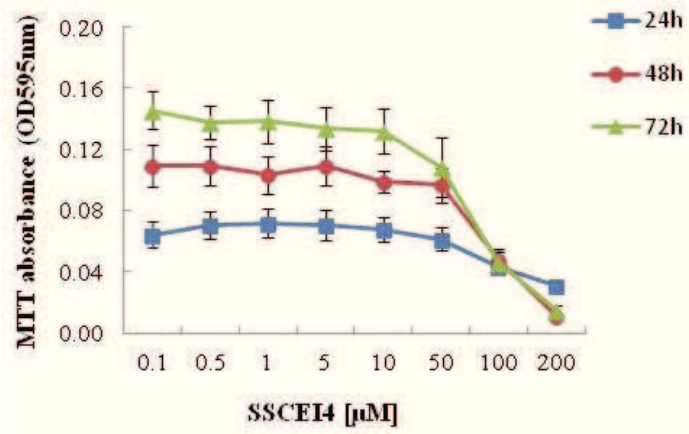

Figure 13. SsCEI 4 inhibits cell growth in U2OS cells in a dose- and time-dependent manner. *To measure the anti-proliferative activity of SsCEI 4, U2OS cells were cultivated in the presence or absence of increasing concentrations of the peptide (0.1-200 µM) for 24, 48 or 72 h. Inhibition of cell growth was assessed by MTT assay and values represent the means ±SD of triplicate data from three independent experiments.*

To assess the cytotoxicity of SsCEI 4 on the cancer cells considered, LDH activity was measured in spent media following 72 h exposure to 50 and 100 µM, using DMSO and 10 nM Bortezomib (BTZ) as controls . As expected, substantial cell death resulted from BTZ supplementation while the LDH activity in cultures exposed to SsCEI 4 was comparable to that of control, indicating that the reduction of cell viability induced by SsCEI 4 was not associated with any cytotoxic effect (**Figure 14**).

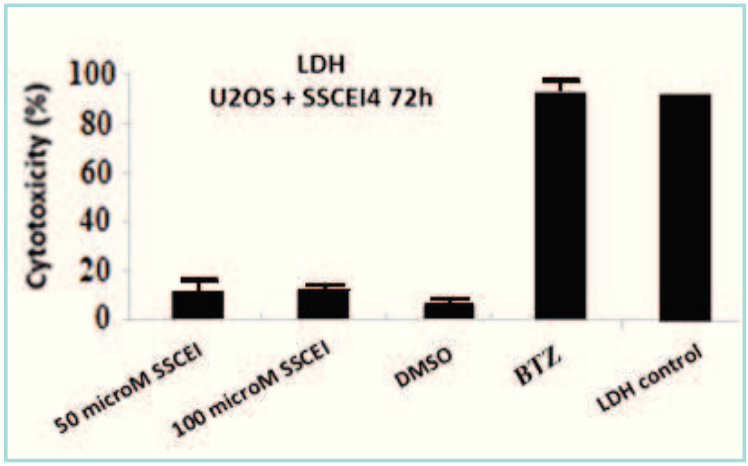

Figure 14*. *LDH release in the culture media was measured to study the cytotoxic of SsCEI 4. *U2OS cell cultures, treated with DMSO alone or with BTZ (10 nM), were used as positive controls*. *U2OS cell cultures were treated with cell lysis buffer to induce maximum LDH leakage (LDH control), DMSO alone or with Bortezomib (BTZ, 10 nM) as controls*. *LDH activity was determined by a fluorescent assay (n=3). Data are reported as percentage of maximum LDH release and values are presented as means±SD*.

2.9 U2OS exposure to high SsCEI 4 doses increases the level of UPS substrates in association with APEH/proteasome downregulation

Proteasome inhibition represents a validated, although challenging, anticancer approach. However, to prevent the adverse effects deriving from indiscriminate cell death, inhibition of the proteasome needs to be tightly controlled or selectively induced in cancer tissues. Therefore, the concept that proteasome activity could be decreased *via* APEH inhibition was investigated in U2OS cancer cell line. To this end, U2OS cells were incubated with increasing SsCEI 4 doses (50 or 100 μM) or with a specific PI (MG132) for 72 h. As shown in **Figure 15**, SsCEI 4 markedly reduced proteasome activity in a dose-dependent manner, reaching its maximum effect at 100 μM, where enzyme activity was decreased by 54%. Under the same conditions, a less marked dose-dependent inhibition of APEH activity (32%) was observed. Notably, MG132 treatment had no detectable effects on APEH activity, suggesting that proteasome modulation should be hierarchically down-stream of APEH inhibition. We next examined the inhibitory effects of SsCEI 4 on the CT-like activity in *cell-free* assays, to confirm that it is not directly targeted by this inhibitor. In these experiments, partially purified proteasome from U2OS cells or the commercially available 20S proteasome from

erythrocytes, were used. As shown in **Figure 16**, SsCEI 4 do not directly downregulate proteasome (either purified from U2OS or from human erythrocytes) function thus demonstrating that its dysfunction occurs *via* a more complex pathway that is triggered by APEH inhibition and has APEH like an important and regulative factor.

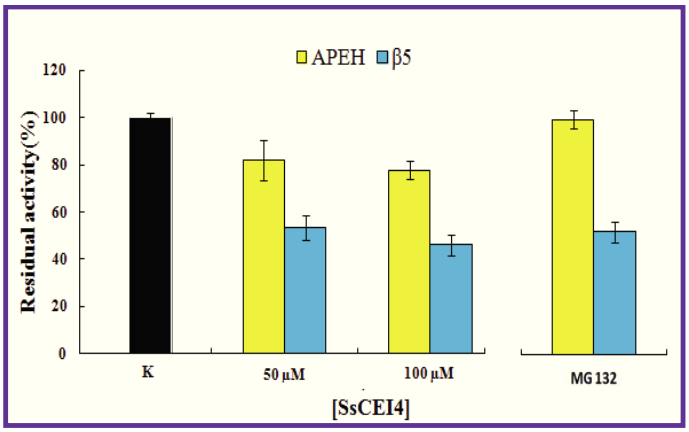

Figure 15. Dose-dependent anti-proliferative activity of SsCEI 4 correlates with downregulation of APEH and proteasomal CT-like subunit at activity level in U2OS cells. *Pre-confluent U2OS cultures were incubated for 72 h with 50 or 100 µM SsCEI 4. Cells untreated or treated with 10 µM MG132 were used as negative or positive controls, respectively. Measurement of APEH or proteasomal CT-like activities were performed on cytoplasmic extracts.*

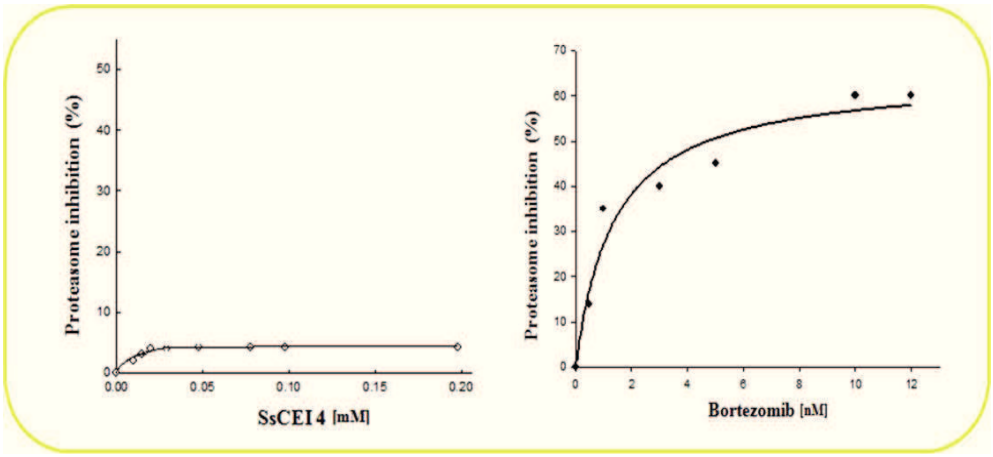

Figure 16. SsCEI 4 not exhibits inhibitory ability towards chymotrypsin-like (CT-like) proteasome activity. *The inhibitory effects of SsCEI 4 or Bortezomib were evaluated on commercially 20S proteasome using the synthetic fluorescent substrate N-Suc-LLVT-AMC (0.080 mM) for the measurement of the CT-like activity. Results are presented as the mean ±*

standard deviation (SD) of triplicate analyses from three independent experiments. SD values lower than 5% were not shown.

To gain insights into the mechanism by which SsCEI 4 induces its anti-proliferative effect, we performed a gene expression analysis of APEH and proteasome on osteosarcoma cell line by qRT-PCR, following treatment with 50 and 100 µM at 72 h, demostrating that it did not cause any significant variation of both gene transcripts (**Figure 17**).

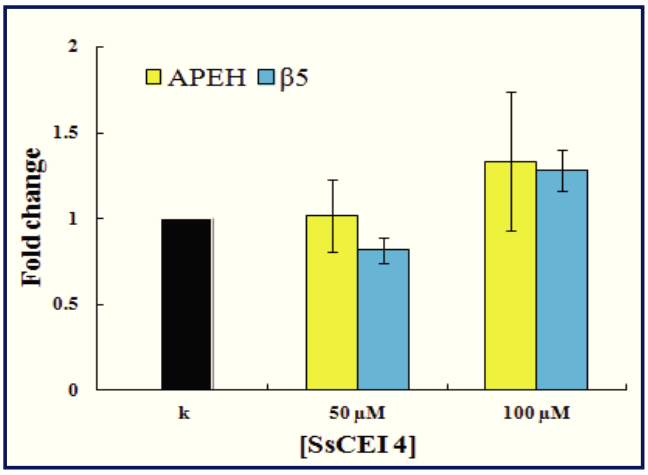

Figure 17. ***Dose-dependent anti-proliferative activity of SsCEI 4 does not correlate with downregulation of APEH and proteasomal CT-like subunit at mRNA level in U2OS cells***. *The mRNA levels of APEH and β-5 subunit were evaluated by qRT-PCR and expressed as fold change in comparison to untreated cells (k).*

Conversely, analysis of protein levels by Western blot revealed that SsCEI 4 caused a marked reduction of APEH and proteasome (40 and 56%, respectively) in osteosarcoma cell line, possibly indicating that the specific downregulation of the APEH and proteasome activities could induce their protein degradation thus contributing to the dysfunction of degradative machinery and to the inhibitory effect of SsCEI 4 on the U2OS viability (**Figure 18**).

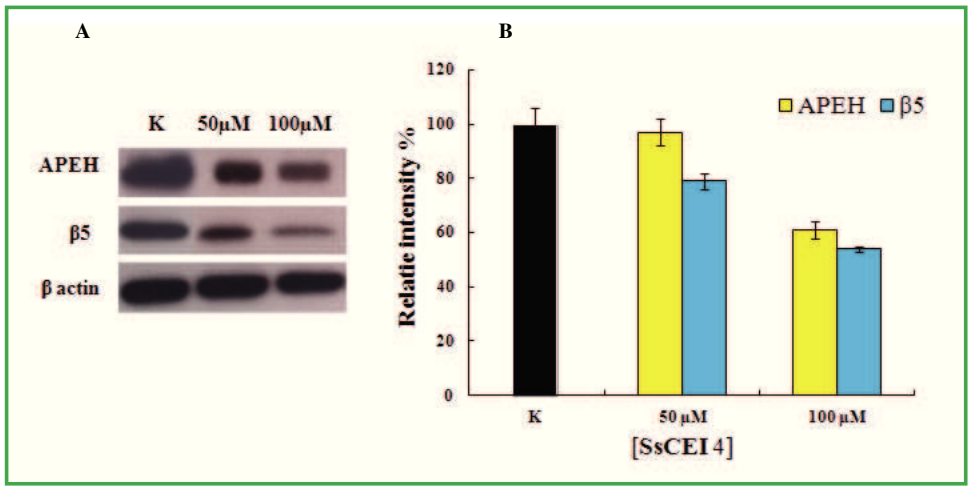

Figure 18. ***Intracellular levels of β-5 and APEH in U2OS cell lysates*** *exposed for 72 h to SsCEI 4 were detected by immunoblot analysis (**A**). Typical Western blot was shown and data from three different analyses were normalized to the density of control protein (β-actin) and expressed as ratio over control (**B**). Results are presented as the mean values ±SD of triplicate analyses from at least three different experiments*.

To finally confirm the reliability of the APEH-mediated strategy to affect UPS activity, the cytoplasm levels of the polyubiquitinylated proteins, which represent the classic hallmark of a direct effect of proteasome inhibition, were evaluated in U2OS cells treated for 72 h with SsCEI 4 at the indicated concentrations (50 and 100 μM). Polyubiquitinylated proteins are normally degraded by the cellular proteasomes, and downregulation of proteasome activity has been shown to substantially suppress bulk intracellular protein turnover [**55**]. As evidenced in **Figure 19**, following incubation with SsCEI 4, we detected in cell extract a dose-dependent increase in the levels of high molecular-mass immunoreactive species (66 kDa to 160 kDa), which are absent in untreated cultures. These signals are indicative of polyubiquitin conjugates in the treated cells, confirming that SsCEI 4 deregulates UPS activity in cancer cells.

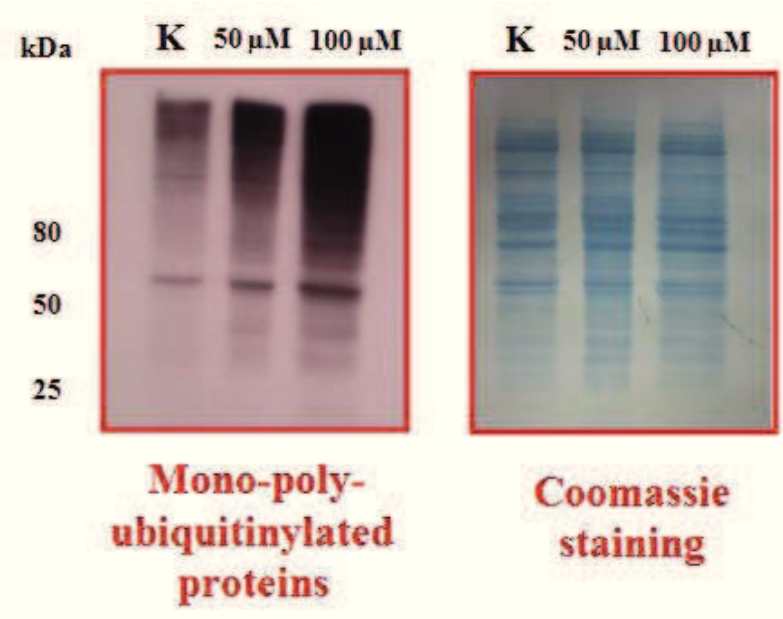

Figure 19. Evaluation of proteasome inhibition marker in U2OS cells incubated with SsCEI 4. *Polyubiquitinated proteins in U2OS cells untreated (K) and treated with SsCEI 4 for 72 h. The membrane PVDF was stained with Coomassie blue after immunodetection. The lane loaded with molecular mass markers [kDa] was shown.*

On the basis of these results, we hypothesized that APEH and proteasome can be functionally related and act as components of a new pathway controlling protein homeostasis and cancer cell proliferation.

2.10 SsCEI 4 induces cell death and G0/G1 phase cell cycle arrest in osteosarcoma cell lines through inhibition of Nf-κB signaling.

To further examine the relationship between SsCEI 4 and the APEH-proteasome pathway, we investigated on the mechanism of cell death involved in the anti-proliferative effect of SsCEI 4 and activated in response to inhibition of APEH-proteasome system in U2OS.

- **Apoptosis**

The correct functioning of the UPS pathway is essential for the degradation of the majority of intracellular proteins. Several key regulatory proteins involved in cell proliferation and differentiation are regulated by proteasome-mediated proteolysis resulting in the activation or inhibition of specific cell signaling pathways [**14**]. Therefore, it is not surprising that a myriad of cell responses and pathways are perturbates as a result of proteasome inhibition. *In vitro* and *in vivo* studies have demonstrated that proteasome inhibitors affect tumor growth by

inducing apoptosis, a genetically programmed mechanism(s) that allows the cell to commit suicide, in several human cancer cells [**89**]. Indeed, caspases, the key proteases activated during apoptosis, are also regulated by the proteasome.

To this end, to examine the contribution of an apoptotic event in SsCEI 4-induced decline of cancer cells viability, caspase 3 activation was measured. Interestingly, results revealed that caspase 3 activity was not improved at increasing doses of SsCEI 4, as shown in **Figure 20**.

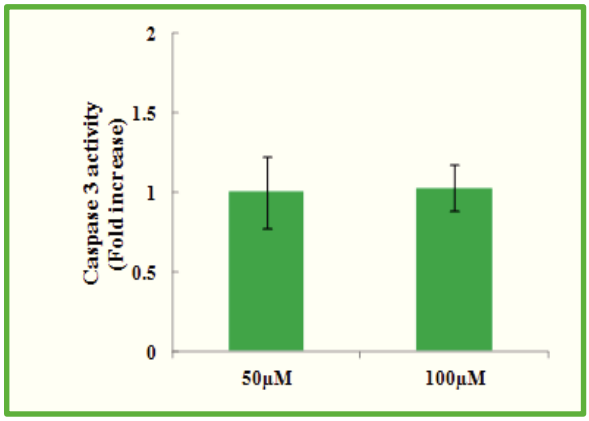

Figure 20. Caspase 3 activity was measured in U2OS cells treated with SsCEI 4*. Pre-confluent U2OS cultures were incubated for 72 h with 50 or 100 µM SsCEI 4. Thereafter, cells were harvested, and used for cytoplasmic extracts preparation. Caspase 3 activity values are expressed as fold increase in comparison to untreated cells. Results were presented as means±SD of triplicate data from three independent experiments.*

This result was further confirmed by Western blot analysis which showed that SsCEI 4 treatment failed to induce the proteolytic cleavage of caspase 3 and the poly(ADP-ribose) polymerase (PARP), two critical events that are a hallmark of apoptosis (**Figure 21**). Therefore, our findings demonstrated that the U2OS anti-proliferative effect elicited by SsCEI 4 does not trigger apoptosis.

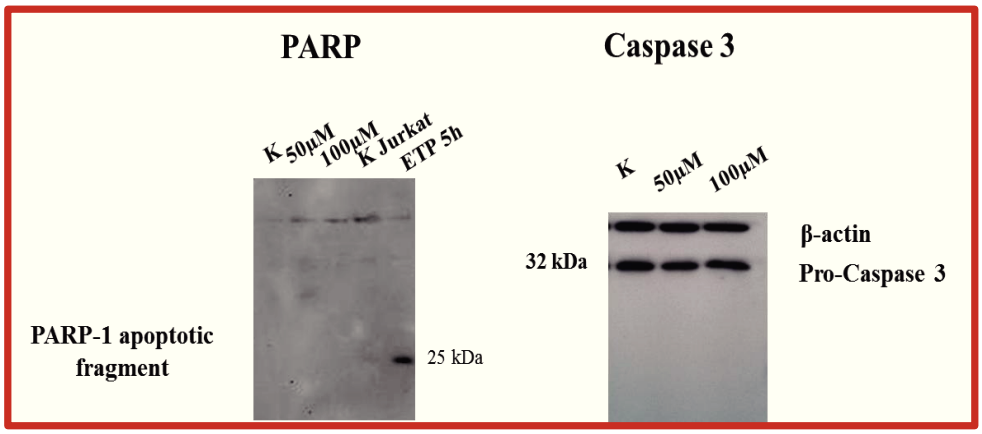

Figure 21. *U2OS cells were treated 72 h with or without 50 and 100 μM SsCEI 4. Cleaved PARP and caspase 3 were evaluated by western blot. Jurkat cells treated with Etoposside (ETP) were used as positive controls.*

- **Autophagy**

The cells have evolved a multitude of pathways that can be used to promote cell killing under appropriate conditions. In this context, apoptosis is the best-characterized form while autophagy, as part of the lysosomal system, is an evolutionarily conserved cellular strategy to engulf and degrade long-lived cytosolic proteins and organelles to provide substrates for energy metabolism and to recycle amino acids, fatty acids, and nucleotides for the biosynthetic needs of cells [**90**]. Generally, autophagy plays dual roles in cellular death or survival: one is to induce type II programmed cell death, which is different from apoptosis and is often termed autophagic cell death, whereas the other is to recycle cellular components to sustain metabolism and to prevent the accumulation of damaged, toxic proteins and organelles during stress [**91**]. A recent study reported that inhibition of the proteasome can induce autophagy in human SHG-44 glioma cells, and inhibition of autophagy increases cell death [**92**]. Typical markers of this mechanism are Beclin 1 and LC3-I/LC3-II. Beclin 1 is a Bcl-2-interacting protein that promotes autophagy and has an important role in cellular proliferation and tumorigenesis. Specifically, Beclin 1 is required for the initiation of the formation of the autophagosome. Microtubule-associated protein light chain 3 (LC3) is synthesized as a proform that is cleaved by a protease to become LC3-I. Indeed, LC3 exists in cells in two forms; one is cytoplasmic, LC3-I (18 kDa) and the other, LC3-II (16kDa) is associated with the autophagosome membrane. Upon initiation of autophagy, the C-terminal

glycine of LC3-I is modified by addition of a phosphatidylethanolamine (PE) to form LC3-II, which translocates rapidly to nascent autophagosomes. The expression level of LC3-II generally correlates with the number of autophagosome. Western blot assessment of the increase in either the LC3-II forms or of the relationship between LC3-II and LC3-I content is currently considered as a simple, quick procedure to verify the presence of cell autophagy [**93**]. LC3 antibody was able to recognize both the upper LC3-I band and the lower LC3-II, which has a faster mobility on immunoblots as a result of the greater hydrophobicity.

To determine the role of autophagy in anti-proliferative effect of SsCEI 4, Western blot analyses were performed. As shown in **Figure 22A**, SsCEI 4 did not affect the expression of Beclin 1 in U2OS cells. In addition, as shown in **Figure 22B**, after 72 h incubation with SsCEI 4 no alteration in the conversion of LC3-I to LC3-II was found. U2OS treated with chloroquine (CQ), which causes accumulation of the lipid-modified LC3, were used as a positive control to confirm the identity of LC3-I and LC3-II. These results suggest that autophagy was not responsible for the anti-proliferative effect of SsCEI 4 observed in U2OS cells.

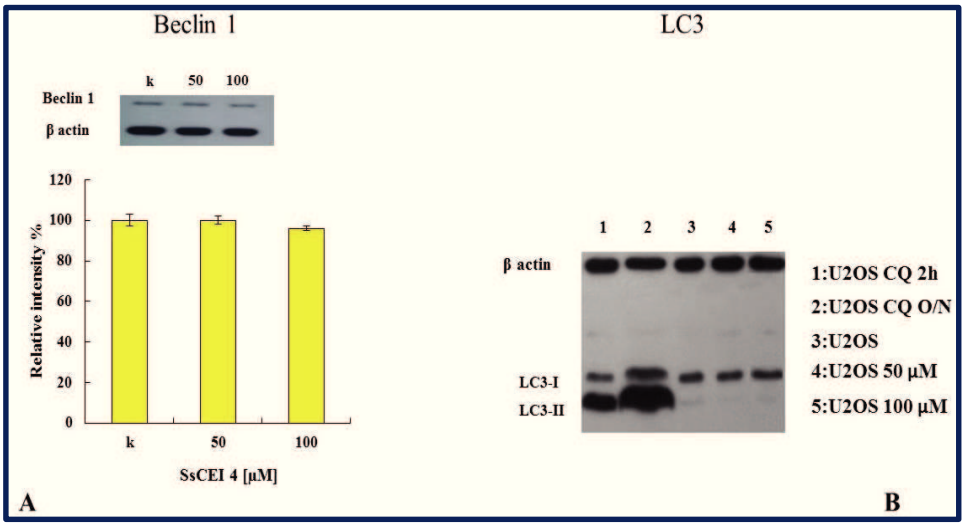

Figure 22. ***Western blot of Beclin 1 (A) and LC3 (B)*** *after treatment of U2OS cells with SsCEI 4 (50 and 100 μM). All the treatments were carried out for 72 h. Results of densitometry of Beclin 1 bands (left panel) are expressed as the mean of relationships between densitometries of Beclin 1 and α actin bands ± SD for three different experiments. The image (right panel) is representative of three different experiments.*

- **Oxidative stress: ROS accumulation**

It was recently reported that proteasome inhibition by bortezomib increased the levels of intracellular ROS levels **[53].** Therefore, we next investigated whether SsCEI 4 triggered an alteration of the redox status by increasing the intracellular ROS in osteosarcoma cancer cells. U2OS were treated with 50 and 100 µM SsCEI 4 from 1 to 48 h and then stained with DCF-DA and analysed by FACS to identify cells bearing ROS. As shown in **Figure 23**, the levels of intracellular ROS did not increase in U2OS cells after exposure to SsCEI 4 for 1 h but same results were obtained upon 48 h treatment (data not shown), suggesting that the alteration of the redox status is not associated with the antiproliferative effect of SsCEI 4.

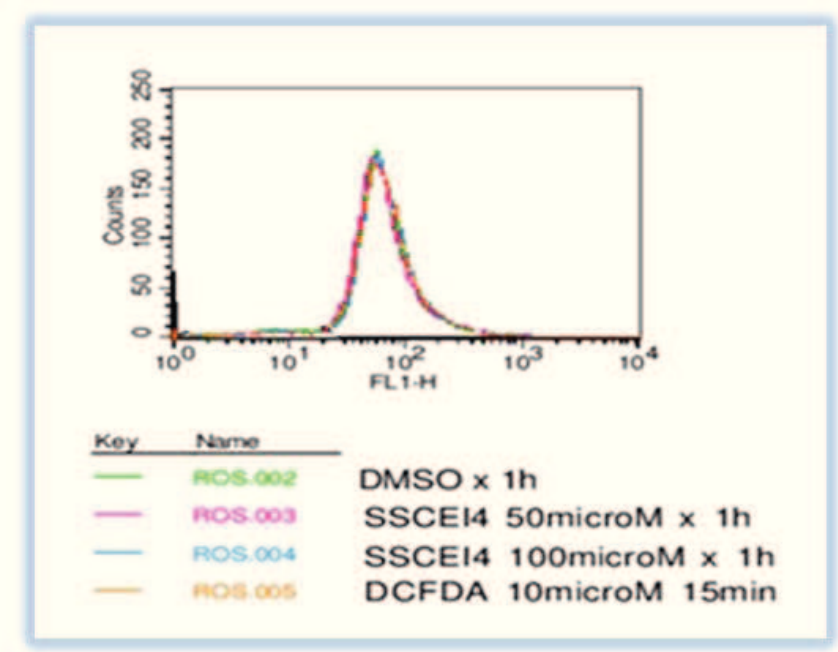

Figure 23. Analysis of intracellular ROS levels by FACS. *U2OS cells were treated with SsCEI 4 (50 and 100 µM) from 1 to 48 h and analyzed respect to untreated cells (green line).*

- **Cell cycle arrest**

To determine whether the antiproliferative activity induced by SsCEI 4 was caused by cell cycle arrest, we examined the effect of SsCEI 4 on cell cycle of U2OS. The percentages of cells in the G0/G1, S and G2/M phases were determined by flow cytometric analysis of propidium iodide stained cells. For these experiments, U2OS cells were exposed to increasing concentrations of SsCEI 5 (50 and 100 µM) and cell cycle profile was evaluated after 24, 48

and 72 h**.** Preliminary data revealed that, in the presence of peptide, the percentage of cells in G0/G1 phase increased in a time and dose-dependent manner, reaching a maximum already at 48 h and at 100 µM (**Figure 24**). Further analyses will be need to investigate the changes in G0/G1 phase-related cycle regulators in response to SsCEI 4 treatment.

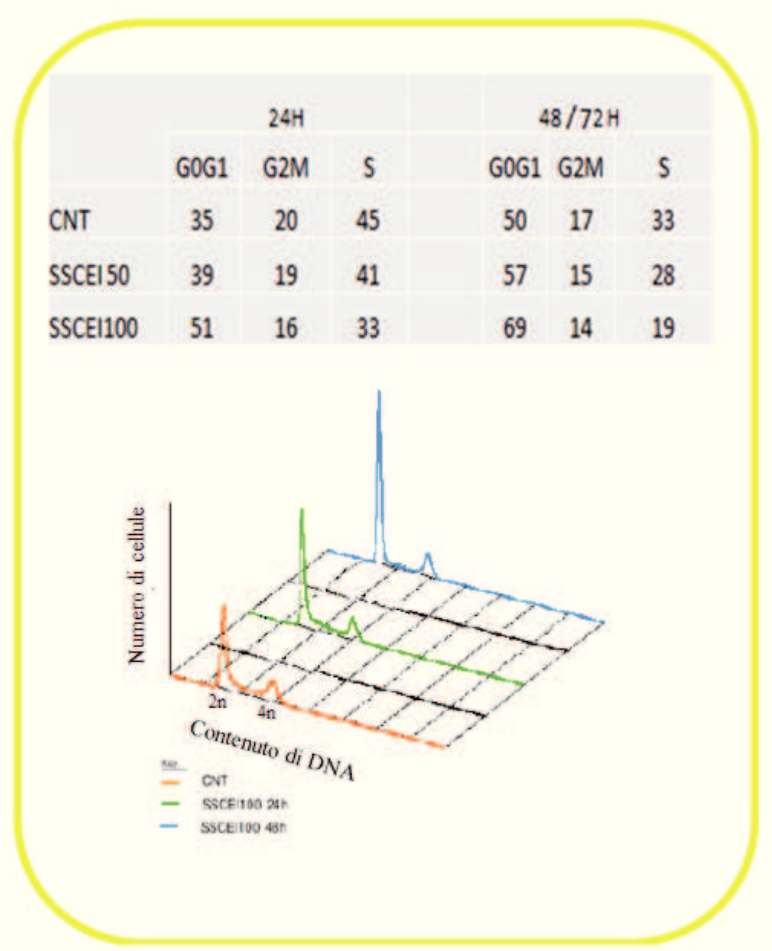

Figure 24. SsCEI 4 induces a G0/G1 cell cycle arrest in U2OS cells*. Cell cycle analysis was performed after exposing U2OS to SsCEI 4 (50 and 100 µM) for 24 h, 48 and 72 h. The experiment shown is a representative example from three different experiments. CNT, control.*

It is reported that a key component of PI mediated growth arrest is inhibition of NF-κB signaling. NF-κB signaling in cancer cells is controlled by the ubiquitin proteasome pathway, which directs the ubiquitination and proteolysis of its inhibitory partner, IκB. Once freed from its inhibitor, NF-κB gets localized in the nucleus where it allows transcription of many genes driving cancer cell proliferation. To confirm the G0/G1 cell cycle arrest, we analyzed the

cytoplasmatic levels of NF-κB in U2OS cells treated with SsCEI 4 by Western Blot. As shown in **Figure 25,** treated U2OS cells exhibited a higher levels of the target protein than control cells, suggesting that this transcription factor could be responsible for the cell-cycle arrest induced by SsCEI 4.

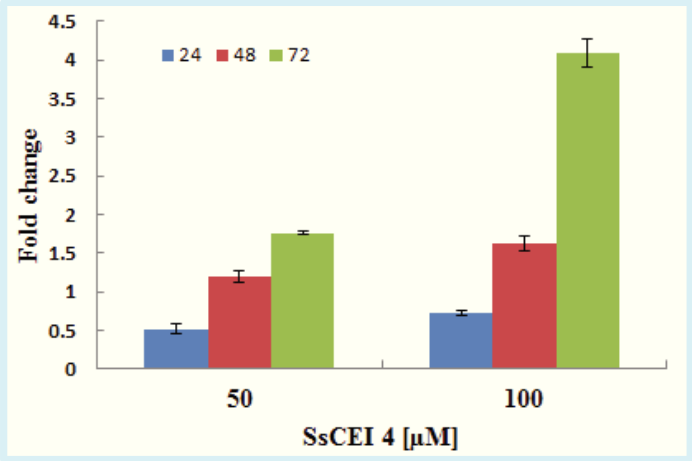

Figure 25. SsCEI 4 increases the cytoplasmic level of NF-κB in U2OS cells. *Cells were treated with SsCEI 4 (50 and 100 μM) for the indicated times and cell extracts were prepared and analyzed by western blot. β-actin was used as a loading control. The values were expressed as average relative intensity as compared to untreated cultures and expressed as means±SD of measurements performed in triplicate.*

2.11 Proteasomal degradation of the cystic fibrosis transmembrane conductance regulator (CFTR) mutated protein is prevented by SsCEI 4

In light of a recently proposed cooperative role for the APEH–proteasome system in the control of protein turnover [**70**], we hypothesised that APEH could be used as a target to indirectly control/modulate proteasome functions. To support this idea, we conducted *in vitro* experiments using the selected APEH inhibitor (SsCEI 4) on the Baby Hamster Kidney (BHK) cell line, stably expressing a mutant protein of the cystic fibrosis transmembrane conductance regulator (CFTR), known as ΔF508 CFTR-3HA (hereafter called CFTR-M), bearing the deletion of Phe508, one of the most common modification in patients with cystic fibrosis. Many of the mutations in the CFTR gene that cause cystic fibrosis interfere with the folding and biosynthetic processing of CFTR molecules in the endoplasmic reticulum. Specifically, some mutations, including the common ΔF508, decrease the efficiency of CFTR folding, reduce the probability of its dissociation from molecular chaperones, and largely

prevent its maturation through the secretory pathway to the plasma membrane. These mutant CFTR molecules are rapidly targeted for proteolysis via the UPS [**85, 94**]. Accordingly, BHK and human bronchial epithelial cells (CFBE41o-DF) expressing CFTR-M were used in this study as a model system to confirm the role of APEH in the coordinated protein-degradation machinery, and steady-state levels of the core glycosylated CFTR-M form (140 kDa) were evaluated by immunoblot analysis. Remarkably, the SsCEI 4 peptide efficiently prevented degradation of CFTR-M at the time intervals considered (24 h and 48 h). As a fact, exposure of BHK cells to 100 µM SsCEI 4 for 48 h induced a marked increase of CFTR-M levels (twenty-fold) (**Figure 26A**, **B**),without any cytotoxic effects (data not shown).

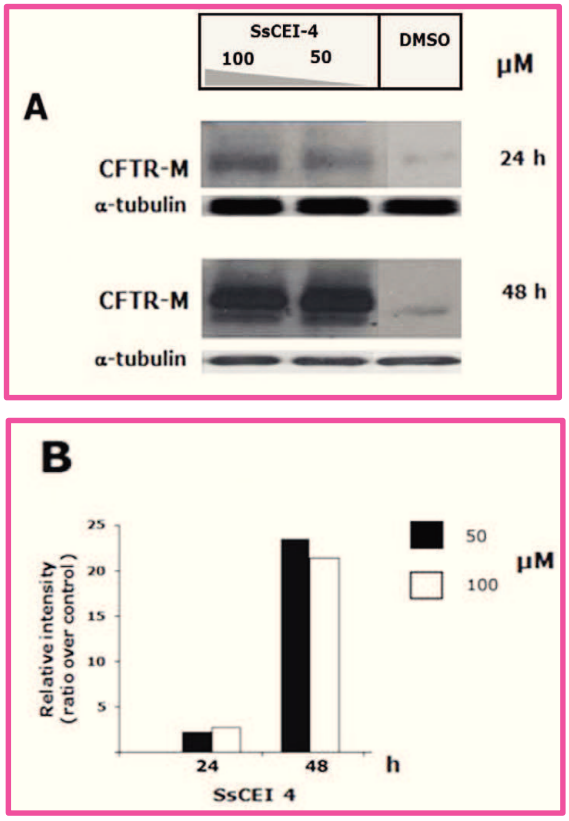

Figure 26. Analysis of the CFTR-M protein accumulation in BHK cells treated with the SsCEI 4. *Representative Immunoblots and associated densitometric analysis for cytosolic CFTR-M accumulation in BHK cells following 24 h and 48 h exposure to 50 µM or 100 µM SsCEI 4 (**A**) Bands were quantified using densitometric analysis and normalized against α-tubulin. The values were expressed as average fold increase as compared to untreated culture (**B**).*

In addition, a dose-dependent inhibition of APEH and proteasome CT-like activities was observed upon 48 h of incubation (similar data on APEH and proteasome activities were measured after 24 h cell exposure) with peptide, as shown in **Figure 27 (C, D)** consistent with the immunoblot results.

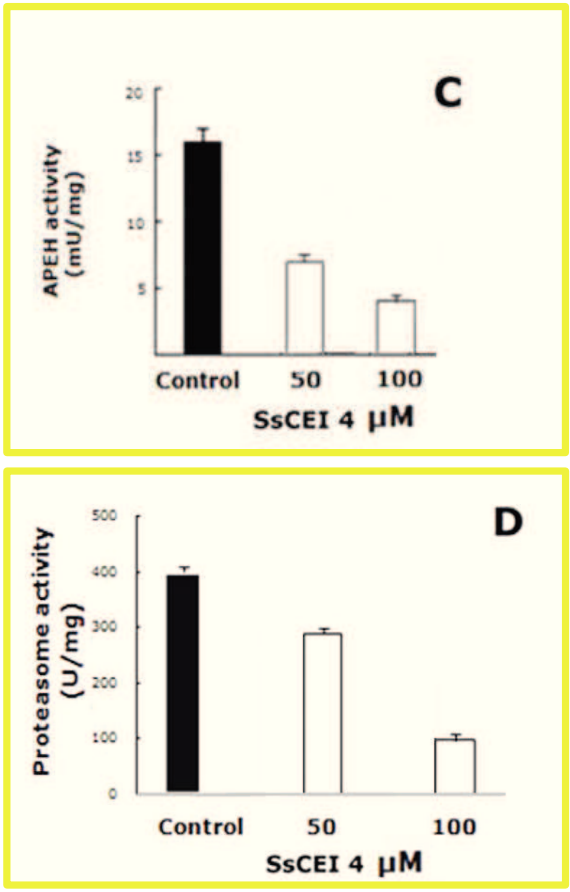

Figure 27. *APEH activity was measured in BHK cells incubated with 50 µM and 100 µM SsCEI 4 (white bars)for 48 h (**C**). CT-like proteasome activities were measured in BHK cells incubated with 50 µM and 100 µM SsCEI 4 (white bars) for 48 h (**D**). Untreated cultures were used as controls (black bars); the data are expressed as means±SD.*

Finally, siRNA technique was used to directly correlate APEH to the protein degradation processes via UPS. For this purpose, the accumulation of CFTR-M was evaluated in CFBE41o-DF cells following transfection with APEH siRNA. As shown in **Figure 28**, APEH siRNA-transfected cells exhibited a considerable reduction of APEH protein levels and a marked accumulation of CFTR-M (eight-fold, data not shown), in contrast to cells transfected with a not specific siRNA which displayed basal levels of APEH and neglectable level of CFTR-M. Therefore, APEH can be seen as an alternative target, whose inhibition by

competitive inhibitor is accompanied by a parallel downregulation of proteasome activity through a yet unknown mechanism.

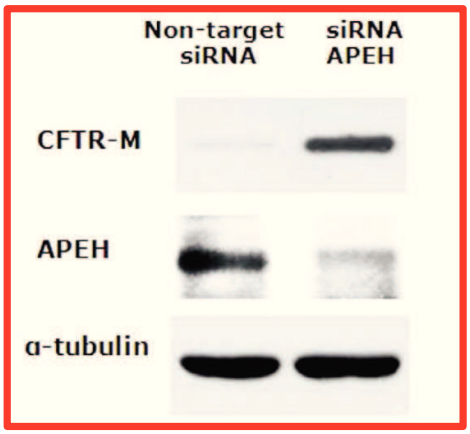

Figure 28. ***Analysis of the CFTR-M protein accumulation in APEH siRNA transfected CFBE41o-DF cells***. *Representative Immunoblots of APEH and CFTR-M accumulation in CFBE41o-DF cells transfected with APEH siRNA. A scrambled, non-targeted siRNA, was used as negative control and α-tubulin was used as loading control*.

3. Conclusions

Conclusions

Proteasome is an abundant multi-enzyme complex that provides the main pathway for the protein turnover or the elimination of misfolded and aggregated proteins. As such, it controls the levels of proteins involved in cell-cycle progression and apoptosis in normal and malignant cells, and has become an important target in anticancer therapies [**95**]. A large number of specific PI molecules have been developed to date [**96**], but despite their indisputable efficacies all of these suffer for negative side-effects. These events represent the major drawback of impairing the activity of a target largely involved in important physiological processes. For these reasons, several studies have suggested that the targeting of functionally related, up-stream or down-stream proteasome effectors [**9**], can be an alternative and a safer way to recover proteasome dysfunction associated with pathological conditions [**11, 55**]. In this study we showed for the first time that, by using a specific APEH inhibitor, proteasome activity could be regulated through an APEH-mediated mechanism, which represents a novel strategy to control UPS functions. Beside these findings, we demonstrated that the stable, selective and non-toxic inhibitor of APEH (SsCEI 4) is able to produce a noticeable downregulation of UPS activity in different cancer cells. Moreover, this molecule represents an attractive template for the design of more potent inhibitors, with potential applications as anticancer and anti-inflammatory agents. APEH has been postulated to serve as a key regulator of N-terminally acetylated proteins [**58**] but the biological effects of disrupting APEH has not been completely understood. As more than 80% of proteins in human cells are N-terminal acetylated [**97**] and protein acetylation is implicated in a variety of essential cellular pathways [**98**], it is thus likely feasible that APEH is involved in these processes. As reported in previous studies, proteasome and APEH act cooperatively in protein turnover [**70, 88**], although the biochemical mechanisms remain to be clarified. In this regard, in contrast to the general idea that N-terminal acetylation protects from degradation, in certain proteins some sequences, which include acetyl groups at the N terminus, were recently found to be involved in degradation signals [**99**]. On the basis of our preliminary results, a direct interaction between APEH and proteasome might be excluded, whereas the hypothesis that APEH can activate or stabilize the proteasome by uncovering the N-tail of a yet unknown negative effector protein cannot be ruled out. Of note, we showed that whereas APEH inhibition triggered an impairment of the proteasome activity, its selective inhibition did not affect APEH functions, likely suggesting that APEH could be an up-stream modulator of the proteasome. Studies aimed at achieving a better understanding of the mechanism/s

responsible for the APEH mediated downregulation of proteasome and at the evaluation of APEH inhibitors in animal cancer model are currently in progress.

4. References

References

1. Voges D, Zwickl P, Baumeister W. The 26S proteasome: A molecular machine designed for controlled proteolysis. *Annu Rev Biochem* (1999); 68: 1015–1068.
2. Kisselev AF, Akopian TN, Castillo V, and Goldberg AL. Proteasome active sites allosterically regulate each other, suggesting a cyclical bite-chew mechanism for protein breakdown. *Mol Cell* (1999); 4: 395–402.
3. Goldberg AL. Protein degradation and protection against misfolded or damaged proteins. *Nature* (2003); 426(6968): 895-9.
4. Groll M, Bajorek M, Köhler A, Moroder L, Rubin DM, Huber R, Glickman MH, Finley D. A gated channel into the proteasome core particle. *Nat Struct Biol* (2000); 7(11): 1062-7.
5. Goldberg AL. Nobel committee tags ubiquitin for distinction. *Neuron* (2005); 45(3): 339-44.
6. Glickman MH, Ciechanover A. The ubiquitin-proteasome proteolytic pathway: destruction for the sake of construction. *Physiol Rev* (2002); 82(2): 373-428.
7. Benaroudj N, Zwickl P, Seemüller E, Baumeister W, Goldberg AL. ATP hydrolysis by the proteasome regulatory complex PAN serves multiple functions in protein degradation. *Mol Cell* (2003); 11(1): 69-78.
8. Schmidt M, Hanna J, Elsasser S, Finley D. Proteasome-associated proteins: regulation of a proteolytic machine. *Biol Chem* (2005); 386(8): 725-37.
9. Smith DM, Kafri G, Cheng Y, Ng D, Walz T, Goldberg AL. ATP binding to PAN or the 26S ATPases causes association with the 20S proteasome, gate opening, and translocation of unfolded proteins. *Mol Cell* (2005); 20(5): 687-98.
10. Kisselev AF, Akopian TN, Woo KM, Goldberg AL. The sizes of peptides generated from protein by mammalian 26 and 20 S proteasomes. Implications for understanding the degradative mechanism and antigen presentation. *J Biol Chem* (1999); 274(6): 3363-71.
11. Saric T, Graef CI, Goldberg AL. Pathway for degradation of peptides generated by proteasomes: a key role for thimet oligopeptidase and other metallopeptidases. *J Biol Chem* (2004); 279(45): 46723-32.
12. Orlowski RZ, Kuhn DJ. Proteasome inhibitors in cancer therapy: lessons from the first decade. *Clin Cancer Res* (2008); 14(6): 1649-57.
13. Glickman MH, Rubin DM, Coux O, Wefes I, Pfeifer G, Cjeka Z, Baumeister W, Fried VA, Finley D. A subcomplex of the proteasome regulatory particle required for ubiquitin-conjugate degradation and related to the COP9-signalosome and eIF3. *Cell* (1998); 94(5): 615-23.
14. Adams J. The proteasome: a suitable antineoplastic target. *Nat Rev Cancer* (2004); 4(5): 349-60.
15. Fisher RI, Bernstein SH, Kahl BS, Djulbegovic B, Robertson MJ, de Vos S, Epner E, Krishnan A, Leonard JP, Lonial S, Stadtmauer EA, O'Connor OA, Shi H, Boral AL, Goy A. Multicenter phase II study of bortezomib in patients with relapsed or refractory mantle cell lymphoma. *J Clin Oncol* (2006); 24(30): 4867-74.

16. Meister S, Schubert U, Neubert K, Herrmann K, Burger R, Gramatzki M, Hahn S, Schreiber S, Wilhelm S, Herrmann M, Jäck HM, Voll RE. Extensive immunoglobulin production sensitizes myeloma cells for proteasome inhibition. *Cancer Res* (2007); 67(4): 1783-92.

17. Dick LR, Fleming PE. Building on bortezomib: second-generation proteasome inhibitors as anti-cancer therapy. Drug Discov Today (2010); 15(5-6): 243-9.

18. Hanahan D, Weinberg RA. The hallmarks of cancer. *Cell* (2000); 100(1): 57-70.

19. Luqman S, Pezzuto JM. NFkappaB: a promising target for natural products in cancer chemoprevention. *Phytother Res* (2010); 24(7): 949-63

20. Li Q, Verma IM. NF-kappaB regulation in the immune system. *Nat Rev Immunol* (2002); 2(10): 725-34.

21. Yang H, Landis-Piwowar KR, Chen D, Milacic V, Dou QP. Natural compounds with proteasome inhibitory activity for cancer prevention and treatment. *Curr Protein Pept Sci* (2008); 9(3): 227-39.

22. Rock KL, Gramm C, Rothstein L, Clark K, Stein R, Dick L, Hwang D, Goldberg AL. Inhibitors of the proteasome block the degradation of most cell proteins and the generation of peptides presented on MHC class I molecules. *Cell* (1994); 78(5): 761-71.

23. Chen W, Lee J, Cho SY, Fine HA. Proteasome-mediated destruction of the cyclin a/cyclin-dependent kinase 2 complex suppresses tumor cell growth *in vitro* and *in vivo*. *Cancer Res* (2004); 64(11): 3949-57.

24. Blagosklonnyh MV. P53: an ubiquitous target of anticancer drugs. *Int J Cancer* (2002); 98: 161-66.

25. Li B, Dou QP. Bax degradation by the ubiquitin/proteasome-dependent pathway: involvement in tumor survival and progression. *Proc Natl Acad Sci U S A* (2000); 97(8): 3850-5.

26. Pagano M, Tam SW, Theodoras AM, Beer-Romero P, Del Sal G, Chau V, Yew PR, Draetta GF, Rolfe M. Role of the ubiquitin-proteasome pathway in regulating abundance of the cyclin-dependent kinase inhibitor p27. *Science* (1995); 269(5224): 682-5.

27. Sun J, Nam S, Lee CS, Li B, Coppola D, Hamilton AD, Dou QP, Sebti SM. CEP1612,a dipeptidyl proteasome inhibitor, induces p21WAF1 and p27KIP1 expression and apoptosis and inhibits the growth of the human lung adenocarcinoma A-549 in nude mice. *Cancer Res* (2001); 61(4): 1280-4.

28. Perkins ND. The Rel/NF-kappa B family: friend and foe. *Trends Biochem Sci* (2000); 25(9): 434-40.

29. Rastogi N, Mishra DP. Therapeutic targeting of cancer cell cycle using proteasome inhibitors. *Cell Div* (2012); 7(1): 26.

30. Diehl JA, Ponugoti B. Ubiquitin-dependent proteolysis in G1/S phase control and its relationship with tumor susceptibility. *Genes Cancer* (2010); 1(7): 717-724.

31. Masamha CP, Benbrook DM. Cyclin D1 degradation is sufficient to induce G1 cell cycle arrest despite constitutive expression of cyclin E2 in ovarian cancer cells. *Cancer Res* (2009); 69(16): 6565-72.

32. Harbour JW, Luo RX, Dei Santi A, Postigo AA, Dean DC. Cdk phosphorylation triggers sequential intramolecular interactions that progressively block Rb functions as cells move through G1. *Cell* (1999); 98(6): 859-69.

33. Abbas T, Dutta A. p21 in cancer: intricate networks and multiple activities. *Nat Rev Cancer* (2009); 9(6): 400-14.

34. Chu IM, Hengst L, Slingerland JM. The Cdk inhibitor p27 in human cancer: prognostic potential and relevance to anticancer therapy. Nat Rev *Cancer* (2008); 8(4): 253-67.

35. Sterz J, Jakob C, Kuckelkorn U, Heider U, Mieth M, Kleeberg L, Kaiser M, Kloetzel PM, Sezer O, von Metzler I. BSc2118 is a novel proteasome inhibitor with activity against multiple myeloma. *Eur J Haematol* (2010); 85(2): 99-107.

36. Mi L, Gan N, Chung FL. Isothiocyanates inhibit proteasome activity and proliferation of multiple myeloma cells. *Carcinogenesis* (2011); 32(2): 216-23.

37. Huang H, Liu N, Zhao K, Zhu C, Lu X, Li S, Lian W, Zhou P, Dong X, Zhao C, Guo H, Zhang C, Yang C, Wen G, Lu L, Li X, Guan L, Liu C, Wang X, Dou QP, Liu J. Sanggenon C decreases tumor cell viability associated with proteasome inhibition. *Front Biosci* (Elite Ed) (2011); 3: 1315-25.

38. Bavi P, Uddin S, Ahmed M, Jehan Z, Bu R, Abubaker J, Sultana M, Al-Sanea N, Abduljabbar A, Ashari LH, Alhomoud S, Al-Dayel F, Prabhakaran S, Hussain AR, Al-Kuraya KS. Bortezomib stabilizes mitotic cyclins and prevents cell cycle progression via inhibition of UBE2C in colorectal carcinoma. *Am J Pathol* (2011); 178(5): 2109-20.

39. McConkey DJ, Zhu K. Mechanisms of proteasome inhibitor action and resistance in cancer. *Drug Resist Updat* (2008); 11(4-5): 164-79.

40. Fridman JS, Lowe SW. Control of apoptosis by p53. *Oncogene* (2003); 22(56): 9030-40.

41. el-Deiry WS. Regulation of p53 downstream genes. *Semin Cancer Biol* (1998); 8(5): 345-57.

42. Yu J, Wang Z, Kinzler KW, Vogelstein B, Zhang L. PUMA mediates the apoptotic response to p53 in colorectal cancer cells. *Proc Natl Acad Sci U S A* (2003); 100(4): 1931-6.

43. Sax JK, El-Deiry WS. p53 downstream targets and chemosensitivity. *Cell Death Differ* (2003); 10(4): 413-7.

44. Oda E, Ohki R, Murasawa H, Nemoto J, Shibue T, Yamashita T, Tokino T, Taniguchi T, Tanaka N. Noxa, a BH3-only member of the Bcl-2 family and candidate mediator of p53-induced apoptosis. *Science* (2000); 288(5468): 1053-8.

45. Sax JK, Fei P, Murphy ME, Bernhard E, Korsmeyer SJ, El-Deiry WS. BID regulation by p53 contributes to chemosensitivity. *Nat Cell Biol* (2002); 4(11): 842-9.

46. Ling YH, Liebes L, Zou Y, Perez-Soler R. Reactive oxygen species generation and mitochondrial dysfunction in the apoptotic response to Bortezomib, a novel proteasome inhibitor, in human H460 non-small cell lung cancer cells. *J Biol Chem* (2003); 278(36): 33714-23.

47. Demasi M, Davies KJ. Proteasome inhibitors induce intracellular protein aggregation and cell death by an oxygen-dependent mechanism. *FEBS Lett* (2003); 542(1-3): 89-94.

48. Davies KJ. Oxidative stress: the paradox of aerobic life. *Biochem Soc Symp* (1995); 61: 1-31.

49. Sedelnikova OA, Redon CE, Dickey JS, Nakamura AJ, Georgakilas AG, Bonner WM. Role of oxidatively induced DNA lesions in human pathogenesis. *Mutat Res* (2010); 704(1-3): 152-9.

50. Adibhatla RM, Hatcher JF. Lipid oxidation and peroxidation in CNS health and disease: from molecular mechanisms to therapeutic opportunities. *Antioxid Redox Signal* (2010); 12(1): 125-69.

51. Bochkov VN, Oskolkova OV, Birukov KG, Levonen AL, Binder CJ, Stöckl J.Generation and biological activities of oxidized phospholipids. *Antioxid Redox Signal* (2010); 12(8): 1009-59.

52. Goldberg AL. Protein degradation and protection against misfolded or damaged proteins. *Nature* (2003); 426(6968): 895-9.

53. Pérez-Galán P, Roué G, Villamor N, Montserrat E, Campo E, Colomer D. The proteasome inhibitor bortezomib induces apoptosis in mantle-cell lymphoma through generation of ROS and Noxa activation independent of p53 status. *Blood* (2006); 107(1): 257-64.

54. Moore HE, Davenport EL, Smith EM, Muralikrishnan S, Dunlop AS, Walker BA, Krige D, Drummond AH, Hooftman L, Morgan GJ, Davies FE. Aminopeptidase inhibition as a targeted treatment strategy in myeloma. *Mol Cancer Ther* (2009); 8(4): 762-70.

55. Polgár L. The prolyl oligopeptidase family. *Cell Mol Life Sci* (2002); 59(2): 349-62.

56. Jones WM, Scaloni A, Manning JM. Acylaminoacyl-peptidase. Methods *Enzymol* (1994); 244: 227-31.

57. Polevoda B, Sherman F. The diversity of acetylated proteins. *Genome Biol* (2002); 3(5): reviews0006.

58. Perrier J, Durand A, Giardina T, Puigserver A. Catabolism of intracellular N-terminal acetylated proteins: involvement of acylpeptide hydrolase and acylase. *Biochimie* (2005); 87(8): 673-85.

59. Sharma KK, Ortwerth BJ. Bovine lens acylpeptide hydrolase. Purification and characterization of a tetrameric enzyme resistant to urea denaturation and proteolytic inactivation. *Eur J Biochem* (1993); 216(2): 631-7.

60. Gogliettino M, Balestrieri M, Cocca E, Mucerino S, Rossi M, Petrillo M, Mazzella E, Palmieri G. Identification and characterisation of a novel acylpeptide hydrolase from

Sulfolobus solfataricus: structural and functional insights. *PLoS One* (2012); 7(5): e37921.

61. Bartlam M, Wang G, Yang H, Gao R, Zhao X, Xie G, Cao S, Feng Y, Rao Z. Crystal structure of an acylpeptide hydrolase/esterase from *Aeropyrum pernix* K1. *Structure* (2004); 12(8): 1481-8.

62. Brunialti EA, Gatti-Lafranconi P, Lotti M. Promiscuity, stability and cold adaptation of a newly isolated acylaminoacyl peptidase. *Biochimie* (2011); 93(9): 1543-54.

63. Nakai A, Yamauchi Y, Sumi S, Tanaka K. Role of acylamino acid-releasing enzyme/oxidized protein hydrolase in sustaining homeostasis of the cytoplasmic antioxidative system. *Planta* (2012); 236(2): 427-36.

64. Palmieri G, Langella E, Gogliettino M, Saviano M, Pocsfalvi G, Rossi M. A novel class of protease targets of phosphatidylethanolamine-binding proteins (PEBP): a study of the acylpeptide hydrolase and the PEBP inhibitor from the archaeon *Sulfolobus solfataricus*. *Mol Biosyst* (2010); 6(12): 2498-507.

65. Cleynen I, Jüni P, Bekkering GE, Nüesch E, Mendes CT, Schmied S, Wyder S, Kellen E, Villiger PM, Rutgeerts P, Vermeire S, Lottaz D. Genetic evidence supporting the association of protease and protease inhibitor genes with inflammatory bowel disease: a systematic review. *PLoS One* (2011); 6(9): e24106.

66. Nguyen KT, Pei D. Purification and characterization of enzymes involved in the degradation of chemotactic N-formyl peptides. *Biochemistry* (2005); 44(23): 8514-22.

67. Chadwick VS, Mellor DM, Myers DB, Selden AC, Keshavarzian A, Broom MF, Hobson CH. Production of peptides inducing chemotaxis and lysosomal enzyme release in human neutrophils by intestinal bacteria in vitro and in vivo. *Scand J Gastroenterol* (1988); 23(1): 121-8.

68. Hobson CH, Roberts EC, Broom MF, Mellor DM, Sherriff RM, Chadwick VS. Radio-immunoassay for formyl methionyl leucyl phenylalanine. I. Development and application to assessment of chemotactic peptide production by enteric bacteria. *J Gastroenterol Hepatol* (1990) ; 5(1): 32-7.

69. Fujino T, Watanabe K, Beppu M, Kikugawa K, Yasuda H. Identification of oxidized protein hydrolase of human erythrocytes as acylpeptide hydrolase. *Biochim Biophys Acta* (2000); 1478(1): 102-12.

70. Shimizu K, Kiuchi Y, Ando K, Hayakawa M, Kikugawa K. Coordination of oxidized protein hydrolase and the proteasome in the clearance of cytotoxic denatured proteins. *Biochem Biophys Res Commun* (2004); 324(1): 140-6.

71. Merker K, Grune T. Proteolysis of oxidised proteins and cellular senescence. *Exp Gerontol* (2000); 35(6-7): 779-86.

72. Fujino T, Tada T, Beppu M, Kikugawa K. Purification and characterization of a serine protease in erythrocyte cytosol that is adherent to oxidized membranes and preferentially degrades proteins modified by oxidation and glycation. *J Biochem* (1998); 124(6): 1077-85.

73. Fujino T, Kojima M, Beppu M, Kikugawa K, Yasuda H, Takahashi K. Identification of the cleavage sites of oxidized protein that are susceptible to oxidized protein

hydrolase (OPH) in the primary and tertiary structures of the protein. *J Biochem* (2000); 127(6): 1087-93.

74. Shimizu K, Ikegami-Kawai M, Takahashi T. Increased oxidized protein hydrolase activity in serum and urine of diabetic rat models. *Biol Pharm Bull* (2009); 32(9): 1632-5.

75. Bulteau AL, Verbeke P, Petropoulos I, Chaffotte AF, Friguet B. Proteasome inhibition in glyoxal-treated fibroblasts and resistance of glycated glucose-6-phosphate dehydrogenase to 20 S proteasome degradation in vitro. *J Biol Chem* (2001); 276(49): 45662-8.

76. Portero-Otín M, Pamplona R, Ruiz MC, Cabiscol E, Prat J, Bellmunt MJ. Diabetes induces an impairment in the proteolytic activity against oxidized proteins and a heterogeneous effect in nonenzymatic protein modifications in the cytosol of rat liver and kidney. *Diabetes* (1999); 48(11): 2215-20.

77. Jones WM, Scaloni A, Bossa F, Popowicz AM, Schneewind O, Manning JM. Genetic relationship between acylpeptide hydrolase and acylase, two hydrolytic enzymes with similar binding but different catalytic specificities. *Proc Natl Acad Sci U S A* (1991); 88(6): 2194-8.

78. Naylor SL, Marshall A, Hensel C, Martinez PF, Holley B, Sakaguchi AY. The DNF15S2 locus at 3p21 is transcribed in normal lung and small cell lung cancer. *Genomics* (1989); 4(3): 355-61.

79. Erlandsson R, Boldog F, Persson B, Zabarovsky ER, Allikmets RL, Sümegi J, Klein G, Jörnvall H. The gene from the short arm of chromosome 3, at D3F15S2, frequently deleted in renal cell carcinoma, encodes acylpeptide hydrolase. *Oncogene* (1991); 6(7): 1293-5.

80. Scaloni A, Jones W, Pospischil M, Sassa S, Schneewind O, Popowicz AM, Bossa F, Graziano SL, Manning JM. Deficiency of acylpeptide hydrolase in small-cell lung carcinoma cell lines. *J Lab Clin Med* (1992); 120(4): 546-52.

81. Yamaguchi M, Kambayashi D, Toda J, Sano T, Toyoshima S, Hojo H. Acetylleucine chloromethyl ketone, an inhibitor of acylpeptide hydrolase, induces apoptosis of U937 cells. *Biochem Biophys Res Commun* (1999); 263(1): 139-42.

82. López-Granero C, Cardona D, Giménez E, Lozano R, Barril J, Aschner M, Sánchez-Santed F, Cañadas F. Comparative study on short- and long-term behavioral consequences of organophosphate exposure: relationship to AChE mRNA expression. *Neurotoxicology* (2014); 40: 57-64.

83. Palmieri G, Catara G, Saviano M, Langella E, Gogliettino M, Rossi M. First Archaeal PEPB-Serine Protease Inhibitor from Sulfolobus solfataricus with Noncanonical Amino Acid Sequence in the Reactive-Site Loop. *J Proteome Res* (2009); 8(1): 327-34.

84. Busse A, Kraus M, Na IK, Rietz A, Scheibenbogen C, Driessen C, Blau IW, Thiel E, Keilholz U. Sensitivity of tumor cells to proteasome inhibitors is associated with expression levels and composition of proteasome subunits. *Cancer* (2008); 112(3): 659-70.

85. Jensen TJ, Loo MA, Pind S, Williams DB, Goldberg AL, Riordan JR. Multiple proteolytic systems, including the proteasome, contribute to CFTR processing. *Cell* (1995); 83(1): 129-35.

86. Wertz IE, Dixit VM. Signaling to NF-kappaB: regulation by ubiquitination. Cold Spring Harb Perspect Biol (2010); 2(3): a003350.

87. Bloom J, Amador V, Bartolini F, DeMartino G, Pagano M. Proteasome-mediated degradation of p21 via N-terminal ubiquitinylation. *Cell* (2003); 115(1): 71-82.

88. Shimizu K, Fujino T, Ando K, Hayakawa M, Yasuda H, Kikugawa K.. Overexpression of oxidized protein hydrolase protect COS-7 cells from oxidative stress-induced inhibition of cell growth and survival. *Biochem Biophys Res Commun* (2003); 304: 766–771.

89. Hideshima T, Mitsiades C, Akiyama M, Hayashi T, Chauhan D, Richardson P, Schlossman R, Podar K, Munshi NC, Mitsiades N, Anderson KC. Molecular mechanisms mediating antimyeloma activity of proteasome inhibitor PS-341. *Blood* (2003); 101(4): 1530-4.

90. Mathew R, White E. Why sick cells produce tumors: the protective role of autophagy. *Autophagy* (2007); 3: 502–5.

91. Shintani T, Klionsky DJ. Autophagy in health and disease: a double edged sword. *Science* (2004); 306: 990–5.

92. Ge PF, Zhang JZ, Wang XF, Meng FK, Li WC, Luan YX, Ling F, Luo YN. Inhibition of autophagy induced by proteasome inhibition increases cell death in human SHG-44 glioma cells. *Acta Pharmacol Sin* (2009); 30(7): 1046-52.

93. Mizushima N. Autophagy: process and function. *Genes Dev* (2007); 21(22): 2861-73.

94. Ward CL, Omura S, Kopito RR Degradation of CFTR by the ubiquitinproteasome pathway. *Cell* (1995); 83: 121–127.

95. McGoldrick CA, Jiang YL, Paromov V, Brannon M, Krishnan K, Stone WL. Identification of oxidized protein hydrolase as a potential prodrug target in prostate cancer. *BMC Cancer* (2014); 14: 77.

96. Nencioni A, Gru¨nebach F, Patrone F, Ballestrero A, Brossart P. Proteasome inhibitors: antitumor effects and beyond. *Leukemia* (2007); 21: 30–36.

97. Arnesen T, Van Damme P, Polevoda B, Helsens K, Evjenth R, Colaert N, Varhaug JE, Vandekerckhove J, Lillehaug JR, Sherman F, Gevaert K. Proteomics analyses reveal the evolutionary conservation and divergence of Nterminal acetyltransferases from yeast and humans. *Proc Natl Acad Sci U S A* (2009); 106: 8157–8162.

98. Kouzarides T. Acetylation: a regulatory modification to rival phosphorylation? *EMBO J* (2000); 19: 1176–1179.

99. Hwang CS, Shemorry A, Varshavsky A. N-terminal acetylation of cellular proteins creates specific degradation signals. *Science* (2010); 327: 973–977.

Chapter 2

5. Introduction

5.1 Conjugated linoleic acid

In the last decade, conjugated linoleic acid (CLA) has been studied intensively because of its unusual biological activities [**1**]. Conjugated LA was discovered quite accidentally when Pariza and Hargraves [**2**] were investigating the carcinogenic properties of grilled beef. To their surprise, the fatty acids present in grilled beef exhibited anticarcinogenic rather than procarcinogenic properties. CLA is a mixture of geometric and positional isomers of linoleic acid (18;2 n-6 or 9,12-cis,cis-octadecadienoic acid, LA) in which the double bonds are conjugated, instead of being in the typical methylene interrupted configuration [**3**]. They are found naturally in ruminant food products such as beef, lamb and dairy because of the process of bacterial biohydrogenation of LA in the rumen [**4-6**]. During the biohydrogenation of linoleic acid to stearic acid, CLA is synthesized as an intermediate by gram-negative bacteria, *Butyrivibrio fibrisolvens* [**7**]. Although 28 different CLA isomers are found in natural food, the major isomer is the cis9-trans11- (c9,t11)-CLA accounting for more than 90% CLA intake in the diet [**8**]. CLA isomers can be prepared commercially by heating LA under alkaline conditions or by partial hydrogenation of LA [**9**]. Health benefits of CLA have been attributed to mainly two of its isomers: c9,t11-CLA and trans10-cis12 (t10,c12)-CLA, which are contained in equal levels (approximately 40–45%) in the mostly common used CLA. Structures of the parent LA, c9,t11- and t10,c12-CLA isomers are shown in **Figure 29**.

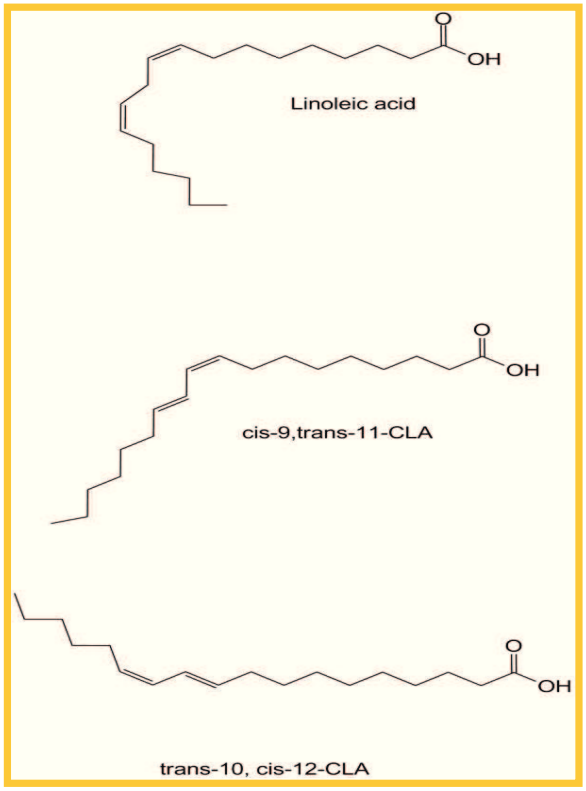

Figure 29. *Chemical structures of linoleic acid and isomers of conjugated acid (CLA)*

In recent years, with the advent of technology, enriched of purified c9,t11-CLA and t10,c12-CLA preparations have become commercially available, leading to studies examining the effects of these individual isomers in health-related disorders using animal models and cell cultures. Most of the studies have used CLA isomer mix, but recent evidence suggests that c9,t11-CLA and t10,c12-CLA may have myriad effects in different biological systems, which often may be similar or opposite. Specifically, CLAs have been shown to have antiadipogenic [**1**], anticarcinogenic [**10**], antiatherogenic [**11**], antidiabetogenic [**12**] and anti-inflammatory properties [**13**] (**Table 2**).

Anti-carcinogenic effects	• Growth Inhibition • Metastasis reduction • Antiproliferative effect • Inhibition angiogenesis • Induction of apoptosis
Anti-adipogenic effects	• Reducing lipid accumulation • Reduction of fat mass • Increasing adipocyte apoptosis
Anti-inflammatory effects	• Antiinflammatory cytokines inhibition • Antiinflammatory ecoisanoid inhibition

Table 2. Biological effects of CLAs in health

5.2 Biological activities of CLA

The biological role of CLA and its purified isomers (c9,t11 and t10,c12) in different models of health-related disorders in cell culture, animals and clinical studies are summarized below [**14, 15**]:

- ***Body fat reduction by CLA***

One aspect of CLA that has drawn much attention is its ability to reduce body fat in animals, first reported in 1995 [**16**]. The availability of purified isomers or CLA enriched in either c9,t11-CLA or t10,c12-CLA isomers prompted new *in vivo* and *in vitro* studies, which identified t10,c12-CLA isomer to be primarily involved in reduction of fat mass, and not the c9,t11-CLA isomer [**17**]. CLA's effect on body fat reduction is suggested to be the result of multiple mechanisms: increasing energy expenditure, reducing lipid accumulation in adipose tissues and/or adipocytes differentiation, increasing adipocyte apoptosis and increasing fatty acid β-oxidation in skeletal muscle [**17**].

- ***Prevention of cardiovascular diseases***

CLA has been reported to reduce atherosclerotic lesions in rabbits and hamsters [**18**]. CLA decreases total cholesterol, triacylglycerides (TG), LDL-cholesterol and increased HDL-cholesterol in a number of animal models [**14**]. CLA affects these parameters through involvement of peroxisome proliferator-activated receptor (PPAR, key for lipogenesis), sterol regulatory element-binding proteins (SREBPs, key for fatty acid synthesis and elongation),

and/or steroyl-CoA desaturase (SCD, key for TG and cholesterol formation) [**14, 19**]. Peroxisome proliferator-activated receptors are ligand-activated nuclear receptors regulating the expression of genes that control lipid and glucose homeostasis, thus modulating the major metabolic disorders predisposing to atherosclerosis [**20**]. Studies with pure isomers suggest that c9,t11-CLA isomer is more effective than t10,c12-CLA isomer in controlling key modulators of lipid metabolism [**21**]. Sterol regulatory element-binding protein 1 isoforms regulate fatty acid and TG synthesis [**22**]. Studies suggest that c9,t11-CLA isomer positively influences lipid metabolism by reduced synthesis and cleavage of hepatic SREBP-1, which in turn is regulated by hepatic LXRa expression [**23**].

Hypertension is also a common pathological state associated with an increased risk of cardiovascular diseases. Nagao et al. have consistently shown that CLA or the t10,c12-CLA isomer decreases blood pressure and hypertension in various rat models prone to develop obesity, diabetes and obesity together, or hypertension [**24**].

- ***Inflammatory response and CLA***

Anti-inflammatory properties of CLA have been reported by reducing inflammation, and modulating the production of cytokines, prostaglandins, and leukotrien B4 [**14, 25, 26**]. However, Poirier *et al*. (2006) reported that the t10,c12-CLA isomer induced inflammatory responses in white adipose tissue [**27**]. Proinflammatory cytokines (TNF-α, IL-β, IL-1, etc.), anti-inflammatory cytokines [IL-10, interferon-γ (IFN-γ), etc.], eicosanoids (prostaglandins, leukotrienes) and nitric oxide (NO) are key inflammatory mediators that are regulated by dietary intake of polyunsaturated fatty acids (PUFA) including ω-6 and ω-3 fatty acids. Specifically, CLA decreases production of inflammatory mediators like prostaglandin PGE2, TNF-α, IL-1β, IL-6 and NO.

- **Anticancer effects by CLA**

CLA has been shown to reduce cancer in a number of animal models, such as skin, colon, mammary, and liver [**14**, **28**]. It has been suggested that CLA not only decreases initiation, promotion, and progression steps of cancer development, but also reduces metastasis of cancer [**14, 28**]. Mechanisms of inhibition of carcinogenesis may include antiproliferative effects, alterations in the components of the cell cycle and induction of apoptosis as well as inhibition of angiogenesis [**28, 29-31**].

Recent work by Ip and colleagues [**32**] demonstrated that CLA reduces the expression of cyclins A and D, that regulate the conversion of G1→S phase of the cell cycle. In addition, diets with CLA moderately increased levels of p16 and p27 cdk inhibitors. CLA feeding is also shown to up-regulate the expression of p53 [**33**], the protein product of a tumor suppressor gene that is frequently mutated in many tumor cells [**34**]. p53 is involved in monitoring the quality of DNA after G1 phase and, if DNA is damaged, will block entry of the cell into S phase by altering the expression of genes involved in growth arrest and promotion [**35**]. Together, these data suggest that CLA could reduce tumor cell proliferation by modifying cell cycle proteins that regulate this process. In addition, dietary CLA induces apoptosis in numerous tissues but the exact mechanism is not established. Specifically, it has been reported that CLA can decrease expression of *bcl-2*, a gene involved in suppression of apoptosis [**36**] and interfere with redox homeostasis inducing ROS formation [**37**]. Moreover, there is evidence in animal studies that fatty acids can decrease protein degradation through the inhibition of proteasome activity, although the exact mechanism is not known [**38**]. Of note, in several studies the prooxidant activity of CLA was associated to its pro-apoptotic effects on cancer cells [**39**] and to the modulatory ability of proteasomal chymotrypsin-like (CT-like) activity.

Potential ways in which CLA could influence tumor cell growth is shown in **Figure 30**.

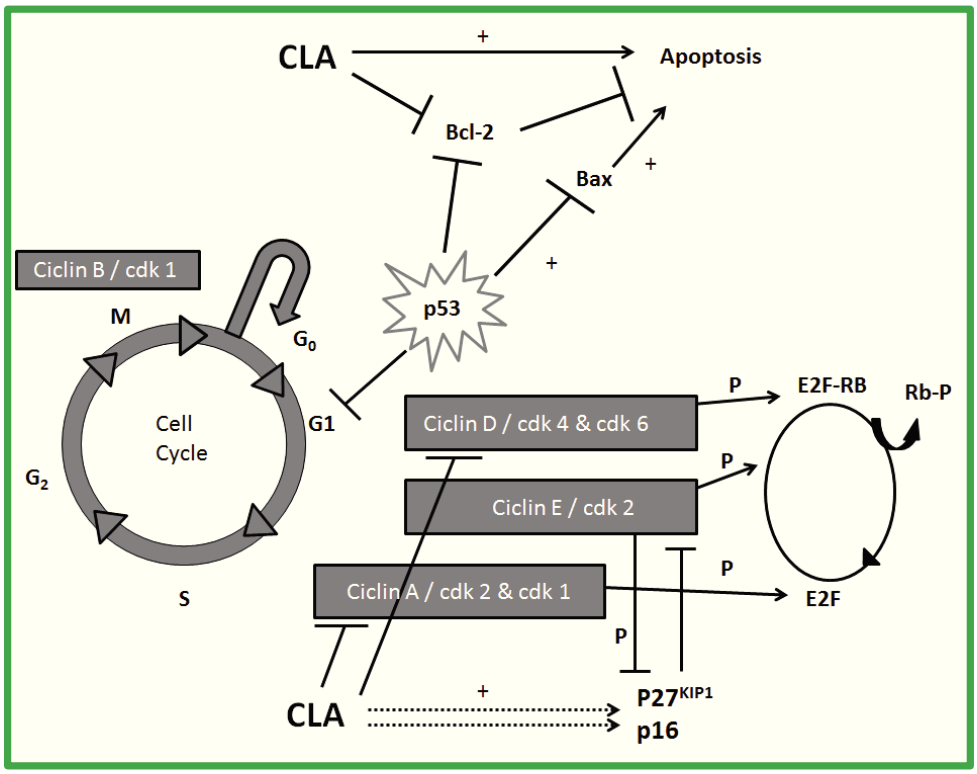

Figure 30. ***Schematic diagram of how CLA may modulate the cell cycle and apoptosis.***

6. Results

6.1 t10,c12-, t9,t11- and c9,t11-CLA isomers differentially inhibit APEH and proteasome

Recent studies have suggested that some fatty acids are able to disrupt the chymotrypsin (CT)-like proteasome activity. Among these, the two major isomers of conjugated linoleic acid (CLA), cis9-trans11 CLA (c9,t11-CLA) and trans10-cis12 CLA (t10,c12-CLA), have shown pro-apoptotic activities in a number of cancer cell lines [**40**] and strong anticancer effects in numerous animal models [**15**]. Interestingly, although the mechanisms are yet poorly understood, their ability to inhibit the proteasome activity *in vitro* [**38**] suggests that this complex enzyme could be their ultimate target. On this background, we have investigated the molecular mechanisms that underlie the interrelationship between APEH and the proteasome, and their eventual regulation by natural compounds including the CLA isomers.

A preliminary investigation of the potential inhibitory effect of CLA isomers on chymotrypsin-like (CT-like) activity of 20S proteasome isoform was carried out. Inhibition analyses were performed by pre-incubating the purified enzyme with increasing amounts of each compound and their half-maximal inhibitory concentrations (IC50) were determined. The curves followed a hyperbolic pattern reaching 100% inhibition with all CLA isomers tested (**Figure 31A-C**), althought t10,c12- and c9,t11-CLA were the best effectors (IC50=14.8±2.0 μM and 31.2±8.8 μM on 20S isoform, respectively). Similar experiments were carried out by using the proteasome inhibitor bortezomib (BTZ) (**Figure 31D**) because of its recognized anti-proliferative activity on cancer cells. As expected, BTZ appeared to target 20S isoform (IC50=1.4±0.3 nM), reaching about 60% of inhibition, while octanoic acid (data not shown), used as a negative control, gave only negligible effects. Next, before to investigate the possible mechanisms underlying the CLA-reduced viability of cancer cells, the potential contribution of APEH was explored. When the ability of these compounds to modulate porcine APEH ($APEH_{pl}$) in cell-free assays was evaluated (**Figure 31E**), only t10,c12-CLA was revealed to affect the enzyme activity in a dose-dependent manner, reaching a maximum inhibition of about 41% (IC50=110.1±11.7 μM), whilst c9t11-CLA was ineffective. In addition the Ki of t10c12- CLA towards $APEH_{pl}$ was 140±20 μM and the Lineweaver-Burk plot revealed a non–competitive inhibition mechanism. Indeed, in the presence of increasing amounts of t10c12-CLA isomer, only the Vmax of $APEH_{pl}$ was affected (**Figure 31F**).

This is the first evidence of a direct inhibition of APEH by a CLA isomer. Moreover, a stereoselective binding in the interaction with APEH and proteasome isoform of the CLA isomers can be proposed together with a specific ability of t10,c12-CLA to inhibit all these enzymes.

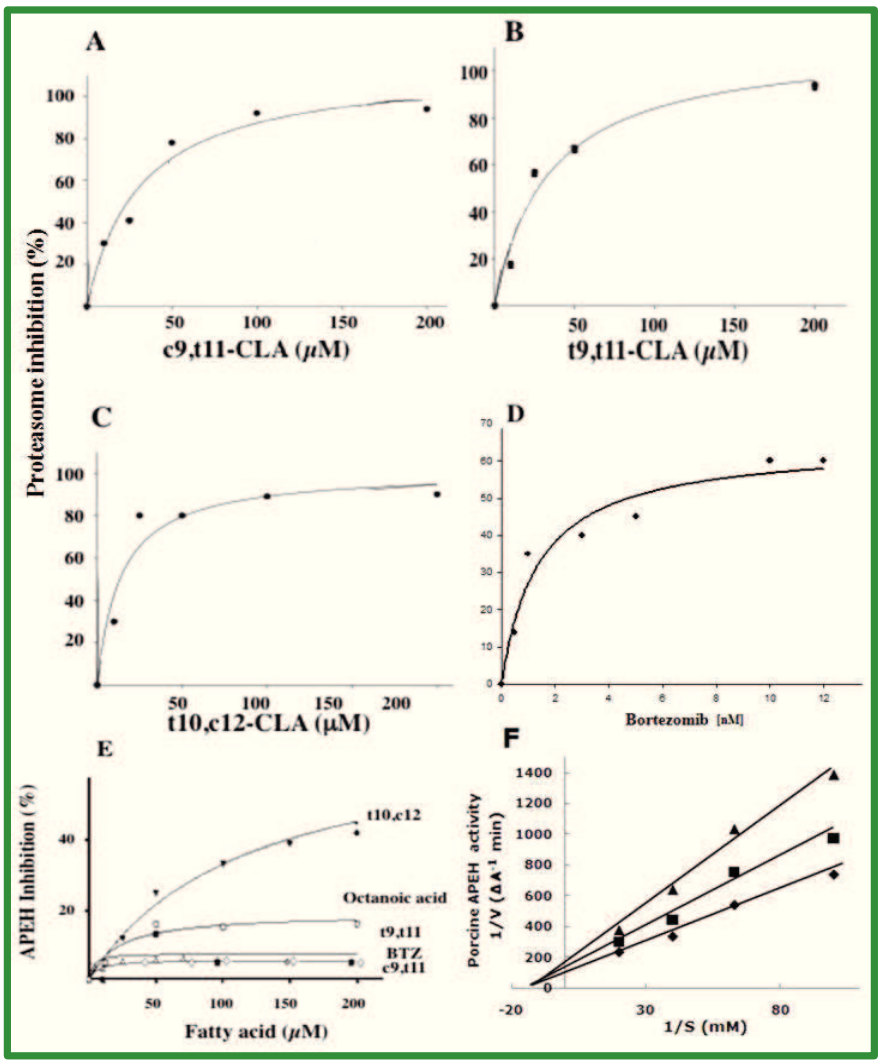

Figure 31. CLA isomers exhibit dissimilar inhibitory ability towards chymotrypsin-like (CT-like) proteasome and APEH activities. *The inhibitory effect of different CLA isomers, namely c9,t11- (**A**), t9,t11- (**B**), t10,c12-CLA (**C**), bortezomib, BTZ (**D**), was evaluated on commercially available pure 20S (black circles) proteasome. The synthetic fluorescent substrate N-Suc-LLVT-AMC (0.080 mM) was used for the measurement of the CT-like activity*

*of the proteasome. The hyperbolic curves indicate the best fits for the data obtained, with IC50 values calculated from the graphs by SigmaPlot 10.0 software. Mixtures treated with DMSO alone were used as blank. The dose-dependent inhibitory effect of c9,t11-, t9,t11-, t10,c12-CLA isomers, octanoic acid or bortezomib on APEH activity was shown (**E**). Inhibition kinetic by increasing t10c12-CLA concentrations: 50 µM (squares) and 100 µM (triangles) (**F**). Enzyme incubated without inhibitors were used as control (diamonds). The inhibition constants, Ki, was determined by the Lineweaver–Burk equation for non-competitive inhibition. Results are presented as the mean ± standard deviation (SD) of triplicate analyses from three independent experiments. SD values lower than 5% were not shown.*

6.2 Cancer cell proliferation is significantly inhibited and associates with caspase 3 activation in melanoma cells exposed to t10,c12-CLA

In evaluating the involvement of APEH and proteasome in the anti-cancer activity of CLA isomers, the growth inhibitory effects were estimated up to 48 h exposure in cell lines belonging to Group I and Group II (**Figure 10-Chapter I**), at two different concentrations (50 and 100 µM). Data shown in **Figure 32** refer to four Group I-cell lines (A375, A375M, Caco-2 and HepG2) and four Group II-cell lines (MDA-MB, Hela, U87 and MCF7), which were chosen for comparative analyses. It is worth to note that the results obtained with all the other Goup I-cell lines (**Figure 10-Chapter I**) did not show any variation in cell viability upon treatments and, therefore, they were not considered for further investigations. Interestingly, the most marked anti-proliferative effect was observed following exposure with t10,c12-CLA on A375 (63%) (**Figure 32B**). A375 cell viability was also greatly influenced by t9,t11-CLA (about 50%) (**Figure 32C**), whereas no significant results were obtained on all cancer cells by octanoic acid (up to 200 µM) treatment, which was used as a negative control (data not shown). To assess if the cytotoxicity was associated to the anti-proliferative events observed on the cancer cells considered, LDH activity was measured in spent media following 24 h exposure to 200 µM c9,t11-, t10,c12-CLA (the most abundant CLA isomers) or to 10 nM BTZ, using octanoic acid as negative control. As expected, substantial cell death resulted from BTZ supplementation while the LDH activity in cultures exposed to CLA isomers was comparable to that of control (**Figure 33A**). Moreover, to examine the contribution of an apoptotic event in CLA-induced decline of cancer cells viability, caspase 3 activation was measured. Unespectedly, results revealed that while caspase 3 activation varied slightly between the different tumor cell lines upon exposure with c9,t11-CLA, a more marked variation was observed by t10,c12-CLA treatment (**Figure 33B**), leading to inversely

correlated measures of cell viability and caspase 3 activation (r^2=0.78; P<0.01) (**Figure 33C**). It's worth to note that, although CLA reduced cell viability in the considered cell lines with no cytotoxicity (LDH release), nevertheless its pro-apoptotic activity couldn't be accounted for the observed cell death, therefore a cytostatic effect cannot be excluded. In addition, proteasome activity was differently downregulated by CLA isomers (data not shown) but it was not significantly correlated with cell viability decrease (r^2=0.046; data not shown), suggesting that proteasome inhibition alone was not liable for the observed anti-proliferative activity of CLAs. Hence, it appears reasonable to hypothesize that an enzyme machinery, such as APEH/proteasome system, could be involved in the marked anti-proliferative and pro-apoptotic activity exerted by t10,c12-CLA through its specific capacity to downregulate both enzymes in cell free assays (**Figure 31**).

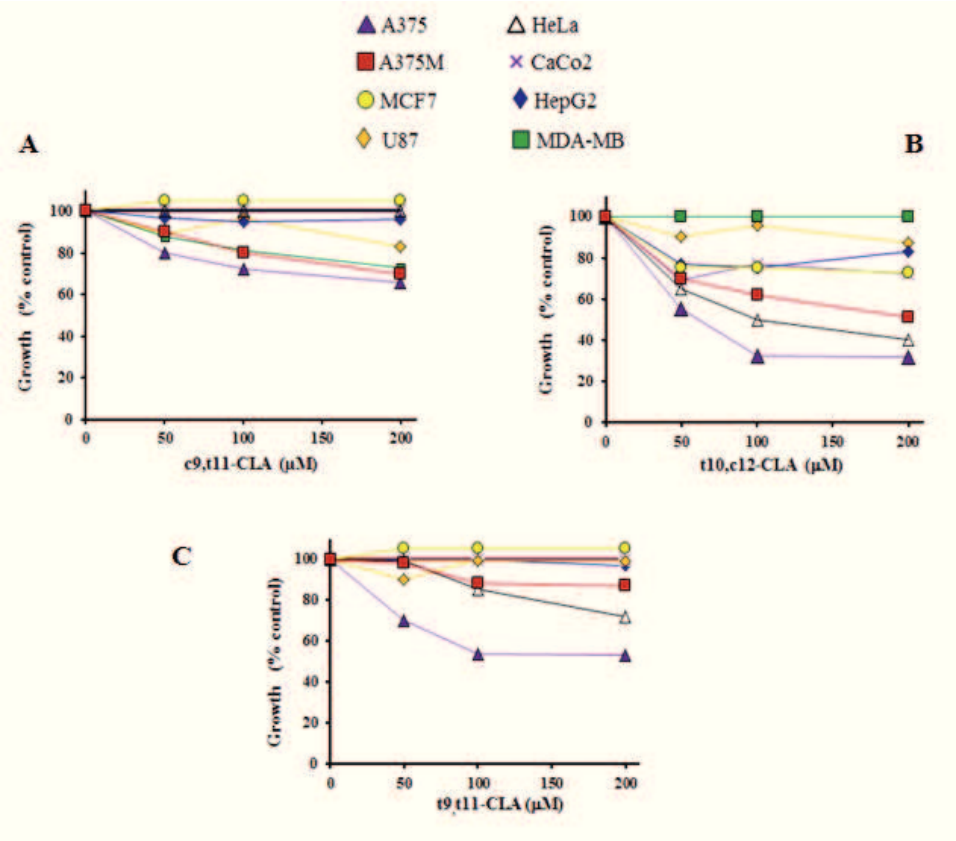

Figure 32. Human cancer cells exhibit differential sensitivity to the anti-proliferative activity of CLA isomers*. The effects of c9,t11 (**A**), t10,c12- (**B**) or t9,t11-CLA isomers (**C**) on cell viability were assessed in eight cancer cell lines exposed for 24 h to increasing concentrations of the CLA isomers. Data are expressed as means ±SD values of triplicate data from three independent experiments. SD values lower than 5% were not shown.*

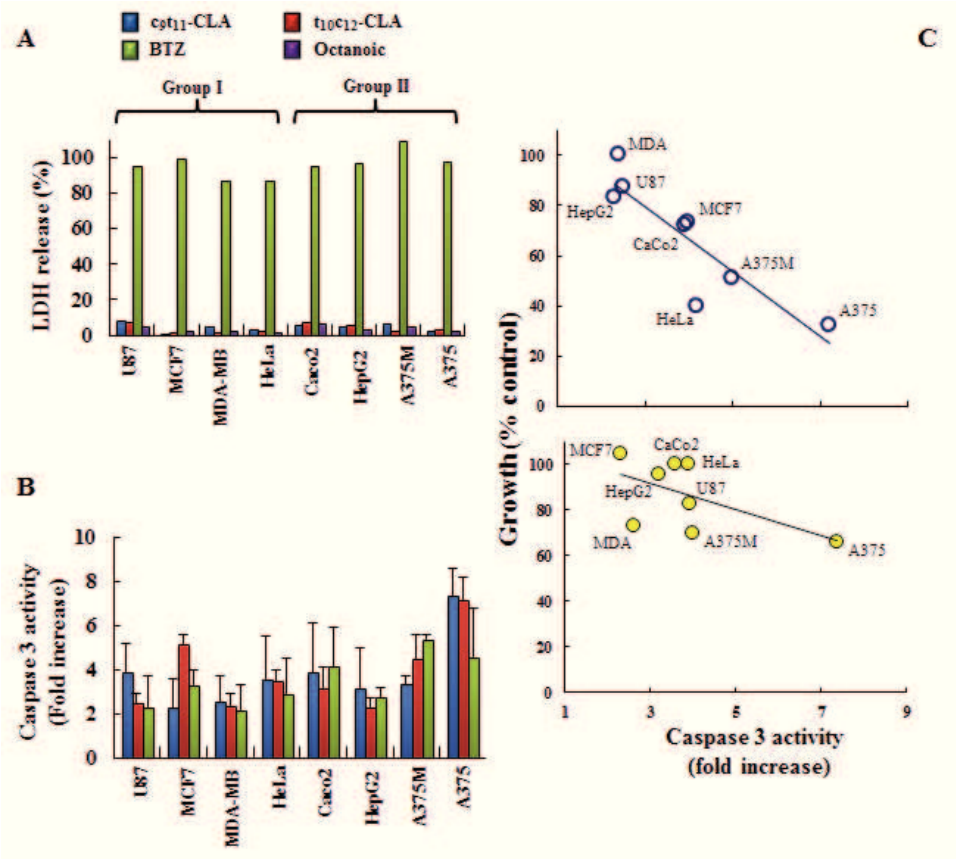

Figure 33. Anti-proliferative ability of t10,c12-CLA correlates with caspase 3 activation. *LDH release (**A**) and caspase 3 activity (**B**) were measured to study the cytotoxic and pro-apoptotic ability of 200 μM of t10,c12- (red bars) or c9,t11-CLA (light blue bars). Cell cultures exposed to octanoic acid (200 μM, violet bars) or to BTZ (10 nM, green bars) were used as negative or positive controls, respectively. Average caspase 3 activity values (fold increase) in cancer cells exposed for 24 h to 200 μM t10,c12- (**C upper panel**) or to c9,t11-CLA (**C lower panel**) were plotted against cell viability (%).*

6.3 t10,c12-CLA decreases glutathione level and APEH/proteasome activity in A375 cells triggering apoptosis in a dose-dependent fashion

On the basis of the marked cell viability reduction (**Figure 32B**) induced by t10,c12-CLA on A375 melanoma cell line, we decided to use this model system for investigations on the different cellular factors (redox status, caspase 3, APEH and proteasome) involved in the apoptotic pathway. In order to define the dose accountable for 50% decrease of cell viability (IC50), A375 cells were exposed for 24 h to a concentration range of t10,c12-CLA or BTZ (from 10 nM to 400 μM), using human fibroblasts as control. The resulting isobologram revealed that the IC50 values were 1.0±0.02 μM or 10.0±0.02 nM for t10,c12-CLA or BTZ,

respectively. Moreover, proliferation data obtained from fibroblasts, even at higher concentration of t10,c12-CLA, further supported the lack of toxic effects (**Figure 34A**). Next, cultures were incubated with increasing t10,c12-CLA doses (50, 100 or 200 μM) and the possible additive effect elicited by sub-toxic amount of BTZ (5 nM) was evaluated in cells co-incubated with t10,c12-CLA for 24 h. The results obtained (**Figure 34B**) demonstrated that the dose-dependent activation of caspase 3 was triggered by t10,c12-CLA, reaching an eightfold increase compared to the control culture. Notably, pro-apoptotic induction, associated with a significant decline in intracellular GSH, was not further improved by BTZ supplementation (**Figure 34C**). Similarly, APEH and proteasome mRNA levels were strongly downregulated by 200 μM t10,c12- CLA treatment (**Figure 35A**, right panel) and only minor alterations were produced by the addition of BTZ (data not shown). Interestingly, while a dose-dependent inhibition of APEH activity was observed, the proteasomal CT-like activity was inhibited to 46 and 50% by 50 and 100 μM t10,c12-CLA, respectively and a less marked effect resulted from cells exposed to 200 μM CLA (25%) (**Figure 35A**, left panel). Moreover, the decline of APEH and β-5 protein expression only occurred at the higher CLA dose ($p<0.05$) (**Figure 35B**). In addition, the noticeable decrease of the anti-apoptotic protein Bcl-2 expression, reaching the maximum reduction of 80%, further supported the role of apoptosis in the anti-proliferative effect of t10,c12-CLA (**Figure 35B**). Finally, we showed that cell exposure to high t10,c12-CLA doses markedly down-regulated the Nrf2 pathway, as evidenced by the declined mRNA levels of some target genes (NQO1 and γGCL), expressed as fold change in comparison to untreated cells (**Figure 36**). These findings support the hypothesis that the combined downregulation of antioxidant/detoxifying defences, APEH/proteasome system and Bcl-2 levels, may play an important role in apoptosis induction triggered by t10,c12-CLA in A375 cells.

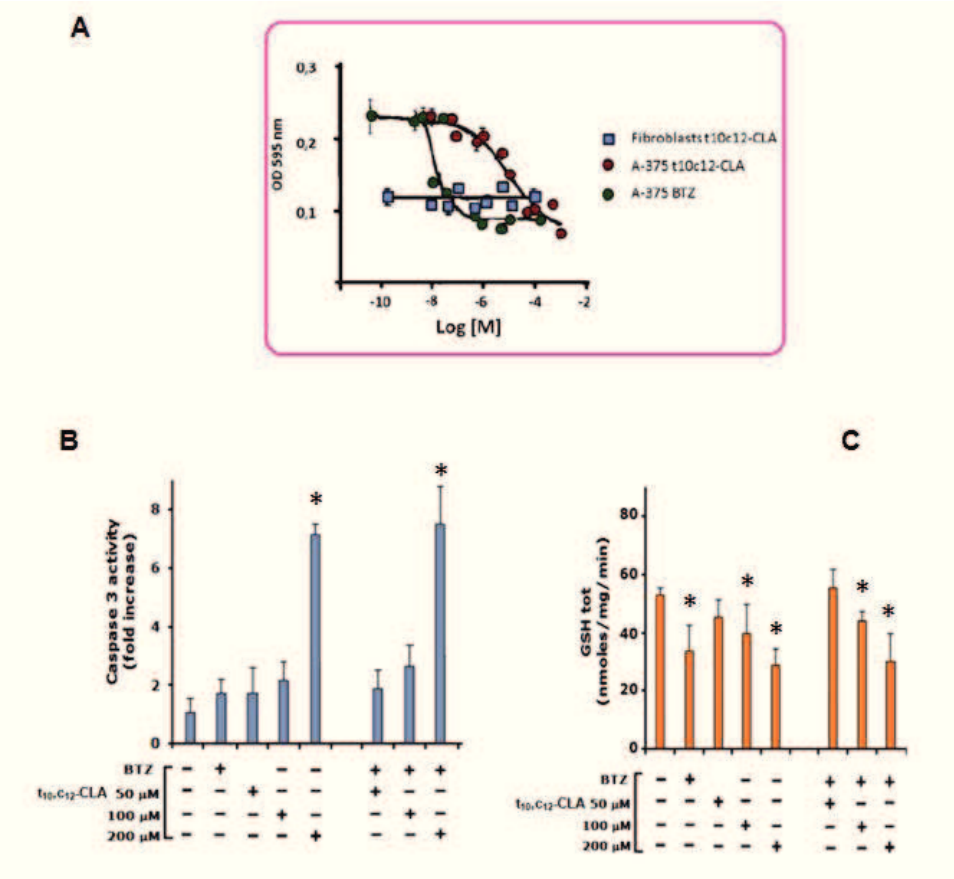

Figure 34. Dose-dependent pro-apoptotic activity of t10,c12-CLA correlates with downregulation of GSH in A375 cells. *Isobologram of A375 cells treated with t10,c12-CLA or BTZ for 24 h is reported in panel* ***A***. *Human fibroblasts exposed to the same t10,c12-CLA concentrations were used as control. Data are expressed as means ±SD values of triplicate data from three independent experiments. Pre-confluent A375 cultures were incubated for 24 h with 50, 100 or 200 µM t10,c12-CLA. Thereafter, cells were harvested, and used for cytoplasmic or mRNA extracts preparation. Cells untreated or treated with 10 nM BTZ were used as negative or positive controls, respectively. Measurement of caspase 3 activity (**B**) and GSH concentration (**C**) were performed on cytoplasmic extracts. Results were presented as means±SD of triplicate data from three independent experiments. *Significantly different (P < 0.01) from respective controls.*

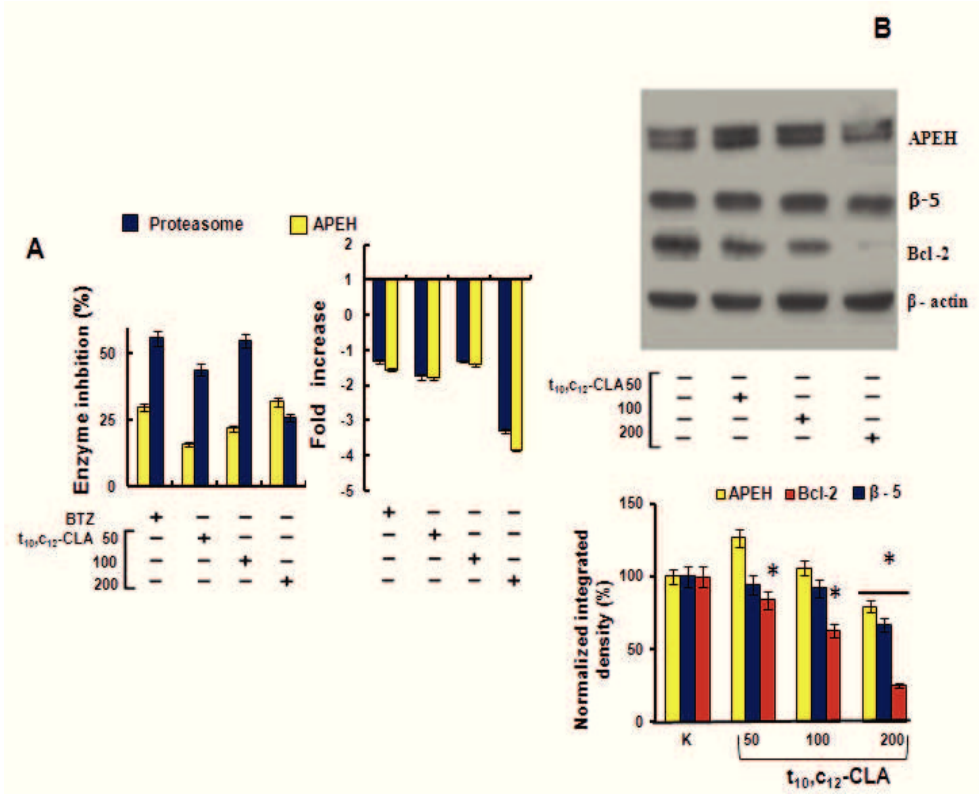

Figure 35. Dose-dependent pro-apoptotic activity of t10,c12-CLA correlates with downregulation of APEH and proteasomal CT-like subunit at both mRNA and activity level in A375 cells. *Pre-confluent A375 cultures were incubated for 24 h with 50, 100 or 200 μM t10,c12-CLA. Thereafter, cells were harvested, and used for cytoplasmic or mRNA extracts preparation. Cells untreated or treated with 10 nM BTZ were used as negative or positive controls, respectively. Measurement of APEH or proteasomal CT-like activities (**A left panel**) were performed on cytoplasmic extracts. The mRNA levels of APEH and β-5 subunit were evaluated by qRT-PCR and expressed as fold change in comparison to untreated cells (**A right panel**). Intracellular levels of Bcl-2, APEH and β-5 were detected by immunoblotting (**B upper panel**). Data on Western blot analysis were normalized to the density of control (β-actin) and the values were expressed as percent value as compared to untreated cultures (K) on triplicate measurements (**B lower panel**). Results were presented as means±SD of triplicate data from three independent experiments. *Significantly different (P < 0.01) from respective controls.*

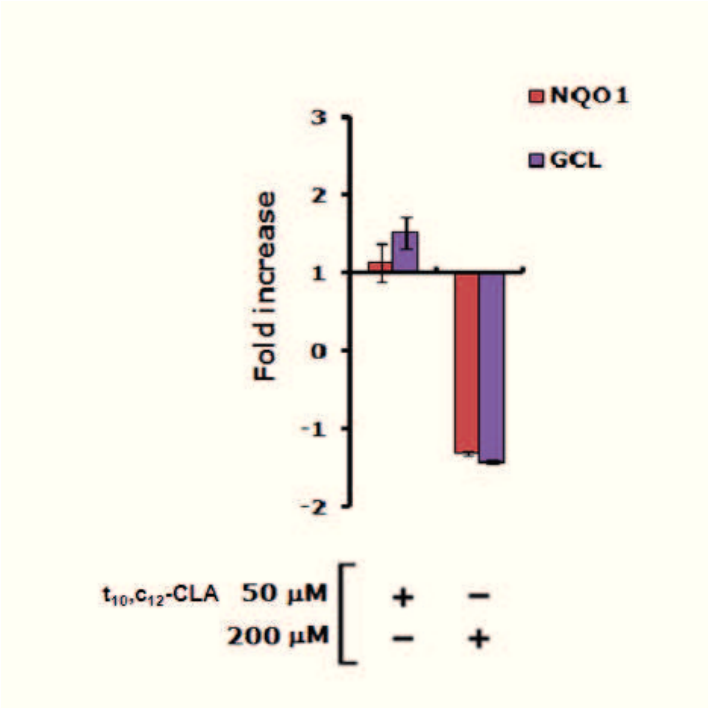

Figure 36. mRNA levels of GCL and NQO1 in A375 cells treated with 50 or 200 µM of t10,c12-CLA for 24 h. *The mRNA levels were evaluated by RT-PCR and expressed as fold change in comparison to untreated cells. *Significantly different (P < 0.01) from respective controls.*

6.4 A375 exposure to high t10,c12-CLA doses increases ROS production in association with apoptotic events and APEH/proteasome downregulation in time-dependent fashion

Time-dependent monitoring of ROS production, APEH and proteasome (β-5) at mRNA and enzyme activity level, was performed to evaluate the effects produced by the exposure to lower (50 µM) or higher (200 µM) t10,c12-CLA concentrations, on pre-confluent A375 cells. Sudden decrease (2 h) of APEH and proteasomal CT-like activities in cells exposed to low doses, correlated with a transient reduction of their mRNA expression. Upon this early response, enzyme activities recovered, reaching a plateau after 8h with values corresponding to 80 or 70% of their starting values, respectively (**Figure 37A**). Similarly, mRNA profiles showed a short-lived gene repression, which quickly recovered towards the stable final values, being approximately one-fold lower than their initial expression level (**Figure 37B**). Conversely, the higher concentration of t10,c12-CLA produced a downshift of APEH activity reaching a plateau with average values of 70% compared to its starting level, whereas a long-term downregulation of proteasomal activity persisted up to 16 h (**Figure 37C**). Interestingly,

two transient minima of mRNA levels were observed after 2 and 6 h, followed by a significant increase until 16 h. After 24 h of incubation, APEH and β-5 expression decreased again reaching the corresponding lowest values (**Figure 37D**). The time-dependent ROS production indicated that the early downregulation of APEH /proteasome enzyme activities could be induced by ROS yield (**Figure 37A**), while a direct modulation of the CLA isomer on both enzymes can possibly contribute to the following decrease of the activity/mRNA levels observed at 200 μM (**Figure 37C, D**). Cell pre-incubation with the antioxidant N-acetyl cysteine (NAC, 5 mM) before the 200 μM CLA exposure (2 or 24 h) resulted in a marked cytotoxic effect (data not shown).

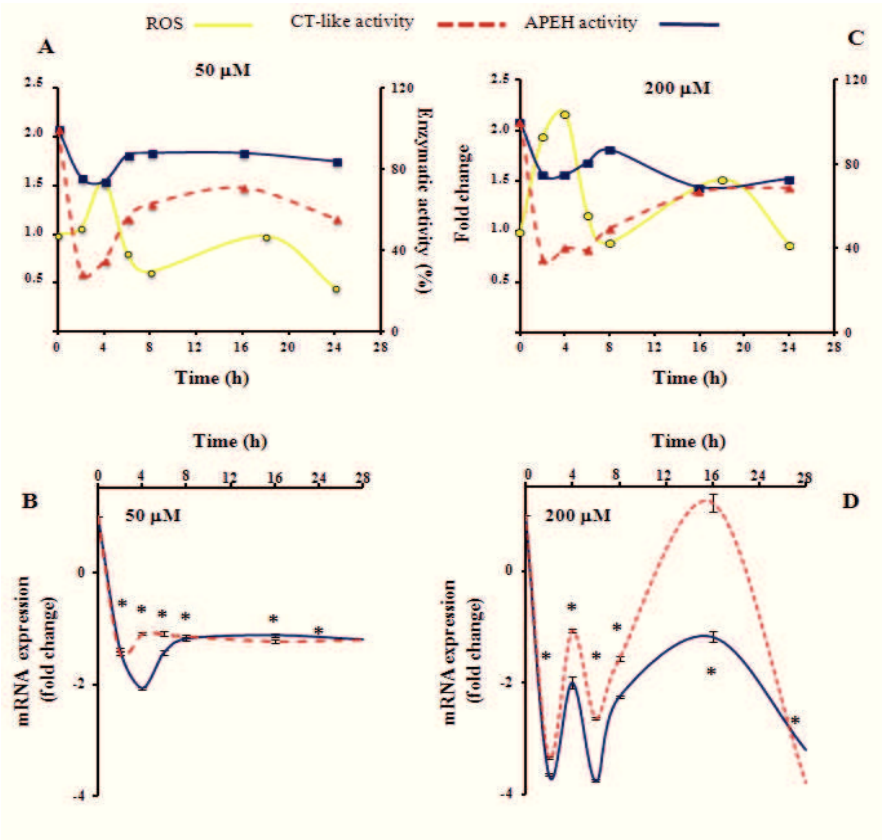

Figure 37. Time-dependent effects of t10,c12-CLA on APEH/proteasome system and on ROS production in A375 cells*. Preconfluent A375 cells were incubated with 50 μM or 200 μM of t10,c12-CLA for the indicated times. After treatments, cytoplasmic cell-extracts were used for the measurement of APEH and proteasomal CT-like activities (**A,C**). The ROS profiles were compared with the time courses of proteasomal CT-like and APEH activity levels (**A,C**). ROS production was assessed as described in materials and methods. cDNAs were synthesized and used for qRT-PCR amplification of APEH and β-5 (**B,D**) at the*

*indicated times. The mRNA levels were finally expressed as fold change in comparison to untreated cells. Results were presented as means±SD of triplicate data from three independent experiments and SD values lower than 5% were not shown. *Significantly different (P< 0.01) from respective controls.*

Finally, time-dependent effects elicited by 200 µM t10,c12- CLA on GSH concentration and caspase 3 activity, together with γGCL mRNA levels, were measured. As shown in **Figure 38A**, the decline of intracellular GSH was followed by caspase 3 activation (after 6-8 h). To investigate the mechanism underlying the pro-oxidant activity of t10,c12-CLA, the mRNA expression of the rate-limiting enzyme responsible for cellular GSH synthesis (namely γGCL) was monitored. As expected, the early activation triggered by CLA isomer (after 2 h) was followed by a transient decrease in mRNA (peaking after 4 h), which temporarily recovered before leading to the downregulation (1.5 fold) of mRNA levels (**Figure 38B**).

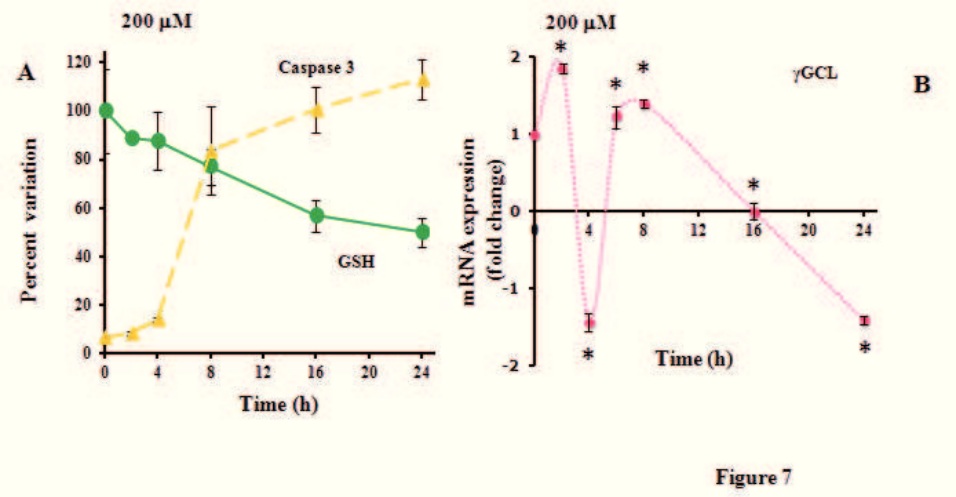

***Figure 38. Time-dependent effects of t10,c12-CLA on caspase 3 and cyto-protective defences on A375 cell**. Pre-confluent A375 cultures were incubated with 200 µM t10,c12-CLA for the indicated times. After treatments, cytoplasmic cell-extracts were used for the measurement of GSH concentration and caspase 3 activity (**A**). GSH and caspase 3 activities were expressed as percent variation in comparison to cells harvested at the beginning or at the end of the incubation, respectively. cDNAs were synthesized and used for qRT-PCR analysis of γGCL transcripts (**B**) at the indicated times. The mRNA levels were finally expressed as fold change in comparison to untreated cells. Results were presented as means±SD of triplicate data from three independent experiments. SD values lower than 5% were not shown. *Significantly different (P < 0.01) from respective controls.*

6.5 Putative APEH binding site for t10,cis12-CLA isomer

In a previous work [**41**], the structural model of the inhibition complex $APEH_{Ss}$-SsCEI protein corroborated by mutagenesis studies, indicated an involvement of the SsCEI *RSL* (shown in paragraph 2.1 *Peptide design and characterization*-Chapter 1) in the interaction with the active site of the enzyme target. The surprising downregulation of APEH by t10,c12-CLA prompted us to undertake a molecular modelling study to look for potential APEH-CLA binding sites. Protein-fatty acid docking analyses were carried out starting from the previously reported structural model of $APEH_{Ss}$ [**41**], herein used for the biochemical investigation. The $APEH_{Ss}$ 3D model, built on the X-ray structure of APEH from *Aeropyrum pernix* [**5**], shows the typical features of a POP family member: a α/β hydrolase catalytic domain with the (Ser-Asp-His) catalytic triad, covered by a central tunnel of an unusual β-propeller domain.

Docking calculations were performed by using the AutoDock simulation package **[43]**. The docked conformations of t10,c12-CLA suggested two putative binding modes that were characterised by different anchoring points for the carboxylate group of the CLA isomer: the positively charged side-chains of either R62 or R507. However, the binding involving the residue R507 appeared to be in conflict with the non-competitive inhibition mechanism indicated by the experimental data, as R507 belongs to the active site of $APEH_{Ss}$ [**41**]. Thus we did not consider this binding approach further. binding of t10,c12-CLA involving R62 residue of the enzyme is in agreement with the non-competitive mechanism of inhibition resulting from cell-free assays. In this case, t10,c12-CLA occupies the β-propeller tunnel, eventually obstructing the passage of the substrate and/or the product (**Figure 39**). Details of the binding mode involving R62 are shown in **Figure 40**: t10,c12-CLA carboxylate group interacts with the side-chains of R62 and S273 of $APEH_{Ss}$, while the long hydrophobic carbon tail of t10,c12-CLA is stabilised by van der Waals interactions with some of the hydrophobic residues that line the b-propeller tunnel of $APEH_{Ss}$. Of note, the interaction mechanism suggested by this docking analysis shares common characteristics with the fatty-acid-binding proteins (FABP) [**44, 45**]. X-ray structural studies have shown that the fatty acid molecule binds to the relatively large FABP inner cavity, and is anchored to a positively-charged arginine residue and a polar amino acid (usually serine or threonin), with the hydrophobic tail again stabilised by van der Waals interactions

with hydrophobic residues. The lack of structural information and the difficulty to predict a sufficiently accurate 3D model for any mammalian APEH have prevented us from performing

modelling studies on mammalian APEHs. However, the functional properties indicate significant similarity between mammalian and archaeal APEHs, showing that both are inhibited by t10,c12-CLA through a non-competitive mechanism (**Figure 31F**), with comparable Ki values. Therefore, we hypothesize that the enzymes from archaeal and mammalian sources could share some common features in their modes of interaction with this inhibitor.

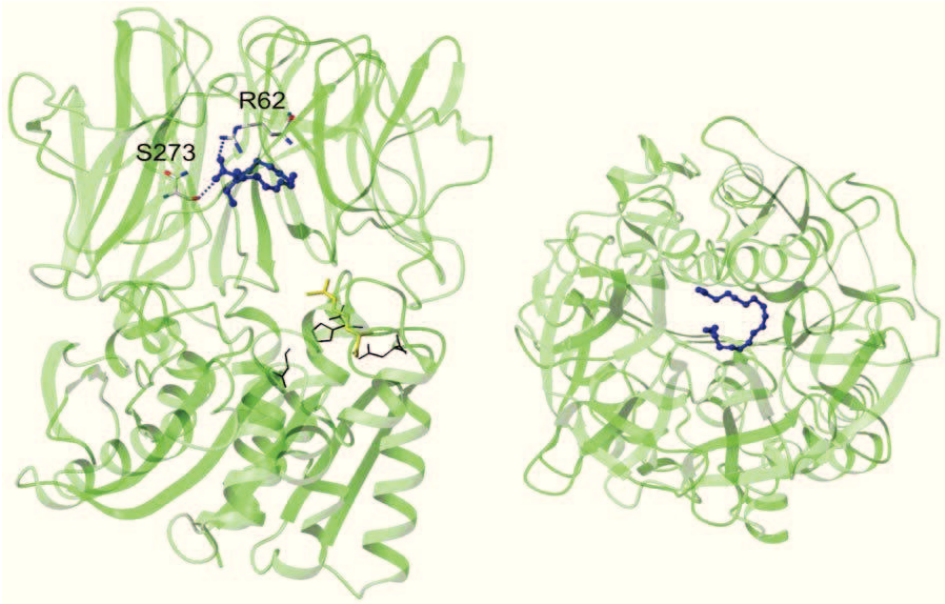

Figure 39*. *Binding mode of the t10,c12-CLA with APEHSs. *Binding mode suggested by docking analysis for t10,c12-CLA (blue; ball-and-stick mode) with APEHSs (cartoon representation; green, left). Protein residues involved in stabilising the interactions with the carboxylic group of the t10,c12-CLA are represented as sticks. The Ser-Asp-His catalytic triad residues are shown as black lines; R507 is shown in yellow. (right) View rotated 90u along the x-axis (the horizontal axis parallel to the image plane).*

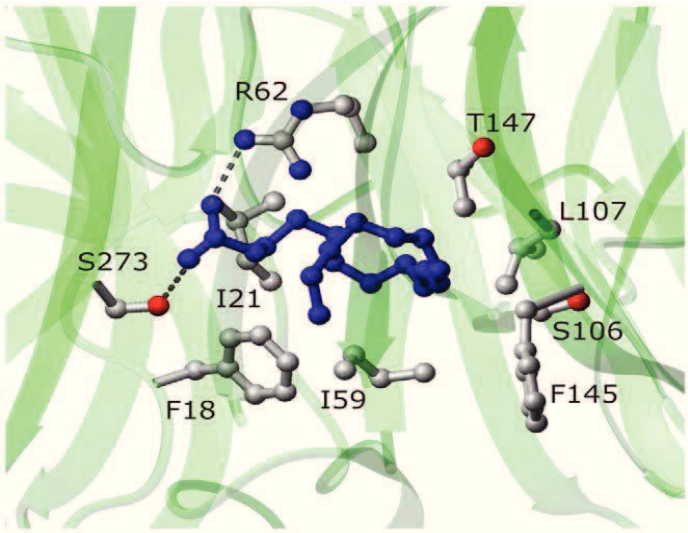

***Figure 40*. Suggested binding site on APEHSs by docking analysis** *for the t10,c12-CLA (blue; ball-and-stick mode) isomer. The relevant* $APEH_{Ss}$ *residues are shown in ball-and-stick representation.*

7. Discussion

Owing to their enhanced metabolic activity, cancer cells require elevated levels of energy to maintain a high rate of cell growth and proliferation. This is also guaranteed by an improved activity of the Ubiquitin-Proteasome System, which is the major pathway for protein turnover in eukaryotes [**46**], providing a secondary antioxidant defence mechanism, in combination with APEH [**47, 48**]. Indeed, protein homeostasis is critically involved in cancer cell survival; thus, one of the major focus in cancer research is targeting the balance between the production and destruction of proteins mediating cell proliferation. In this context, proteasome inhibition represents a novel strategy against many tumoral diseases, triggering an increase in apoptosis and decrease in cellular growth. Accordingly, in the last decade, research and development of new compounds able to down-regulate proteasome functions have attracted growing attention. It is known that the pro-apoptotic ability of CLA mixture (c9,t11- and t10,c12-CLA; 50:50) or its individual isomers, affects tumor cell proliferation via different biochemical pathways involving apoptotic or survival genes (Bcl-2, p21, p53). The efficacy of these isomers in inhibiting the cancer cell viability was highly influenced by the model system used, within a concentration range of 1-200 μmol/L and treatment lasting 1-11 days [**28**]. Specifically, t10,c12-CLA has revealed a more efficient activity, respect to c9,t11-CLA isomer, in modulating apoptosis or cell cycle. In human prostatic carcinoma cells, t10,c12-CLA anticancer effect associates to decreased Bcl-2 and increased p21(WAF1/Cip1) mRNA levels [**49**] while in human colon or bladder cancer cells it was accompanied by the activation of ATF/NAG-1 [**50**] or Insulin Growth Factor signaling [**51**]. Moreover, it was reported that t10,c12-CLA was able to down-regulate Fatty Acid Synthase [**52**] or antioxidant defence systems [**53-55**] in different human cancer cells. In such a context, the purpose of this study was to explore the relationship between the anti-proliferative properties and the ability of CLA isomers to down-regulate the APEH/proteasome system in cancer cells, taking into account the role of cellular redox status in these processes. We firstly evaluated the effects of CLA isomers on purified proteasome and APEH in cell free assays, showing that t10,c12-CLA was the only isomer able to efficiently inhibit both enzymes, which appeared functionally correlated, in a cancer cell panel. Intriguingly, the link observed between caspase 3 activation and cell viability in t10,c12-CLA treated cells, supported the apoptosis role in the anti-proliferative effects specifically induced by this isomer. The higher susceptibility to the t10,c12-CLA treatment of A375 melanoma cell line, showing the highest basal levels of APEH/proteasome, is consistent

with the involvement of this system in cell survival. Unfortunately, this hypothesis cannot be extended to all the tested cell lines showing high constitutive enzymatic levels. In addition, we demonstrated that early ROS production triggered by higher t10,c12-CLA doses, along with the combined downregulation of NF-E2-related factor 2-Antioxidant responsive elements (Nrf2-ARE) pathway and proteasome-APEH activity/expression levels, was likely responsible for the programmed A375 cell death. However, these results couldn't be further investigated by using antioxidants (NAC) and t10,c12-CLA combination in cell treatment (data not shown) due to NAC toxicity on A375 cells [**56**]. The endogenous oxidative stress rarely leads to damage, because a healthy cell generally possesses a powerful antioxidant defence to inactivate ROS. However, when cellular antioxidants are compromised, as occurs in the context of external environmental challenges, cell death is the expected outcome. By contrast, in several tumoral cells, hyperactivation of endogenous sources of ROS, which generates the observed increased levels of these molecules, results in a state of chronic oxidative stress [**57**, **10**]. It is well established that GSH plays an important role in cancer development and treatment, as it can protect against DNA damages produced by ROS and electrophilic chemicals [**58**]. Generally, in various types of cancerous cells and solid tumors, elevated GSH levels are observed, making these cells and tissues less susceptible to chemotherapy by increasing the resistance to oxidative stress. However, although chronic ROS exposure confers several advantages to cancer cells, by stimulating proliferation and maintaining the transformed phenotype [**59**], excessive ROS yield may induce cell cycle arrest and apoptosis. Therefore, redox state modulation in tumoral cells has been indicated as a possible target for cancer [**60**] or, specifically, for melanoma treatment [**61**].

In this context, our results, showing the increased intracellular GSH levels in A375 cells, were in agreement with studies reporting the central role played by redox homeostasis in the control of melanoma survival, proliferation and invasiveness [**62**]. Moreover, the association of pro-oxidant activity of t10,c12-CLA with anti-proliferative effect, was consistent with literature [**53, 54**] and conformed to the activities of recently discovered proteasome inhibitors, triggering ROS production in melanoma cells through oxidative stress activation [**63, 64**]. In addition, although the downregulation of the Nrf2 pathway, was accompanied by the caspase 3 activation in cells exposed to high t10,c12-CLA doses, nevertheless there is not necessarily a direct cause/effect between these two events. In accordance with the importance of Nrf2 downregulation in tumor growth reduction and in enhancing the efficacy of

chemotherapeutic agents [**65**], the use of t10,c12-CLA in combination with specific APEH/proteasome inhibitors could represent an effective strategy for melanoma treatment. To sum up, t10,c12-CLA-induced oxidative stress was detectable at very early times, as revealed by the increase of DCF fluorescence (**Figure 37C**), downregulation of γGCL expression (**Figure 38B**) and the following decline of intracellular thiols (**Figure 38A**). Hence, it is reasonable to hypothesize that the oxidative stress and the Nrf2-activation, triggered by t10,c12-CLA, are upstream processes contributing to the APEH/proteasome downregulation (**Figure 41**) [**66-68**] which culminate in activation of caspase 3. The finding of time progression events provides additional insights toward understanding the CLA-activated mechanisms, which are involved in the anticarcinogenic effects of these compounds, particularly the t10,c12-CLA isomer, in melanoma cancer cells. Further research are needed to support the role played by APEH in the downregulation of cancer cell viability.

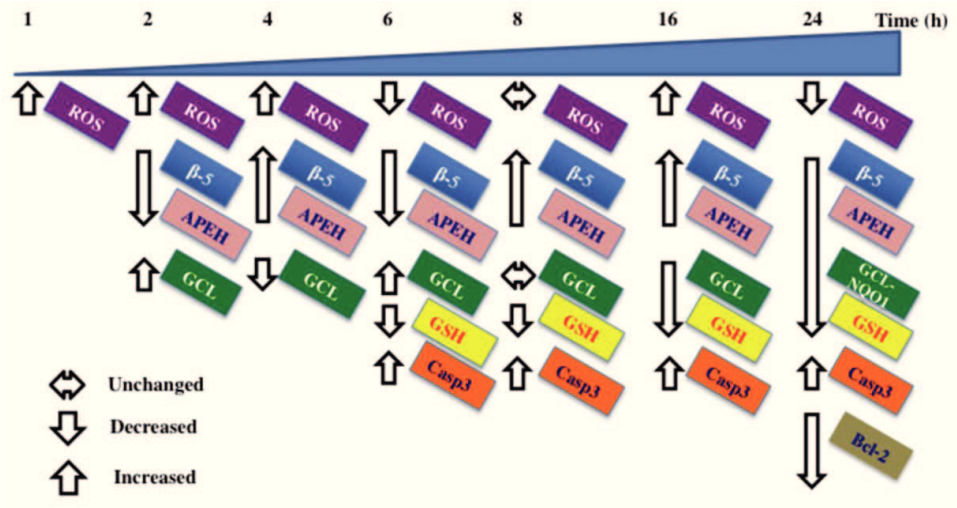

Figure 41. ***Summary diagram***. *In the scheme early ROS yield (after 1 h), triggered by cells exposure to 200 μM t10,c12-CLA, led to the transient decline of the detoxifying APEH/proteasome system and the improved γGCL expression, following the increased nuclear translocation of Nrf2. During the next 10 h, the partial recovery of β-5 and APEH transcription paralleled the reduced GCL expression and intracellular GSH levels resulting in the increased apoptosis (caspase 3 activity, casp3). After 24 h incubation, the simultaneous decline of β-5, APEH, γGCL and NQO1 transcriptional levels and of intracellular GSH are associated with decreased cell viability likely via apoptosis enhancement (as evidenced by increased casp3 activity and Bcl-2 degradation).*

In conclusion, in the light of all the results reported, it can be assumed that the selected APEH inhibitors t10,c12-CLA and SsCEI 4 are able to activate different cellular responses in diverse tumor cell lines. This could be due to the specific nature of these compounds. Indeed, t10,c12-CLA isomer is a natural molecule which is known to exert multiple functions and therefore several fundamental processes, including not only protein degradation machinery but also apoptotic pathways and antioxidative defence systems, could be strongly altered in melanoma A375 cells. Conversely, SsCEI 4 is a synthetic and very selective peptide designed as APEH inhibitor and, for this reason, possibly involved in the specific downregulation of APEH-proteasome system and protein turnover processes in osteosarcoma U2OS cells. Hovewer, further analysis will be necessary to deepen the molecular mechanisms activated in response to APEH-proteasome inhibition.

8. References

References

1. Pariza MW, Park Y, Cook ME. The biologically active isomers of conjugated linoleic acid. *Prog Lipid Res* (2001); 40(4): 283-98.
2. Pariza MW, Hargraves WA. A beef-derived mutagenesis modulator inhibits initiation of mouse epidermal tumors by 7,12-dimethylbenz[a]anthracene. *Carcinogenesis* (1985); 6(4): 591-3.
3. Decker EA. The role of phenolics, conjugated linoleic acid, carnosine, and pyrroloquinoline quinone as nonessential dietary antioxidants. *Nutr Rev* (1995); 53(3): 49-58.
4. Chin SF, Liu W, Storkson JM, Ha YL, Pariza MW. Dietary sources of conjugated dienoic isomers of linoleic acid, a newly recognized class of anticarcinogens. *J Food Compos Anal* (1992); 5: 185-197.
5. Lin H, Boylston TD, Chang MJ, Luedecke LO, Shultz TD. Survey of the conjugated linoleic acid contents of dairy products. *J Dairy Sci* (1995); 78(11): 2358-65.
6. Parodi PW. Cows' milk fat components as potential anticarcinogenic agents. J Nutr (1997); 127(6): 1055-60.
7. Lawson RE, Moss AR, Givens DI. The role of dairy products in supplying conjugated linoleic acid to man's diet: a review. *Nutr Res Rev* (2001); 14(1): 153-72.
8. Fritsche JRR, Steinhart H. Formation, contents, and estimation of daily intake of conjugated linoleic acid isomers and trans-fatty acids in foods. *Advances in Conjugated Linoleic Acid Research* (1999); 1: 378 – 96.
9. Banni S. Conjugated linoleic acid metabolism. *Curr Opin Lipidol* (2002); 13(3): 261-6.
10. Belury MA. Inhibition of carcinogenesis by conjugated linoleic acid: potential mechanisms of action. *J Nutr* (2002); 132(10): 2995-8.
11. Koba K, Akahoshi A, Yamasaki M, Tanaka K, Yamada K, Iwata T, Kamegai T, Tsutsumi K, Sugano M. Dietary conjugated linolenic acid in relation to CLA differently modifies body fat mass and serum and liver lipid levels in rats. *Lipids* (2002); 37(4): 343-50.
12. Ryder JW, Portocarrero CP, Song XM, Cui L, Yu M, Combatsiaris T, Galuska D, Bauman DE, Barbano DM, Charron MJ, Zierath JR, Houseknecht KL. Isomer-specific antidiabetic properties of conjugated linoleic acid. Improved glucose tolerance, skeletal muscle insulin action, and UCP-2 gene expression. *Diabetes* (2001); 50(5): 1149-57.
13. Yang M, Cook ME. Dietary conjugated linoleic acid decreased cachexia, macrophage tumor necrosis factor-alpha production, and modifies splenocyte cytokines production. *Exp Biol Med* (Maywood) (2003); 228(1): 51-8.
14. Bhattacharya A, Banu J, Rahman M, Causey J, Fernandes G. Biological effects of conjugated linoleic acids in health and disease. *J Nutr Biochem* (2006); 17(12): 789-810.
15. Park Y. Conjugated linoleic acid (CLA): Good or bad trans fat? *Journal of Food Composition and Analysis* 22S (2009): S4–S12.

16. Park Y, Albright KJ, Liu W, Cook ME, Pariza MW. Dietary conjugated linoleic acid (CLA) reduces body fat content and isomers of CLA are incorporated into phospholipid fraction. *IFT Book of Abstract* (1995), 183.

17. Park Y, Pariza MW. Mechanisms of body fat modulation by conjugated linoleic acid (CLA). *Food Research International* (2007); 40: 311–323.

18. Kritchevsky D, Tepper SA, Wright S, Czarnecki SK, Wilson TA, Nicolosi RJ.Conjugated linoleic acid isomer effects in atherosclerosis: growth and regression of lesions. Lipids (2004); 39(7): 611-6.

19. Choi Y, Park Y, Pariza MW, Ntambi JM. Regulation of stearoyl-CoA desaturase activity by the trans-10, cis-12 isomer of conjugated linoleic acid in HepG2 cells. *Biochem Biophys Res Commun* (2001); 284: 689– 93.

20. Pineda Torra I, Gervois P, Staels B. Peroxisome proliferator-activated receptor alpha in metabolic disease, inflammation, atherosclerosis and aging. *Curr Opin Lipidol* (1999); 10(2): 151-9.

21. Moya-Camarena SY, Vanden Heuvel JP, Blanchard SG, Leesnitzer LA, Belury MA. Conjugated linoleic acid is a potent naturally occurring ligand and activator of PPARalpha. *J Lipid Res* (1999); 40(8): 1426-33.

22. Pai JT, Guryev O, Brown MS, Goldstein JL. Differential stimulation of cholesterol and unsaturated fatty acid biosynthesis in cells expressing individual nuclear sterol regulatory element-binding proteins. *J Biol Chem* (1998); 273(40): 26138-48.

23. Roche HM, Noone E, Sewter C, Mc Bennett S, Savage D, Gibney MJ, O'Rahilly S, Vidal-Puig AJ. Isomer-dependent metabolic effects of conjugated linoleic acid: insights from molecular markers sterol regulatory element-binding protein-1c and LXRalpha. Diabetes (2002); 51(7): 2037-44.

24. Inoue N, Nagao K, Hirata J, Wang YM, Yanagita T. Conjugated linoleic acid prevents the development of essential hypertension in spontaneously hypertensive rats. *Biochem Biophys Res Commun* (2004); 323(2): 679-84.

25. Changhua L, Jindong Y, Defa L, Lidan Z, Shiyan Q, Jianjun X. Conjugated linoleic acid attenuates the production and gene expression of proinflammatory cytokines in weaned pigs challenged with lipopolysaccharide. *J Nutr* (2005); 135: 239–44.

26. Yu Y, Correll PH, Vanden Heuvel JP. Conjugated linoleic acid decreases production of pro-inflammatory products in macrophages: evidence for a PPAR gamma-dependent mechanism. *Biochim Biophys Acta* (2002); 1581: 89– 99.

27. Poirier H, Shapiro JS, Kim RJ, Lazar MA. Nutritional supplementation with trans-10,cis-12-conjugated linoleic acid induces inflammation of white adipose tissue. Diabetes (2006); 55(6): 1634-41.

28. Kelley NS, Hubbard NE, Erickson KL. Conjugated linoleic acid isomers and cancer. *The Journal of Nutrition* (2007); 137:2599–2607

29. Majumder B, Wahle KW, Moir S, Schofield A, Choe SN, Farquharson A, Grant I, Heys SD. Conjugated linoleic acids (CLAs) regulate the expression of key apoptotic genes in human breast cancer cells. *FASEB J* (2002); 16(11): 1447-9.

30. Masso-Welch PA, Zangani D, Ip C, Vaughan MM, Shoemaker S, Ramirez RA, Ip MM. Inhibition of angiogenesis by the cancer chemopreventive agent conjugated linoleic acid. *Cancer Res* (2002); 62(15): 4383-9.

31. Palombo JD, Ganguly A, Bistrian BR, Menard MP. The antiproliferative effects of biologically active isomers of conjugated linoleic acid on human colorectal and prostatic cancer cells. *Cancer Lett* (2002); 177(2): 163-72.

32. Ip C, Dong Y, Thompson HJ, Bauman DE, Ip MM. Control of rat mammary epithelium proliferation by conjugated linoleic acid. Nutr *Cancer* (2001); 39(2): 233-8.

33. Belury MA. Inhibition of carcinogenesis by conjugated linoleic acid: potential mechanisms of action. *J Nutr* (2002); 132(10): 2995-8.

34. Schafer KA. The cell cycle: a review. *Vet Pathol* (1998); 35(6): 461-78.

35. Leake R. The cell cycle and regulation of cancer cell growth. Ann N Y Acad Sci (1996); 784: 252-62.

36. Ip C, Ip MM, Loftus T, Shoemaker S, Shea-Eaton W. Induction of apoptosis by conjugated linoleic acid in cultured mammary tumor cells and premalignant lesions of the rat mammary gland. *Cancer Epidemiol Biomarkers Prev* (2000); 9(7): 689-96.

37. Schönfeld P, Wojtczak L. Fatty acids as modulators of the cellular production of reactive oxygen species. *Free Radic Biol Med* (2008); 45(3): 231-41.

38. Hamel FG. Preliminary report: inhibition of cellular proteasome activity by free fatty acids. *Metabolism* (2009); 58(8): 1047-9.

39. Devery R, Miller A, Stanton C. Conjugated linoleic acid and oxidative behaviour in cancer cells. *Biochem Soc Trans* (2001); 29: 341-344.

40. Serini S, Piccioni E, Merendino N, Calviello G. Dietary polyunsaturated fatty acids as inducers of apoptosis: implications for cancer. Apoptosis (2009); 14:135-152.

41. Palmieri G, Langella E, Gogliettino M, Saviano M, Pocsfalvi G, Rossi M. A novel class of protease targets of phosphatidylethanolamine-binding proteins (PEBP): a study of the acylpeptide hydrolase and the PEBP inhibitor from the archaeon Sulfolobus solfataricus. Mol Biosyst (2010); 6: 2498–2507.

42. Bartlam M, Wang G, Yang H, Gao R, Zhao X, Xie G, Cao S, Feng Y, Rao Z. Crystal structure of an acylpeptide hydrolase/esterase from Aeropyrum pernix K1. Structure (2004); 12: 1481–1488.

43. Morris GM, Goodsell DS, Halliday RS, Huey R, Hart WE, Belew RK, Olson AJ. Automated docking using Lamarckian genetic algorithm and an empirical binding free energy function. J Comput Chem (1998); 19: 1639-1662.

44. Sacchinettini JC, Scapin G, Gopaul D, Gordon JI. Refinement of the structure of Escherichia coli-derived rat intestinal fatty acid binding protein with bound oleate to 1.75-A resolution. Correlation with the structures of the apoprotein and the protein with bound palmitate. J Biol Chem (1992); 267: 23534–45.

45. Hamilton JA. Fatty acid interactions with proteins: what X-ray crystal and NMR solution structures tell us. Progr Lipid Res (2004); 43: 177–99.

46. Ciechanover A. Intracellular protein degradation: from a vague idea through the lysosome and the ubiquitin-proteasome system and onto human diseases and drug targeting. Neurodegener Dis (2012); 10: 7-22.

47. Shimizu K, Kiuchi Y, Ando K, Hayakawa M, Kikugawa K . Coordination of oxidized protein hydrolase and the proteasome in the clearance of cytotoxic denatured proteins. Biochem Biophys Res Commun (2004); 324: 140-146.

48. Shimizu K, Fujino T, Ando K, Hayakawa M, Yasuda H, Kikugawa K. Overexpression of oxidized protein hydrolase protect COS-7 cells from oxidative stress-induced inhibition of cell growth and survival. Biochem Biophys Res Commun (2003); 304: 766-771.

49. Ochoa JJ, Farquharson AJ, Grant I, Moffat LE, Heys SD, Wahle KW. Conjugated linoleic acids (CLAs) decrease prostate cancer cell proliferation: different molecular mechanisms for cis-9, trans-11 and trans-10, cis-12 isomers. Carcinogenesis (2004);25(7):1185-91.

50. Lee SH, Yamaguchi K, Kim JS, Eling TE, Safe S, Park Y, Baek SJ. Conjugated linoleic acid stimulates an anti-tumorigenic protein NAG-1 in an isomer specific manner. Carcinogenesis (2006);27(5):972-81.

51. Jung JI, Cho HJ, Kim J, Kwon DY, Park JH. trans-10,cis-12 conjugated linoleic acid inhibits insulin-like growth factor-I receptor signaling in TSU-Pr1 human bladder cancer cells. J Med Food (2010); 13:13-19.

52. Lau DS, Archer MC. The 10t,12c isomer of conjugated linoleic acid inhibits fatty acid synthase expression and enzyme activity in human breast, colon, and prostate cancer cells. Nutr Cancer (2010) ;62: 116-121.

53. Hsu YC, Ip MM. Conjugated linoleic acid-induced apoptosis in mouse mammary tumor cells is mediated by both G protein coupled receptor-dependent activation of the AMP-activated protein kinase pathway and by oxidative stress. Cell Signal (2011); 231: 2013-2020.

54. Bergamo P, Luongo D, Rossi M. Conjugated linoleic acidmediated apoptosis in Jurkat T cells involves the production of reactive oxygen species. Cell Physiol Biochem (2004); 14: 57-64.

55. Ou L, Wu Y, Ip C, Meng X, Hsu YC, Ip MM. Apoptosis induced by t10,c12-conjugated linoleic acid is mediated by an atypical endoplasmic reticulum stress response. J Lipid Res (2008);49(5):985-94.

56. Yang J, Su Y, Richmond A. Antioxidants tiron and N-acetyl-Lcysteine differentially mediate apoptosis in melanoma cells via a reactive oxygen species- independent NF-κB pathway. Free Radic Biol Med (2007); 42: 1369–1380.

57. Franco R, Sánchez-Olea R, Reyes-Reyes EM, Panayiotidis MI. Environmental toxicity, oxidative stress and apoptosis: Menage a trios. Mutat Res (2009); 674: 3-22.

58. Ballatori N, Krance SM, Notenboom S, Shi S, Tieu K, Hammond CL. Glutathione dysregulation and the etiology and progression of human diseases. Biol Chem (2009); 390(3): 191-214.

59. Fried L, Arbiser JL. The reactive oxygen-driven tumor: relevance to melanoma. Pigment Cell. Melanoma Res (2008); 21: 117-122.

60. Trachootham D, Alexandre J, Huang P. Targeting cancer cells by ROS-mediated mechanisms: a radical therapeutic approach? Nat Rev Drug Discov (2009); 8: 579-591.

61. Fruehauf JP, Trapp V. Reactive oxygen species: an Achilles' heel of melanoma. Expert Rev Anticancer Ther (2008); 8: 1751–1757.

62. Govindarajan B, Sligh JE, Vincent BJ, Li M, Canter JA, Nickoloff BJ, Rodenburg RJ, Smeitink JA, Oberley L, Zhang Y, Slingerland J, Arnold RS, Lambeth JD, Cohen C, Hilenski L, Griendling K, Martínez-Diez M, Cuezva JM, Arbiser JL. Overexpression of Akt converts radial growth melanoma to vertical growth melanoma. J Clin Invest (2007); 117: 719-729.

63. Qiao S, Lamore SD, Cabello CM, Lesson JL, Muñoz-Rodriguez JL, Wondrak GT. Thiostrepton is an inducer of oxidative and proteotoxic stress that impairs viability of human melanoma cells but not primary melanocytes. Biochem Pharmacol (2012);83(9):1229-40.

64. Brohem CA, Massaro RR, Tiago M, Marinho CE, Jasiulionis MG, de Almeida RL, Rivelli DP, Albuquerque RC, de Oliveira TF, de Melo Loureiro AP, Okada S, Soengas MS, de Moraes Barros SB, Maria-Engler SS. Proteasome inhibition and ROS generation by 4-nerolidylcatechol induces melanoma cell death. Pigment Cell Melanoma Res (2012); 25(3): 354-69.

65. Ren D, Villeneuve NF, Jiang T, Wu T, Lau A, Toppin HA, Zhang DD. Brusatol enhances the efficacy of chemotherapy by inhibiting the Nrf2-mediated defense mechanism. Proc Natl Acad Sci U S A (2011); 108(4): 1433-8.

66. Reinheckel T, Sitte N, Ullrich O, Kuckelkorn U, Davies KJ, Grune T. Comparative resistance of the 20S and 26S proteasome to oxidative stress. Biochem J (1998);335 (Pt 3): 637-42.

67. Chapple SJ, Siow RC, Mann GE. Crosstalk between Nrf2 and the proteasome: Therapeutic potential of Nrf2 inducers in vascular disease and aging. Int J Biochem Cell Biol (2012); 44: 1315-1320.

68. Aiken CT, Kaake RM, Wang X, Huang L Oxidative stressmediated regulation of proteasome complexes. Mol Cell Proteomics (2011); 10: R110.006924.

9. Materials and Methods

9.1 Reagents

Pure fatty acids (octanoic acid, c9,t11-, t9,t11- and t10,c12-CLA isomers), caspase-3 fluorometric Assay Kits were purchased from Sigma-Aldrich. DMEM/F12, DMEM, L-glutamine, penicillin-streptomycin and FBS were from Gibco-BRL. Porcine liver APEH was obtained by Takara. 20S human proteasome was purchased from Boston Biochem. Bortezomib (BTZ) was obtained by Santa Cruz Biothecnology. Chemicals of the highest purity were from Sigma-Aldrich or Calbiochem.

9.2 Peptide design, synthesis and characterization

The peptides were prepared as amidated derivatives by solidphase synthesis (synthesis scale, 0.1 mmoles), following standard Fmoc/tBu protocols. A rink amide resin (substitution, 0.57 mmol/g) and amino acid derivatives with standard protection were used in all of the syntheses. Cleavage from the solid support was performed by treatment with a trifluoroacetic acid (TFA)/triisopropylsilane/ water (90:5:5, v/v/v) mixture for 90 min at room temperature. The crude peptides were precipitated in cold ether, dissolved in a water/acetonitrile (1:1, v/v) mixture and lyophilised. The peptides were purified by reverse-phase HPLC using a semipreparative 561 cm ID C18 monolythic Onyx column, applying a linear gradient of 0.05% TFA in acetonitrile from 10% to 70% over 8 min at a flow rate of 15 mL/min. Peptide purity and identity were confirmed by liquid chromatography–mass spectrometry analysis.

9.3 Gel filtration analysis of synthetic peptides

Gel filtration chromatography was performed on a BioSep SEC-S2000 column equilibrated with 50 mM phosphate buffer pH 6.8, at a flow rate of 1.0 mL/min. A standard curve was built using a set of synthetic peptides with molecular weights between 1.500 amu and 2.500 amu. For this purpose, peptide aliquots were injected onto the column and a plot of KD versus log10 molecular weights (MW) was obtained, where KD=(Ve-Vo)/(VTVo), Ve is the elution volume of the sample, and VT and Vo are the total and void volumes of the column, respectively.

9.4 Circular dichroism spectroscopy

CD spectra were obtained on a Jasco J-715 spectropolarimeter with 400 μL of 8.0×10^{-7} M protein in 5 mM Tris–HCl pH 7.5. Hellman quartz cells of 0.1-cm-path length were used in

the far UV (190–250 nm). The temperature of the sample cell was regulated by a PTC-348 WI thermostat and thermal CD was performed from 250 to 195 nm by raising the cell temperature from 37 °C to 77 °C. The thermal CD spectra were signal-averaged by combining three scans and the baseline was corrected by subtracting a buffer spectrum. The samples were then cooled back to 37 °C to monitor the final folding of the peptides.

9.5 Enzyme assays

APEH activity was measured spectrophotometrically using the chromogenic substrate acetyl-Ala-pNA (Bachem). The reaction mixture (1 mL) containing pure APEH (38 ng) or an appropriate amount of cell extract in 50 mM Tris-HCl buffer pH 7.5 (Tris Buffer), was preincubated at 37 °C for 2 min. Then, 1 mM acetyl-Ala-pNA was added and the release of p-nitroanilide ($\varepsilon 410 = 8800\ M^{-1}\ cm^{-1}$) was measured by recording the absorbance increase at 410 nm on a Cary 100 Scan (Varian) UV/Vis spectrophotometer, equipped with a thermostated cuvette compartment. APEH activity was expressed in IU. The synthetic fluorescent substrate N-succinyl-Leu-Leu-Val-Tyr-7-amido-4-methylcoumarin (N-Suc-LLVT-AMC) was used for the measurement of the CT-like activity of the proteasome, at a final concentration of 0.080 mM. The reaction mixture (0.9 mL) containing appropriate amount of proteasome was preincubated as above, in Tris buffer. N-Suc-LLVT-AMC was added, and the release of the fluorescent product (7-AMC) was monitored for 5 min in a Perkin–Elmer LS 50B fluorimeter. The excitation and emission wavelengths were 380 nm and 460 nm, respectively.

The carboxypeptidase Y, elastase, thrombin, trypsin and subtilisin activities were also evaluated according to previously published methods.

9.6 Enzyme inhibitory assays

Protease inhibitor activities of the peptides (SsCEI 4 and CF3-lmph) and fatty acids were carried out using a fixed amount of APEH or partially purified proteasome (3–5 nM and 0.12 mg/mL, respectively), and increasing peptide or fatty acid concentrations. Mixtures were pre-incubated for 30 min at 37 °C before the addition of the substrate, and the enzymatic activities were followed as described above. Inhibitory cell free assays were also performed on APEH and proteasome partially purified from Caco-2, A375 and U2OS cells at 37 °C in Tris buffer pH 7.5.

The time-dependent inhibition of SsCEI 4 towards APEH was assessed. Mixtures containing appropriate amounts of each inhibitor and APEH were pre-incubated for 20 min at 37 °C; they were then diluted (1:5) into the standard assay mixture, which contained the substrate only. The enzymatic activity was followed as described above. Control samples were prepared by pre-incubating the same amounts of APEH without the inhibitors and then diluted in the standard assay mixture. To determine the mechanisms of APEH inhibition (Ki), Lineweaver−Burk double reciprocal plots of data at increasing inhibitor and substrate concentrations were constructed.

9.7 Cells, culture conditions and treatments

Human hepatoma cells (HepG2) were seeded ($2x10^4$cells/cm^2) and grown in MEM (Gibco Invitrogen; Milano) medium supplemented with 2 mM L-glutamine, 1% nonessential amino acids and 10% FBS. Colon carcinoma (Caco-2), cervical carcinoma (Hela), glioblastoma (U87), melanoma (A375, A375M, PNP, Sk-mel, LCM, LCP), osteosarcoma (U2OS, SaOS) and mammary adenocarcinoma (MCF7, MDA-MB) were seeded ($1x10^4$cells/cm^2) and grown in DMEM supplemented with 10% FBS, 2 mM L-glutamine. The cells were harvested at the pre-confluent stage and used for cytoplasmic or mRNA extract preparation.

Differentiated Caco-2 cells were studied between passages 12 and 22. The cells were split using trypsin-EDTA solution and plated in 6-well plates at a density of 8x104 cells/mL and the medium was replaced every 2–3 days. Under these conditions, the cells reached visual confluence after 7 days and the differentiated stage two weeks later. Then, the differentiated cells were incubated for 48 h with the different substances.

Normal human dermal fibroblast (NDHF) within 8th passage were seeded at a density of $2x10^4$ cells/cm^2 and cultured in fibroblast growth medium (FGM-2; Lonza, Milan, Italy) containing 2% FBS, 50 μg/mL gentamycin and amphotericin B, 10μg/mL fibroblast growth factor and insulin. BHK21 cells (kindly donated by Dr. David Y Thomas, McGill University Montreal Canada) were cultured in DMEM/F12, 5% FBS, 1 mM L-glutamine, 200 μg/mL methotrexate, and 100units/mL penicillin-streptomycin. Cells were incubated in a humidified atmosphere at 37 °C in 5% CO_2. Stock solutions of SsCEI peptides, fatty acids or bortezomib (BTZ) were prepared by dissolving in dimethyl sulphoxide (DMSO) and further dilutions were carried out in DMEM. Cells were treated with fatty acids or BTZ and control culture were exposed to the same amount of DMSO.

BHK cells stably expressing CFTR-M (kindly donated by Dr. David Y Thomas, McGill University Montreal Canada) were plated in 12-well plates, to a confluence of 60% for the 24-h incubations, and 40% for 48-h exposure to PIs. These treatments were initiated 24-h after the plating of the cells. Phase-contrast images of the cells were taken just before the lysis of the cells for protein analysis, using a Lica DM6000 inverted microscope.

9.8 Antibodies

The following antibodies were used: anti-APEH antibody (sc-102311; Santa Cruz Biotechnology); anti-NF-kB/p65 antibody (Thermo Scientific); anti-p21Waf1 antibody (Exbio); pan Ab-5 anti-actin antibody (clone ACTN05, Thermo Scientific); anti-Bcl-2 (340576-BD PharmingenTM); anti-proteasome 20S β-5 subunit (BML-PW8895-0025; Enzo Life Science); anti-caspase 3 (Santa Cruz Biotechnology); anti-PARP (Abcam); anti-LC3 e anti-Beclin-1 (Autophagy Antibody Sampler Kit, Cell Signaling Technology) and monoclonal antibodies against polyubiquitinylated proteins conjugated with horseradish peroxidase (FK2H, Enzo, Life Science). The ΔF508CFTR-3HA protein was detected with an anti HA monoclonal antibody (Covance).

9.9 Protein extraction and Western blotting analysis

Following the treatments, the cells were washed three times with ice cold phosphate-buffered saline and collected immediately at 4 °C in lysis buffer (1% Triton X-100, 0.1% SDS, 20 mM Tris-HCl, pH 8.0, 150 mM NaCl, 0.5% sodium deoxycholate and complete protease inhibitors [Roche]). The lysates were centrifuged at 10,000xg for 15 min at 4 °C. The protein concentrations in the clear supernatants were determined (BCA protein assay reagent kit; Pierce) before their use in enzymatic assays or SDS–PAGE. In brief, for Western blotting, aliquots (30 μg) were run on SDS-PAGE (8% or 12.5%) and then electroblotted onto PVDF membranes (ImmobilonTM, Millipore). The membranes were next incubated with primary antibodies and then with the appropriate dilution of secondary antibody (1 h at 37 °C). At the end of this time, the immunocomplexes formed were visualised by enhanced chemiluminescence and autoradiography according to the manufacturer protocol (Amersham Biosciences) and quantified by densitometric analysis with ChemiDoc XRS (Bio-Rad). Protein expression data was quantified with Quantity One Software (Bio-Rad).

9.10 MTT-based cytotoxicity assay

The colorimetric 3-(4,5-dimethylthiazol-2)-2,5- diphenyltetrazolium bromide (MTT) (Sigma Aldrich, Milan) assay was used to quantify cell viability. Briefly, cells were incubated in 96 well microplates in the appropriate complete medium with standardized densities for 24 h as pre-incubation process. The medium was removed and replaced by medium containing different doses of the different compounds for 24h (CLA isomers) or 24, 48 and 72 h (peptides). Following treatment, the medium was removed and the cells were incubated with DMEM w/o red phenol with 0.5 mg/ml MTT for additional 2 to 4h at 37 °C. After removal of the medium and MTT, cells in each plate were incubated with 0.1 M HCl/ isopropanol to dissolve the MTT-formazan crystals. Absorbance at 590 nm was recorded with a plate reader (Bio Rad mod 680). The relative number of viable cells was expressed as a percentage of the control.

9.11 Apoptosis assays

The pro-apoptotic ability of the peptides or CLA isomers were assayed by measuring the caspase 3 activity using fluorometric kits, according to the manufacturer instructions. These assays were based on hydrolysis of the substrate acetyl-Asp-Glu-Val-Asp-7-amido-4-methylcoumarin (Ac-DEVD-AMC) by caspase 3. The release of the 7-AMC moiety in protein extracts prepared from the differently treated cells was evaluated by fluorimetry (excitation 360 nm, emission 460 nm). Their amounts were calculated by means of a standard curve prepared with pure AMC, and following normalization for protein content, the activities were expressed as nmoles AMC/mg protein/min.

9.12 Cytotoxicity assay

The release of LDH (Lactate dehydrogenase) was used as the marker for cell toxicity [48]. The culture supernatants were sampled at the end of the incubations and centrifuged (4,000xg, 5 min, and 4 °C). Aliquots of the clear supernatant (10 µL) were incubated with 190 µL reaction buffer (200 mM Tris/HCl, pH 8.0, 0.7 mM p-iodonitrotetrazolium violet, 50 mM L-lactic acid, 0.3 mM phenazine methoxysulphate, 0.4 mM NAD,) for 30 min at 37 °C. Absorbance was measured at 490 nm and the results were expressed as percentages of total LDH release from control cultures treated with 1% (w/v) Triton X-100 and calculated as: [(experimental value - blank value)/(total lysis -blank value)-100].

9.13 ROS detection

DCF-DA (2',7'-dichlorofluorescein diacetate) was used to determine the amount of ROS production. DCF-DA working solution was added to the medium to reach 10 μM and then incubated at 37 °C for 15 min in the dark. Cells were harvested by trypsinization, washed with PBS and kept on ice for detection by FACScan (Becton Dickinson, USA) equipped with a 488 nm argon laser using a band pass filter of 530 nm.

9.14 Cell cycle analysis

U2OS cells were treated with the indicated concentrations of SsCEI 4 for 24, 48 and 72 h. The cells were then harvested, washed with PBS, and then stained with 50 μg /mL of propidium iodide containing 0.1% Triton X-100 in citrate buffer, and 100 μg/mL RNase A. The stained cells were then analyzed for DNA content using a FACS Calibur flow cytometer (BD Biosciences) and differences in cell cycle between treated *versus* untreated cells were analysed using ModFit LT software. The experiment was performed in triplicate.

9.15 Intracellular redox status and cell viability assessment

Intracellular concentration of reduced and oxidized glutathione (GSH and GSSG, respectively) were quantified using the 5,5'-dithiobis(2-nitrobenzoic acid)-GSSG reductase recycling assay. GSSG content was preliminarily evaluated in cytosolic extracts of treated or untreated cells upon the addition of 10 mM 1-methyl-2-vinylpyridinium trifluoromethanesulfonate (a specific GSH scavenger). Notably,

owing to the minor contribution given by GSSG (less than 5%) to the total intracellular thiol concentration, the latter was finally expressed as nmol GSH/mg protein. Pro-apoptotic and cytotoxic ability of CLA isomers were assayed by measuring caspase 3 and the activity of lactate dehydrogenase (LDH) in the spent media, respectively. The caspase 3 activity, measured at 37 °C and pH 7.5, was

expressed as fold increase compared to the control culture. The LDH release, measured at 37 °C and pH 8.2, was expressed as percentages of total LDH released from cultures treated with 1% (w/v) Triton X-100 and calculated as: [(experimental value-blank value)/(total lysis-blank value)-100].

9.16 Small interfering RNA transfection

The siRNA is purchased from Sigma (siRNAID SASI_ Hs01_00240856 and SASI_Hs01_00240857), and CFBE41o-DF espressing ΔF508 CFTR were kindly provided by Dr. J. P. Clancy Department of Pediatrics, the University of Alabama at Birmingham, Birmingham, AL, USA. CFBE41o-DF cells at $5x10^4$ cells/well were cultured over-night on 12-well plates and transfected 24 h after with APEH siRNA at a final concentration of 50 nM. using Lipofectamine 2000, according to the manufacturer's instruction. Non-targeting siRNA was used as a negative control. After 72 hours of transfection, cells are lysed in RIPA buffer and protein levels were determined by western blotting.

9.17 RNA isolation and quantitative real-time PCR analysis

mRNA expression levels of APEH and β-5 proteasome subunit were determined in treated or untreated cells to investigate on the functional relationship existing between APEH and proteasome activities and on their involvement in the anticancer activity of APEH inhibitors. In addition, the mRNA expression of NADH quinone oxidoreductase (NQO1) and of gamma Glutamylcysteine Ligase (γGCL), which is the limiting enzyme in the GSH synthesis, were also measured to further demonstrate the CLA ability to down-regulate intracellular redox status via the Nrf2 pathway.

Total RNA was isolated from the human cell lines (~106 cells aliquots) according to the SV Total RNA Isolation System (Promega) protocol, with an on column DNase I step. Total RNA concentrations were determined using a Qubit® Fluorometer (Invitrogen). RNAs were then reverse transcribed using the Transcriptor First Strand cDNA Synthesis Kit (Roche). 100 ng of reverse transcribed complementary DNA, and its dilution series to calculate the efficacy of primers, were amplified by quantitative real-time PCR (qRT-PCR) on an iCycleriQ™ (Bio-Rad) using 300 nM gene-specific primers, Maxima® SYBR Green/Fluorescein qPCR Master Mix (2X) (Fermentas) and the following PCR conditions: 1 cycle at 95 °C for 10min, and 40 cycles of 95 °C for 15s , 60 °C for 30s, and 72 °C for 30s. The expression level of β-actin gene was used as an internal control for normalization (ref gene). Raw cycle threshold values (Ct values) obtained for the target genes were compared to the Ct value obtained for the ref gene. The final graphical data were derived from the R=(Etarget)ΔCt_target (control - sample)/(Eref)ΔCt_ref (control - sample) formula, where "control" cells were fibroblasts or

A375/U2OS line, and "sample" cells were the tumor lines. In time course analysis the expression levels were normalized to those of untreated cells at Time=0.

Universal Probe Library Assay Design Center (https://www.roche-appliedscience.com/sis/rtpcr/upl/index.jsp?id=UP030000) was used for designing primers.

The primers utilized were:

APEH, 5'-CCCCATTCATCCTTTGTCAC-3' and 5'-AAAGCCCATCTTGCAAAGC-3';

β-5, 5'-CATGGGCACCATGATCTGT-3' and 5'-GAAATCCGGTTCCCTTCACT-3';

γGCL, 5'-GACAAAACACAGTTGGAACAGC-3'and 5'-CAGTCAAATCTGGTGGCATC-3';

NQO1, 5'-CAGCTCACCGAGAGCCTAGT-3' and 5'-GAGTGAGCCAGTACGATCAGTG-3';

β-actin, 5'-CCAACCGCGAGAAGATGA-3' and 5'-CCAGAGGCGTACAGGGATAG-3'.

9.18 Statistical analysis

All data were obtained from triplicate analyses of three different preparations. Data were presented as means±SD. Statistical analysis and IC50 values were calculated with the SigmaPlot 10.0 software through a non-linear curve-fitting method and using a simple binding isotherm equation. Groups were compared by Student's t test, and $P<0.05$ was considered as significant.

OPEN ACCESS Freely available online

PLoS one

Acylpeptide Hydrolase Inhibition as Targeted Strategy to Induce Proteasomal Down-Regulation

Gianna Palmieri[1☯*], Paolo Bergamo[2☯], Alberto Luini[5], Menotti Ruvo[3], Marta Gogliettino[1], Emma Langella[3], Michele Saviano[4], Ramanath N. Hegde[5], Annamaria Sandomenico[3], Mose Rossi[1]

1 Institute of Protein Biochemistry, National Research Council (CNR-IBP), Napoli, Italy, **2** Institute of Food Sciences, National Research Council (CNR-ISA), Avellino, Italy, **3** Institute of Biostructure and Bioimaging, National Research Council (CNR-IBB), Napoli, Italy, **4** Institute of Crystallography, National Council of Research of Italy (CNR-IC), Bari, Italy, **5** Telethon Institute of Genetics and Medicine (TIGEM), Napoli, Italy

Abstract

Acylpeptide hydrolase (APEH), one of the four members of the prolyl oligopeptidase class, catalyses the removal of N-acylated amino acids from acetylated peptides and it has been postulated to play a key role in protein degradation machinery. Disruption of protein turnover has been established as an effective strategy to down-regulate the ubiquitin-proteasome system (UPS) and as a promising approach in anticancer therapy. Here, we illustrate a new pathway modulating UPS and proteasome activity through inhibition of APEH. To find novel molecules able to down-regulate APEH activity, we screened a set of synthetic peptides, reproducing the reactive-site loop of a known archaeal inhibitor of APEH (SsCEI), and the conjugated linoleic acid (CLA) isomers. A 12-mer SsCEI peptide and the trans10-cis12 isomer of CLA, were identified as specific APEH inhibitors and their effects on cell-based assays were paralleled by a dose-dependent reduction of proteasome activity and the activation of the pro-apoptotic caspase cascade. Moreover, cell treatment with the individual compounds increased the cytoplasm levels of several classic hallmarks of proteasome inhibition, such as NFkappaB, p21, and misfolded or polyubiquitinylated proteins, and additive effects were observed in cells exposed to a combination of both inhibitors without any cytotoxicity. Remarkably, transfection of human bronchial epithelial cells with APEH siRNA, promoted a marked accumulation of a mutant of the cystic fibrosis transmembrane conductance regulator (CFTR), herein used as a model of misfolded protein typically degraded by UPS. Finally, molecular modeling studies, to gain insights into the APEH inhibition by the trans10-cis12 CLA isomer, were performed. Our study supports a previously unrecognized role of APEH as a negative effector of proteasome activity by an unknown mechanism and opens new perspectives for the development of strategies aimed at modulation of cancer progression.

Citation: Palmieri G, Bergamo P, Luini A, Ruvo M, Gogliettino M, et al. (2011) Acylpeptide Hydrolase Inhibition as Targeted Strategy to Induce Proteasomal Down-Regulation. PLoS ONE 6(10): e25888. doi:10.1371/journal.pone.0025888

Editor: Arun Rishi, Wayne State University, United States of America

Received June 30, 2011; **Accepted** September 12, 2011; **Published** October 10, 2011

Funding: The fundings for this study were from the project MoMa n. 1/014/06/0 of the Agenzia Spaziale Italiana. The funders had no role in study design, data collection and analysis, decision to publish, or preparation of the manuscript.

Competing Interests: The authors have declared that no competing interests exist.

☯ These authors contributed equally to this work.

* E-mail: g.palmieri@ibp.cnr.it

Introduction

In all living cells, proteolysis is essential in the control of many basic processes, including protein quality control, cell-cycle progression, signal transduction, apoptosis, and gene expression. One of the major players in the regulation of intracellular proteolysis is the ubiquitin-proteasome system (UPS) [1]. This is a complex enzymatic machine that primarily contributes to the cytoplasmic turnover of a vast majority of proteins in mammalian cells and it is tightly controlled by a number of endogenous regulators. Due to the multiple roles of UPS, it is essential in eukaryotes and its dysfunction can have deleterious effects in cells and for the organism as a whole. UPS dysregulation has been implicated in a number of pathologies such as autoimmune, neurodegenerative diseases and viral infections, and it is considered a novel therapeutic target for tackling tumoral diseases [2–6]. Indeed, protein homeostasis is critically involved in cancer cell survival thus, targeting the balance between the production and destruction of proteins mediating cell proliferation, has become a major focus in cancer research. Accordingly, over the past decade, several studies have been focused on the development of specific proteasome inhibitors (PIs), which have relevant anticancer effects and particularly on those involving in the repression of nuclear factor-κ (NF-κ B) signalling, and in the promotion of apoptosis in transformant cells [7,8].

The first evidence of the pro-apoptotic activity of PIs was shown in U937 human monoblast cells [9]. In 2003, the PI bortezomib (Velcade® or PS341) has been approved by the Food and Drug Administration for the treatment of multiple myeloma, which confirmed the efficacy of PIs in blocking cancer progression. However, like other PIs, bortezomib has several relevant adverse events [10,11] and, at present, increasing research efforts are aimed at reducing these negative side-effects through the use of inhibitors with reversible and time-limited binding activity and increased bioavailability. Recent studies have suggested that some fatty acids are able to disrupt the chymotrypsin (CT)-like proteasome activity. Among these, the two major isomers of conjugated linoleic acid (CLA), cis9-trans11 CLA (c_9t_{11}-CLA) and trans10-cis12 CLA ($t_{10}c_{12}$-CLA), have shown pro-apoptotic activities in a number of cancer cell lines [12] and strong

anticancer effects in numerous animal models [13]. Interestingly, although the mechanisms are yet poorly understood, their ability to inhibit the proteasome activity *in vitro* [14] suggests that this complex enzyme could be their ultimate target.

Acylpeptide hydrolase (APEH; also known as acylaminoacyl peptidase or oxidised protein hydrolase) is one of the four members of the prolyl oligopeptidase class (POP, clan SC, family S9); it catalyses the removal of N-acylated amino acids from acetylated peptides and has been recently recognised as having a role in the coordinated protein-degradation machinery in Cos-7 cells [15], and in the modulation of cancer progression [16].

On this background, we have investigated the molecular mechanisms that underlie the interrelationship between APEH and the proteasome, and their eventual regulation by natural or synthetic compounds including peptides reproducing the reactive site loop (RSL) of an archaeal APEH inhibitor (SsCEI, *Sulfolobus solfataricus* chymotrypsin-elastase inhibitor) [17], and the c_9t_{11}-CLA and $t_{10}c_{12}$-CLA isomers. Two molecules that selectively inhibit APEH and induce, in parallel, a down-regulation of proteasome activity have been identified. Moreover, a direct correlation between APEH inhibition and proteasome down-regulation has been established using a specific APEH siRNA probe. A molecular docking analysis has been also carried out to predict the CLA-enzyme binding sites. Therefore, this study shows that proteasome functions can be upstream regulated by APEH, and that inhibition of APEH activity appears to be an important event in controlling the proteasome dysfunction associated with pathological conditions, opening new important and challenging perspectives for the development of novel strategies in cancer therapy.

Results and Discussion

Peptide design and characterisation

The recent identification and characterisation of an endogenous inhibitor protein of APEH in S. solfataricus (SsCEI) [17,18], was the starting point for the present study and the S. solfataricus APEH (APEHSs) was used, in a first instance, as a model protein for molecular investigation. On the basis of the RSL of SsCEI, a set of four peptides, differing in size and nature at their P1 site, were designed and synthesized. Peptides SsCEI 1 and SsCEI 2 correspond to residues 119–134 and 123–134 of the SsCEI protein, respectively, and include the P1-P′1 (L126-E127) binding site which is reportedly involved in protease inhibition (Figure S1). The shorter variant (SsCEI 2), starting with the N-terminus of RSL, was designed to minimise peptide length while maintaining intact the RSL binding site. Two further peptides were projected, SsCEI 3 and SsCEI 4, to replace the P1 residue Leu with Ala, which is the preferred amino acid in the substrates of mammalian APEHs. The sequences of these peptides are reported in Table 1. Amidation at the C-terminal end was introduced to mimic the amino acid stretch within the protein backbone, whereas the amino termini of peptides were not acetylated to prevent substrate-like effects when in contact with APEH. Peptide structures within SsCEI protein inhibitor are predicted to be random/extended, as they have to be free in adopting the best conformation needed to dock the target proteases. Circular dichroism (CD) spectroscopy analyses were carried out to obtain information on the secondary structures of peptides outside the context of the native protein. Interestingly, the CD spectra measured between the 190 nm and 250 nm demonstrated that, except for SsCEI 4 which was largely unstructured (Figure S2), these peptides have well defined secondary structures in water. Specifically, CD spectra of SsCEI 2 and SsCEI 4 at 37°C, despite the single mutation, showed markedly different profiles, suggesting that the Leu→Ala substitution at the P1 site induces significant conformational alterations. CD spectra of SsCEI 2 featured canonical 'α-helix' curves with surprising fidelity (Figure S2). These data are in agreement with the role that the RSLs have in the native inhibitor proteins, and suggest a strong tendency of these peptides to adopt different conformations following even minimal sequence modifications.

CD spectra were also recorded in the temperature range between 37°C and 77°C, with increasing temperature steps of 10°C. Under these conditions, SsCEI 2 and SsCEI 3 showed considerable structural stability, as seen by the poor influence of temperature on their conformation (Figure S2). SsCEI 1 was not examined due to its poor stability in aqueous solution at the concentrations required for these analyses. These findings indicate that, in our model, the backbone architecture of the inhibitory loop is imposed by its specific amino acid sequence, and that the protein scaffold does not constrain the conformation of the RSL.

Given the relevant contents of β-sheet structures observed in SsCEI 2 and SsCEI 3, we next investigated the oligomerization properties of these peptides to exclude the occurrence of macroscopic aggregates. For this purpose, 100 μM solutions of peptides SsCEI 2, SsCEI 3 and SsCEI 4 were analysed by size-exclusion chromatography, and their apparent molecular masses were extrapolated from a calibration curve. As shown in Table 1, SsCEI 2, SsCEI 3 and SsCEI 4 were essentially monomers, suggesting that the secondary structures detected by CD were not a result of non-specific self-association, but seemed to be an intrinsic property of the peptides.

APEHSs is specifically and efficiently inhibited by SsCEI 2 and t10c12-CLA isomer

Preliminary experiments were aimed at investigating the possible interaction/inhibition between APEHSs and the peptides SsCEI 2, SsCEI 3 and SsCEI 4. Inhibition analyses were performed by pre-incubating the enzyme with increasing amounts

Table 1. Synthetic peptides used in this study.

Peptide	Theoretical mass value (Da)	Measured mass value (Da±SD)	P1 P′1
SsCEI 1	1818.12	n.d.	YAIDTILL EIKNINAD
SsCEI 2	1355.61	1961±265	TILL EIKNINAD
SsCEI 3	1766.04	2012±150	YAIDTILA EIKNINAD
SsCEI 4	1313.53	1986±28	TILA EIKNINAD

Peptides were synthesized with a free amino group at the N-terminus and an amidic group at the C-terminus. The apparent MWs of SsCEI peptides were determined by gel filtration chromatography. The calibration curve (R2 = 0.995) was obtained using a set of synthetic peptides. Data reported are the result of three independent determinations.

doi:10.1371/journal.pone.0025888.t001

of these compounds and their half-maximal inhibitory concentrations (IC50) were determined. The calibration curve for SsCEI 2 followed a hyperbolic pattern with an IC50 value of 9.8±1.0 μM as calculated using Ac-Leu-pNA as reporter substrate; however, in the presence of SsCEI 3 and SsCEI 4 no detectable decrease in the APEHSs activity was observed (Figure 1A). Therefore, APEHSs interacts with and is inhibited only by SsCEI 2 which has a Leu on the P1 site, suggesting that the residue on this position has a major role in the recognition with the target protease. Moreover, among the fatty acids tested, only the t10c12-CLA isomer was able to dose-dependently reduce APEHSs activity with an IC50 value of 80±2.0 μM, whilst no significant modulatory effect was observed using c9t11-CLA isomer (Figure 1B). Notably, APEHSs activity followed a Michaelis–Menten kinetic, both in the absence and in the presence of SsCEI 2 but only the Michaelis constant (Km) was affected by increasing concentrations of substrate, suggesting that SsCEI 2 behaved as a competitive inhibitor. It was confirmed by plotting the data according to the Lineweaver–Burk equation (data not shown), which allowed the calculation of a Ki value for SsCEI-2 of 1.00±0.02 μM. In contrast, in the presence of increasing amounts of t10c12-CLA isomer, only the Vmax of APEHSs was affected, indicating a non-competitive inhibition mechanism for t10c12-CLA, with a Ki value of 140±20 μM.

Mammalian APEHs are inhibited by SsCEI peptides and t10c12-CLA

The inhibition activity of SsCEI peptides was also assessed using mammalian APEHs purified from both porcine liver and human colon carcinoma intestinal cells (Caco-2). These two enzymes share more than 90% sequence identity, as calculated by the ClustalW algorithm (http://www.ebi.ac.uk/Tools/msa/clustalw2/). Ac-Ala–pNA was again used as the preferential substrate for these mammalian APEHs. As shown in Figure 1C, both SsCEI 2 and SsCEI 4 dose-dependently decreased porcine APEH activity, although to different extents (IC50 values were 142±30 μM and 84±16 μM, respectively). Comparable IC50 values were obtained using human APEH (data not shown). Moreover, the affinity of SsCEI 4 towards porcine APEH was revealed by a Ki value of 4.0±0.8 μM, as determined by the Lineweaver-Burk plot, which also showed that SsCEI 4 is a competitive inhibitor of this enzyme (Figure 1E). The greater efficacy of SsCEI 4 over SsCEI 2, can be ascribed to the preference for an Ala residue, with respect to leucine, at the P1 site, assuming that the SsCEI–APEH association occurs in a substrate-like manner. Data also suggested that the additional N-terminal residues in SsCEI 3 (Table 1), negatively affected the inhibition capacity towards both APEHSs and mammalian APEH (Figure 1A, C).

Next, the modulatory effects of CLA isomers on porcine APEH were investigated. The dose-dependent reduction of enzyme activity followed a hyperbolic pattern in the presence of t10c12-CLA isomer with an IC50 value of 105±23 μM (Figure 1D), whilst c9t11-CLA was ineffective. In addition the Ki of t10c12-CLA towards porcine APEH was 140±20 μM and the Lineweaver-Burk plot revealed a non–competitive inhibition mechanism. This is the first evidence of a direct inhibition of APEH by a CLA isomer.

SsCEI 4 and t10c12-CLA are selective, time-dependent and non covalent APEH inhibitors

The selectivity of SsCEI 2 and SsCEI 4 for porcine APEH (hereafter APEH) were analysed in biochemical assays using a panel of eukaryotic serine proteases comprising trypsin, α-chymotrypsin, elastase, carboxypeptidase Y, subtilisin and thrombin. Results showed that SsCEI 4 has no detectable effects on the proteases tested. In contrast, SsCEI 2 displayed an inhibition activity towards bovine α-chymotrypsin. The inhibition curve also followed a hyperbolic pattern with increasing SsCEI 2 concentrations, and gave an IC50 value of 21.9±6.4 μM (Figure S3). To further examine the SsCEI 4 specificity towards APEH, its inhibition activity was determined in a reaction mixture containing the entire set of proteases reported above. Under these conditions the inhibition efficiency and the Ki of SsCEI 4 towards APEH were comparable to those measured in the presence of the APEH alone (data not shown).

To investigate the molecular inhibition mechanisms of SsCEI 4 and t10c12-CLA, time-dependent experiments were carried out. Of note, SsCEI 4 and t10c12-CLA inhibited APEH (100% and 43%, respectively) only after pre-incubation with the enzyme for at least 20 min, suggesting that they behave as time-dependent inhibitors. Moreover, to exclude the formation of adducts or degradation products between SsCEI 4 and its protease target APEH, we analysed the incubation mixtures by reverse-phase HPLC chromatography. The lack of new peaks in the HPLC chromatogram and invariability of peak area suggested that neither peptide degradation nor covalent binding with APEH occurred under the assay conditions (Figure S3). Data thus indicated that SsCEI 4 is a highly selective, time-dependent and non covalent inhibitor of APEH.

Proteasomal degradation of the cystic fibrosis transmembrane conductance regulator (CFTR) mutated protein is prevented by SsCEI 4 and t10c12-CLA

The enzymatic stability of SsCEI 4 in 10% FBS was evaluated as previously reported [19] and the peptide was completely stable for at least one week under the assay conditions (data not shown).

In light of a recently proposed cooperative role for the APEH–proteasome system in the control of protein turnover [15], we hypothesised that APEH could be used as a target to indirectly control/modulate proteasome functions. To support this idea, we conducted in vitro experiments using the selected APEH inhibitors (SsCEI 4 or t10c12-CLA) on the Baby Hamster Kidney (BHK) cell line stably expressing a mutant protein of the cystic fibrosis transmembrane conductance regulator (CFTR), known as ΔF508 CFTR-3HA (hereafter called CFTR-M), bearing the deletion of Phe508, one of the most common modification in patients with cystic fibrosis. Many of the mutations in the CFTR gene that cause cystic fibrosis interfere with the folding and biosynthetic processing of CFTR molecules in the endoplasmic reticulum. Specifically, some mutations, including the common ΔF508, decrease the efficiency of CFTR folding, reduce the probability of its dissociation from molecular chaperones, and largely prevent its maturation through the secretory pathway to the plasma membrane. These mutant CFTR molecules are rapidly targeted for proteolysis via the UPS [20–22].

Accordingly, BHK and human bronchial epithelial cells (CFBE41o-DF) expressing CFTR-M were used in this study as a model system to confirm the role of APEH in the coordinated protein-degradation machinery, and steady-state levels of the core-glycosylated CFTR-M form (140 kDa) were evaluated by immunoblot analysis. Remarkably, the SsCEI 4 peptide and the t10c12-CLA isomer efficiently prevented degradation of CFTR-M at the time intervals considered (24 h and 48 h). As a fact, exposure of BHK cells to 100 μM SsCEI 4 for 48 h or to 100 μM t10c12-CLA for 24 h induced a marked increase of CFTR-M levels (twenty- and five-fold, respectively) (Figure 2A, B, C), without any cytotoxic effects (data not shown). In addition, a dose-

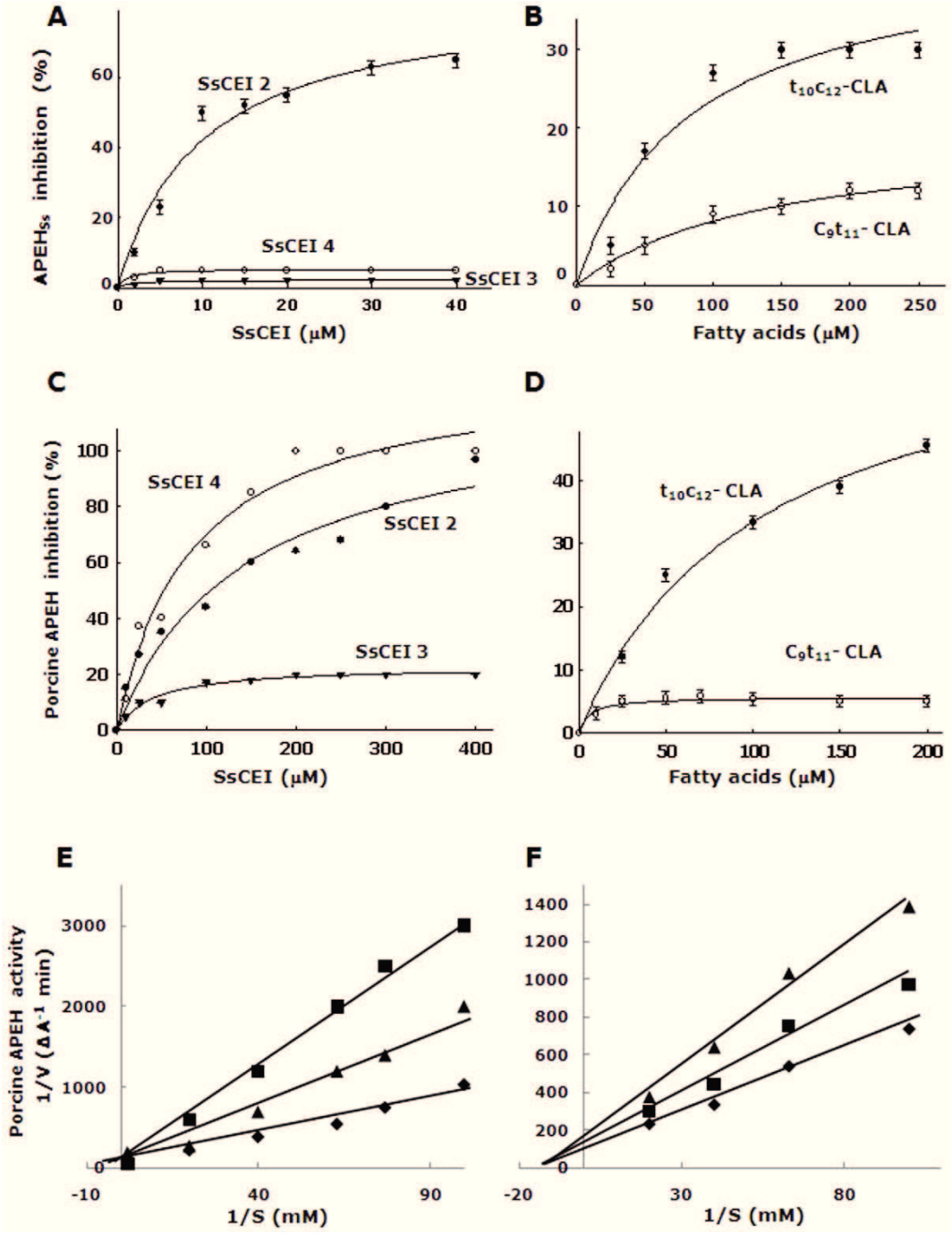

Figure 1. Kinetic analysis of SsCEIs and CLA isomers towards APEHs. Binding of increasing concentrations of the SsCEI peptides (A), and CLA isomers (B) to $APEH_{Ss}$. Binding of SsCEI peptides (C), and $t_{10}c_{12}$-CLA (D) to porcine APEH. The hyperbolic curves indicate the best fits for the data obtained, with IC_{50} values calculated from the graphs. Inhibition kinetics analyses with porcine APEH (0.5 nM) at increasing SsCEI 4 concentrations: 100 μM (triangles) and 150 μM (squares) (E). Similarly, inhibition kinetics by increasing $t_{10}c_{12}$-CLA concentrations: 50 μM (squares) and 100 μM (triangles) (F). Enzyme incubated without inhibitors were used as control (diamonds) (E, F). The inhibition constants, Ki, were determined by the Lineweaver–Burk equation for competitive and non-competitive inhibition, respectively.
doi:10.1371/journal.pone.0025888.g001

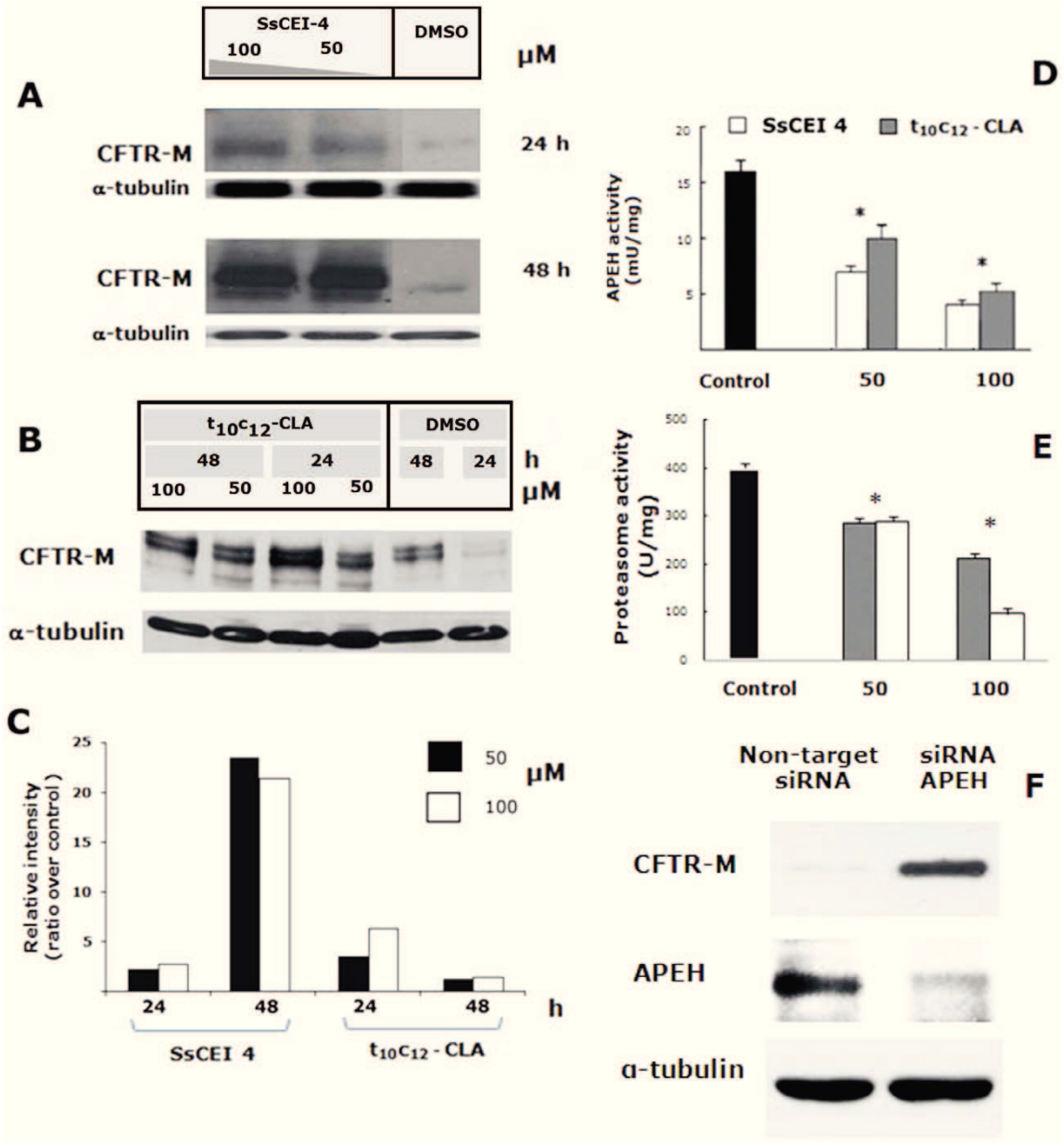

Figure 2. Analysis of the CFTR-M protein accumulation in BHK cells treated with the SsCEI 4 and $t_{10}c_{12}$-CLA and in APEH siRNA transfected CFBE41o-DF cells. Representative Immunoblots and associated densitometric analysis for cytosolic CFTR-M accumulation in BHK cells following 24 h and 48 h exposure to 50 μM or 100 μM SsCEI 4 (A), and to 50 μM or 100 μM $t_{10}c_{12}$-CLA (B). Bands were quantified using densitometric analysis and normalized against α-tubulin. The values were expressed as average fold increase as compared to untreated culture (C). APEH activity was measured in BHK cells incubated with 50 μM and 100 μM SsCEI 4 (white bars) or $t_{10}c_{12}$-CLA (grey bars) for 48 h (D). CT-like proteasome activities were measured in BHK cells incubated with 50 μM and 100 μM SsCEI 4 (white bars) or t10c12-CLA (gray bars) for 48 h (E). Untreated cultures were used as controls (black bars); the data are expressed as means±SD. *Significantly different ($P<0.005$) from the control (D, E). Representative Immunoblots of APEH and CFTR-M accumulation in CFBE41o-DF cells transfected with APEH siRNA. A scrambled, non-targeted siRNA, was used as negative control and α-tubulin was used as loading control (F).
doi:10.1371/journal.pone.0025888.g002

dependent inhibition of APEH and proteasome CT-like activities was observed upon 48 h of incubation (similar data on APEH and proteasome activities were measured after 24 h cell exposure) with both compounds, as shown in Figure 2D, E consistent with the immunoblot results.

Finally, siRNA technique was used to directly correlate APEH to the protein degradation processes via UPS. For this purpose, the accumulation of CFTR-M was evaluated in CFBE41o-DF cells following transfection with APEH siRNA. As shown in Figure 2F, APEH siRNA-transfected cells exhibited a considerable reduction

of APEH protein levels and a marked accumulation of CFTR-M (eight-fold, data not shown) (Figure 2F), in contrast to cells transfected with a not specific siRNA which displayed basal levels of APEH and neglectable level of CFTR-M. Therefore, APEH can be seen as an alternative target, whose inhibition by competitive as well as non-competitive inhibitors is accompanied by a parallel down-regulation of proteasome activity through a yet unknown mechanism.

SsCEI 4 and t10c12-CLA down-regulate APEH and proteasome activities in cancer cells

Proteasome inhibition represents a validated, although challenging, anticancer approach. However, to prevent the adverse effects deriving from indiscriminate cell death, inhibition of the proteasome needs to be tightly controlled or selectively induced in cancer tissues. Therefore, the concept that proteasome activity could be decreased via APEH inhibition was investigated in a cancer cell line. To this end, differentiated human colon carcinoma Caco-2 cells were treated with SsCEI 4, t10c12-CLA or with a specific PI (MG132) for 48 h. As shown in Figure 3A, SsCEI 4 and t10c12-CLA markedly reduced APEH activity in a dose-dependent manner, reaching their maximum effect at 200 μM, where enzyme activity was decreased by 70% and 50%, respectively. Under the same conditions MG132 treatment had no detectable effects.

We next examined the inhibitory effects of SsCEI 4 and t10c12-CLA on the CT-like proteasomal activity in Caco-2 cells and in cell-free assays. In these latter experiments, partially purified proteasome fractions from Caco-2 cells were used instead of the commercially available 20S proteasome or immunoproteasome. Indeed, it has been reported that in neoplastic cell lines the CT-like proteasomal activity, as well as the sensitivity to different PIs, is greatly influenced by the highly variable proteasome subunit composition [23].

Therefore, cell exposure to SsCEI 4 and t10c12-CLA, produced a dose-dependent decrease (up to 45% of the residual activity) of the CT-like proteasome activity with respect to the untreated cultures, whereas partially purified proteasome was not affected by these compounds (Figure 3C, D), thus confirming that it is not directly targeted by these inhibitors.

Next, we evaluated the effects of SsCEI 4 and t10c12-CLA treatment on the activation of caspases. As shown in Figure 3B,

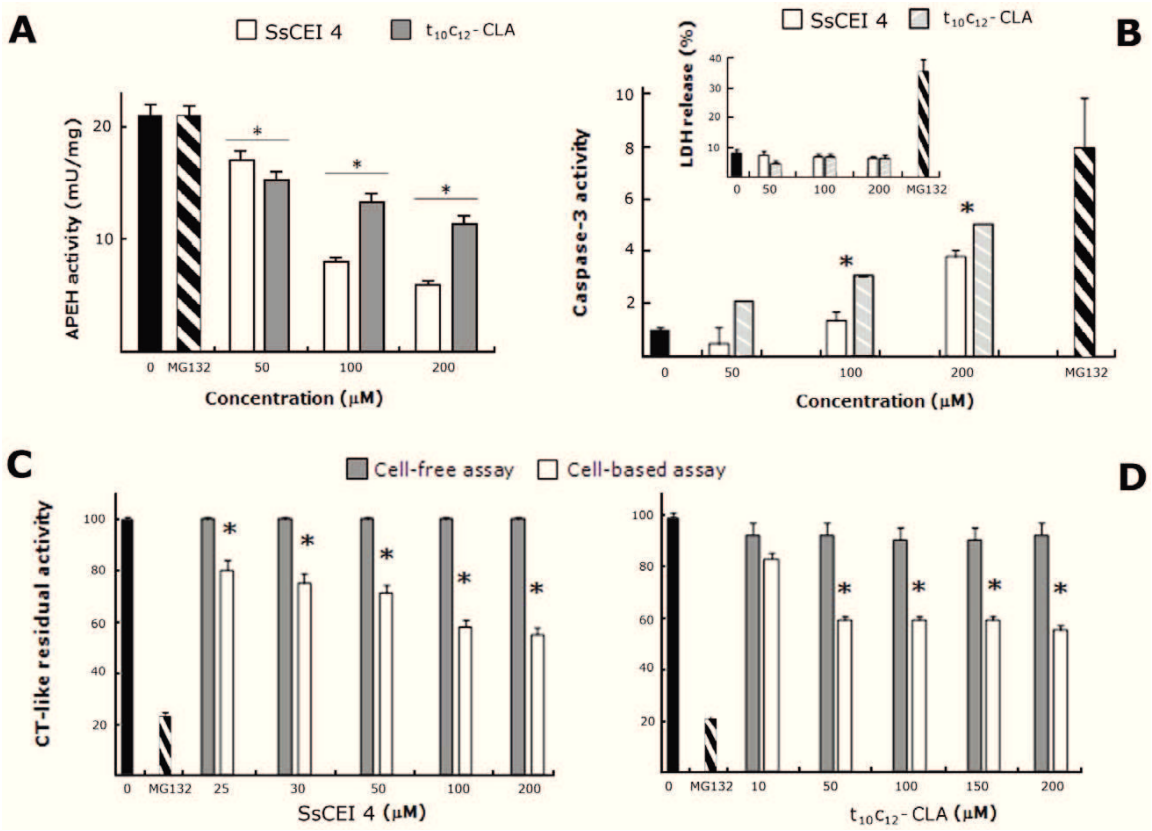

Figure 3. Down-regulation of the proteasome/APEH enzyme system by the SsCEI 4 and $t_{10}c_{12}$-CLA in Caco-2 cells. APEH activity was measured in Caco-2 cells incubated with 50 μM, 100 μM and 200 μM SsCEI 4 (white bars) or $t_{10}c_{12}$-CLA (gray bars) for 48 h (A). Proteasomal CT-like activity was measured in cell-free system (a partially purified proteasome fraction from differentiated Caco-2 cells, gray bars) and in Caco-2 cells (white bars) treated with increasing concentrations of SsCEI 4 (C) or $t_{10}c_{12}$-CLA (D). Caspase-3 activities and LDH release were measured upon 48 h incubations of Caco-2 cells with increasing concentrations of SsCEI 4 (white bars) and $t_{10}c_{12}$-CLA (striped grey bars) (B). The cytotoxic effect of the different treatments was evaluated by measuring the LDH release in the culture media (B insert). Cell-free protein mixtures, or Caco-2 cell cultures, treated with DMSO alone (black bars) or with MG132 (10 μM) (striped black bars) were used as positive controls. The data are expressed as means±SD. *Significantly different ($P<0.005$) from respective controls.
doi:10.1371/journal.pone.0025888.g003

caspase-3 activity, a key effector of apoptosis, was improved at increasing doses of either SsCEI 4 or t10c12-CLA. This was not associated with any cytotoxic effect even at the highest concentration (200 μM), as indicated by the lactate dehydrogenase (LDH) activity levels which remained comparable to those of controls (Figure 3B insert).

Therefore, our results, consistently with the reporting coordinated functions of proteasome and APEH in protein turnover [15], add the relevant information that proteasome modulation could occur via a complex pathway which has APEH like an important and regulative factor. Moreover, since APEH activity is not influenced by cell treatment with the specific PI MG132 (Figure 3A), proteasome modulation should be hierarchically down-stream of APEH inhibition. This view is also corroborated by the observation that APEH and proteasome seem to have no direct interactions, as they are distinctly eluted from gel filtration columns loaded with protein extracts obtained from SsCEI 4-treated or untreated Caco-2 cells (Figure S4). Further investigations aimed at a better understanding of the molecular mechanism underlying the proteasome inhibition by APEH are currently in progress.

The combined use of SsCEI 4 and $t_{10}c_{12}$-CLA improves the inhibition of proteasome activity, triggers apoptosis and increases the level of UPS substrates in Caco-2 cells

To finally confirm the reliability of the APEH-mediated strategy to affect UPS activity, several readouts were evaluated in differentiated Caco-2 cells treated with SsCEI 4 and t10c12-CLA, alone or in combination. Caco-2 cells were incubated for 48 h with SsCEI 4, t10c12-CLA (200 μM), or an equimolar mixture (100 μM each) of both compounds. The commercially inhibitors of APEH (ebelactone) or the proteasome (MG132) were used as positive controls.

Cell exposure to SsCEI 4 or t10c12-CLA saw 40% reduction in the proteasomal CT-like activity, with a more marked decrease (about 73%) resulting from their combined use (Figure 4A). A similar behaviour was observed when APEH activity was monitored (data not shown), which supports the hypothesis of an additive effect (combination index; $CI = 1$) [24] produced by SsCEI 4 and t10c12-CLA on the target protease. However, due to the difficulties in the setting-up the large number of variables which possibly affect the formation of enzyme–inhibitor-substrate complexes, we were unable to reproduce the additive effects on the proteasome or APEH activities in cell-free assays.

To evaluate the pro-apoptotic effects arising from cell exposure to a mixture of SsCEI 4 and t10c12-CLA, we measured caspase-3 and caspase-8 activities as these enzymes have been reported to be essential for the proteasome-induced apoptosis cascade [6,25]. Specifically, caspase-3 was significantly increased by SsCEI 4 or t10c12-CLA (about two-fold in both cases; $P<0.01$), with a further improvement produced by their combination (about four-fold), in comparison to untreated cultures. Although caspase-8 activity was less intense, it showed a profile similar to that of caspase-3, further supporting the view that cell death occurs by an apoptotic mechanism (Figure 4B). These data are in agreement with the well-established association between proteasomal inhibition and apoptosis induction, and confirm the additive effects produced by using a mixture of SsCEI 4 and t10c12-CLA on the caspase cascade in cancer cells. Notably, the toxicity resulting from the APEH-mediated inhibition of proteasome activity, as indicated by the treatment with SsCEI 4, t10c12-CLA or ebelactone, was significantly lower than that observed in culture incubated with MG132 (Figure 4B insert).

Moreover, the immunoblot analysis, showing that the levels of APEH in cells were not affected by any of these treatments, clearly indicated that the APEH down-regulation resulted from an enzyme inhibition process, rather than a reduction in protein expression. Cell exposure to SsCEI 4 and t10c12-CLA, alone or in combination, produced an increase of well-known proteasome substrates (p21Waf1 and NF-κB, two-fold or four-fold, respectively; Figure 4C, D). These findings are consistent with the idea that the relationship between apoptosis and the accumulation of damaged or short-lived regulatory proteins has a prominent role in controlling the homeostasis of cancer cells [22]. Cytoplasmic increase of NF-κB levels is indeed regarded as a major hallmark of apoptotic cells, since NF-κB nuclear translocation, following I-κB degradation by UPS and gene transcription, is a well-established mechanism of cell growth. Proteasome inhibition in cancer cells leads to a reduced rate of I-κB degradation, and to a longer persistence of NF-κB in the cytoplasm [26,27]. In the same way, accumulation of p21Waf1, a negative regulator of the cell division cycle, is a direct evidence of increased apoptosis and of reduced proteasome activity, since it has been reported that its degradation occurs through N-terminal as well as internal lysine ubiquitinylation [28].

Polyubiquitinylated proteins are normally degraded by the cellular proteasomes, and down-regulation of proteasome activity has been shown to substantially suppress bulk intracellular protein turnover [29]. As evidenced in Figure 4E, following incubation with SsCEI 4, t10c12-CLA (alone or in combination), ebelactone or MG132, we detected in cell extract the presence of high-molecular-mass immunoreactive species (66 kDa to 160 kDa) which are absent in untreated cultures. These signals are indicative of polyubiquitin conjugates in the treated cells, confirming that these compounds deregulate UPS activity in cancer cells.

As a whole, our in vitro results demonstrate that APEH inhibition by SsCEI 4 and t10c12-CLA treatments is associated with increased levels of the typical markers of proteasome inhibition without any cytotoxic effect. Although pro-apoptotic activities of CLA mixtures and their ability to induce an increase of the cytoplasm levels of NF-κB and p21Waf1 have been previously reported [30,31], to our knowledge this is the first study showing that their effects are mediated, at least in part, by the APEH/proteasome system, suggesting a possible mechanism by which CLA isomers exert their anticancer activity.

Putative APEH binding site for $t_{10}cis_{12}$-CLA isomer

In light of these outcomes, APEH inhibition represents a novel strategy to regulate proteasome activity, with potential applications in biomedical fields. Knowledge of the enzyme–inhibitor binding sites at the molecular level is pivotal for our understanding of the underlying mechanisms, as well as for the design of novel and more efficient inhibitors. In a previous work [17], the structural model of the inhibition complex APEHSs-SsCEI protein corroborated by mutagenesis studies, indicated an involvement of the SsCEI RSL in the interaction with the active site of the enzyme target. Therefore, it is conceivable to assume that the competitive inhibition of APEHSs by SsCEI 4 peptide occurs through a similar binding-mode.

The surprising down-regulation of APEH by t10c12-CLA and the finding of additional non-competitive APEH binding pockets apart from the active site, prompted us to undertake a molecular modelling study to look for potential APEH-CLA binding sites. Protein-fatty acid docking analyses were carried out starting from the previously reported structural model of APEHSs [17], herein used for the biochemical investigation. The APEHSs 3D model, built on the X-ray structure of APEH from Aeropyrum pernix

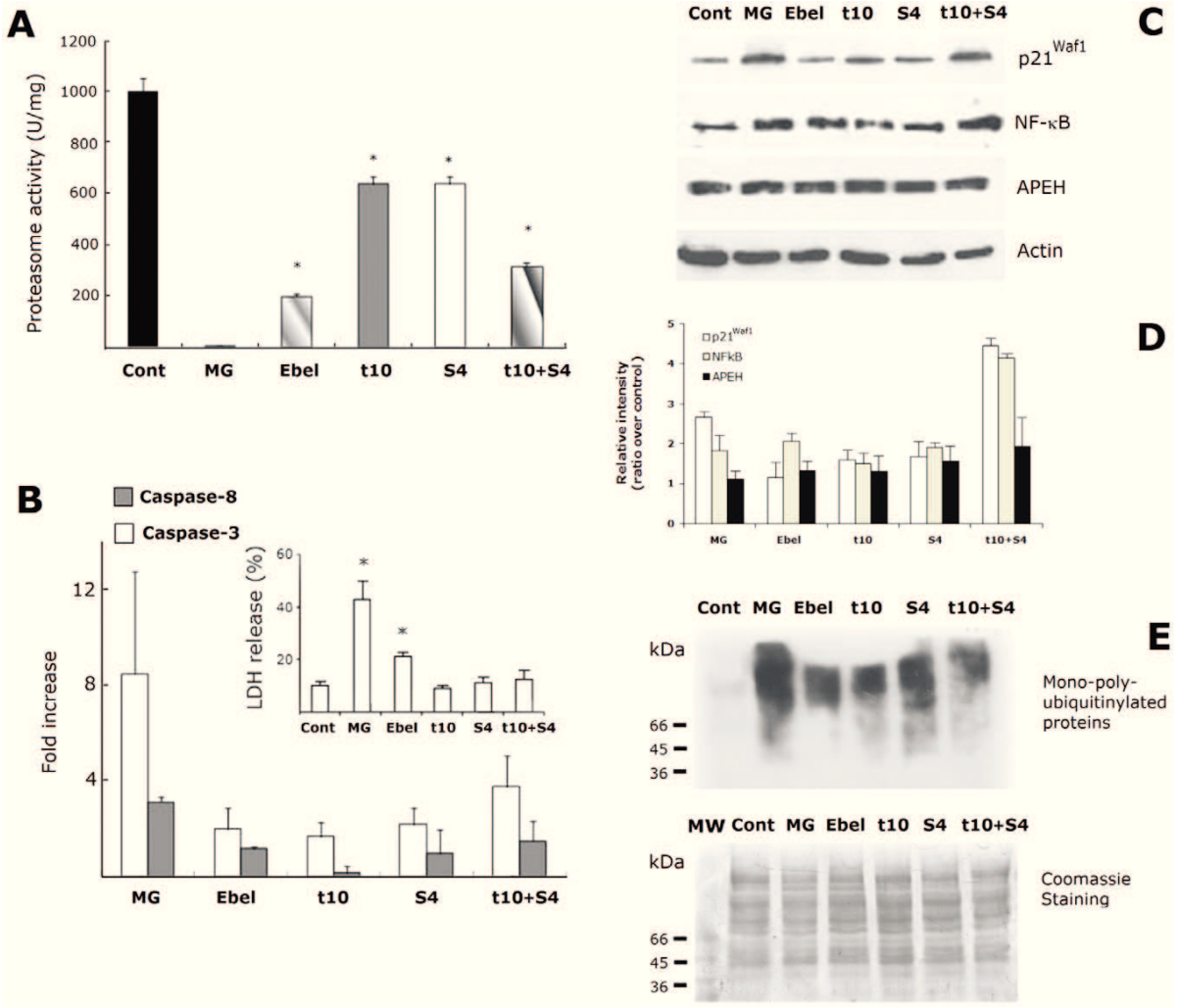

Figure 4. Evaluation of proteasome inhibition markers in Caco-2 cells incubated with SsCEI-4 and $t_{10}c_{12}$-CLA, alone or in combination. Caco-2 cells were treated (48 h) with 10 μM MG132 (MG), 100 μM ebelactone (Ebel), 200 μM SsCEI 4 (S4), $t_{10}c_{12}$-CLA (t10), or with a mixture of both (t10+S4). Cells exposed to DMSO alone were used as the controls (black bar). The data are expressed as means±SD. *Significantly different ($P<0.005$) from the control (A). Caspase-3 (white bars) and caspase-8 (grey bars) activities measured as fold increase in comparison to untreated cells (B). The cytotoxic effect of the different treatments was evaluated by measuring the LDH release in the culture media (B insert). Representative immunoblots of the expression of p21Waf1, NF-κB, and APEH in Caco-2 cell exposed for 48 h to MG, Ebel, S4, t10 or with a mixture of both (t10+S4) (C). Data on Western blot analysis are expressed as the density ratio of target to control (β-actin) in arbitrary units. The values were expressed as average relative intensity as compared to untreated cultures and expressed as means±SD of measurements performed in triplicate (D). Protein ubiquitinylation in Caco-2 cell exposed for 48 h to MG, Ebel, S4, t10 or with a mixture of both (t10+S4) (E, upper panel). Upon the immunodetection, the membrane was stained with Coomassie blue. The lane loaded with molecular mass markers [MW kDa] was shown (lower panel).
doi:10.1371/journal.pone.0025888.g004

[32], shows the typical features of a POP family member: a α/β-hydrolase catalytic domain with the (Ser-Asp-His) catalytic triad, covered by a central tunnel of an unusual β-propeller domain.

Docking calculations were performed by using the AutoDock simulation package [33]. The docked conformations of t10c12-CLA suggested two putative binding modes that were characterised by different anchoring points for the carboxylate group of the CLA isomer: the positively charged side-chains of either R62 or R507. However, the binding involving the residue R507 appeared to be in conflict with the non-competitive inhibition mechanism indicated by the experimental data, as R507 belongs to the active site of APEHSs [17]. Thus we did not consider this binding approach further. binding of t10c12-CLA involving R62 residue of the enzyme is in agreement with the non-competitive mechanism of inhibition resulting from cell-free assays. In this case, t10c12-CLA occupies the β-propeller tunnel, eventually obstructing the passage of the substrate and/or the product (Figure 5). Details of the binding mode involving R62 are shown in Figure 6: t10c12-CLA carboxylate group interacts with the side-chains of R62 and S273 of APEHSs, while the long hydrophobic carbon tail of t10c12-CLA is stabilised by van der Waals interactions with some of the hydrophobic residues that line the β-propeller tunnel of APEHSs.

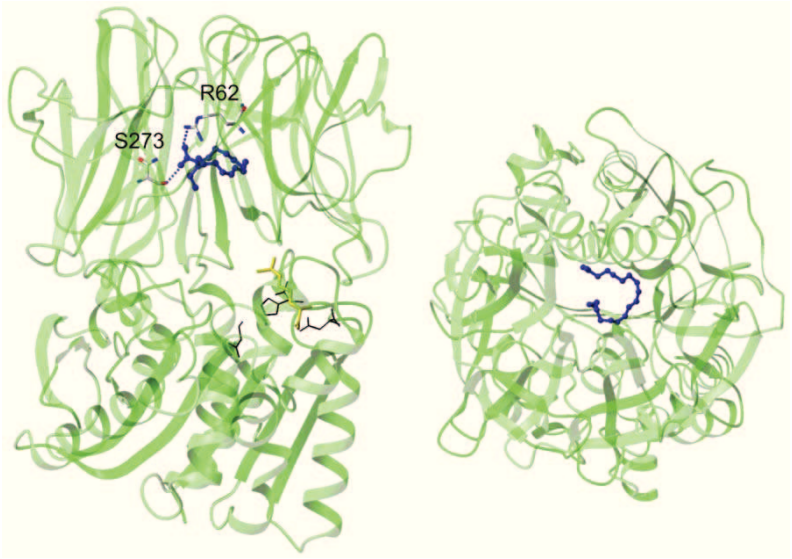

Figure 5. Binding mode of the $t_{10}c_{12}$-CLA with $APEH_{Ss}$. Binding mode suggested by docking analysis for $t_{10}c_{12}$-CLA (blue; ball-and-stick mode) with $APEH_{Ss}$ (cartoon representation; green, left). Protein residues involved in stabilising the interactions with the carboxylic group of the $t_{10}c_{12}$-CLA are represented as sticks. The Ser-Asp-His catalytic triad residues are shown as black lines; R507 is shown in yellow. (right) View rotated 90° along the x-axis (the horizontal axis parallel to the image plane).
doi:10.1371/journal.pone.0025888.g005

Of note, the interaction mechanism suggested by this docking analysis shares common characteristics with the fatty-acid-binding proteins (FABP) [34,35]. X-ray structural studies have shown that the fatty acid molecule binds to the relatively large FABP inner cavity, and is anchored to a positively-charged arginine residue and a polar amino acid (usually serine or threonin), with the hydrophobic tail again stabilised by van der Waals interactions with hydrophobic residues.

The lack of structural information and the difficulty to predict a sufficiently accurate 3D model for any mammalian APEH have prevented us from performing modelling studies on mammalian APEHs. However the functional properties indicate significant similarity between mammalian and archaeal APEHs, showing that both are inhibited by SsCEI 4 peptide in a competitive manner (Figure 1E) or by t10c12-CLA through a non-competitive mechanism (Figure 1F), with comparable Ki values. Therefore, we hypothesise that the enzymes from archaeal and mammalian sources could share some common features in their modes of interaction with these inhibitors suggesting that APEHSs can be used as an initial model system for the early design of novel inhibitors of mammalian APEH.

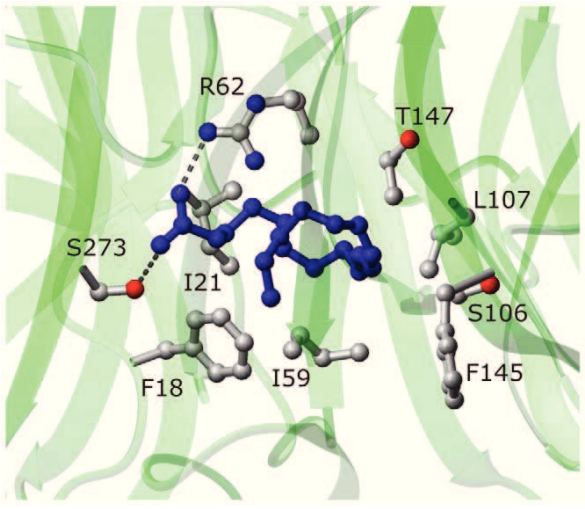

Figure 6. Suggested binding site on $APEH_{Ss}$.by docking analysis for the $t_{10}c_{12}$-CLA (blue; ball-and-stick mode) isomer. The relevant $APEH_{Ss}$ residues are shown in ball-and-stick representation.
doi:10.1371/journal.pone.0025888.g006

Conclusions

Proteasome is an abundant multi-enzyme complex that provides the main pathway for the protein turnover or the elimination of misfolded and aggregated proteins. As such, it controls the levels of proteins involved in cell-cycle progression and apoptosis in normal and malignant cells, and has become an important therapeutic target in anticancer therapies. A large number of specific PI molecules have been developed to date [36], but despite their indisputable efficacies all of these suffer for negative side-effects. These events represent the major drawback of impairing the activity of a target largely involved in physiological processes. For these reasons, several studies have suggested that the targeting of functionally related, up-stream or down-stream proteasome effectors [29], can be an alternative and a safer way to recover proteasome dysfunction associated with pathological conditions [29,37,38].

In this study we showed for the first time that, by using a set of selected APEH inhibitors, proteasome activity can be regulated through an APEH-mediated mechanism which represents a novel strategy to control UPS functions. Beside these findings, we demonstrated that the stable, selective and non toxic inhibitors of APEH (a synthetic peptide and a CLA isomer) are able to produce a noticeable down-regulation of UPS activity in cells. Moreover,

these molecules represent attractive templates for the design of more potent inhibitors, with potential applications as anticancer and anti-inflammatory agents. In addition, the synergistic effects resulting from their combined use strongly suggest that chimeric compounds, including competitive and non-competitive inhibitors, with increased specificity and enhanced activity, can be investigated and developed.

APEH has been postulated to serve as a key regulator of N-terminally acetylated proteins [39] but the biological effects of disrupting APEH has not been completely understood. As more than 80% of proteins in human cells are N-terminal acetylated [40–42] and protein acetylation is implicated in a variety of essential cellular pathways [43], it is thus likely feasible that APEH is involved in these processes.

As reported in previous studies, proteasome and APEH act cooperatively in protein turnover [15,44], although the biochemical mechanisms remain to be clarified. In this regard, in contrast to the general idea that N-terminal acetylation protects from degradation, in certain proteins some sequences which include acetyl groups at the N-terminus were recently found to be involved in degradation signals [45,46]. On the basis of our preliminary results, a direct interaction between APEH and proteasome might be excluded, whereas the hypothesis that APEH can activate or stabilise the proteasome by uncovering the N-tail of a yet unknown negative effector protein cannot be ruled out. Of note, we showed that whereas APEH inhibition triggered an impairment of the proteasome activity, its selective inhibition did not affect APEH functions, likely suggesting that APEH could be an up-stream modulator of the proteasome. Studies aimed at achieving a better understanding of the mechanism/s responsible for the APEH-mediated down-regulation of proteasome and at the evaluation of APEH inhibitors in animal cancer model are currently in progress.

Materials and Methods

Reagents

Pure c_9t_{11}- and $t_{10}c_{12}$-CLA isomers and caspase-3 and -8 fluorometric Assay Kits were purchased from Sigma-Aldrich. DMEM/F12, DMEM, L-glutamine, penicillin-streptomycin and FBS were from Gibco-BRL. Porcine liver APEH was obtained by Takara. Chemicals of the highest purity were from Sigma-Aldrich or Calbiochem.

Peptide design, synthesis and characterisation

The peptides were prepared as amidated derivatives by solid-phase synthesis (synthesis scale, 0.1 mmoles), following standard Fmoc/tBu protocols [47]. A rink amide resin (substitution, 0.57 mmol/g) and amino acid derivatives with standard protection were used in all of the syntheses. Cleavage from the solid support was performed by treatment with a trifluoroacetic acid (TFA)/tri-isopropylsilane/water (90:5:5, v/v/v) mixture for 90 min at room temperature. The crude peptides were precipitated in cold ether, dissolved in a water/acetonitrile (1:1, v/v) mixture and lyophilised. The peptides were purified by reverse-phase HPLC using a semi-preparative 5×1 cm ID C18 monolythic Onyx column, applying a linear gradient of 0.05% TFA in acetonitrile from 10% to 70% over 8 min at a flow rate of 15 μL/min. Peptide purity and identity were confirmed by liquid chromatography–mass spectrometry analysis.

Gel filtration analysis of synthetic peptides

Gel filtration chromatography was performed on a BioSep SEC-S2000 column equilibrated with 50 mM phosphate buffer pH 6.8, at a flow rate of 1.0 mL/min. A standard curve was built using a set of synthetic peptides with molecular weights between 1.500 amu and 2.500 amu. For this purpose, peptide aliquots were injected onto the column and a plot of KD versus log10 molecular weights (MW) was obtained, where KD = (Ve-Vo)/(VT-Vo), Ve is the elution volume of the sample, and VT and Vo are the total and void volumes of the column, respectively.

Circular dichroism spectroscopy

CD spectra were obtained on a Jasco J-715 spectropolarimeter with 400 μL of 8.0×10-7 M protein in 5 mM Tris–HCl pH 7.5. Hellman quartz cells of 0.1-cm-path length were used in the far UV (190–250 nm). The temperature of the sample cell was regulated by a PTC-348 WI thermostat and thermal CD was performed from 250 to 195 nm by raising the cell temperature from 37°C to 77°C. The thermal CD spectra were signal-averaged by combining three scans and the baseline was corrected by subtracting a buffer spectrum. The samples were then cooled back to 37°C to monitor the final folding of the peptides.

Purification of APEHs and proteasome

APEH from Sulfolobus solfataricus was purified as previously reported [17]. Partial purification of human APEH and proteasome was carried out from protein extracts of Caco-2 cell. Briefly, protein extracts (500 μg) were fractionated by gel filtration chromatography on a Superdex 200 PC 3.2/30 column connected to a SMART System (Pharmacia) equilibrated in buffer 50 mM Tris-HCl, pH 7.5, 100 mM NaCl, at 0.1 mL/min. The eluted fractions were assayed using the specific substrates for APEH and the proteasome. The active fractions were collected and used for further analysis.

Enzyme assays

Porcine liver APEH activity was measured spectrophotometrically using the chromogenic substrate acetyl-Ala-pNA (Bachem). The reaction mixture (1 mL) containing pure APEH (38 ng) or an appropriate amount of cell extract in 50 mM Tris-HCl buffer pH 7.5 (Tris Buffer), was preincubated at 37°C for 2 min. Then, 1 mM acetyl-Ala-pNA was added and the release of p-nitroanilide (ε410 = 8800 M-1 cm-1) was measured by recording the absorbance increase at 410 nm on a Cary 100 Scan (Varian) UV/Vis spectrophotometer, equipped with a thermostated cuvette compartment. APEH activity was expressed in IU. The APEHSs activity was measured using acetyl-Leu-pNA (0.1 mM) (Sigma) as substrate. The reaction mixture (1 mL) containing the appropriate amount of enzyme in 25 mM Tris-HCl buffer pH 7.5, was preincubated at 80°C for 2 min. Then, 0.1 mM acetyl-Leu-pNA was added and the release of p-nitroanilide was measured, following the standard assay procedure described above.

The synthetic fluorescent substrate N-succinyl-Leu-Leu-Val-Tyr-7-amido-4-methylcoumarin (N-Suc-LLVT-AMC) was used for the measurement of the CT-like activity of the proteasome, at a final concentration of 0.080 mM. The reaction mixture (0.9 mL) containing appropriate amount of proteasome was preincubated as above, in Tris buffer. N-Suc-LLVT-AMC was added, and the release of the fluorescent product (7-AMC) was monitored for 5 min in a Perkin–Elmer LS 50B fluorimeter. The excitation and emission wavelengths were 380 nm and 460 nm, respectively.

The carboxypeptidase Y, elastase, thrombin, trypsin and subtilisin activities were also evaluated according to previously published methods [18].

Enzyme inhibitory assays

Protease inhibitor activities of the SsCEI peptides and the CLA isomers were carried out using a fixed amount of APEH or

partially purified proteasome (3–5 nM and 0.12 mg/mL, respectively), and increasing the SsCEI and CLA isomer concentrations. Mixtures were pre-incubated for 30 min at 37°C before the addition of the substrate, and the enzymatic activities were followed as described above. Protease inhibitor activities of the SsCEI peptides and the CLA isomers were determined towards APEHSs. The protease and increasing concentrations of the inhibitors were mixed and preincubated for 30 min at 80°C before the addition of the specific substrate. The residual enzymatic activity was determined using the assay procedure described above.

The time-dependent inhibition of SsCEI 4 and t10c12-CLA towards APEH was assessed. Mixtures containing appropriate amounts of each inhibitor and of APEH were pre-incubated for 20 min at 37°C; they were then diluted (1:5) into the standard assay mixture, which contained the substrate only. The enzymatic activity was followed as described above. Control samples were prepared by pre-incubating the same amounts of APEH without the inhibitors and then diluted in the standard assay mixture.

The additive effects elicited by cell exposure to SsCEI 4 and t10c12-CLA was calculated accordingly to the Chou and Talalay equation (CI = D1/[(DM)1×[fa/(1-fa)]1/m1+D2/[DM2×[fa/(1-fa)] 1/m2) [24].

HPLC analysis of SsCEI peptides incubated with the target enzyme

The experiments were conducted at 37°C in 50 mM Tris buffer, pH 7.5. Solutions of SsCEI 4 and porcine APEH were incubated for up to 2 h at optimal concentrations (4 μM SsCEI 4 and 100 μM APEH) to guarantee a high degree of enzymatic inhibition. At specific time intervals, 195 μL aliquots were taken, and the reaction was stopped by addition of 5 μL TFA. The samples were then analysed directly by reverse-phase HPLC (Dionex BioLC) on a μBondapak C18 column (3.9×300 mm, Waters), eluted with a linear gradient (0–60% acetonitrile in 0.1% TFA) at a flow rate of 1 ml/min. Control peptide samples were incubated in the absence of the purified enzymes and run in parallel.

Antibodies

The following antibodies were used: anti-APEH antibody (sc-102311; Santa Cruz Biotechnology); anti-NF-κB/p65 antibody (Thermo Scientific); anti-p21Waf1 antibody (Exbio); pan Ab-5 anti-actin antibody (clone ACTN05, Thermo Scientific); and monoclonal antibodies against polyubiquitinylated proteins conjugated with horseradish peroxidase (FK2H, Enzo, Life Science). The ΔF508CFTR-3HA protein was detected with an anti HA monoclonal antibody (Covance).

Cell culture

BHK cells stably expressing CFTR-M (kindly donated by Dr. David Y Thomas, McGill University Montreal Canada) were cultured in DMEM/F12, 5% FBS, 1 mM L-glutamine, 200 μg/mL methotrexate, and 100 units/mL penicillin-streptomycin, at 37°C in a humidified 5% CO2 atmosphere. The cells were plated in 12-well plates, to a confluence of 60% for the 24-h incubations, and 40% for 48-h exposure to PIs. These treatments were initiated 24-h after the plating of the cells. Phase-contrast images of the cells were taken just before the lysis of the cells for protein analysis, using a Lica DM6000 inverted microscope.

Caco-2 cells (ATCC) were cultivated in DMEM supplemented with 10% FBS, 1 mM glutamine and 100 units/mL penicillin-streptomycin at 37°C in a humidified 5% CO2 atmosphere. The cells were studied between passages 12 and 22. The cells were split using trypsin-EDTA solution and plated in 6-well plates at a density of 8×104 cells/mL and the medium was replaced every 2–3 days. Under these conditions, the cells reached visual confluence after 7 days and the differentiated stage two weeks later. The differentiated cells were incubated for 48 h with the different substances.

Protein extraction and Western blotting analysis

Following the treatments, the BHK and Caco-2 cells were washed three times with ice cold phosphate-buffered saline and collected immediately at 4°C in lysis buffer (1% Triton X-100, 0.1% SDS, 20 mM Tris-HCl, pH 8.0, 150 mM NaCl, 0.5% sodium deoxycholate and complete protease inhibitors [Roche]). The lysates were centrifuged at 10,000×g for 15 min at 4°C. The protein concentrations in the clear supernatants were determined (BCA protein assay reagent kit; Pierce) before their use in enzymatic assays or SDS–PAGE. In brief, for Western blotting, aliquots were run on SDS-PAGE (8% or 12.5%) and then electroblotted onto nitrocellulose (Schleicher & Schuell) or PVDF membranes (Immobilon^{TM}, Millipore). The membranes were next incubated with primary antibodies and then with the appropriate dilution of secondary antibody (1 h at 37°C). At the end of this time, the immunocomplexes formed were visualised by enhanced chemiluminescence and autoradiography according to the manufacturer protocol (Amersham Biosciences) and quantified by densitometric analysis with ChemiDoc XRS (Bio-Rad). Protein expression data was quantified with Quantity One Software (Bio-Rad).

Apoptosis assays

The pro-apoptotic ability of the peptides and the CLA isomers were assayed by measuring the caspase-3 and caspase-8 activities using fluorometric kits, according to the manufacturer instructions. These assays were based on hydrolysis of the substrate acetyl-Asp-Glu-Val-Asp-7-amido-4-methylcoumarin (Ac-DEVD-AMC) or acetyl-Ile-Glu-Thr-Asp-7-amino-4-methyl coumarin (Ac-IETD-AMC) by caspase-3 and caspase-8, respectively. The release of the 7-AMC moiety in protein extracts prepared from the differently treated cells was evaluated by fluorimetry (excitation 360 nm, emission 460 nm). Their amounts were calculated by means of a standard curve prepared with pure AMC, and following normalisation for protein content, the activities were expressed as nmoles AMC/mg protein/min.

Cytotoxicity assay

The release of LDH was used as the marker for cell toxicity [48]. The culture supernatants were sampled at the end of the incubations and centrifuged (4,000×g, 5 min, and 4°C). Aliquots of the clear supernatant (10 μL) were incubated with 190 μL reaction buffer (200 mM Tris/HCl, pH 8.0, 0.7 mM p-iodonitrotetrazolium violet, 50 mM L-lactic acid, 0.3 mM phenazine methoxysulphate, 0.4 mM NAD,) for 30 min at 37°C. Absorbance was measured at 490 nm and the results were expressed as percentages of total LDH release from control cultures treated with 1% (w/v) Triton X-100 and calculated as: [(experimental value - blank value)/(total lysis -blank value)−100].

Docking calculations

The AutoDock (version 4.0) programme package [33] was chosen to dock t10c12-CLA into the large inner cavity of the APEHSs enzyme. The previously reported atomic coordinates of the APEHSs model [17], were used in the calculations. Amber

charges and polar hydrogens were added to the protein using the PDB2PQR server (http://pdb2pqr-1.wustl.edu/pdb2pqr/). The ligand coordinates were generated by the PRODRG server (http://davapc1.bioch.dundee.ac.uk/prodrg/), and subsequently energy minimised using the Insight II package; atom charges and active torsions were defined using AutoDockTools. Affinity grids with dimensions 80×80×90 points (with spacings of 0.375 Å) were centred approximately in the middle of the enzyme β-propeller central tunnel and were large enough to cover the entire inner cavity of the enzyme subunit. The Lamarckian genetic algorithm and the pseudo-Solis and Wets methods were used for the conformational search. The maximum number of energy evaluations was set to 2.5×107 and a maximum number of 2.7×105 genetic algorithm operations were generated on a single population of 150 individuals. The operator weights for crossover, mutation, and elitism were set as the default parameters: 0.80, 0.02, and 1.0, respectively. One hundred runs were performed. The resultant docked conformations of the ligand were clustered and ranked according to the default AutoDockTools scoring function using a RMSD deviation of 3.5 Å. The MOLMOL programme was used for the molecular visualisation and analysis [49].

Small interfering RNA transfection

The siRNA is purchased from Sigma (siRNAID SASI_Hs01_00240856 and SASI_Hs01_00240857), and CFBE41o-DF espressing ΔF508 CFTR were kindly provided by Dr. J. P. Clancy Department of Pediatrics, the University of Alabama at Birmingham, Birmingham, AL, USA. CFBE41o-DF cells at 5×104 cells/well were cultured over-night on 12-well plates and transfected 24 h after with APEH siRNA at a final concentration of 50 nM. using Lipofectamine 2000, according to the manufacturer's instruction. Non-targeting siRNA was used as a negative control. After 72 hours of transfection, cells are lysed in RIPA buffer and protein levels were determined by western blotting

Statistical analysis

All data were obtained from triplicate analyses of three different preparations. Data were presented as means ±S.D. Statistical analysis and IC50 values were calculated with the SigmaPlot 10.0 software through a non-linear curve-fitting method and using a simple binding isotherm equation. Groups were compared by Student's t test, and $P<0.05$ was considered as significant.

Supporting Information

Figure S1 Amino acid sequence of SsCEI protein.
(PDF)

Figure S2 Far-UV CD spectra of the SsCEI peptides at different temperatures.
(PDF)

Figure S3 Binding of increasing concentration of the SsCEI peptides (as indicated) to a-chymotrypsin.
(PDF)

Figure S4 Gel filtration chromatography on a Superdex 200 column of protein extract from Caco-2 cells treated with 200 μM of SsCEI 4.
(PDF)

Author Contributions

Conceived and designed the experiments: GP PB MRu AL. Performed the experiments: GP PB MG AS EL RH. Analyzed the data: GP PB MRo. Contributed reagents/materials/analysis tools: MRo MS. Wrote the paper: GP PB MRu.

References

1. Ciechanover A (2005) Proteolysis: from the lysosome to ubiquitin and the proteasome. Nat Rev Mol Cell Biol 6: 79–87.
2. Schwartz AL, Ciechanover A (2009) Targeting proteins for destruction by the ubiquitin system: implications for human pathobiology. Annu Rev Pharmacol Toxicol 49: 73–96.
3. Shah IM, Di Napoli M (2007) The ubiquitin-proteasome system and proteasome inhibitors in central nervous system diseases. Cardiovasc Hematol Disord Drug Targets 7: 250–273.
4. Rajkumar SV, Richardson PG, Hideshima T, Anderson KC (2005) Proteasome inhibition as a novel therapeutic target in human cancer. J Clin Oncol 23: 630–639.
5. Naujokat C, Sezer O, Zinke H, Leclere A, Hauptmann S, et al. (2000) Proteasome inhibitors induced caspase-dependent apoptosis and accumulation of p21WAF1/Cip1 in human immature leukemic cells. Eur J Haematol 65: 221–236.
6. Drexler HCA (1997) Activation of the cell death program by inhibition of proteasome function, Proc Natl Acad Sci USA 94: 855–860.
7. Palombella VJ, Rando OJ, Goldberg AL, Maniatis T (1994) The ubiquitinproteasome pathway is required for processing the NF-κB1 precursor protein and the activation of NF-κB. Cell 78: 773–785.
8. Nencioni A, Grunebach F, Patrone F, Ballestrero A, Brossart P (2007) Proteasome inhibitors: antitumor effects and beyond. Leukemia 21: 30–36.
9. Vlahakis SR, Badley AD (2006) Influence of proteasome inhibitors on apoptosis. Curr Opin Clin Nutr Metab Care 9: 42–47.
10. Orlowski RZ, Kuhn DJ (2008) Proteasome Inhibitors in Cancer Therapy: Lessons from the First Decade. Clin Cancer Res 14: 1649–1657.
11. Landis-Piwowar KR, Milacic V, Chen D, Yang H, Zhao Y, et al. (2006) The proteasome as a potential target for novel anticancer drugs and chemosensitizers. Drug Resist Updat 9: 263–273.
12. Serini S, Piccioni E, Merendino N, Calviello G (2009) Dietary polyunsaturated fatty acids as inducers of apoptosis: implications for cancer. Apoptosis 14: 135–152.
13. Park Y (2009) Conjugated linoleic acid (CLA): Good or bad trans fat? J Food Compos Anal 22S: S4–S12.
14. Hamel FG (2009) Preliminary report: inhibition of cellular proteasome activity by free fatty acids. Metabolism 58: 1047–1049.
15. Shimizu K, Kiuchi Y, Ando K, Hayakawa M, Kikugawa K (2004) Coordination of oxidized protein hydrolase and the proteasome in the clearance of cytotoxic denatured proteins. Biochem Biophys Res Commun 324: 140–146.
16. Scaloni A, Jones W, Pospischil M, Sassa S, Schneewind O, et al. (1992) Deficiency of acylpeptide hydrolase in small-cell lung carcinoma cell lines. J Lab Clin Med 120: 546–552.
17. Palmieri G, Langella E, Gogliettino M, Saviano M, Pocsfalvi G, et al. (2010) A novel class of protease targets of phosphatidylethanolamine-binding proteins (PEBP): a study of the acylpeptide hydrolase and the PEBP inhibitor from the archaeon Sulfolobus solfataricus. Mol Biosyst 6: 2498–2507.
18. Palmieri G, Catara G, Saviano M, Langella E, Gogliettino M, et al. (2009) First Archaeal PEPB-Serine Protease Inhibitor from Sulfolobus solfataricus with Noncanonical Amino Acid Sequence in the Reactive-Site Loop. J Proteome Res 8: 327–334.
19. Ponticelli S, Marasco D, Tarallo V, Albuquerque RJ, Mitola S, et al. (2008) Modulation of angiogenesis by a tetrameric tripeptide that antagonizes vascular endothelial growth factor receptor 1. J Biol Chem 283: 34250–34259.
20. Cheng SH, Gregory RJ, Marshall J, Paul S, Souza DW, et al. (1990) Defective intracellular transport and processing of CFTR is the molecular basis of most cystic fibrosis. Cell 63: 827–834.
21. Ward CL, Omura S, Kopito RR (1995) Degradation of CFTR by the ubiquitin-proteasome pathway. Cell 83: 121–127.
22. Jensen TJ, Loo MA, Pind S, Williams DB, Goldberg AL, et al. (1995) Multiple proteolytic systems, including the proteasome, contribute to CFTR processing. Cell 83: 129–135.
23. Busse A, Kraus M, Na IK, Rietz A, Scheibenbogen C, et al. (2008) Sensitivity of tumor cells to proteasome inhibitors is associated with expression levels and composition of proteasome subunits. Cancer 112: 659–670.
24. Chou TC, Talalay P (1984) Quantitative analysis of dose-effect relationships: the combined effects of multiple drugs or enzyme inhibitors. Adv Enzyme Regul 22: 27–55.
25. Suzuki Y, Nakabayashi Y, Takahashi R (2001) Ubiquitin-protein ligase activity of X-linked inhibitor of apoptosis protein promotes proteasomal degradation of caspase-3 and enhances its anti-apoptotic effect in Fas-induced cell death. Proc Natl Acad Sci USA 98: 8662–8667.

26. Hideshima T, Chauhan D, Richardson P, Mitsiades C, Mitsiades N, et al. (2002) NF-kappa B as a therapeutic target in multiple myeloma. J Biol Chem 277: 16639–16647.
27. Wertz IE, Dixit VM (2010) Signaling to NF-kappaB: regulation by ubiquitination. Cold Spring Harb Perspect Biol 2010 Mar;2(3): a003350. (Ed. Louis M. Staudt and Michael Karin).
28. Bloom J, Amador V, Bartolini F, DeMartino G, Pagano M (2003) Proteasome-mediated degradation of p21 via N-terminal ubiquitinylation. Cell 115: 71–82.
29. Moore HE, Davenport EL, Smith EM, Muralikrishnan S, Dunlop AS, et al. (2009) Aminopeptidase inhibition as a targeted treatment strategy in myeloma. Mol Cancer Ther 8: 762–770.
30. Wahle KWJ, Heys SD, Rotondo D (2004) Conjugated linoleic acids: are they beneficial or detrimental to health? Progr Lipid Res 43: 553–587.
31. Reynolds CM, Roche HM (2010) Conjugated linoleic acid and inflammatory cell signalling. Prostaglandins Leukot Essent Fatty Acids 82: 199–204.
32. Bartlam M, Wang G, Yang H, Gao R, Zhao X, et al. (2004) Crystal structure of an acylpeptide hydrolase/esterase from Aeropyrum pernix K1. Structure 12: 1481–1488.
33. Morris GM, Goodsell DS, Halliday RS, Huey R, Hart WE, et al. (1998) Automated docking using Lamarckian genetic algorithm and an empirical binding free energy function. J Comput Chem 19: 1639–1662.
34. Sacchinettini JC, Scapin G, Gopaul D, Gordon JI (1992) Refinement of the structure of Escherichia coli-derived rat intestinal fatty acid binding protein with bound oleate to 1.75-A resolution. Correlation with the structures of the apoprotein and the protein with bound palmitate. J Biol Chem 267: 23534–45.
35. Hamilton JA (2004) Fatty acid interactions with proteins: what X-ray crystal and NMR solution structures tell us. Progr Lipid Res 43: 177–99.
36. Nencioni A, Grünebach F, Patrone F, Ballestrero A, Brossart P (2007) Proteasome inhibitors: antitumor effects and beyond. Leukemia 21: 30–36.
37. Saric T, Graef CI, Goldberg AL (2004) Pathway for degradation of peptides generated by proteasomes: a key role for thimet oligopeptidase and other metallopeptidases. J Biol Chem 279: 46723–46732.
38. Ichinose Y, Genka K, Koike T, Kato H, Watanabe Y, et al. (2003) Randomized double-blind placebo controlled trial of bestatin in patients with resected stage I squamous-cell carcinoma. J Natl Cancer Inst 95: 605–610.
39. Perrier J, Durand A, Giardina T, Puigserver A (2005) Catabolism of intracellular N-terminal acetylated proteins: involvement of acylpeptide hydrolase and acylase. Biochimie 87: 673–685.
40. Arnesen T, Van Damme P, Polevoda B, Helsens K, Evjenth R, et al. (2009) Proteomics analyses reveal the evolutionary conservation and divergence of N-terminal acetyltransferases from yeast and humans. Proc Natl Acad Sci U S A 106: 8157–8162.
41. Goetze S, Qeli E, Mosimann C, Staes A, Gerrits B, et al. (2009) Identification and functional characterization of N-terminally acetylated proteins in Drosophila melanogaster. PLoS Biol 7: e1000236.
42. Boissel JP, Kasper TJ, Bunn HF (1988) Cotranslational amino-terminal processing of cytosolic proteins. Cell-free expression of site-directed mutants of human hemoglobin. J Biol Chem 263: 8443–8449.
43. Kouzarides T (2000) Acetylation: a regulatory modification to rival phosphorylation? EMBO J 19: 1176–1179.
44. Shimizu K, Fujino T, Ando K, Hayakawa M, Yasuda H, et al. (2003) Overexpression of oxidized protein hydrolase protect COS-7 cells from oxidative stress-induced inhibition of cell growth and survival. Biochem Biophys Res Commun 304: 766–771.
45. Ben Saadon R, Fajerman I, Ziv T, Hellman U, Schwartz AL, et al. (2004) The tumor suppressor protein p16(INK4a) and the human papillomavirus oncoprotein-58 E7 are naturally occurring lysine-less proteins that are degraded by the ubiquitin system. Direct evidence for ubiquitination at the N-terminal residue. J Biol Chem 279: 41414–41421.
46. Hwang CS, Shemorry A, Varshavsky A (2010) N-terminal acetylation of cellular proteins creates specific degradation signals. Science 327: 973–977.
47. Fields GB, Noble RL (1990) Solid phase peptide synthesis utilizing 9-fluorenylmethoxycarbonyl amino acids. Int J Pept Protein Res 35: 161–214.
48. Decker T, Lohmann-Matthes ML (1988) A quick and simple method for the quantitation of lactate dehydrogenase release in measurements of cellular cytotoxicity and tumor necrosis factor (TNF) activity. J Immunol Methods 115: 61–69.
49. Koradi R, Billeter M, Wüthrich K (1996) MOLMOL: a program for display and analysis of macromolecular structures. J Mol Graph 14: 51–5, 29–32.

Journal of Medicinal Chemistry

Article

pubs.acs.org/jmc

Small Peptide Inhibitors of Acetyl-Peptide Hydrolase Having an Uncommon Mechanism of Inhibition and a Stable Bent Conformation

A. Sandomenico,[†] A. Russo,[†] G. Palmieri,[‡] P. Bergamo,[§] M. Gogliettino,[‡] L. Falcigno,[†,⊥] and M. Ruvo,*[,†]

[†]Istituto di Biostrutture e Bioimmagini, CNR, via Mezzocannone 16, 80134, Napoli, Italy

[‡]Istituto di Biochimica delle Proteine, CNR, via P. Castellino, 111, 80132, Napoli, Italy

[§]Istituto di Scienze degli Alimenti, CNR, via Roma 64, 83100, Avellino, Italy

[⊥]Dipartimento di Scienze Chimiche, Università di Napoli Federico II, via Cinthia, 80143, Napoli, Italy

Supporting Information

ABSTRACT: Acyl peptide hydrolase (APEH) catalyzes the removal of acetyl-amino acids from the N-terminus of peptides and cytoplasmic proteins. Due to the role played in several diseases, and to the growing interest around N-terminal acetylation, studies on APEH structure, function, and inhibition are attracting an ever increasing attention. We have therefore screened a random tetrapeptide library, N-capped with selected groups, and identified a trifluoroacetylated tetrapeptide (CF_3-lmph) which inhibits the enzyme with a K_i of 24.0 ± 0.8 μM. The inhibitor is selective for APEH, shows an uncommon uncompetitive mechanism of inhibition, and in solution adopts a stable bent conformation. CF_3-lmph efficiently crosses cell membranes, blocking the cytoplasmic activity of APEH; however, it triggers a mild pro-apoptotic effect as compared to other competitive and noncompetitive inhibitors. The unusual inhibition mechanism and the stable structure make the new compound a novel tool to investigate enzyme functions and a useful scaffold to develop more potent inhibitors.

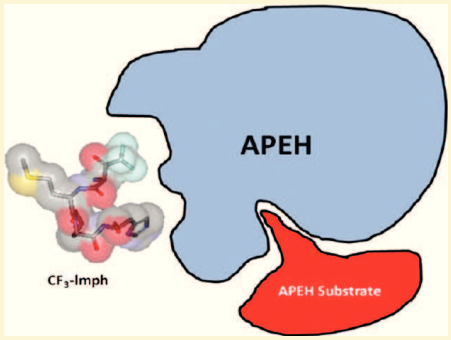

INTRODUCTION

Acyl peptide hydrolase (APEH) is a ubiquitous enzyme that belongs to the prolyl-oligopeptidase (POP) family of proteins. It mostly catalyzes the removal of *N*-acetyl-amino acids from the N-terminus of short peptides deriving from protein degradation processes and bearing residues with small hydrophobic side chains on position 1.[1] It has been also postulated for many years that it could be a key regulator of protein N-terminal acetylation; however, only very recently it has been shown that APEH can process a large set of full length cytoplasmic proteins, thus suggesting that their structure and function can be tightly regulated by the activity of this enzyme.[2] Indeed, treatment of cells with potent and highly specific APEH inhibitors leads to an accumulation of N-terminal acetylated proteins over the nonacetylated variants and to a sustained proliferation of mouse T cells, an effect not observed in untreated cells. Because a relevant fraction of cellular proteins is N-terminally acetylated[3] and this modification plays a critical role in the protein folding/misfolding process, thus on protein fate,[4] an obvious involvement of APEH in the protein turnover mechanism has been also hypothesized.[2,5]

We have recently demonstrated that APEH can influence the activity of proteasomes,[6] a well-established target for a number of cancer diseases, including multiple myeloma.[7,8] APEH inhibitors have a potential as antitumor agents working as indirect regulators of the proteasome activity or more in general of the ubiquitin proteasome system (UPS).[5,9] In particular, we have reported that competitive inhibitors of APEH derived from the reactive site loop (RSL) of the first protein inhibitor of APEH isolated from the archaeon *Sulfolobus solfataricus*, SsCEI,[10] block the enzyme activity by a mechanism that leads to a concomitant downregulation of proteasome function, inducing a potent pro-apoptotic stimulus in human colon carcinoma cells (Caco-2). Remarkably, the same effects are seen using, alone or in combination with the peptide inhibitor, the $trans_{10}$-cis_{12} isomer of conjugated linoleic acid (CLA), which instead shows a noncompetitive mechanism of APEH inhibition. These findings open a new important perspective for the development of APEH inhibitors, especially in the field of multiple myeloma, an incurable tumor disease whose current treatments are mainly based on the use of proteasome inhibitors.[6] A further important role for APEH has been hypothesized in neurodegenerative diseases, such as Alzheimer's disease (AD), because administration of the acetylcholinesterase inhibitor dichlorvos to rat hippocampal slices also efficiently inhibits enzyme activity, and this correlates with improved synaptic efficacy.[11]

Received: October 7, 2011

   dx.doi.org/10.1021/jm2013375 | J. Med. Chem. XXXX, XXX, XXX–XXX

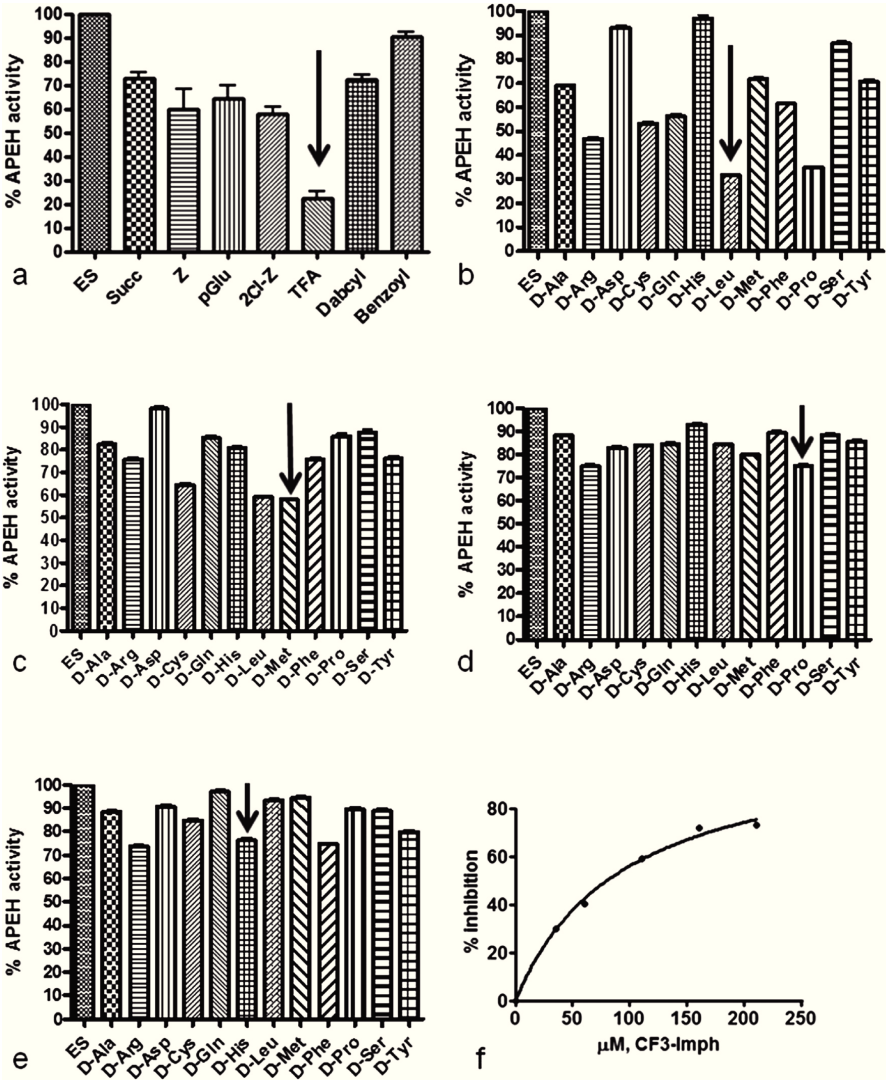

Figure 1. Iterative screening of the Yi-X1-X2-X3-X4 library to identify APEH inhibitors. The library was assembled in a simplified format (see Marasco et al.[12]) using a reduced set of residues accounting for all the different chemical groups present on natural amino acid side chains. D-Amino acids were used to obtain enzymatically stable peptides. Also the N-terminus was modified by a set of carboxylic acids in order to explore the chemical space around the N-terminus where APEH is known to operate. In part a, a plot with inhibition by the first sublibraries, distinguishable by the different carboxylic acids on the N-terminus, is reported. In part b, a plot with inhibition by the second set of sublibraries all N-terminally trifluoroacetylated, distinguishable by the different residues on position X1, is reported. In part c, a plot with inhibition by the third set of sublibraries, all having in common TFA-D-Leu, distinguishable by the different residues on position X2, is reported. In part d, a plot with inhibition by the fourth set of sublibraries, all having in common TFA-D-Leu-D-Met, distinguishable by the different residues on position X3, is reported. In part e, a plot with inhibition by the fifth set of sublibraries, all having in common TFA-D-Leu-D-Met-D-Pro, distinguishable by the different residues on position X4, is reported. In part f, the binding of TFA-D-Leu-D-Met-D-Pro-D-His to porcine liver APEH using acetyl-Ala-pNA as substrate is reported. The hyperbolic curve indicates the best fit for the percentage inhibition data obtained, and the IC_{50} value was calculated from the graph.

To further investigate the role played by APEH and their inhibitors on cell activity, we have undertaken the screening of a random library made of short synthetic peptides to select new compounds able to modulate the enzyme functions. Peptides are particularly suitable for this purpose for their capability to mimic the structures of natural substrates and of modulating enzyme activity by different mechanisms; in particular, small linear peptides could best fit in catalytic pockets and, given the high flexibility, they can adopt suitable conformations in an effective and timely way. Random screenings are very useful in this instance, as the protein structure is unknown and inhibitors cannot be designed on a rational basis. In addition, libraries of small peptides made of three to four residues and containing only subsets of amino acids are of particular interest for the rapid identification of small hits, which more favorably can be converted to more rigid and stable organic scaffolds.[12]

In this study, we have identified N-terminally modified small peptides (average MW 500−600 amu), selected from completely random synthetic libraries, which inhibit APEH in a very specific manner. The most active molecule also exhibits an uncommon mechanism of inhibition and a bent conformation induced by the presence of a D-proline on

dx.doi.org/10.1021/jm2013375 | J. Med. Chem. XXXX, XXX, XXX−XXX

position 3. The peptide is not toxic compared to the commercially available APEH inhibitor ebelactone, efficiently crosses cell membranes, and blocks the activity of APEH in cancer cells. Although it exhibits only minor effects on cell proliferation and caspase 3 activity, its novel mechanism of action opens new perspectives for the understanding of the cellular processes involving APEH and the mechanisms associated to the parallel inhibition of proteasome activity.[6]

RESULTS

Library Preparation and Characterization. After the synthesis of the first library, an average 10 mg amount of material was obtained. Assuming an average MW of 600 amu and considering the synthesis scale of 20 μmoles, a rough 83% yield could be calculated. Data from amino acid analysis of peptide pools performed on the first (complexity 12^4 = 20 736 peptides) and second library (complexity 12^3 = 1728 peptides) were in agreement with a pretty equimolar distribution of peptide components within the mixtures. The third library (complexity 12^2 = 144 peptides) was not characterized. LC-MS analysis of a 12-component mixtures also suggested that peptide components were essentially at the same concentration within mixtures. The synthesis of single peptides proceeded very smoothly. After HPLC purification, an average 50% yield was obtained. After semipreparative purification, tetrapeptides were all >95% pure, as determined by RP-HPLC as well as LC-MS analyses.

Library Screening. After the first screening step, the sublibrary trifluoroacetylated on the N-terminus was selected as the most active in inhibiting the APEH activity. It indeed provided an overall 78% enzyme inhibition at a concentration of 200 μM (see Figure 1a).

From the screening of the second library, tested at 40 μM, pools having D-Leu, D-Pro, and D-Arg on position X1 were selected as the most active. They provided inhibition of 67%, 64%, and 51%, respectively (Figure 1b). Testing of these sublibraries in a range of concentrations between 10 and 200 μM allowed the selection of the library with D-Leu as the most active (not shown). The 12 pools of the third library with TFA and D-Leu at the N-terminus were assayed at 100 μM. Pools with D-Cys(Acm), D-Met, and D-Leu were selected for the dose–response test and, as shown in Figure 1c, the library with D-Met on the X2 position was then selected for resynthesis. The 12 pools of the fourth library having the N-terminal common sequence TFA-D-Leu-D-Met were tested at 50 μM. In this assay, only pools with D-Pro and D-Arg on position X3 inhibited the enzyme (both 21%, Figure 1d). A dose–response test allowed selection of the pool with D-Pro as the candidate for resynthesis (not shown). The fifth library, composed of twelve single tetrapeptides, was tested at 50 μM. As reported in Figure 1e, peptides having D-Arg, or D-His, or D-Phe, or D-Tyr on position X4 were capable of inhibiting APEH for more than 25%; however, after testing in a dose–response assay, the peptide of sequence TFA-D-Leu-D-Met-D-Pro-D-His-NH_2 (hereafter termed only CF_3-lmph), was the one selected as an efficient inhibitor, as it was the only peptide able to block enzyme activity in a dose-dependent fashion. In Figure 2a the drawing structure of the selected tetrapeptide is reported, whereas in Figure 2b and 2c the structure of the inactive TFA-D-Leu-D-Met-D-Pro-D-Ala-NH_2 and TFA-D-Leu-D-Met-D-Pro-D-Asp-NH_2 (hereafter termed CF_3-lmpa and CF_3-lmpd, respectively), used as negative controls in the subsequent experiments, are reported.

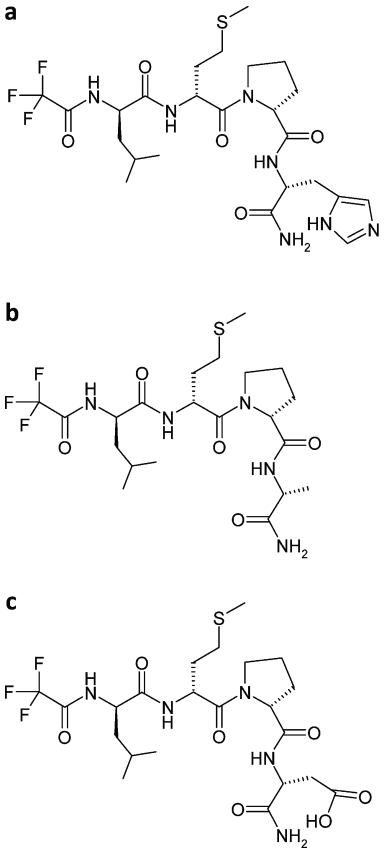

Figure 2. (a) Drawing structure of the selected active tetrapeptide TFA-D-Leu-D-Met-D-Pro-D-His-NH_2 (named CF_3-lmph). (b and c) The structures of the inactive variants TFA-D-Leu-D-Met-D-Pro-D-Ala-NH_2 and TFA-D-Leu-D-Met-D-Pro-D-Asp-NH_2 (termed CF_3-lmpa and CF_3-lmpd, respectively), used as negative control in the subsequent experiments, are shown.

Assessment of Peptide Selectivity and Mechanism of Inhibition. The inhibition activity of CF_3-lmph peptide was assessed using APEH purified from porcine liver, which shares more than 90% sequence identity with the homologous human enzyme. The selectivity of CF_3-lmph toward APEH was initially evaluated in biochemical assays using a panel of eukaryotic proteases (trypsin, α-chymotrypsin, elastase, carboxypeptidase Y, subtilisin, and proteinase K). Results (Table 3) show that the best protein target for CF_3-lmph was APEH with a maximum of 72% inhibition reached at 150 μM. This inhibition did not increase even using the peptide at 1 mM. The inhibition curve of porcine APEH followed a hyperbolic pattern with increasing inhibitor concentrations and gave an IC_{50} value of 98.0 ± 6.4 μM (Figure 1f). The affinity of CF_3-lmph toward porcine APEH was witnessed by a K_i value of 24.0 ± 0.8 μM. Data indicated that the peptide was also able to slightly affect carboxypeptidase activity (Table 3), reaching a maximum of 30% inhibition at 1.0 mM; the IC_{50} was only 210 ± 0.8 μM (see Figure SI 1 in Supporting Information). To determine the mechanism of APEH inhibition, we set out to use the peptide in several inhibition experiments, varying both substrate and peptide concentrations. Data are reported in Figure 3 as the classical Lineweaver–Burk double reciprocal plot, and the straight lines obtained at different inhibitor concentrations

dx.doi.org/10.1021/jm2013375 | J. Med. Chem. XXXX, XXX, XXX–XXX

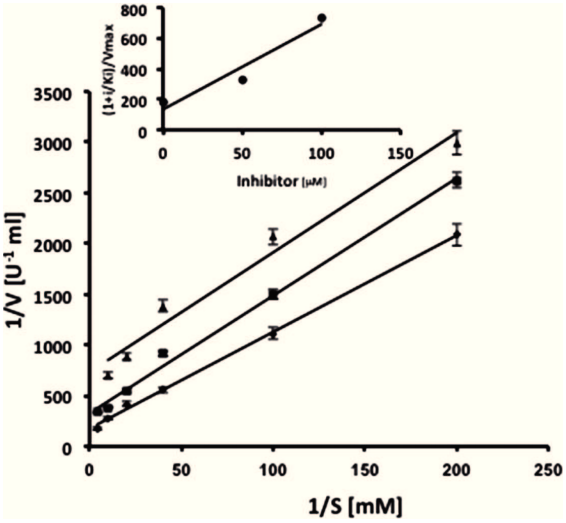

Figure 3. Double-reciprocal plots of the velocity against substrate (Ac-Ala-pNA) concentration at three different CF_3-lmph concentrations (no inhibitor ◆, 50 μM ■, and 100 μM ▲). The velocity of the reaction is expressed as μmol of *p*-nitroaniline released/min/mL of enzyme on incubation at 37 °C. K_i value was determined from the equation of the uncompetitive inhibition (see insert for a plot of $[(1 + i/K_i)/V_{max}]$ vs inhibitor concentration).

resulted in a series of parallel lines, which indicate that the tetrapeptide acts as a typical uncompetitive inhibitor. This very uncommon type of inhibition is based on a mechanism where the inhibitor binds to the enzyme, enhancing the binding of the substrate (so reducing K_m), but, due to a reduced reaction rate of the resultant enzyme−inhibitor−substrate complex, V_{max} is also decreased.[13]

Also the activity of the acetylated and nonacetylated variants was tested against porcine APEH to assess the role of the N-terminal trifluoroacetyl group. As reported in Figure 4, the

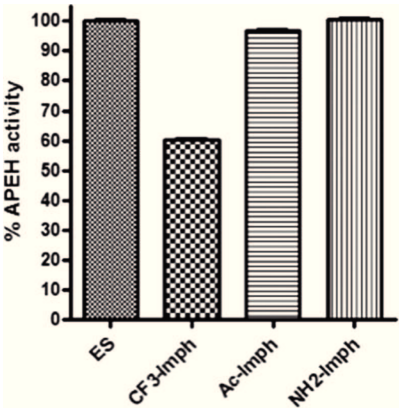

Figure 4. APEH inhibition by CF_3-lmph and the corresponding acetylated and NH_2-free peptides. Only the trifluoroacetylated peptide shows inhibition.

presence of this moiety confers a high specificity to peptide activity, because no enzyme inhibition was seen with the acetylated and the NH_2-free peptides.

Circular Dichroism. CF_3-lmph was characterized by CD and NMR spectroscopy in order to determine its conformational preferences and a possible correlation between its structure and the inhibition activity. For this purpose, CD spectra of the peptide at both pH 7.0 and pH 5.0 were acquired. In parallel also the CD spectrum of the N-terminally free variant was investigated under the same conditions. As can be seen in Figure 5, the peptide adopted a well-organized structure

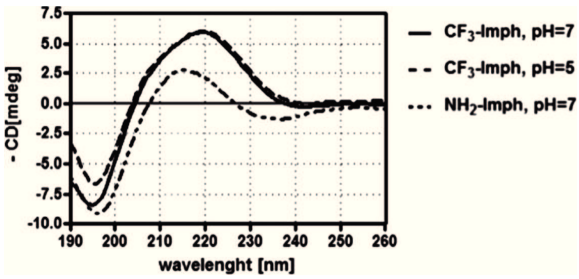

Figure 5. CD spectra of CF_3-lmph at pH 5.0 (solid line) and 7.0 (dashed line) at 200 μM. The spectrum of the NH_2-free peptide at pH 7.0 and at the same concentration (dotted line) is also reported. CD values at all wavelengths have been multiplied by −1 to take into account for the presence of all D residues.

with a minimum at 195 nm and a maximum at 220 nm. Considering the presence of all-D amino acids, which normally show inverted values, these spectra suggest that the peptide has a twisted or bent conformation at both pH values and that the structure is not grossly affected, at a qualitative level, by removing the trifluoroacetyl group.

NMR Spectroscopy. NMR investigation was performed on both the tetrapeptide inhibitor CF_3-lmph and on the inactive analogue CF_3-lmpa. The ala[4] variant, instead of that used as control in biochemical as well as cellular assays, was chosen because of its higher solubility at millimolar concentration.

NMR analyses in plain water showed that the two peptides CF_3-lmph and CF_3-lmpa adopt very similar conformations. Indeed, they showed comparable proton chemical shifts (Tables SI 1a, SI 1b of the Supporting Information), αCH chemical shifts deviations from random coil values[14] (Figure SI 2 of the Supporting Information) and NOE patterns. Interproton distances, evaluated from NOE intensities, were used in restrained molecular dynamics simulations to obtain solution molecular models of both peptides. Starting models were energy-minimized in a cubic box of water using Gromacs 4.0 program, as described in the Supporting Information. Before starting the dynamics simulations, the systems were further energy-minimized adding the NMR restraints, and the solvent was relaxed by a 200 ps MD at 300 K. Then, for each peptide, two simulations were run for 10 ns with (r) and without (u) NMR restraints to evaluate the stability of the peptide structure. The backbone root-mean-square deviations (rmsd) of both peptides along the trajectory at 300 K show small deviations (∼1−1.5 Å) from the starting model, either for the restrained or for unrestrained molecular dynamics simulations, pointing to a stable structure over the observation time. The structural stability is well represented by the backbone superposition of molecular frames, collected during the last 2 ns of restrained MD simulations, of CF_3-lmph (rmsd 0.25 ± 0.10 Å) and CF_3-lmpa (rmsd of 0.34 ± 0.24 Å), and reported in Figure 6a and 6b. It should be noted that no structural differences were observed from restrained (r) and unrestrained (u) molecular dynamics simulations, and the

dx.doi.org/10.1021/jm2013375 | J. Med. Chem. XXXX, XXX, XXX−XXX

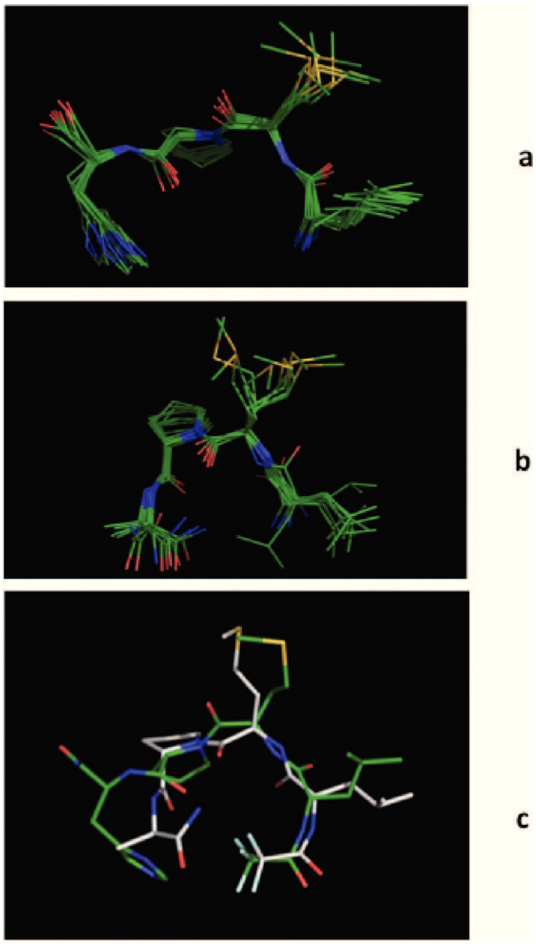

Figure 6. Backbone superposition of ten molecular frames collected during the last 2 ns of restrained molecular dynamics for (a) CF_3-lmph; (b) CF_3-lmpa. (c) Backbone superposition of CF_3-lmph (green) and CF_3-lmpa (gray) molecular models after 10 ns of restrained molecular dynamics.

comparison of the final r and u structures showed backbone rmsd of 0.34 Å and 0.20 Å for CF_3-lmph and CF_3-lmpa, respectively. The final molecular models obtained by restrained molecular dynamics simulations showed a good agreement with experimental NMR data and were chosen as representative of peptide structures. They look very similar in the conserved region (see Figure 6c) with a global backbone rmsd of 0.21 Å.

Cell Assays. The pro-apoptotic/cytotoxic effect produced by APEH inhibition was preliminarily investigated in HeLa cells exposed for 24 h to increasing concentrations of a widely used noncompetitive APEH inhibitor (i.e., ebelactone).[15] The marked (5-fold) increase of caspase 3 was produced by cell incubation with 30 and 50 μM ebelactone ($P < 0.001$) whereas its maximum cytotoxic effect (28%) was produced by cell exposure to 100 μM concentration. (Figure 7a).

Next, to determine the influence of CF_3-lmph or the control peptide TFA-D-Leu-D-Met-D-Pro-D-Asp-NH_2 (CF_3-lmpd) on cell viability, cell proliferation was evaluated upon exposure of HeLa cells for 24 h to increasing concentrations of the selected peptides. The dose-dependent antiproliferative effect was produced by cell exposure to different ebelactone concentrations (positive control), but only minor changes were

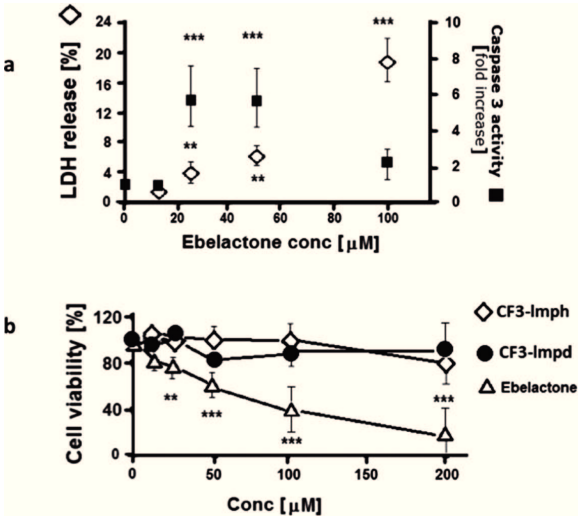

Figure 7. Pro-apoptotic and toxic effect of ebelactone on HeLa cells. The modulation of a commercially available APEH inhibitor on cell viability was preliminarily evaluated on HeLa cells. Caspase 3 activity and LDH release was evaluated upon 24 h exposure with increasing concentrations of ebelactone (a). Caspase 3 activity was expressed as fold increase as compared to untreated culture. Culture media from untreated culture were used as control, and those from cells exposed to 1% TritonX-100 were used as positive control (100% release). The dose-dependent effect CF_3-lmph (open titled squares) or with the control peptide CF_3-lmpd (black circles) on cell viability was compared with that produced by ebelactone treatment (white triangles) (b). The data from triplicate analysis from three different experiments are expressed as means ± SD. ***, ** Significantly different $P < 0.005$ or 0.01, from respective controls.

produced by the treatment with CF_3-lmph or CF_3-lmpd (Figure 7b).

In order to evaluate the ability of the peptide to inhibit APEH in in vitro experimental models, two cancer cell lines (A375 and HeLa) were exposed for 24 h with increasing concentrations of CF_3-lmph or of the control peptide CF_3-lmpd. As shown in Figure 8a and 8b, CF_3-lmph markedly reduced APEH activity in a dose-dependent manner, reaching their maximum effect at 150 μM, where enzyme activity was decreased in HeLa and in A375 cells by 80% and 50%, respectively. Notably, undetectable inhibition resulted from the treatment with CF_3-lmpd control peptide.

To determine the effects of CF_3-lmph or CF_3-lmpd on cell viability, their cytotoxic or pro-apoptotic effects were also studied. As apoptosis has been associated with APEH inhibition,[16] the caspase 3 activity, a key enzyme in the apoptotic cascade, was measured upon the cell treatments. Specifically, cells exposed to 100 or 150 μM CF_3-lmph, triggered a mild, but significant, increase in caspase 3 activity as compared with cells incubated with the same amount of control peptide ($P < 0.01$ or 0.005). In addition, undetectable toxicity, measured as LDH release in the medium, resulted from the CF_3-lmph-mediated inhibition of APEH (Figure 8c, 8d insert).

DISCUSSION AND CONCLUSIONS

Aminopeptidases are known to be essential for basic physiological processes, such as protein maturation[17] and cell cycle control.[18] Their inhibition disrupts protein turnover, leading to decreased cell survival and proliferation; thus,

dx.doi.org/10.1021/jm2013375 | J. Med. Chem. XXXX, XXX, XXX–XXX

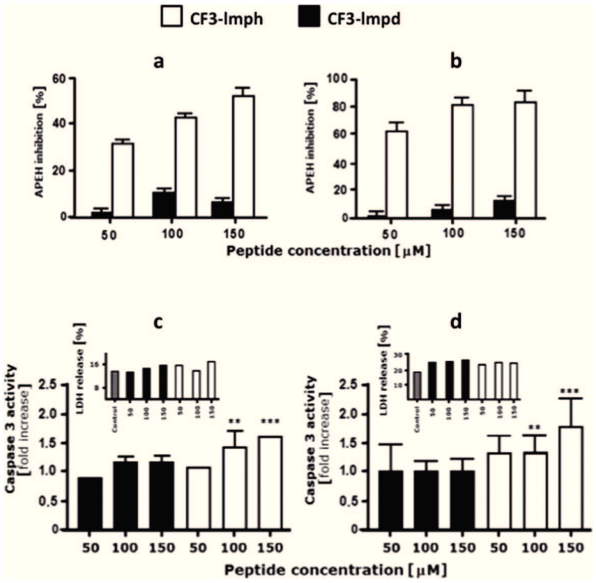

Figure 8. Down-regulation of APEH activity by CF_3-lmph in HeLa and A375 cells. APEH activity was measured in HeLa (a) or A375 (b) cells incubated with 50 μM, 100 μM and 150 μM CF_3-lmph (white bars) or with the control peptide CF_3-lmpd (black bars) for 24 h. Caspase-3 activities and LDH release were measured in HeLa (c) or A375 cells (d). The cytotoxic effect of the different treatments was evaluated by measuring the LDH release in the culture media. Media from untreated culture were used as control (gray bars). Media from cells exposed to 1% Triton X-100 were used as positive control (c, d insert). The data are expressed as means ± SD. ***, ** Significantly different $P < 0.005$ or 0.01, from respective controls.

targeting this pathway has been indicated as a suitable approach for anticancer therapies.[19,20] Also a role in protein structure and function regulation has been persistently evoked due to its capability to remove acetyl-amino acids from the N-terminus of a large set of cytoplasmic proteins,[2] which, depending on the presence/absence of this small post-translational modification, could not properly fold and thus be tagged for degradation.[4,6] A more extensive understanding of APEH functions is thus needed, also in view of the recently reported involvement in the regulation of proteasome activity, and this necessarily involves the development of specific modulators of enzymatic activity and a more detailed view of its interaction network and of related modulators. In this instance, enzyme inhibitors and interactors, with different mechanisms of action and structure, can play a major role, as they enable elucidation of downstream effects mediated by processed substrates or by interrupted or promoted interactions.

With the aim of developing new APEH inhibitors, we have prepared and screened a complex library of synthetic peptides modified on the N-terminus by a set of diverse chemical groups in order to investigate the space around the enzyme site of action and also to prevent undesired substrate-like behaviors of the peptides exposed to the enzyme. After five iterative rounds of screening and resynthesis needed to elucidate the whole peptide structure, we have identified the peptide CF_3-lmph as the one best inhibiting APEH in vitro. At variance with inhibitors previously described, the one we report in this study shows an uncommon uncompetitive mechanism of inhibition which is generally characterized by the binding of inhibitors to enzyme: substrate (ES) complexes and their inactivation induced by a delay in the release of processed substrates.

CF_3-lmph shows selectivity toward APEH, because, among the different serine proteases we have tested, it only blocks to a limited extent (30%) carboxypeptidase Y, with an IC_{50} which is more than twice that exhibited toward APEH (about 210 μM for carboxypeptidase Y and about 98 μM for APEH). The inhibition specificity is also demonstrated by the lack of activity of the acetylated and NH_2-free variants, indicating a direct involvement of fluorine atoms in the recognition and blocking of the ES complex. This is consistent with the observation that several organophosphorus compounds such as chlorpyrifos, dichlorvos, and naled, which share with the peptide the multihalogenated structure, also inhibit APEH.[21] We can thus reasonably hypothesize that halogens (bromine, fluorine, and chlorine), or more generally, highly electronegative centers, are likely an important discriminant for enzyme recognition.

Also the presence of D-histidine on position 4 of the tetrapeptide is very important for activity, and indeed mutants bearing D-Ala or D-Asp on the same position are not active. It is important to point out that the conformations of the inactive CF_3-lmpa and NH_2-lmph peptides are essentially identical to that of the active CF_3-lmph, with a bent conformation around the D-proline residue on position 3. This suggests that, beyond fluorines, the imidazole ring on the histidine side chain plays a crucial role in binding and inhibiting APEH. Again, given the strong structural similarity between imidazole and triazole rings, which are the core structures of many potent serine hydrolase inhibitors, we can reasonably speculate that the peptide shares with these at least one recognition site. Note that the peptide we have isolated in our screening does not apparently mimic any of the substrates recently identified for APEH,[2] still in agreement with the observation that CF_3-lmph does not bind into the catalytic pocket. Nevertheless, because potent triazole inhibitors have been isolated with competition assays, we can presume that the peptide inhibitor recognizes APEH on a region nearby the catalytic site.

While a role for APEH has been more clearly delineated in neurodegenerative diseases,[11] the occurrence of different phenotypic outcomes on cells treated with APEH inhibitors renders much more elusive the involvement of this enzyme in cancer.[9] The opposed effects observed certainly depend on the different experimental settings and cell lines utilized in the various studies; however, we cannot exclude that they could be associated to the mechanism of action of the diverse APEH inhibitors used, thus introducing a further level of complexity toward the understanding of the overall role played by this enzyme in cell homeostasis. We have recently reported that competitive APEH inhibition in Caco-2 cancer cells by SsCEI peptides reproducing the RSL of a proteic APEH inhibitor is paralleled by a downregulation of proteasome functions and an increase of caspase 3 activity that, in turn, induce a sustained and strong reduction of cell proliferation.[6] A similar effect is observed when the same cells are treated with the non-competitive inhibitor $trans_{10}$-cis_{12} CLA that binds the enzyme on a site adjacent to the catalytic pocket. Further, the effects are synergistic when the two compounds are used in combination.[6] On the contrary, the use of other competitive APEH inhibitors on mouse T cells strongly stimulates cell proliferation.[2]

To try to further address this very important aspect, we have used CF_3-lmph, along with an inactive control, to stimulate two different cell lines, A375 and HeLa, which are melanoma and cervical cancer cell lines, respectively. Though the peptide very

dx.doi.org/10.1021/jm2013375 | J. Med. Chem. XXXX, XXX, XXX–XXX

efficiently crosses cell membranes, reduces enzyme activity in the cytoplasm, and is not toxic compared to other known inhibitors, for example ebelactone (see Figure 7a), it only slightly affects cell proliferation, inducing a reduction in cell vitality which is negligible compared to that of controls and to that previously observed in Caco-2 cells treated with competitive and noncompetitive inhibitors.[6] As also shown on mouse T cells, which even tend to proliferate when treated with APEH competitive inhibitors, this effect is certainly explained by the different cell lines used, which could display a different set of substrates, or by their metabolic status, but we cannot exclude that also the different mechanism of inhibition could influence cell proliferation by affecting or altering the network of interactions that regulates the functions of APEH. This hypothesis opens a new intriguing question regarding the role played by APEH nonsubstrate interactors, which are so far completely unknown.

We have identified the first uncompetitive APEH inhibitor, which is selective, has a conformationally defined structure, and contains molecular determinants common to other known inhibitors. In contrast to competitive inhibitors, which lose potency as substrate concentration rises, uncompetitive inhibitors become more potent as the substrate concentration increases in an inhibited open system.[22] This can be a significant advantage in vivo when the physiological context exposes the enzyme to high levels of substrate concentrations.

Despite the low potency in the micromolar range, the structural properties, the ease of synthesis, and unusual mechanism of action make this tetrapeptide an appealing and innovative tool for the systematic design of a new class of more potent and less toxic protease inhibitors, which may complement the active site-targeted molecules in future therapeutic applications.

EXPERIMENTAL SECTION

Materials. Protected amino acids for the synthesis of peptides were from GL-Biochem (Shanghai, PRC) and Novabiochem (Laufelfingen, Switzerland). Coupling agents were from GL-Biochem (Shanghai, PRC); solvents, such as acetonitrile (CH_3CN), dimethylformamide (DMF), and methanol (CH_3OH), were from Sigma-Aldrich (Milan, Italy). Chemicals for the preparation of libraries and enzymes for biochemical assays, including caspase-3 fluorimetric Assay Kits, and other chemicals of the highest purity were also from Sigma-Aldrich (Milan, Italy). Dulbecco's Modified Eagle Medium (DMEM), L-glutamine, penicillin–streptomycin, and fetal bovine serum (FBS) for cell culture were from Gibco-BRL. Porcine liver APEH was obtained by Takara. Acetyl-Ala-pNA was from Bachem.

Peptide Library Design, Synthesis, and Characterization. Peptide libraries were designed in a simplified format as reported in Marasco et al.[12] By this approach, a small set of amino acids is chosen to represent the chemical space occupied by very short peptides which can be seen as precursors or templates of small molecular scaffolds. Preferentially, only non natural or D-amino acids are included in these sets in order to potentially select enzyme-resistant new peptides. The set used here, reported in Table 1, includes aspartic acid as representative of amino acids with acidic side chains, arginine and histidine representing basic amino acids, glutamine and S-acetamidomethyl(Acm)-cysteine representing residues with amides on the side chain, phenylalanine and tyrosine as being representative of aromatic residues, serine representing residues with hydroxyl groups, leucine and methionine representing bulky hydrophobic amino acids, and alanine representing amino acids with small hydrophobic side chains. Proline was used to eventually select peptides with bent conformations. Note that histidine was used as an additional basic residue also by virtue of its aromaticity. The choice of this set of residues was also determined by their difference in MW in order to facilitate eventual identification of active components by tandem mass spectrometry methods.[12] As APEH is capable of removing acetyl-amino acids from the N-terminus of peptides and proteins, we set out to not acetylate the peptides but instead to introduce, on the N-terminal position, seven groups (see Table 2) with very different physicochemical properties in order to (i) prevent substrate-like effects and (ii) explore the chemical space around the N-terminal residue. These groups were chosen to introduce charges (succinic acid), aromatic groups (phenyl, Z, and 6-Cl-Z), bulky polyaromatic rings (Dabcyl), and small hydrophilic groups (trifluoroacetic acid (TFA) and pyroglutamate). The library was synthesized by the solid-phase method on a global 140 μmol scale following the Fmoc/tBu methodology.[23] Fmoc deprotection was achieved by treatment with

Table 1. Set of Amino Acids Used To Assemble the Tetrapeptide Library of General Formula Y_i-X_1-X_2-X_3-X_4-NH_2 on the X Position

N	building block, three-letter code	protected derivative used for the X positions
1	D-Ala	N^{α}-Fmoc-alanine
2	D-Arg	N^{α}-Fmoc-arginine (N^{Γ}-pentamethyldihydrobenzofuran)
3	D-Asp	N^{α}-Fmoc-aspartic acid (*tert*-butyl ester)
4	D-Cys(Acm)	N^{α}-Fmoc-cysteine(S-acetamydomethyl)
5	D-Gln	N^{α}-Fmoc-glutamine (N^{δ}-trityl)
6	D-His	N^{α}-Fmoc-histidine(N^{ϵ}-trityl)
7	D-Leu	N^{α}-Fmoc-leucine
8	D-Met	N^{α}-Fmoc-methionine
9	D-Phe	N^{α}-Fmoc-phenylalanine
10	D-Pro	N^{α}-Fmoc-proline
11	D-Ser	N^{α}-Fmoc- serine(*O-tert*-butyl-ether)
12	D-Tyr	N^{α}-Fmoc-tyrosine(*O-tert*-butyl-ether)

Table 2. Set of Carboxylic Acids Used To Modify the Tetrapeptide Library of General Formula Yi-X1-X2-X3-X4-NH_2 on the Yi Position

	Y_i	
N	building block	derivative used for modifying the N-terminus
1	Succ	succinic anhydride
2	Z	benzyloxycarbonyl-OSu
3	pGlu	pyroglutamic acid
4	2Cl-Z	2Cl-benzyloxycarbonyl-OSu
5	TFA	trifluoroacetic acid
6	Dabcyl	Dabcyl-OSu
7	benzoyl	benzoic acid

Table 3. Inhibition Profile of CF_3-lmph[a]

enzyme	pH	IC_{50} [μM]	maximal concentration tested [μM]	maximal inhibition [%]
APEH	7.5	98.0	1000	72
chymotrypsin	8.0*	>1000	1000	<1
elastase	8.0*	>1000	1000	<1
trypsin	8.0*	>1000	1000	<1
carboxypeptidase Y	7.0	210	1000	30
subtilisin	7.5	>1000	1000	<1
proteinase K	7.5	>1000	1000	<1

[a]The IC_{50} values of the tetrapeptide inhibitor were determined in 50 mM Tris-HCl (supplemented with 20 mM $CaCl_2$*) saline buffer at the optimal pH for the enzyme–substrate pair and at increasing concentrations, of CF_3-lmph, up to 1.0 mM.

dx.doi.org/10.1021/jm2013375 | J. Med. Chem. XXXX, XXX, XXX–XXX

30% piperidine in DMF. Couplings with amino acids or nonactivated carboxylic acids (3, 5, and 7 in Table 2) were performed by activating, with 1 equiv of HATU, 2 equiv of DIEA, and 10 equiv of Fmoc-protected amino acids or carboxylic acids. Random positions were obtained by coupling equimolar mixtures of the chosen set of amino acids used in very large excess to suppress preferential acylations deriving from differences in reactivity.

The first library was prepared by four sequential incorporations of mixtures of the 12 amino acids; the resin batch was then split into 7 identical aliquots to which the 7 different carboxylic acids were coupled. Subsequent libraries, identified by the iterative screening, were prepared in the same way and on the same synthesis scale. In the last step, 12 single peptides were prepared and purified before screening. Complex peptide mixtures were characterized by pool amino acid analysis comparing experimental amino acid distribution with those calculated assuming an equimolar distribution of all components in the pools. Single peptides and mixtures up to 12 components were easily characterized by LC-MS as reported elsewhere, identifying peptides by MW determination and in some cases by sequence assignment by tandem mass spectrometry. Cleavage of peptide mixtures from the resin was afforded by treatment with TFA−triisopropylsilane (TIS)−H_2O mixtures (90:5:5, v/v/v) and subsequent precipitation in cold diethyl ether. Single peptides were purified by semipreparative RP-HPLC on an ONYX 10 × 1 cm i.d. C18 monolithic column, operating at 15 mL/min, using H_2O and CH_3CN as eluents, both supplemented with 0.05% TFA. Gradients were chosen on the basis of peptide sequences. Libraries and single peptides were prepared as amidated derivatives. Canonical Fmoc-protected D-amino acids were used in all syntheses. D-Cys(Acm) was also introduced as the corresponding Fmoc derivative. A RINK amide resin with a 0.57 mmol/g substitution level was used in all syntheses. Most couplings and deprotection reactions were performed at room temperature for 5 min. In some specific cases, microwaves were used to improve reaction yields. A common kitchen microwave oven used at the minimum power was utilized for this purpose. Microwave-assisted couplings and deprotection reactions were carried out for 1.5 min with repeated 5 s on−off cycles. Cleavages were carried out in the same way for 1 min. After lyophilization, peptide material was dissolved in dimethyl sulfoxide (DMSO) at 10 mg/mL and stored frozen until use. Single peptides were characterized by RP-HPLC and LC-MS using an ONYX 50 × 2 mm i.d. C18 monolithic column, operating at 0.6 mL/min, using H_2O (eluent A) and CH_3CN (eluent B) as eluents, both supplemented with 0.05% TFA. Gradients were from 2% to 45% of eluent B in 9 min. Detection was achieved with a photodiode array set between 200 and 320 nm and with an ion trap mass spectrometer (Deca XP, ThermoFisher). Purity was checked on chromatograms extracted at 214 nm and on TIC (total ion current) traces obtained by full scans between 200 and 2000 m/z. Identity of peptides was confirmed by MW determination and tandem mass analyses. Peptides were all >95% pure, as determined by RP-HPLC and LC-MS analyses.

Enzyme Inhibition Assay and Screening of the Peptide Library. Porcine liver APEH activity was measured spectrophotometrically using the chromogenic substrate acetyl-Ala-pNA. The reaction mixture (0.2 mL) containing pure APEH (0.5 nM) in 50 mM Tris-HCl buffer, pH 7.5 (Tris buffer), was preincubated at 37 °C for 2 min. Then, 25 μM acetyl-Ala-pNA was added and the release of *p*-nitroanilide ($\varepsilon_{410\ nm}$ = 8800 M^{-1} cm^{-1}) was measured by recording the absorbance increase at 410 nm on a BIOTEK multiwavelength plate reader, equipped with a thermostatted compartment. APEH activity was expressed in IU. Assays were performed in 96-well polyethylene plates in duplicates or triplicates.

Inhibition by library components was carried out by using a fixed concentration of APEH (0.5 nM) and fixed concentrations of libraries as described below. Depending on the screening steps, peptide mixtures or single peptides were preincubated with the enzyme for 30 min at 37 °C before addition of the substrate, and the enzymatic activity was then followed as described above. Each inhibition experiment was carried out in duplicate wells. The first library (seven sublibraries) was screened in duplicate at a global concentration of 200 μM, assuming an average peptide molecular weight of 600 amu. Data were processed, averaging values from duplicate wells, and the slope was calculated by linear regression analysis. The percentage of inhibition was determined by comparing slopes from inhibition assays with that from the control experiment. To confirm and strengthen results after each screening step, dose−response assays with the positive mixtures were performed at concentrations ranging between 10 and 200 μM. In the second screening step, the 12 libraries bearing the trifluoroacetyl (TFA) group on the N-terminus were screened at a nominal concentration of 40 μM, assuming again an average MW of 600 amu. The same average molecular weight was assumed for the subsequent third (library concentration 100 μM) and fourth screening round (50 μM). Single peptides in the final fifth step were purified and characterized by LC-MS, assessing purity and identity. They were assayed at a concentration of 50 μM.

Enzyme Assays with APEH and Other Enzymes. Porcine liver APEH activity was measured spectrophotometrically using the chromogenic substrate acetyl-Ala-pNA. The reaction mixture (1 mL) containing pure APEH (38 ng) or an appropriate amount of cell extract in Tris buffer was preincubated at 37 °C for 2 min. Then, 25 μM acetyl-Ala-pNA was added and the release of *p*-nitroanilide (ε_{410} = 8800 M^{-1} cm^{-1}) was measured by recording the absorbance increase at 410 nm on a Cary 100 Scan (Varian) UV/vis spectrophotometer, equipped with a thermostatted cuvette compartment. APEH activity was expressed in IU. The carboxypeptidase Y, elastase, chymotrypsin-like activity of proteasome, trypsin, and subtilisin activities were evaluated according to previously published methods.[24] Proteinase K activity was measured according to the manufacturer's instructions.

Protease inhibiting activities of the selected peptides were carried out using a fixed amount of enzymes (5 nM) and increasing peptide concentrations, up to 1 mM. Mixtures were preincubated for 30 min at 37 °C before the addition of the substrate, and the enzymatic activities were followed as described above. To determine the mechanism of APEH inhibition, Lineweaver−Burk double reciprocal plots of data at increasing inhibitor and substrate concentrations were constructed. For this experiment, APEH (5 nM) was incubated, with or without inhibitor at 50 μM and 100 μM concentrations, and assayed at increasing substrate concentrations. The reciprocals of the rate of the substrate hydrolysis for each inhibitor concentration were plotted against the reciprocals of the substrate concentrations. The inhibition constant K_i was determined by the Lineweaver−Burk equation for the uncompetitive type of inhibition $[1/V = 1/V_{max} \times (1 + i/K_i) + (K_m/V_{max}) \times 1/S]$.

Circular Dichroism Analysis. CD spectra were obtained on a Jasco J-715 spectropolarimeter for peptide solutions at 2.0 × 10^{-4} M concentration in 5 mM Tris−HCl, pH 7.0, or in acetate buffer, pH 5.0, 25 °C. Hellma quartz cells of 1-cm path length were used in the far UV (190−250 nm). The temperature of the sample cell was regulated by a PTC-348 WI thermostat. Spectra were signal-averaged over three scans and baseline-corrected by subtracting a buffer spectrum. Due to the presence of only D residues, the entire spectrum was multiplied by −1.

NMR Analysis. NMR characterization of peptides was performed in water at 25 °C. Samples were prepared by dissolving weighted amounts of each peptide in water (spectroscopic purity), adding D_2O (ARMAR, isotopic purity 99,8%) for a final ratio 90/10 v/v. Final concentrations were ca. 2.0−2.5 mM. Details concerning NMR analyses are reported in the Supporting Information.

Molecular Dynamics (MD) Simulations. MD simulations were performed as reported in the Supporting Information.

Cell Cultures. Human melanoma (A375) and cervical cancer cells (HeLa), kindly donated by Dr. Rosanna Palumbo (IBB, CNR), were cultivated in DMEM supplemented with 10% FBS, 1 mM glutamine, and 100 units/mL penicillin−streptomycin at 37 °C in a humidified 5% CO_2 atmosphere. The cells were split using trypsin−ethylendiaminetetraacetic acid (EDTA) solution and plated in six-well plates at a density of 8 × 10^4 cells/mL, and the medium was replaced every 2−3 days. Cells at 60−70% confluence were incubated with the selected peptides at different concentrations.

Apoptosis Assays. The pro-apoptotic ability of the tetrapeptides were assayed by measuring the caspase-3 activity using fluorometric

kits, according to the manufacturer instructions. These assays were based on hydrolysis of the substrate acetyl-Asp-Glu-Val-Asp-7-amido-4-methylcoumarin (Ac-DEVD-AMC) by caspase-3. The release of the 7-AMC moiety in protein extracts prepared from the differently treated cells was evaluated by fluorimetry (excitation 360 nm, emission 460 nm). Their amounts were calculated by means of a standard curve prepared with pure AMC, and following normalization for protein content, the activities were calculated as nmoles AMC/mg protein and expressed as fold increase as compared to control culture.

Cytotoxicity Assays. The release of LDH was used as the marker for cell toxicity.[25] The culture supernatants were sampled at the end of the incubations and centrifuged (4000*g*, 5 min, and 4 °C). Aliquots of the clear supernatant (10 μL) were incubated with 190 μL of reaction buffer (200 mM Tris/HCl, pH 8.0, 0.7 mM *p*-iodonitrotetrazolium violet, 50 mM L-lactic acid, 0.3 mM phenazine methoxysulfate, 0.4 mM NAD) for 30 min at 37 °C. Absorbance was measured at 490 nm, and the results were expressed as percentages of total LDH release from control cultures treated with 1% (w/v) Triton X-100 and calculated as:

$$[(\text{experimental value} - \text{blank value})/(\text{total lysis} - \text{blank value}) - 100]$$

Statistical Analysis. Data were obtained from triplicate analyses of three different preparations, and the results were expressed as means ± SD. Statistical analysis and IC_{50} values were calculated with the SigmaPlot 10.0 software through a nonlinear curve-fitting method and using a simple binding isotherm equation. Groups were compared by Student's *t* test, and $P < 0.05$ was considered as significant.

■ ASSOCIATED CONTENT

Supporting Information

Methods for NMR and MD simulations. A plot with dose−response carboxypeptidase Y inhibition. A plot with chemical shift deviations from random-coil values. This material is available free of charge via the Internet at http://pubs.acs.org.

■ AUTHOR INFORMATION

Corresponding Author

*Phone: 0039-081-2536644; fax: 0039-081-2534574; e-mail: menotti.ruvo@unina.it.

Notes

The authors declare no competing financial interest.

■ ACKNOWLEDGMENTS

The authors thank Dr. Giuseppe Perretta for his valuable assistance with peptide synthesis and Mr. Leopoldo Zona for kindly assisting during NMR experiments. The project has been partly funded by project FIRB MERIT N. RBNE08NKH7_003 (MIUR) to M.R. and by CNR.

■ ABBREVIATIONS USED

Acm, Acetamidomethyl; Caco-2, Human colon carcinoma cells; A375, Human melanoma cells; HeLa, Human cervical cancer cells; DMEM, Dulbecco's Modified Eagle Medium; DMSO, Dimethylsulfoxide; EDTA, Ethylendiamine-tetra-acetic acid; FBS, Fetal Bovine Serum; TFA, Trifluoroacetic acid; TIS, Tri-isopropylsilane

■ REFERENCES

(1) Perrier, J.; Durand, A.; Giardina, T.; Puigserver, A. Catabolism of intracellular N-terminal acetylated proteins: involvement of acylpeptide hydrolase and acylase. *Biochimie* **2005**, *87*, 673−685.

(2) Adibekian, A.; Martin, B. R.; Wang, C.; Hsu, K. L.; Bachovchin, D. A.; Niessen, S.; Hoover, H.; Cravatt, B. F. Click-generated triazole ureas as ultrapotent in vivo-active serine hydrolase inhibitors. *Nat. Chem. Biol.* **2011**, *7*, 469−478.

(3) Narita, K. Isolation of acetylpeptide from enzymic digests of TMV-protein. *Biochim. Biophys. Acta* **1958**, *28*, 184−191.

(4) Forte, G. M.; Pool, M. R.; Stirling, C. J. N-terminal acetylation inhibits protein targeting to the endoplasmic reticulum. *PLoS Biol.* **2011**, *9*, e1001073.

(5) Shimizu, K.; Kiuchi, Y.; Ando, K.; Hayakawa, M.; Kikugawa, K. Coordination of oxidized protein hydrolase and the proteasome in the clearance of cytotoxic denatured proteins. *Biochem. Biophys. Res. Commun.* **2004**, *324*, 140−146.

(6) Palmieri, G.; Bergamo, P.; Luini, A.; Ruvo, M.; Gogliettino, M.; Langella, E.; Saviano, M.; Hegde, R.; Sandomenico, A.; Rossi, M. Acyl Peptide hydrolase Inhibition as targeted strategy to induce proteasomal dysfunction. *PLoS One* **2011**, *6* (10), e25888.

(7) Orlowski, R. Z.; Kuhn, D. J. Proteasome inhibitors in cancer therapy: lessons from the first decade. *Clin. Cancer Res.* **2008**, *14*, 1649−1657.

(8) Landis-Piwowar, K. R.; Milacic, V.; Chen, D.; Yang, H.; Zhao, Y.; Chan, T. H.; Yan, B.; Dou, Q. P. The proteasome as a potential target for novel anticancer drugs and chemosensitizers. *Drug Resist. Updates* **2006**, *9*, 263−273.

(9) Scaloni, A.; Jones, W.; Pospischil, M.; Sassa, S.; Schneewind, O.; Popowicz, A. M.; Bossa, F.; Graziano, S. L.; Manning, J. M. Deficiency of acylpeptide hydrolase in small-cell lung carcinoma cell lines. *J. Lab. Clin. Med.* **1992**, *120*, 546−552.

(10) Palmieri, G.; Langella, E.; Gogliettino, M.; Saviano, M.; Pocsfalvi, G.; Rossi, M. A novel class of protease targets of phosphatidylethanolamine-binding proteins (PEBP): a study of the acylpeptide hydrolase and the PEBP inhibitor from the archaeon Sulfolobus solfataricus. *Mol. Biosyst.* **2010**, *6*, 2498−2507.

(11) Olmos, C.; Sandoval, R.; Rozas, C.; Navarro, S.; Wyneken, U.; Zeise, M.; Morales, B.; Pancetti, F. Effect of short-term exposure to dichlorvos on synaptic plasticity of rat hippocampal slices: involvement of acylpeptide hydrolase and alpha(7) nicotinic receptors. *Toxicol. Appl. Pharmacol.* **2009**, *238*, 37−46.

(12) Marasco, D.; Perretta, G.; Sabatella, M.; Ruvo, M. Past and future perspectives of synthetic peptide libraries. *Curr. Protein Pept. Sci.* **2008**, *9*, 447−467.

(13) Segel, I. H. Enzyme kinetics; Wiley Interscience: New York, 1975; pp 161−166.

(14) Wishart, D. S.; Sykes, B. D.; Richards, F. M. Relationship between nuclear magnetic resonance chemical shift and protein secondary structure. *J. Mol. Biol.* **1991**, *222*, 311−333.

(15) Abe, F.; Aoyagi, T. Physiological roles of ectoenzymes indicated by the use of aminopeptidase inhibitors. In *Ectopeptidases. CD13/Aminopeptidase N and CD26/Dipeptidylpeptidase IV in Medicine and Biology*; Langner, J., Ansorge, S., Eds.; 2002.

(16) Yamaguchi, M.; Kambayashi, D.; Toda, J.; Sano, T.; Toyoshima, S.; Hojo, H. Acetylleucine chloromethyl ketone, an inhibitor of acylpeptide hydrolase, induces apoptosis of U937 cells. *Biochem. Biophys. Res. Commun.* **1999**, *263*, 139−142.

(17) Moerschell, R. P.; Hosokawa, Y.; Tsunasawa, S.; Sherman, F. The specificities of yeast methionine aminopeptidase and acetylation of amino-terminal methionine in vivo. Processing of altered iso-1-cytochromes c created by oligonucleotide transformation. *J. Biol. Chem.* **1990**, *265*, 19638−19643.

(18) Constam, D. B.; Tobler, A. R.; Rensing-Ehl, A.; Kemler, I.; Hersh, L. B.; Fontana, A. Puromycin-sensitive aminopeptidase. Sequence analysis, expression, and functional characterization. *J. Biol. Chem.* **1995**, *270*, 26931−26939.

(19) Wickstrom, M.; Larsson, R.; Nygren, P.; Gullbo, J. Amino-peptidase N (CD13) as a target for cancer chemotherapy. *Cancer Sci.* **2011**, *102*, 501−508.

(20) Moore, H. E.; Davenport, E. L.; Smith, E. M.; Muralikrishnan, S.; Dunlop, A. S.; Walker, B. A.; Krige, D.; Drummond, A. H.; Hooftman, L.; Morgan, G. J.; Davies, F. E. Aminopeptidase inhibition as a targeted treatment strategy in myeloma. *Mol. Cancer Ther.* **2009**, *8*, 762−770.

724 (21) Casida, J. E.; Quistad, G. B. Serine hydrolase targets of
725 organophosphorus toxicants. *Chem. Biol. Interact.* **2005**, *157−158*,
726 277−283.
727 (22) Westley, A. M.; Westley, J. Enzyme inhibition in open systems.
728 Superiority of uncompetitive agents. *J. Biol. Chem.* **1996**, *271*, 5347−
729 52.
730 (23) Fields, G. B.; Noble, R. L. Solid phase peptide synthesis utilizing
731 9-fluorenylmethoxycarbonyl amino acids. *Int. J. Pept. Protein Res.* **1990**,
732 *35*, 161−214.
733 (24) Palmieri, G.; Catara, G.; Saviano, M.; Langella, E.; Gogliettino,
734 M.; Rossi, M. First Archaeal PEPB-Serine Protease Inhibitor from
735 Sulfolobus solfataricus with Noncanonical Amino Acid Sequence in
736 the Reactive-Site Loop. *J. Proteome Res.* **2009**, *8*, 327−334.
737 (25) Decker, T.; Lohmann-Matthes, M. L. A quick and simple
738 method for the quantitation of lactate dehydrogenase release in
739 measurements of cellular cytotoxicity and tumor necrosis factor
740 (TNF) activity. *J. Immunol. Methods* **1988**, *115*, 61−69.

OPEN ACCESS Freely available online

PLOS ONE

RedOx Status, Proteasome and APEH: Insights into Anticancer Mechanisms of t10,c12-Conjugated Linoleic Acid Isomer on A375 Melanoma Cells

Paolo Bergamo[1], Ennio Cocca[2¤], Rosanna Palumbo[3], Marta Gogliettino[2¤], Mose Rossi[2¤], Gianna Palmieri[2*¤]

1 Institute of Food Sciences, National Research Council (CNR-ISA), Avellino, Italy, **2** Institute of Protein Biochemistry, National Research Council (CNR-IBP), Napoli, Italy, **3** Institute of Biostructure and Bioimaging, National Research Council (CNR-IBB), Napoli, Italy

Abstract

This study describes the investigation of the efficiency of conjugated linoleic acid (CLA) isomers in reducing cancer cells viability exploring the role of the oxidative stress and acylpeptide hydrolase (APEH)/proteasome mediated pathways on pro-apoptotic activity of the isomer trans10,cis12 (t10,c12)-CLA. The basal activity/expression levels of APEH and proteasome (β-5 subunit) were preliminarily measured in eight cancer cell lines and the functional relationship between these enzymes was clearly demonstrated through their strong positive correlation. t10,c12-CLA efficiently inhibited the activity of APEH and proteasome isoforms in *cell-free* assays and the negative correlation between cell viability and caspase 3 activity confirmed the pro-apoptotic role of this isomer. Finally, modulatory effects of t10,c12-CLA on cellular redox status (intracellular glutathione, mRNA levels of antioxidant/detoxifying enzymes activated through NF-E2-related factor 2, Nrf2, pathway) and on APEH/β-5 activity/expression levels, were investigated in A375 melanoma cells. Dose- and time-dependent variations of the considered parameters were established and the resulting pro-apoptotic effects were shown to be associated with an alteration of the redox status and a down-regulation of APEH/proteasome pathway. Therefore, our results support the idea that these events are involved in ROS-dependent apoptosis of t10,c12-CLA-treated A375 cells. The combined inhibition, triggered by t10,c12-CLA, *via* the modulation of APEH/proteasome and Nrf2 pathway for treating melanoma, is suggested as a subject for further *in vivo* studies.

Citation: Bergamo P, Cocca E, Palumbo R, Gogliettino M, Rossi M, et al. (2013) RedOx Status, Proteasome and APEH: Insights into Anticancer Mechanisms of t10,c12-Conjugated Linoleic Acid Isomer on A375 Melanoma Cells. PLoS ONE 8(11): e80900. doi:10.1371/journal.pone.0080900

Editor: Salvatore V Pizzo, Duke University Medical Center, United States of America

Received May 16, 2013; **Accepted** October 17, 2013; **Published** November 19, 2013

Funding: This research was supported by MERIT grant project no. RBNE08YFN3_009 and PON grant project 2007-2013, PON01_01802. The funders have no role in study design, data collection and analysis, decision to publish, or preparation of the manuscript.

Competing interests: The authors declare that no competing interests exist.

* E-mail: g.palmieri@ibp.cnr.it

¤ Current address: Institute of Biosciences and Bioresources, National Research Council (CNR-IBBR), Napoli, Italy

Introduction

Oxidative stress is a dynamic status characterized by an imbalance between the production of reactive oxygen species (ROS) and the activity and availability of antioxidants. Organisms have developed a hierarchy of defence strategies to deal with oxidative stress in which antioxidants (molecules and enzymes) provide the first defensive mechanism, and proteolytic systems act as secondary defences [1]. Among intracellular antioxidants, reduced glutathione (GSH) plays a central role in the maintenance of the thiol-disulfide redox state in mammalian cells and its deregulation is responsible for apoptosis evasion [2], colonizing ability [3] and multidrug resistance of cancer cells [4]. Interestingly, alterations in redox status are known to lead the induction of apoptosis in cancer cells and its decrease represents a molecular mechanism whereby anti-cancer agents reduces malignant cell survival [5].

The proteasome is a multi-catalytic protease responsible for intracellular protein degradation and dysregulation of its activity has been implicated in the pathogenesis of many diseases, including cancer. Proteasome inhibition has recently emerged as an attractive target for anticancer therapy [6]; the rationale for such targeting arose from the concept that in cancer cells, likely because of their higher metabolic rate, proteasome functionality is more crucial than in untransformed cells. Of note, during oxidative stress, the higher activity of 20S proteasome core enzymes aimed at counteracting the accumulation of oxidatively damaged proteins, greatly contributes to secondary anti-oxidative defences [1]. However, a delicate balance between cellular redox status and

proteasome activity is clearly indicated by ROS production during the initiation of apoptotic signalling triggered by bortezomib (BTZ, Velcade), a widely used proteasome inhibitor [7-10] and the impairment of proteasome activity by oxidative stress [11,12].

Due to substrate specificity, 20S enzymes only cleave a limited percentage of peptide bonds in proteins [13] and complete conversion to amino acids is carried out by cytosolic exo- and endo-peptidases which play an important role in cleaving proteasomal produced peptides [14]. Among these proteases, acylpeptide hydrolase (APEH), also named Acylaminoacyl Peptidase or Oxidised Protein Hydrolase, catalyses the removal of N-acylated amino acids from acetylated peptides and was hypothesized to participate in the coordinated degradation of oxidatively modified proteins [15,16].

Conjugated linoleic acid (CLA) is a collective term used to describe the positional and geometric isomers of this fatty acid. Among the eight possible isomers, cis9,trans11 (c9,t11-CLA) and trans10,cis12 (t10,c12-CLA) have attracted considerable attention for their putative health benefits [17]. The commercially available CLA mixture, containing approximately equal amounts of these isomers, exhibited antitumor activity against a broad range of cancer cell types [18] and hindered the growth of numerous types of tumors [19,20]. Of note, similarly to proteasome inhibitors, in several studies the pro-oxidant activity of CLA was associated to its pro-apoptotic effects on cancer cells [21-23] and the modulatory ability of CLA on APEH and proteasomal chymotrypsin-like (CT-like) activities was demonstrated [24,25]. In addition, CLA ability to influence redox status through the activation of NF-E2-related factor 2 (Nrf2) *in vivo* was recently demonstrated [24,26]. The dissociation of Nrf2 from the Kelch-like (Keap1) triggered by electrophile or oxidative stress induces its nuclear translocation and the down-stream activation of genes coding for highly specialized antioxidant and detoxifying proteins. In addition, although Nrf2 has been indicated as a potential target in anticancer therapy [27], nevertheless, to our knowledge, its involvement in the anticancer activity of CLA has not been yet investigated.

Herein, the cellular redox status along with the reduced cancer cell viability induced by CLA isomers, were investigated in relation to the APEH/proteasome system. To this aim, we examined the basal expression/activity level of proteasome and APEH and the anti-proliferative activities elicited by three different CLA isomers (c9,t11-, t9,t11- or t10,c12-CLA) in eight randomly selected cancer cell lines. Interestingly, we identified APEH/proteasome and Nrf2 pathways as the key factors involved in the pro-apoptotic effects of t10,c12-CLA on the A375 melanoma cell lines, revealed to be the best suited experimental model.

Materials and Methods

Materials

Pure fatty acids (octanoic acid, c9,t11-, t9,t11- and t10,c12-CLA isomers), caspase 3 fluorometric assay kit were from Sigma-Aldrich. DMEM, L-glutamine, penicillin-streptomycin and fetal bovine serum (FBS) were from Gibco-BRL. Porcine liver APEH was obtained from Takara. 20S, 20Si, 26S human proteasome were purchased from Boston Biochem. Bortezomib (BTZ) was obtained by Santa Cruz Biothecnology. The following antibodies were used: anti-APEH antibody (sc-102311; Santa Cruz Biotechnology); pan Ab-5 anti-actin antibody (clone ACTN05, Thermo Scientific); anti-Bcl-2 (340576-BD Pharmingen™); anti-proteasome 20S β-5 subunit (BML-PW8895-0025; Enzo Life Science). All chemicals were obtained from Sigma-Aldrich or Calbiochem.

Enzyme assays

APEH activity was measured spectrophotometrically using the chromogenic substrate acetyl-Ala-pNA (Bachem) as described before [25]. The reaction mixture containing pure APEH or an appropriate amount of cell extract was incubated at 37 °C in 50 mM Tris-HCl, pH 7.5 (Tris Buffer).

The fluorescent substrate N-succinyl-Leu-Leu-Val-Tyr-7-amido-4-methylcoumarin (N-Suc-LLVT-AMC) was used for measurement of the CT-like activity of the proteasome, both in *cell free* assays and in cancer cell extracts, at a final concentration of 0.080 mM at 37 °C in Tris buffer pH 7.5, following the procedure described in Palmieri et al. [25].

Enzyme inhibitory assays

Protease inhibition activities of CLA isomers and fatty acids were carried out using a fixed amount of commercially available APEH or 20S, 20Si, 26S proteasomes (3-5 nM or 0.12 mg/mL, respectively), and increasing concentrations of fatty acid. Mixtures were pre-incubated for 30min at 37 °C in 50 mM Tris-HCl buffer pH 7.5, before addition of the specific substrate, and the enzymatic activities were followed as described above.

Inhibitory *cell free* assays were also performed on APEH and proteasome partially purified from A375 cells at 37 °C in Tris buffer pH 7.5 according to a published protocol [25] and the IC_{50} (concentration required for obtaining 50% of the maximum effect measured) values were determined (data not shown). These values, using the considered CLA isomers, were comparable to those obtained with the commercially available porcine APEH (sharing more than 90% of sequence identity with human APEH as calculated by the ClustalW algorithm http://www.genome.jp/tools/clustalw/) and human proteasomes, therefore these enzymes were hereafter used in this study.

Cells, culture conditions and treatments

Human hepatoma cells (HepG2) were seeded ($2x10^4$cells/cm^2) and maintained for 24h in MEM (Gibco Invitrogen; Milano) medium supplemented with 2 mM L-glutamine, 1% nonessential amino acids and 10% FBS. Colon carcinoma (Caco-2), cervical carcinoma (Hela), glioblastoma (U87), melanoma (A375, A375M) and mammary adenocarcinoma (MCF7, MDA-MB) were seeded ($1x10^4$cells/cm^2) and grown in DMEM supplemented with 10% FBS, 2 mM L-glutamine. HepG2, Hela, U87, Caco-2, MCF7, MDA-MB, A375 and A375 metastatic melanoma (A375M) cell lines were obtained by ATCC (LCG standards, Milano, Italy). Normal human dermal fibroblast (NDHF) within 8th passage were seeded at a density

of $2x10^4$ cells/cm^2 and cultured in fibroblast growth medium (FGM-2; Lonza, Milan, Italy) containing 2% FBS, 50 µg/mL gentamycin and amphotericin B, 10µg/mL fibroblast growth factor and insulin. BHK21 cells (kindly donated by Dr. David Y Thomas, McGill University Montreal Canada) were cultured in DMEM/F12, 5% FBS, 1 mM L-glutamine, 200 µg/mL methotrexate, and 100units/mL penicillin-streptomycin. Cells were incubated in a humidified atmosphere at 37 °C in 5% CO_2.

Stock solutions of fatty acids or bortezomib (BTZ) were prepared by dissolving in dimethyl sulphoxide (DMSO) to the final concentration of 1 M or 8.6 mM, respectively, and further dilutions were carried out in DMEM. Cells were treated with fatty acids or BTZ and control culture were exposed to the same amount of DMSO.

MTT-based cytotoxicity assay

The colorimetric 3-(4,5-dimethylthiazol-2)-2,5-diphenyltetrazolium bromide (MTT) (Sigma Aldrich, Milan) assay was used to quantify cell viability. Briefly, cells were incubated in 96 well microplates in the appropriate complete medium with standardized densities for 24h as pre-incubation process. The medium was removed and replaced by medium containing different doses of the different CLA-isomers for 24h. Following treatment, the medium was removed and the cells were incubated with DMEM w/o red phenol with 0.5 mg/ml MTT for additional 2 to 4h at 37 °C. After removal of the medium and MTT, cells in each plate were incubated with 0.1 M HCl/ isopropanol to dissolve the MTT-formazan crystals. Absorbance at 590 nm was recorded with a plate reader (Bio Rad mod 680). The relative number of viable cells was expressed as a percentage of the control.

Cytosolic cell extracts and Western blotting analysis

Following the treatments, cells were washed three times with ice cold phosphate-buffer saline (PBS) and cytosolic extracts were prepared accordingly to a published procedure [26]. Protein concentrations were determined in supernatants by BCA protein assay reagent kit (Pierce). Western blotting analyses were performed as previously described [25].

Intracellular redox status and cell viability assessment

Intracellular concentration of reduced and oxidized glutathione (GSH and GSSG, respectively) were quantified using the 5,5'-dithiobis(2-nitrobenzoic acid)-GSSG reductase recycling assay [26]. GSSG content was preliminarily evaluated in cytosolic extracts of treated or untreated cells upon the addition of 10 mM 1-methyl-2-vinylpyridinium trifluoromethanesulfonate (a specific GSH scavenger). Notably, owing to the minor contribution given by GSSG (less than 5%) to the total intracellular thiol concentration, the latter was finally expressed as nmol GSH/mg protein.

Pro-apoptotic and cytotoxic ability of CLA isomers were assayed by measuring caspase 3 and the activity of lactate dehydrogenase (LDH) in the spent media, respectively [25]. The caspase 3 activity, measured at 37 °C and pH 7.5, was expressed as fold increase compared to the control culture. The LDH release, measured at 37 °C and pH 8.2, was expressed as percentages of total LDH released from cultures treated with 1% (w/v) Triton X-100 and calculated as: [(experimental value-blank value)/(total lysis-blank value)-100].

ROS detection

DCF-DA (2',7'-dichlorofluorescein diacetate) was used to determine the amount of ROS production. DCF-DA working solution was added to the medium to reach 10 µM and then incubated at 37 °C for 15min in the dark. Cells were harvested by trypsinization, washed with PBS and kept on ice for detection by FACScan (Becton Dickinson, USA) equipped with a 488 nm argon laser using a band pass filter of 530 nm.

RNA isolation and quantitative real-time PCR analysis

mRNA expression levels of APEH and β-5 proteasome subunit were determined in treated or untreated cells to investigate on the functional relationship existing between APEH and proteasome activities and on their involvement in the anticancer activity of CLA. In addition, the mRNA expression of NADH quinone oxidoreductase (NQO1) and of gamma Glutamylcysteine Ligase (γGCL), which is the limiting enzyme in the GSH synthesis, were also measured to further demonstrate the CLA ability to down-regulate intracellular redox status via the Nrf2 pathway.

Total RNA was isolated from the human cell lines (~10^6 cells aliquots) according to the SV Total RNA Isolation System (Promega) protocol, with an on column DNase I step. Total RNA concentrations were determined using a Qubit® Fluorometer (Invitrogen). RNAs were then reverse transcribed using the Transcriptor First Strand cDNA Synthesis Kit (Roche). 100 ng of reverse transcribed complementary DNA, and its dilution series to calculate the efficacy of primers, were amplified by quantitative real-time PCR (qRT-PCR) on an iCycleriQ™ (Bio-Rad) using 300 nM gene-specific primers, Maxima® SYBR Green/Fluorescein qPCR Master Mix (2X) (Fermentas) and the following PCR conditions: 1 cycle at 95 °C for 10min, and 40 cycles of 95 °C for 15s , 60 °C for 30s, and 72 °C for 30s.

The expression level of β-actin gene was used as an internal control for normalization (ref gene). Raw cycle threshold values (Ct values) obtained for the target genes were compared to the Ct value obtained for the ref gene. The final graphical data were derived from the $R=(E_{target})^{\Delta Ct\_target\ (control\ -\ sample)}/(E_{ref})^{\Delta Ct\_ref\ (control\ -\ sample)}$ formula [28], where "control" cells were fibroblasts or A375 line, and "sample" cells were the tumor lines. In time-course analysis the expression levels were normalized to those of untreated cells at Time=0.

Universal Probe Library Assay Design Center (https://www.roche-appliedscience.com/sis/rtpcr/upl/index.jsp?id=UP030000) was used for designing primers.

The primers utilized were:

APEH, 5'-CCCCATTCATCCTTTGTCAC-3' and 5'-AAAGCCCATCTTGCAAAGC-3';

β-5, 5'-CATGGGCACCATGATCTGT-3' and 5'-GAAATCCGGTTCCCTTCACT-3';

γGCL, 5'-GACAAAACACAGTTGGAACAGC-3'and 5'-CAGTCAAATCTGGTGGCATC-3';

NQO1, 5'-CAGCTCACCGAGAGCCTAGT-3' and 5'-GAGTGAGCCAGTACGATCAGTG-3';
β-actin, 5'-CCAACCGCGAGAAGATGA-3' and 5'-CCAGAGGCGTACAGGGATAG-3'.

Statistical analysis

All data were obtained from triplicate analyses of three different preparations, and presented as means ±S.D. Statistical analysis and IC_{50} values were calculated with SigmaPlot 10.0 software through a non-linear curve-fitting method and using a simple binding isotherm equation. Groups were compared by Student's *t* test, and $P<0.05$ was considered as significant.

Results

t10,c12-, t9,t11- and c9,t11-CLA isomers differentially inhibit APEH and proteasome

A preliminary investigation of the potential inhibitory effect of CLA isomers on chymotrypsin-like (CT-like) activity of proteasome isoforms (20S, 20Si and 26S), was carried out. Inhibition analyses were performed by pre-incubating the purified enzyme with increasing amounts of each compound and their half-maximal inhibitory concentrations (IC_{50}) were determined. The curves followed a hyperbolic pattern reaching 100% inhibition with all the proteasomes (Figure 1A-C) and CLA isomers tested, althought t10,c12- and c9,t11-CLA were the best effectors (IC_{50}=14.8±2.0 μM and 31.2±8.8 μM on 20S isoform and 1.1±0.2 μM and 6.4±1.0 μM on 20Si isoform for t10,c12- and c9,t11-CLA, respectively). Similar experiments were carried out by using the proteasome inhibitor bortezomib (BTZ) (Figure **1D**) because of its recognized anti-proliferative activity on cancer cells. As expected, BTZ appeared to target both 20S (IC_{50}=1.4±0.3 nM) and 20Si (IC_{50}=2.1±0.5 nM) isoforms indiscriminately, reaching about 60% of inhibition in both cases, while octanoic acid (data not shown), used as a negative control, gave only negligible effects.

Next, before to investigate the possible mechanisms underlying the CLA-reduced viability of cancer cells, the potential contribution of APEH was explored. When the ability of these compounds to modulate APEH in *cell-free* assays was evaluated (Figure **1E**), only t10,c12-CLA was revealed to affect the enzyme activity in a dose-dependent manner, reaching a maximum inhibition of about 41% (IC_{50}=110.1±11.7 μM) as calculated by SigmaPlot 10.0 software.

Therefore, a stereoselective binding in the interaction with APEH and proteasome isoforms of the CLA isomers can be proposed together with a specific ability of t10,c12-CLA to inhibit all these enzymes .

APEH and proteasome expression at both mRNA and protein level correlates with their enzyme activity in cancer cell lines

In evaluating the involvement of APEH and proteasome in the anti-cancer effects of CLA isomers, we decided to examine the basal expression/activity levels of these enzymes in eight cancer cell lines (at their pre-confluent stage) to select the best cellular candidate for further investigations. As shown in Figure 2A, when basal specific APEH activity was plotted against the corresponding proteasomal chymotrypsin-like (CT-like) activity, a significant positive correlation was found (r^2=0.988, P=<0.01), supporting the idea of a functional relationship between these two enzymes which could act in cooperation for degradation of damaged proteins [15,16]. Moreover, on the basis of gene expression analysis and intracellular protein levels (Figure 2B and 2C), the different cancer cells could be divided into two groups displaying low (U87, HeLa, MDA-MB and MCF7: Group I) or high (A375, A375M, HepG2 and $Caco_2$: Group II) protein, activity and transcript levels of APEH and proteasome (β-5 subunit). Data on the immunoproteasome subunit (β-5i subunit) were not reported due to the low detectable levels in all the cancer cells investigated. These findings suggested that cells exhibiting high basal activity and expression levels of APEH and proteasome could be highly dependent on these enzyme functions and therefore more sensitive to their down-regulation.

Cancer cell proliferation is significantly inhibited and associates with caspase 3 activation in cells exposed to t10,c12-CLA

The susceptibility of cell lines belonging to Group I and Group II to the growth inhibitory effects of CLA isomers was estimated upon 24h exposure at concentrations ranging from 50 to 200 μM. Data indicated that only A375, A375M and MDA-MB cells exhibited a moderate reduction (<40%) of cell viability by c9,t11-CLA treatment (Figure 3A), while a more marked anti-proliferative effect was observed following cell exposure with t10,c12-CLA on HeLa, A375M and A375 (40, 51 and 63% respectively) (Figure 3B). A375 cell viability was also greatly influenced by t9,t11-CLA (about 50%) (Figure 3C), whereas no significant results were obtained on all cancer cells by octanoic acid (up to 200 μM) treatment, which was used as a negative control (data not shown).

To assess the cytotoxicity and antiproliferative activity of the most abundant CLA isomers on the cancer cells considered, LDH activity was measured in spent media following 24h exposure to 200 μM c9,t11-, t10,c12-CLA or to 10 nM BTZ, using octanoic acid as negative control. As expected, substantial cell death resulted from BTZ supplementation while the LDH activity in cultures exposed to CLA isomers was comparable to that of control (Figure 4A). Moreover, to examine the contribution of an apoptotic event in CLA-induced decline of cancer cells viability, caspase 3 activation was measured. Interestingly, results revealed that while caspase 3 activation varied slightly between the different tumor cell lines upon exposure with c9,t11-CLA, a more marked variation was observed by t10,c12-CLA treatment (Figure 4B), leading to inversely correlated measures of cell viability and caspase 3 activation (r^2=0.78; P<0.01) (Figure 4C). It's worth to note that, although CLA reduced cell viability in the considered cell lines with no cytotoxicity (LDH release), nevertheless its pro-apoptotic activity couldn't be accounted for the observed cell death, therefore a cytostatic effect cannot be excluded.

In addition, proteasome activity was differently down-regulated by CLA isomers (Figure S1) but it was not significantly correlated with cell viability decrease (r^2=0.046;

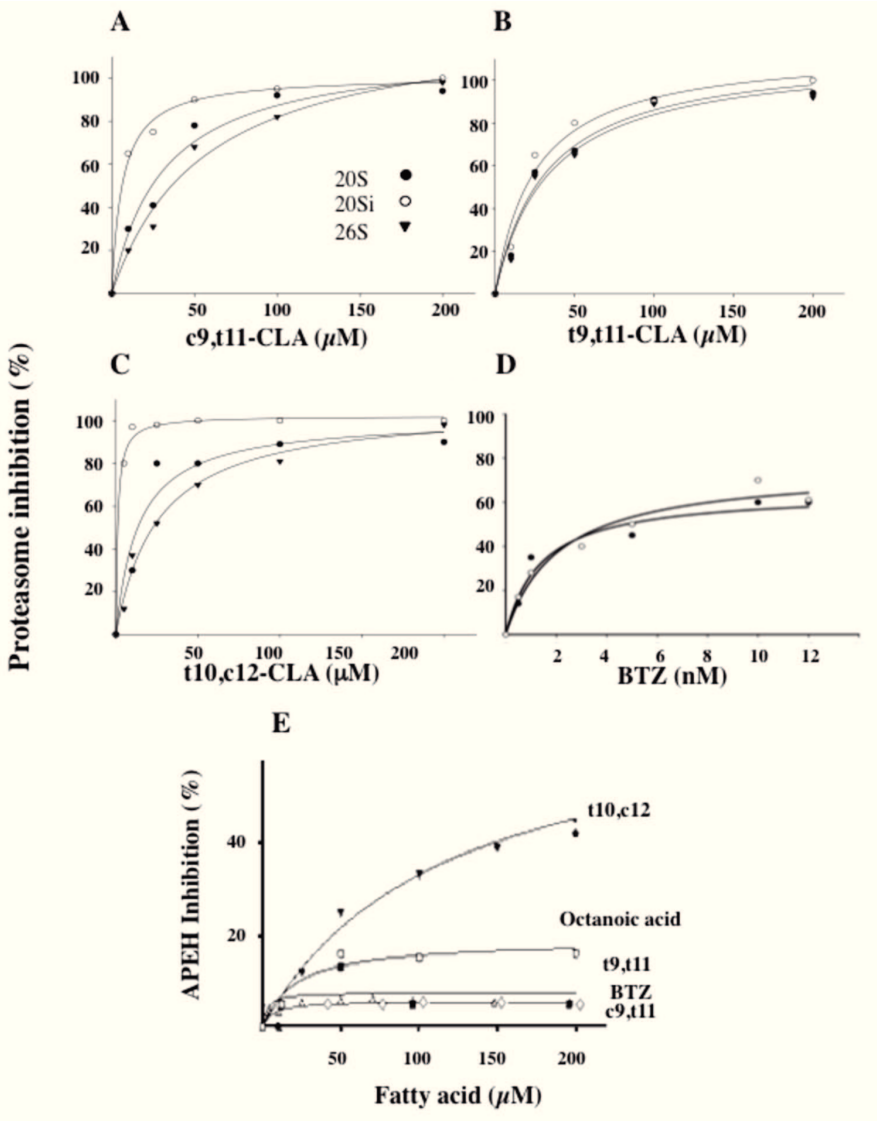

Figure 1. Fatty acids and CLA isomers exhibit dissimilar inhibitory ability towards chymotrypsin-like (CT-like) proteasome and APEH activities. The inhibitory effect of different CLA isomers, namely c9,t11- (**A**), t9,t11- (**B**), t10,c12-CLA (**C**), bortezomib, BTZ (**D**), was evaluated on commercially available pure 20S (black circles), 20Si (white circles) and 26S (black triangles) proteasomes. The synthetic fluorescent substrate N-Suc-LLVT-AMC (0.080 mM) was used for the measurement of the CT-like activity of the proteasomes. The hyperbolic curves indicate the best fits for the data obtained, with IC50 values calculated from the graphs by SigmaPlot 10.0 software. Mixtures treated with DMSO alone were used as blank. The dose-dependent inhibitory effect of c9,t11-, t9,t11-, t10,c12-CLA isomers, octanoic acid or bortezomib on APEH activity was shown (**E**). Results are presented as the mean ± standard deviation (SD) of triplicate analyses from three independent experiments. SD values lower than 5% were not shown.

doi: 10.1371/journal.pone.0080900.g001

data not shown), suggesting that proteasome inhibition alone was not liable for the observed anti-proliferative activity of CLAs. Hence, it appears reasonable to hypothesize that an enzyme machinery, such as APEH/proteasome system, could be involved in the marked anti-proliferative and pro-apoptotic activity exerted by t10,c12-CLA through its specific capacity to down-regulate both enzymes (Figure 1).

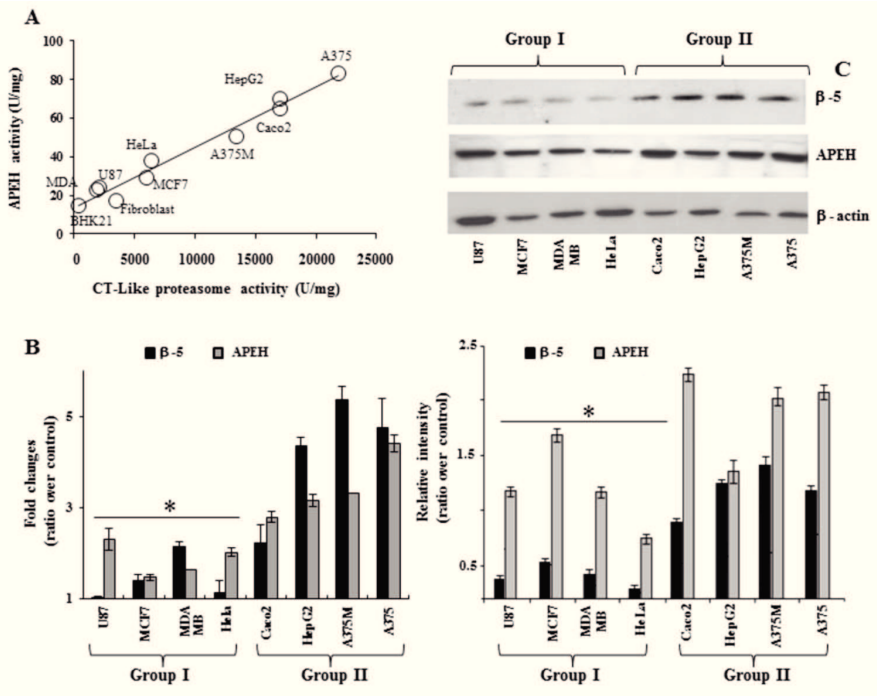

Figure 2. Human cancer cell lines may be grouped according to the basal enzyme activities and expression levels of APEH and proteasome. Cells from eight human cancer lines (U87, MCF7, MDA-MB, HeLa, $Caco_2$, HepG2, A375M, A375) and non-cancerous cells (BHk21, fibroblasts) were harvested at the pre-confluent stage and used for cytoplasmic or mRNA extract preparation. Basal APEH and proteasomal CT-like activities were measured in cytoplasmic extracts (A). The mRNA levels of APEH and β-5 subunit were evaluated by qRT-PCR and expressed as fold change in comparison to expressed levels in human fibroblast (B). Intracellular levels of β-5 and APEH were detected by immunoblotting (C upper panel). Typical Western blot was shown and data from three different analyses were normalized to the density of control protein (β-actin) and expressed as ratio over control (C lower panel). Results are presented as the mean values ±SD of triplicate analyses from at least three different experiments. *Significantly different ($P < 0.01$) from respective controls.

doi: 10.1371/journal.pone.0080900.g002

t10,c12-CLA decreases glutathione level and APEH/ proteasome activity in A375 cells triggering apoptosis in a dose-dependent fashion

On the basis of the marked cell viability reduction (Figure 3B) induced by t10,c12-CLA on A375 melanoma cell line, we decided to use this model system for investigations on the different cellular factors (redox status, caspase 3, APEH and proteasome) involved in the apoptotic pathway.

In order to define the dose accountable for 50% decrease of cell viability (IC_{50}), A375 cells were exposed for 24h to a concentration range of t10,c12-CLA or BTZ (from 10 nM to 400 μM), using human fibroblasts as control. The resulting isobologram revealed that the IC_{50} values were 1.0±0.02 μM or 10.0±0.02 nM for t10,c12-CLA or BTZ, respectively. Moreover, proliferation data obtained from fibroblasts, even at higher concentration of t10,c12-CLA, further supported the lack of toxic effects (Figure 5A).

Next, cultures were incubated with increasing t10,c12-CLA doses (50, 100 or 200 μM) and the possible additive effect elicited by sub-toxic amount of BTZ (5 nM) was evaluated in cells co-incubated with t10,c12-CLA for 24h. The results obtained (Figure 5B) demonstrated that the dose-dependent activation of caspase 3 was triggered by t10,c12-CLA, reaching an eightfold increase compared to the control culture. Notably, pro-apoptotic induction, associated with a significant decline in intracellular GSH, was not further improved by BTZ supplementation (Figure 5B). Similarly, APEH and proteasome mRNA levels were strongly down-regulated by 200 μM t10,c12-CLA treatment (Figure 5C, right panel) and only minor alterations were produced by the addition of BTZ (data not shown). Interestingly, while a dose-dependent inhibition of APEH activity was observed, the proteasomal CT-like activity was inhibited to 46 and 50% by 50 and 100 μM t10,c12-CLA, respectively and a less marked effect resulted from cells exposed to 200 μM CLA (25%) (Figure 5C, left panel). Moreover, the decline of APEH and β-5 protein expression only occurred at the higher CLA dose ($p<0.05$) (Figure 5D). In addition, the noticeable decrease of the anti-apoptotic protein Bcl-2 expression, reaching the maximum reduction of 80%, further supported the role of apoptosis in the anti-proliferative

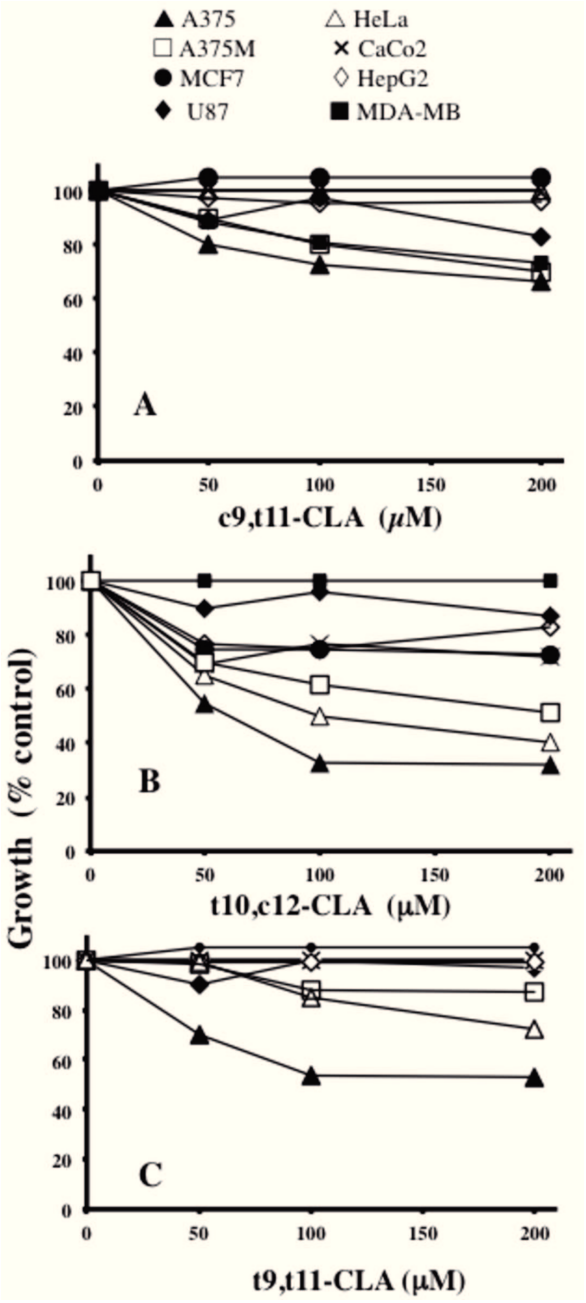

Figure 3. Human cancer cells exhibit differential sensitivity to the anti-proliferative activity of CLA isomers. The effects of c9,t11 (A), t10,c12- (B) or t9,t11-CLA isomers (C) on cell viability were assessed in eight cancer cell lines exposed for 24h to increasing concentrations of the CLA isomers. Data are expressed as means ±SD values of triplicate data from three independent experiments. SD values lower than 5% were not shown.

doi: 10.1371/journal.pone.0080900.g003

effect of t10,c12-CLA (Figure 5D). Finally, we showed that cell exposure to high t10,c12-CLA doses markedly down-regulated the Nrf2 pathway, as evidenced by the declined mRNA levels of some target genes (NQO1 and γGCL), expressed as fold change in comparison to untreated cells (Figure S2).

These findings support the hypothesis that the combined down-regulation of antioxidant/detoxifying defences, APEH/proteasome system and Bcl-2 levels, may play an important role in apoptosis induction triggered by t10,c12-CLA in A375 cells.

A375 exposure to high t10,c12-CLA doses increases ROS production in association with apoptotic events and APEH/proteasome down-regulation in time-dependent fashion

Time-dependent monitoring of ROS production, APEH and proteasome (β-5) at mRNA and enzyme activity level, was performed to evaluate the effects produced by the exposure to lower (50 μM) or higher (200 μM) t10,c12-CLA concentrations, on pre-confluent A375 cells. Sudden decrease (2h) of APEH and proteasomal CT-like activities in cells exposed to low doses, correlated with a transient reduction of their mRNA expression. Upon this early response, enzyme activities recovered, reaching a plateau after 8h with values corresponding to 80 or 70% of their starting values, respectively (Figure 6A). Similarly, mRNA profiles showed a short-lived gene repression, which quickly recovered towards the stable final values, being approximately one-fold lower than their initial expression level (Figure 6B). Conversely, the higher concentration of t10,c12-CLA produced a downshift of APEH activity reaching a plateau with average values of 70% compared to its starting level, whereas a long-term down-regulation of proteasomal activity persisted up to 16h (Figure 6C). Interestingly, two transient minima of mRNA levels were observed after 2 and 6h, followed by a significant increase until 16h. After 24h of incubation, APEH and β-5 expression decreased again reaching the corresponding lowest values (Figure 6D).

The time-dependent ROS production indicated that the early down-regulation of APEH /proteasome enzyme activities could be induced by ROS yield (Figure 6A), while a direct modulation of the CLA isomer on both enzymes can possibly contribute to the following decrease of the activity/mRNA levels observed at 200 μM (Figure 6C,D). Cell pre-incubation with the antioxidant N-acetyl cysteine (NAC, 5 mM) before the 200 μM CLA exposure (2 or 24h) resulted in a marked cytotoxic effect (data not shown).

Finally, time-dependent effects elicited by 200 μM t10,c12-CLA on GSH concentration and caspase 3 activity, together with γGCL mRNA levels, were measured. As shown in Figure 7A, the decline of intracellular GSH was followed by caspase 3 activation (after 6-8h). To investigate the mechanism underlying the pro-oxidant activity of t10,c12-CLA, the mRNA expression of the rate-limiting enzyme responsible for cellular GSH synthesis (namely γGCL) was monitored. As expected, the early activation triggered by CLA isomer (after 2h) was followed by a transient decrease in mRNA (peaking after 4h),

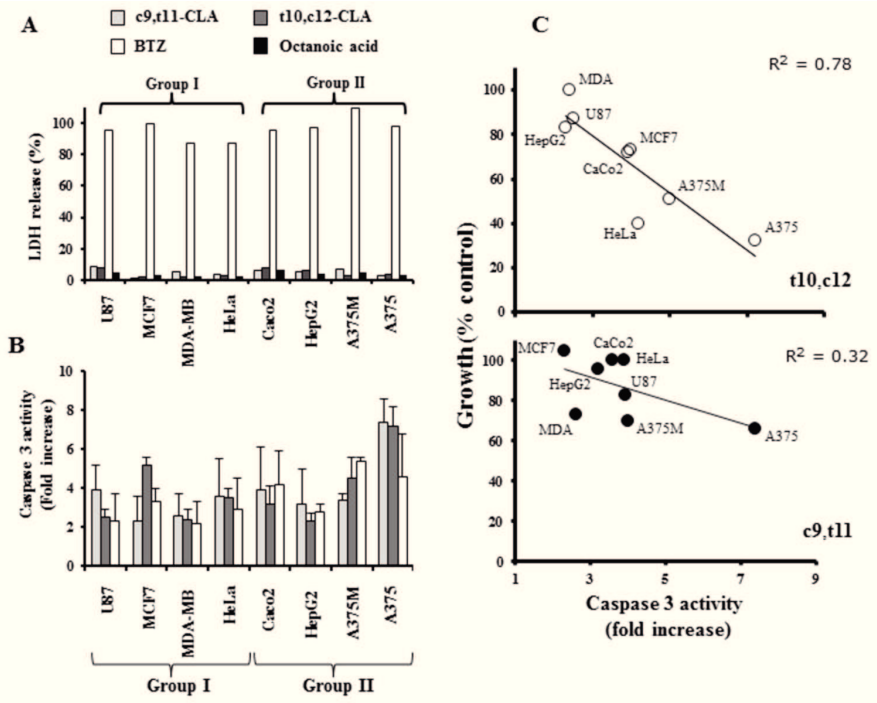

Figure 4. Anti-proliferative ability of t10,c12-CLA correlates with caspase 3 activation. LDH release (A) and caspase 3 activity (B) were measured to study the cytotoxic and pro-apoptotic ability of 200 μM of t10,c12- (dark grey bars) or c9,t11-CLA (light grey bars). Cell cultures exposed to octanoic acid (200 μM, black bars) or to BTZ (10 nM, white bars) were used as negative or positive controls, respectively. Average caspase 3 activity values (fold increase) in cancer cells exposed for 24h to 200 μM t10,c12- (C upper panel) or to c9,t11- CLA (C lower panel) were plotted against cell viability (%).

doi: 10.1371/journal.pone.0080900.g004

which temporarily recovered before leading to the down-regulation (1.5 fold) of mRNA levels (Figure 7B).

Discussion

Owing to their enhanced metabolic activity, cancer cells require elevated levels of energy to maintain a high rate of cell growth and proliferation. This is also guaranteed by an improved activity of the Ubiquitin-Proteasome System, which is the major pathway for protein turnover in eukaryotes [29], providing a secondary antioxidant defence mechanism, in combination with APEH [15,16]. Indeed, protein homeostasis is critically involved in cancer cell survival; thus, one of the major *focus* in cancer research is targeting the balance between the production and destruction of proteins mediating cell proliferation. In this context, proteasome inhibition represents a novel strategy against many tumoral diseases, triggering an increase in apoptosis and decrease in cellular growth. Accordingly, in the last decade, research and development of new compounds able to down-regulate proteasome functions have attracted growing attention.

It is known that the pro-apoptotic ability of CLA mixture (c9,t11- and t10,c12-CLA; 50:50) or its individual isomers, affects tumor cell proliferation *via* different biochemical pathways involving apoptotic or survival genes (Bcl-2, p21, p53). The efficacy of these isomers in inhibiting the cancer cell viability was highly influenced by the model system used, within a concentration range of 1-200 μmol/L and treatment lasting 1-11 days [18]. Specifically, t10,c12-CLA has revealed a more efficient activity, respect to c9,t11-CLA isomer, in modulating apoptosis or cell cycle. In human prostatic carcinoma cells, t10,c12-CLA anticancer effect associates to decreased Bcl-2 and increased p21(WAF1/Cip1) mRNA levels [30] while in human colon or bladder cancer cells it was accompanied by the activation of ATF/NAG-1 [31] or Insulin Growth Factor signaling [32]. Moreover, it was reported that t10,c12-CLA was able to down-regulate Fatty Acid Synthase [33] or antioxidant defence systems [21,22,34] in different human cancer cells.

In such a context, the purpose of this study was to explore the relationship between the anti-proliferative properties and the ability of CLA isomers to down-regulate the APEH/ proteasome system in cancer cells, taking into account the role of cellular redox status in these processes.

We firstly evaluated the effects of CLA isomers on purified proteasomes and APEH in *cell free* assays, showing that t10,c12-CLA was the only isomer able to efficiently inhibit both enzymes, which appeared functionally correlated, in a cancer cell panel.

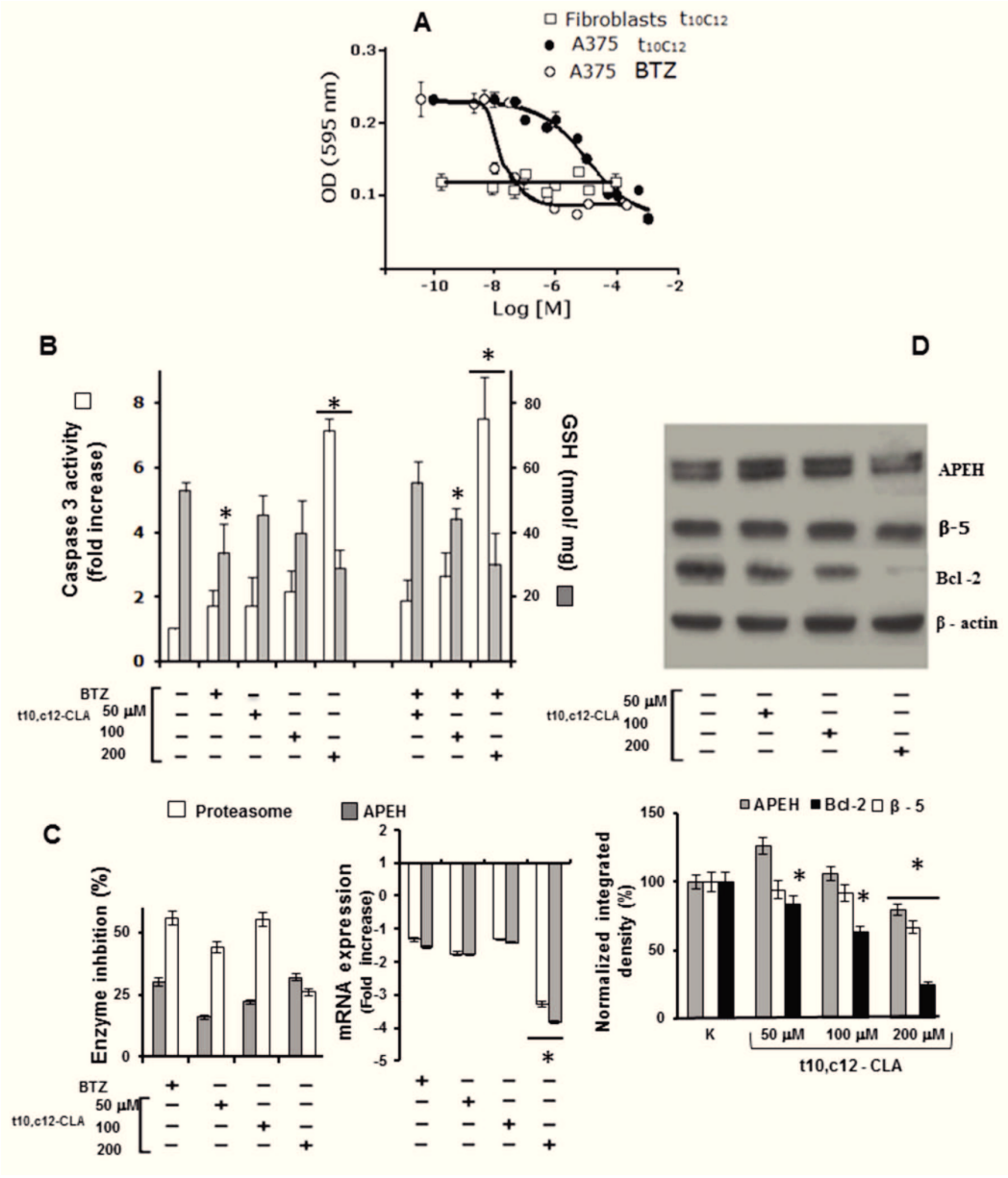

Figure 5. Dose-dependent pro-apoptotic activity of t10,c12-CLA correlates with down-regulation of GSH, APEH and proteasomal CT-like subunit at both mRNA and activity level in A375 cells. Isobologram of A375 cells treated with t10,c12-CLA or BTZ for 24h is reported in panel A. Human fibroblasts exposed to the same t10,c12-CLA concentrations were used as control. Data are expressed as means ±SD values of triplicate data from three independent experiments. Pre-confluent A375 cultures were incubated for 24h with 50, 100 or 200 µM t10,c12-CLA. Thereafter, cells were harvested, and used for cytoplasmic or mRNA extracts preparation. Cells untreated or treated with 10 nM BTZ were used as negative or positive controls, respectively. Measurement of GSH concentration (B), caspase 3 activity (B) and APEH or proteasomal CT-like activities (C left panel) were performed on cytoplasmic extracts. The mRNA levels of APEH and β-5 subunit were evaluated by qRT-PCR and expressed as fold change in comparison to untreated cells (C right panel). Intracellular levels of Bcl-2, APEH and β-5 were detected by immunoblotting (D upper panel). Data on Western blot analysis were normalized to the density of control (β-actin) and the values were expressed as percent value as compared to untreated cultures (K) on triplicate measurements (D lower panel). Results were presented as means ±SD of triplicate data from three independent experiments. *Significantly different ($P < 0.01$) from respective controls.

doi: 10.1371/journal.pone.0080900.g005

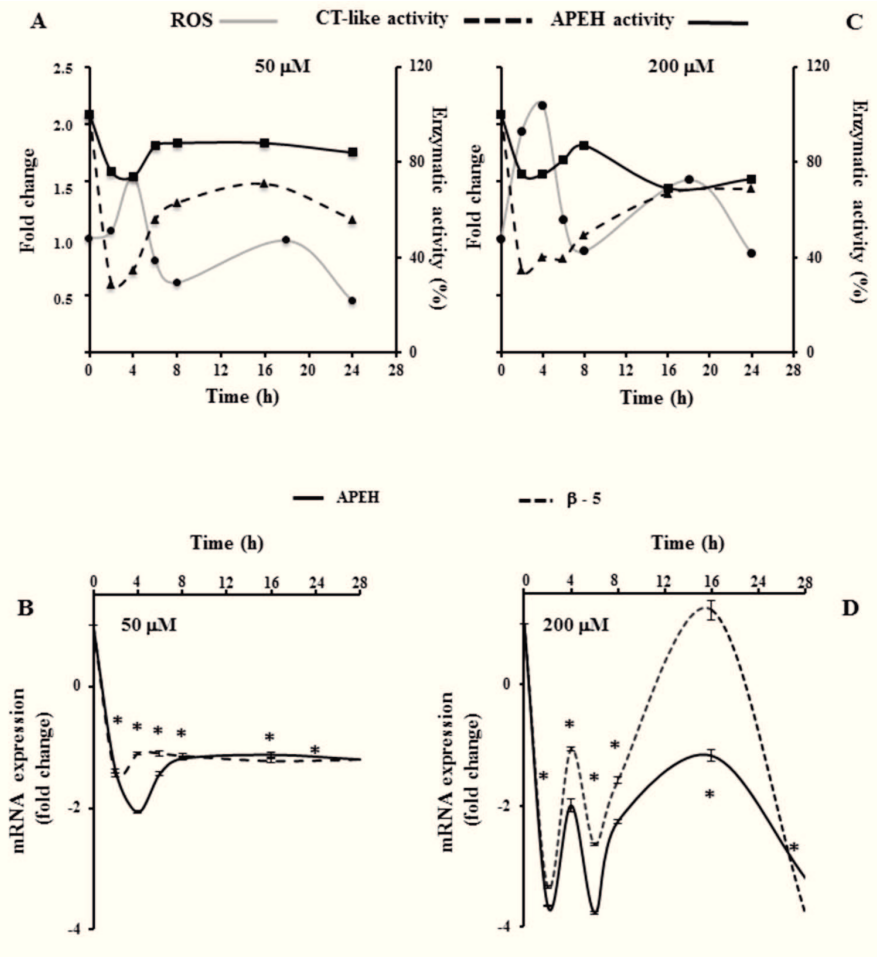

Figure 6. Time-dependent effects of t10,c12-CLA on APEH/proteasome system and on ROS production in A375 cells. Pre-confluent A375 cells were incubated with 50 µM or 200 µM of t10,c12-CLA for the indicated times. After treatments, cytoplasmic cell-extracts were used for the measurement of APEH and proteasomal CT-like activities (A,C). The ROS profiles were compared with the time courses of proteasomal CT-like and APEH activity levels (A,C). ROS production was assessed as described in materials and methods. cDNAs were synthesized and used for qRT-PCR amplification of APEH and β-5 (B,D) at the indicated times. The mRNA levels were finally expressed as fold change in comparison to untreated cells. Results were presented as means ±SD of triplicate data from three independent experiments and SD values lower than 5% were not shown. *Significantly different ($P < 0.01$) from respective controls.

doi: 10.1371/journal.pone.0080900.g006

Intriguingly, the link observed between caspase 3 activation and cell viability in t10,c12-CLA treated cells, supported the apoptosis role in the anti-proliferative effects specifically induced by this isomer. The higher susceptibility to the t10,c12-CLA treatment of A375 melanoma cell line, showing the highest basal levels of APEH/proteasome, is consistent with the involvement of this system in cell survival. Unfortunately, this hypothesis cannot be extended to all the tested cell lines showing high constitutive enzymatic levels. In addition, we demonstrated that early ROS production triggered by higher t10,c12-CLA doses, along with the combined down-regulation of NF-E2-related factor 2-Antioxidant responsive elements (Nrf2-ARE) pathway and proteasome-APEH activity/expression levels, was likely responsible for the programmed A375 cell death. However, these results couldn't be further investigated by using antioxidants (NAC) and t10,c12-CLA combination in cell treatment (data not shown) due to NAC toxicity on A375 cells [35].

The endogenous oxidative stress rarely leads to damage, because a healthy cell generally possesses a powerful antioxidant defence to inactivate ROS. However, when cellular antioxidants are compromised, as occurs in the context of

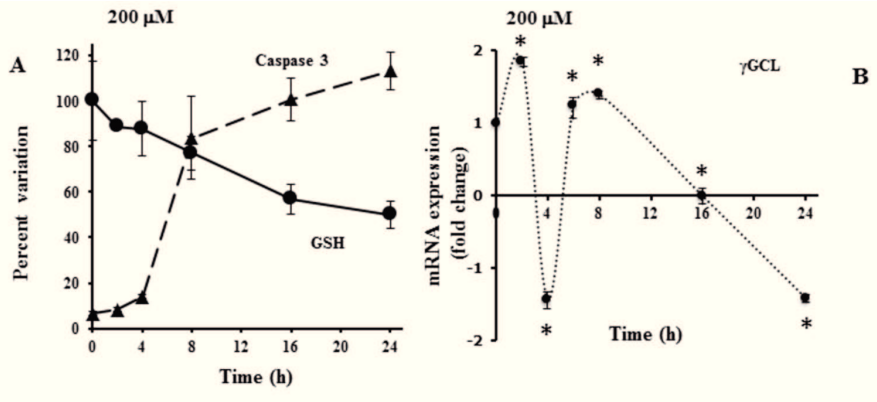

Figure 7. Time-dependent effects of t10,c12-CLA on caspase 3 and cyto-protective defences on A375 cell. Pre-confluent A375 cultures were incubated with 200 µM t10,c12-CLA for the indicated times. After treatments, cytoplasmic cell-extracts were used for the measurement of GSH concentration and caspase 3 activity (A). GSH and caspase 3 activities were expressed as percent variation in comparison to cells harvested at the beginning or at the end of the incubation, respectively. cDNAs were synthesized and used for qRT-PCR analysis of γGCL transcripts (B) at the indicated times. The mRNA levels were finally expressed as fold change in comparison to untreated cells. Results were presented as means ±SD of triplicate data from three independent experiments. SD values lower than 5% were not shown. *Significantly different ($P < 0.01$) from respective controls.

doi: 10.1371/journal.pone.0080900.g007

external environmental challenges, cell death is the expected outcome. By contrast, in several tumoral cells, hyperactivation of endogenous sources of ROS, which generates the observed increased levels of these molecules, results in a state of chronic oxidative stress [2,15]. It is well established that GSH plays an important role in cancer development and treatment, as it can protect against DNA damages produced by ROS and electrophilic chemicals [36]. Generally, in various types of cancerous cells and solid tumors, elevated GSH levels are observed, making these cells and tissues less susceptible to chemotherapy by increasing the resistance to oxidative stress. However, although chronic ROS exposure confers several advantages to cancer cells, by stimulating proliferation and maintaining the transformed phenotype [37], excessive ROS yield may induce cell cycle arrest and apoptosis. Therefore, redox state modulation in tumoral cells has been indicated as a possible target for cancer [38] or, specifically, for melanoma treatment [39].

In this context, our results, showing the increased intracellular GSH levels in A375 cells, were in agreement with studies reporting the central role played by redox homeostasis in the control of melanoma survival, proliferation and invasiveness [40]. Moreover, the association of pro-oxidant activity of t10,c12-CLA with anti-proliferative effect, was consistent with literature [21,22] and conformed to the activities of recently discovered proteasome inhibitors, triggering ROS production in melanoma cells through oxidative stress activation [41,42]. In addition, although the down-regulation of the Nrf2 pathway, was accompanied by the caspase 3 activation in cells exposed to high t10,c12-CLA doses , nevertheless there is not necessarily a direct cause/effect between these two events. In accordance with the importance of Nrf2 down-regulation in tumour growth reduction and in enhancing the efficacy of chemotherapeutic agents [43], the use of t10,c12-CLA in combination with specific APEH/ proteasome inhibitors could represent an effective strategy for melanoma treatment.

To sum up, t10,c12-CLA-induced oxidative stress was detectable at very early times, as revealed by the increase of DCF fluorescence (Figure **6C**), down-regulation of γGCL expression (Figure **7B**) and the following decline of intracellular thiols (Figure **7A**). Hence, it is reasonable to hypothesize that the oxidative stress and the Nrf2-activation, triggered by t10,c12-CLA, are upstream processes contributing to the APEH/proteasome down-regulation (Figure **8**) [11,44,45] which culminate in activation of caspase 3.

The finding of time progression events provides additional insights toward understanding the CLA-activated mechanisms, which are involved in the anticarcinogenic effects of these compounds, particularly the t10,c12-CLA isomer, in melanoma cancer cells. Further research are needed to support the role played by APEH in the down-regulation of cancer cell viability.

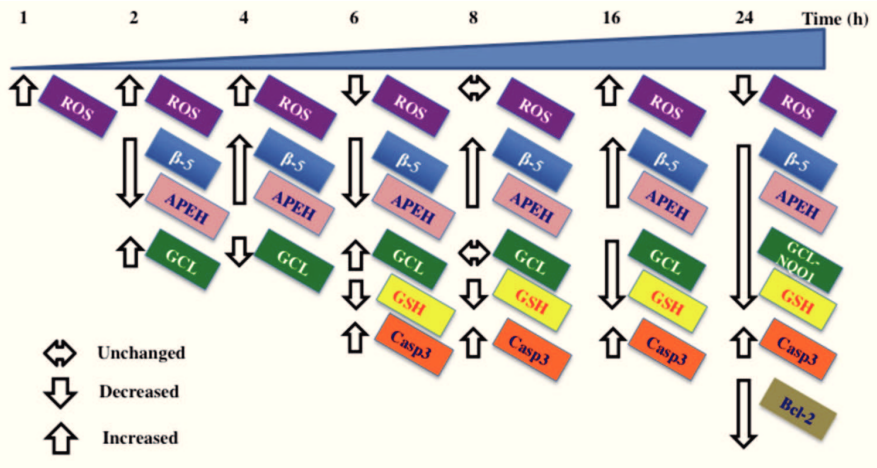

Figure 8. Summary diagram. In the scheme early ROS yield (after 1h), triggered by cells exposure to 200 μM t10,c12-CLA, led to the transient decline of the detoxifying APEH/proteasome system and the improved γGCL expression, following the increased nuclear translocation of Nrf2. During the next 10h, the partial recovery of β-5 and APEH transcription paralleled the reduced GCL expression and intracellular GSH levels resulting in the increased apoptosis (caspase 3 activity, casp3). After 24h incubation, the simultaneous decline of β-5, APEH, γGCL and NQO1 transcriptional levels and of intracellular GSH are associated with decreased cell viability likely *via* apoptosis enhancement (as evidenced by increased casp3 activity and Bcl-2 degradation).

doi: 10.1371/journal.pone.0080900.g008

Supporting Information

Figure S1. Proteasome activity is differently down-regulated by CLA isomers. Proteasomal CT-like activity was measured in eight cancer cell lines exposed to 200 µM of t10,c12- (dark grey bars) or c9,t11-CLA (light grey bars). Cell cultures exposed to octanoic acid (200 µM, black bars) or to BTZ (10 nM, white bars) were used as negative or positive controls, respectively. Data are expressed as means ±SD values of triplicate data from three independent experiments, SD values lower than 5% were not shown.
(PDF)

Figure S2. mRNA levels of GCL and NQO1 in A375 cells treated with 50 or 200 µM of t10,c12-CLA for 24h. The mRNA levels were evaluated by RT-PCR and expressed as fold change in comparison to untreated cells. *Significantly different ($P < 0.01$) from respective controls.
(PDF)

Author Contributions

Conceived and designed the experiments: GP PB EC. Performed the experiments: MG RP PB. Analyzed the data: GP RP MR PB. Contributed reagents/materials/analysis tools: GP EC MR. Wrote the manuscript: GP MG PB.

References

1. Grune T, Davies KJ (1997) Breakdown of oxidized proteins as a part of secondary antioxidant defenses in mammalian cells. Biofactors 6: 165-172. doi:10.1002/biof.5520060210. PubMed: 9259998.
2. Franco R, Sánchez-Olea R, Reyes-Reyes EM, Panayiotidis MI (2009) Environmental toxicity, oxidative stress and apoptosis: Menage a trios. Mutat Res 674: 3-22. doi:10.1016/j.mrgentox.2008.11.012. PubMed: 19114126.
3. Carretero J, Obrador E, Anasagasti MJ, Martin JJ, Vidal-Vanaclocha F et al. (1999) Growth-associated changes in glutathione content correlate with liver metastatic activity of b16 melanoma cells. Clin Exp Metastas 17: 567-574. doi:10.1023/A:1006725226078. PubMed: 10845555.
4. Lai GM, Moscow JA, Alvarez MG, Fojo AT, Bates SE (1991) Contribution of glutathione and glutathione-dependent enzymes in the reversal of adriamycin resistance in colon carcinoma cell lines. Int J Cancer 49: 688-695. doi:10.1002/ijc.2910490511. PubMed: 1682279.
5. Chandra J (2009) Oxidative stress by targeted agents promotes cytotoxicity in hematologic malignancies. Antioxid Redox Signal 11: 1123-1137. doi:10.1089/ars.2008.2302. PubMed: 19018667.
6. Schwartz AL, Ciechanover A (2009) Targeting proteins for destruction by the ubiquitin system: implications for human pathobiology. Annu Rev Pharmacol Toxicol 49: 73–96. doi:10.1146/annurev.pharmtox.051208.165340. PubMed: 18834306.
7. Ling YH, Liebes L, Zou Y, Perez-Soler R (2003) Reactive oxygen species generation and mitochondrial dysfunction in the apoptotic response to Bortezomib, a novel proteasome inhibitor, in human H460 non-small cell lung cancer cells. J Biol Chem 278: 33714-33723. doi: 10.1074/jbc.M302559200. PubMed: 12821677.
8. Pérez-Galán P, Roué G, Villamor N, Montserrat E, Campo E et al. (2006) The proteasome inhibitor bortezomib induces apoptosis in mantle-cell lymphoma through generation of ROS and Noxa activation independent of p53 status. Blood 107: 257-264. doi:10.1182/blood-2005-05-2091. PubMed: 16166592.
9. Yu C, Rahmani M, Dent P, Grant S (2004) The hierarchical relationship between MAPK signaling and ROS generation in human leukemia cells undergoing apoptosis in response to the proteasome inhibitor Bortezomib. Exp Cell Res 295: 555-566. doi:10.1016/j.yexcr.2004.02.001. PubMed: 15093752.
10. Wu M, Bian Q, Liu Y, Fernandes AF, Taylor A et al. (2009) Sustained oxidative stress inhibits NF-kappaB activation partially via inactivating the proteasome. Free Radic Biol Med 46: 62-69. doi:10.1016/j.freeradbiomed.2008.09.021. PubMed: 18948189.
11. Reinheckel T, Sitte N, Ullrich O, Kuckelkorn U, Davies KJ et al. (1998) Comparative resistance of the 20S and 26S proteasome to oxidative stress. Biochem J 335: 637-642. PubMed: 9794805.
12. Fribley A, Zeng Q, Wang CY (2004) Proteasome inhibitor PS-341 induces apoptosis through induction of endoplasmic reticulum stress-reactive oxygen species in head and neck squamous cell carcinoma cells. Mol Cell Biol 24: 9695-9704. doi:10.1128/MCB.24.22.9695-9704.2004. PubMed: 15509775.
13. Kisselev AF, Akopian TN, Woo KM, Goldberg AL (1999) The size of peptides generated from protein by mammalian 26 and 20S proteasomes. J Biol Chem 274: 3363–3371. doi:10.1074/jbc.274.6.3363. PubMed: 9920878.
14. Reits E, Neijssen J, Herberts C, Benckhuijsen W, Janssen L et al. (2004) A major role for TPPII in trimming proteasomal degradation products for MHC class I antigen presentation. Immunity 20: 495–506. doi:10.1016/S1074-7613(04)00074-3. PubMed: 15084277.
15. Shimizu K, Kiuchi Y, Ando K, Hayakawa M, Kikugawa K (2004) Coordination of oxidized protein hydrolase and the proteasome in the clearance of cytotoxic denatured proteins. Biochem Biophys Res Commun 324: 140–146. doi:10.1016/j.bbrc.2004.08.231. PubMed: 15464994.
16. Shimizu K, Fujino T, Ando K, Hayakawa M, Yasuda H et al. (2003) Overexpression of oxidized protein hydrolase protect COS-7 cells from oxidative stress-induced inhibition of cell growth and survival. Biochem Biophys Res Commun 304: 766–771. doi:10.1016/S0006-291X(03)00657-0. PubMed: 12727222.
17. Dilzer A, Park Y (2012) Implication of conjugated linoleic acid (CLA) in human health. Crit Rev Food Sci Nutr 52: 488-513. doi: 10.1080/10408398.2010.501409. PubMed: 22452730.
18. Kelley NS, Hubbard NE, Erickson KL (2007) Conjugated linoleic acid isomers and cancer. J Nutr 137: 2599-2607. PubMed: 18029471.
19. Belury MA (2002) Dietary conjugated linoleic acid in health: physiological effects and mechanisms of action. Annu Rev Nutr 22: 505–531. doi:10.1146/annurev.nutr.22.021302.121842. PubMed: 12055356.
20. Lee KW, Lee HJ, Cho HY, Kim YJ (2005) Role of the conjugated linoleic acid in the prevention of cancer. Crit Rev Food Sci Nutr 45: 135–144. doi:10.1080/10408690490911800. PubMed: 15941017.
21. Hsu YC, Ip MM (2011) Conjugated linoleic acid-induced apoptosis in mouse mammary tumor cells is mediated by both G protein coupled receptor-dependent activation of the AMP-activated protein kinase pathway and by oxidative stress. Cell Signal 231: 2013-2020.
22. Bergamo P, Luongo D, Rossi M (2004) Conjugated linoleic acid-mediated apoptosis in Jurkat T cells involves the production of reactive oxygen species. Cell Physiol Biochem 14: 57-64. doi: 10.1159/000076927. PubMed: 14976407.
23. Devery R, Miller A, Stanton C (2001) Conjugated linoleic acid and oxidative behaviour in cancer cells. Biochem Soc Trans 29: 341-344. doi:10.1042/BST0290341. PubMed: 11356179.
24. Bergamo P, Gogliettino M, Palmieri G, Cocca E, Maurano F et al. (2011) Conjugated linoleic acid protects against gliadin-induced depletion of intestinal defences. Mol Nutr Food Res 55: S248-S256. doi:10.1002/mnfr.201100295. PubMed: 21954188.
25. Palmieri G, Bergamo P, Luini A, Ruvo M, Gogliettino M et al. (2011) Acylpeptide hydrolase inhibition as targeted strategy to induce proteasomal down-regulation. PLOS ONE 6: e25888. doi:10.1371/journal.pone.0025888. PubMed: 22016782.
26. Bergamo P, Maurano F, Rossi M (2007) Phase 2 enzymes induction by Conjugated Linoleic Acid improves lupus-associated oxidative stress. Free Radic Biol Med 43: 71-79. doi:10.1016/j.freeradbiomed.2007.03.023. PubMed: 17561095.
27. Magesh S, Chen Y, Hu L (2012) Small molecule modulators of Keap1-Nrf2-ARE pathway as potential preventive and therapeutic agents. Med Res Rev 32: 687-726. doi:10.1002/med.21257. PubMed: 22549716.
28. Pfaffl MW (2001) A new mathematical model for relative quantification in real-time RT-PCR. Nucleic Acids Res 29: e45. doi:10.1093/nar/29.9.e45. PubMed: 11328886.
29. Ciechanover A (2012) Intracellular protein degradation: from a vague idea through the lysosome and the ubiquitin-proteasome system and onto human diseases and drug targeting. Neurodegener Dis 10: 7-22. doi:10.1159/000334283. PubMed: 22327508.

30. Ochoa JJ, Farquharson AJ, Grant I, Moffat LE, Heys SD et al. (2004) Conjugated linoleic acids (CLAs) decrease prostate cancer cell proliferation: different molecular mechanisms for cis-9, trans-11 and trans-10, cis-12 isomers. Carcinogenesis 25: 1185–1191. doi:10.1093/carcin/bgh116. PubMed: 14976130.
31. Lee SH, Yamaguchi K, Kim JS, Eling TE, Safe S et al. (2006) Conjugated linoleic acid stimulates an anti-tumorigenic protein NAG-1 in an isomer specific manner. Carcinogenesis 27: 972-981. doi:10.1093/carcin/bgi268. PubMed: 16286461.
32. Jung JI, Cho HJ, Kim J, Kwon DY, Park JH (2010) trans-10,cis-12 conjugated linoleic acid inhibits insulin-like growth factor-I receptor signaling in TSU-Pr1 human bladder cancer cells. J Med Food 13: 13-19. doi:10.1089/jmf.2009.1201. PubMed: 20136431.
33. Lau DS, Archer MC (2010) The 10t,12c isomer of conjugated linoleic acid inhibits fatty acid synthase expression and enzyme activity in human breast, colon, and prostate cancer cells. Nutr Cancer 62: 116-121. PubMed: 20043266.
34. Ou L, Wu Y, Ip C, Meng X, Hsu YC et al. (2008) Apoptosis induced by t10,c12-conjugated linoleic acid is mediated by an atypical endoplasmic reticulum stress response. J Lipid Res 49: 985-994. doi:10.1194/jlr.M700465-JLR200. PubMed: 18263853.
35. Yang J, Su Y, Richmond A (2007) Antioxidants tiron and N-acetyl-L-cysteine differentially mediate apoptosis in melanoma cells via a reactive oxygen species- independent NF-κB pathway. Free Radic Biol Med 42: 1369–1380. doi:10.1016/j.freeradbiomed.2007.01.036. PubMed: 17395010.
36. Ballatori N, Krance SM, Notenboom S, Shi S, Tieu K et al. (2009) Glutathione dysregulation and the etiology and progression of human diseases. Biol Chem 390: 191-214. PubMed: 19166318.
37. Fried L, Arbiser JL (2008) The reactive oxygen-driven tumor: relevance to melanoma. Pigment Cell. Melanoma Res 21: 117–122.
38. Trachootham D, Alexandre J, Huang P (2009) Targeting cancer cells by ROS-mediated mechanisms: a radical therapeutic approach? Nat Rev Drug Discov 8: 579-591. doi:10.1038/nrd2803. PubMed: 19478820.
39. Fruehauf JP, Trapp V (2008) Reactive oxygen species: an Achilles' heel of melanoma. Expert Rev Anticancer Ther 8: 1751–1757. doi:10.1586/14737140.8.11.1751. PubMed: 18983235.
40. Govindarajan B, Sligh JE, Vincent BJ, Li M, Canter JA et al. (2007) Overexpression of Akt converts radial growth melanoma to vertical growth melanoma. J Clin Invest 117: 719–729. doi:10.1172/JCI30102. PubMed: 17318262.
41. Qiao S, Lamore SD, Cabello CM, Lesson JL, Muñoz-Rodriguez JL et al. (2012) Thiostrepton is an inducer of oxidative and proteotoxic stress that impairs viability of human melanoma cells but not primary melanocytes. Biochem Pharmacol 83: 1229-1240. doi:10.1016/j.bcp.2012.01.027. PubMed: 22321511.
42. Brohem CA, Massaro RR, Tiago M, Marinho CE, Jasiulionis MG et al. (2012) Proteasome inhibition and ROS generation by 4-nerolidylcatechol induces melanoma cell death. Pigment Cell. Melanoma Res 25: 354-369.
43. Ren D, Villeneuve NF, Jiang T, Wu T, Lau A et al. (2011) Brusatol enhances the efficacy of chemotherapy by inhibiting the Nrf2-mediated defense mechanism. Proc Natl Acad Sci U S A 108: 1433–1438. doi:10.1073/pnas.1109656108. PubMed: 21205897.
44. Chapple SJ, Siow RC, Mann GE (2012) Crosstalk between Nrf2 and the proteasome: Therapeutic potential of Nrf2 inducers in vascular disease and aging. Int J Biochem Cell Biol 44: 1315-1320. doi:10.1016/j.biocel.2012.04.021. PubMed: 22575091.
45. Aiken CT, Kaake RM, Wang X, Huang L (2011) Oxidative stress-mediated regulation of proteasome complexes. Mol Cell Proteomics 10: R110.006924. PubMed: 21543789.

 DOI 10.1002/mnfr.201100295 *Mol. Nutr. Food Res.* 2011, *55*, S248–S256

RESEARCH ARTICLE

Conjugated linoleic acid protects against gliadin-induced depletion of intestinal defenses

Paolo Bergamo[1], Marta Gogliettino[2], Gianna Palmieri[2], Ennio Cocca[2], Francesco Maurano[1], Rosita Stefanile[1], Marco Balestrieri[2], Giuseppe Mazzarella[1], Chella David[3] and Mauro Rossi[1]

[1] Istituto di Scienze dell'Alimentazione, Consiglio Nazionale delle Ricerche (CNR-ISA), Avellino, Italy
[2] Istituto di Biochimica delle Proteine, Consiglio Nazionale delle Ricerche (CNR-IBP), Napoli, Italy
[3] Department of Immunology, Mayo Clinic College of Medicine, Rochester, MN, USA

Received: May 2, 2011
Revised: July 1, 2011
Accepted: July 13, 2011

Scope: The involvement of oxidative stress in gluten-induced toxicity has been evidenced in vitro and in clinical studies but has never been examined in vivo. We recently demonstrated the protective activity of conjugated linoleic acid (CLA), which functions by the activation of nuclear factor erythroid 2-related factor2 (Nrf2), a key transcription factor for the synthesis of antioxidant and detoxifying enzymes (phase 2). Here, we evaluate the involvement of nuclear factor erythroid 2-related factor2 in gliadin-mediated toxicity in human Caco-2 intestinal cells and in gliadin-sensitive human leukocyte antigen-DQ8 transgenic mice (DQ8) and the protective activity of CLA.

Methods and results: Gliadin effects in differentiated Caco-2 cells and in DQ8 mice, fed with a gliadin-containing diet with or without CLA supplementation, were evaluated by combining enzymatic, immunochemical, immunohistochemical, and quantitative real-time PCR (qRT-PCR) assays. Gliadin toxicity was accompanied by downregulation of phase 2 and elevates proteasome-acylpeptide hydrolase activities in vitro and in vivo. Notably, gliadin was unable to generate severe oxidative stress extent or pathological consequences in DQ8 mice intestine comparable to those found in celiac patients and the alterations produced were hampered by CLA.

Conclusion: The beneficial effects of CLA against the depletion of crucial intestinal cyto-protective defenses indicates a novel nutritional approach for the treatment of intestinal disease associated with altered redox homeostasis.

Keywords:
Conjugated linoleic acid / Gluten toxicity / Nrf2-mediated defenses / Proteasome-acylpeptide hydrolase activity

1 Introduction

Celiac disease (CD) is a chronic inflammatory pathology of the small intestine, resulting from a complex interplay between environmental and genetic factors [1]. Indeed, the main wheat gluten protein (gliadin) and related proteins from rye and barley represent the environmental factors responsible for the immunotoxic response in CD patients [2]. During the past few years, significant progress has been made in clarifying the different factors that contribute to the pathogenesis of CD. In addition, the presence of human

Correspondence: Dr. Paolo Bergamo, Istituto di Scienze dell' Alimentazione, Consiglio Nazionale delle Ricerche (CNR-ISA), via Roma 64, 83100, Avellino, Italy
E-mail: p.bergamo@isa.cnr.it
Fax: +39-825-299105

Abbreviations: APEH, acylpeptide hydrolase; **CD,** celiac disease; **CLA,** conjugated linoleic acid; **GCL,** γ-glutamylcysteine ligase; **GFD,** gluten-free diet; **GSHtot,** total thiols; **GSSG,** glutathione disulfide; **GST,** glutathione *S*-transferase; **HO-1,** heme oxygenase-1; **IAP,** intestinal alkaline phosphatase; **MGFD,** Modified GFD; **NQO1,** NAD(P)H:quinone oxidoreductase; **Nrf2,** nuclear factor erythroid 2-related factor 2; **PC,** protein-bound carbonyls; **pt-glia,** peptic–triptic digest of gliadin; **StD,** standard diet; **tTG,** tissue transglutaminase

leukocyte antigen (HLA) class II DQ2 and/or DQ8 [3] has been linked to the events leading to gluten toxicity and intestinal damage; however, their presence is necessary but not sufficient for the development of such disease [4]. Transgenic mice expressing human leukocyte antigen-DQ8 in the absence of endogenous mouse class II genes, nontransgenic for human CD4 [5] (DQ8 mice) are widely used for investigating gluten sensitivity [6–8], but in the absence of immunization, gluten is generally well tolerated by the intestine of both DQ8 or DQ2 mice as oral tolerance is still operative [8, 9]. However, despite the large amount of data on immunological factors, the biochemical mechanisms underlying gluten toxicity are not completely understood.

Among the different mechanisms, oxidative stress has been implicated in the pathophysiology of CD by clinical evidence [10] and by in vitro studies [11] but the underlying mechanisms are still unclear. Indeed, oxidants and/or a defective antioxidant defense play a crucial role in the generation of the oxidative stress implicated in the pathogenesis of inflammatory diseases. The epithelium of the small intestine is a dynamic system that is continuously renewed by a differentiation process, and redox status has an important role in these stages. Moreover, owing to the constant exposure to potentially noxious substances, intestinal mucosa is endowed with efficient defenses to preserve cellular integrity and tissue homeostasis. Among these defenses, the nuclear factor erythroid 2-related factor2 (Nrf2) transcription factor has been recognized as the key regulator [12], and its activation, via the modification of cysteine residues of Kelch-like ECH-associated protein 1 (Keap1) in the cytoplasm, triggers Nrf2 release from the Keap1/Nrf2 complex. The ensuing translocation of Nrf2 into the nucleus activates the transcription of a battery of genes coding for antioxidant and detoxifying proteins (phase 2 enzymes: γ-glutamylcysteine ligase, GCL; glutathione *S*-transferase, GST; glutathione peroxidase, GSHPx; NAD(P)H:quinone oxidoreductase, NQO1; and heme oxygenase-1, HO-1) [13].

Besides the Nrf2 pathway, several proteases have been reported to play a detoxifying role by degrading oxidatively damaged cytosolic proteins. The ubiquitin–proteasome pathway plays a key role in a broad array of cellular processes (cell cycle, apoptosis, and differentiation) [14], and the proteolytic activity of the proteasome, a major multicomponent enzymatic system, controls and regulates the accumulation of potentially cytotoxic protein aggregates in an ATP- and ubiquitin-independent manner [15]. Additionally, acylpeptide hydrolase (APEH), a novel serine-peptidase enzyme belonging to the prolyl-oligopeptidase family, was recently demonstrated to contribute to the proteasome-mediated elimination of potentially cytotoxic proteins [16].

The potential protective effect displayed by n-3 PUFA on inflammatory bowel disease has been recently reviewed [17] and similarly to n-3 PUFA, conjugated linoleic acid (CLA) has been recognized to promote beneficial effects in animal models of several pathologies, including inflammatory, autoimmune diseases [18], and experimentally induced colitis [19]. In these studies, the modulatory activity of n-3 PUFA and CLA on the peroxisome proliferator-activated receptor γ-NF-κB pathway was demonstrated to contribute to the anti-inflammatory activities of these compounds. In addition, our recent data showing the ability of CLA to enhance Nrf2-mediated defenses in vitro and in vivo raises the possibility that CLA can also exert its protective effects through this mechanism of action [20].

The major objective of this study was to evaluate the detrimental effects of gluten on intestinal antioxidant and detoxifying defenses in vitro and in vivo and to investigate the protective effects of CLA against gluten-induced toxicity in the small intestine of DQ8 mice.

2 Materials and methods

2.1 Reagents

An isomeric mixture of CLA (38.5% t10, c12, 37.4% c9, t11), known as TonalinTM, was from Natural. *N*-Suc-LLVY-AMC, BSA, α-lactalbumin, and other chemicals of the highest purity were from Sigma-Aldrich (St. Louis, MO, USA) or Calbiochem (La Jolla, CA, USA).

2.2 Cell culture and in vitro experiments

The Caco-2 cell line was obtained from the American Type Culture Collection (ATCC, Gaithersburg, MD, USA) and was studied between passages 16 and 35. This is a well-described cell line that spontaneously differentiates and becoming morphologically and functionally similar to enterocytes, and therefore differentiated cells. Unless otherwise specified, in the present study, cells after 21 days postseeding (differentiated) were incubated for 48 h at 37°C with 1 mg/mL of a peptic–tryptic digest of gliadin (pt-glia) or with the same amount of α-lactalbumin (control) prepared according to a published protocol [21].

2.3 In vivo experiments

Transgenic DQ8 mice were bred and maintained in pathogen-free conditions at our animal facility and used at the age of 6–12 wk. All procedures for the use of laboratory animals met the guidelines of the Italian Ministry of Health (permission accreditation no. 164/99-A). Animals were from a colony reared for several generations on a gluten-free diet (GFD) (Altromin-MT-mod, Rieper S.p.A. Italy).

Gluten toxicity in vivo was initially studied in animal groups ($n = 9$ each) fed for 3 wk with a standard diet (StD) or with a GFD. As the StD and GFD differed in both soy and

wheat proteins, we subsequently used a modified GFD (MGFD), adding only wheat proteins to the GFD to specifically analyze the in vivo toxicity of gluten (Supporting Information Table 1). Four groups of female DQ8 mice ($n = 9$ each) were used, and two of these groups were switched to MGFD for 3 wk. Starting from 2 days before the change of diet and during the trial, two groups of animals (one fed with GFD and the other with MGFD) were intraorally administered 20 mg of CLA/day (five times/wk). At the end of this time, the mice were sacrificed. The amount of CLA administered, upon normalization to the body surface area [22], corresponded to a dose (4.9 g/day) comparable to that used in the clinical trials [23]. All mice were maintained under strict pathogen-free conditions and had free access to drinking water.

2.4 Protein extract and brush border membrane vesicle preparation

Cytosolic and nuclear extracts from Caco-2 cells and intestinal tissue were prepared by using the previously published protocols [20] and, if not used immediately, the prepared extracts were frozen on dry ice and stored in aliquots at −80°C. Before their use, protein concentration was determined by protein assay (Bio-Rad). Brush border membrane vesicles were prepared from small intestine samples (approx., 10 mg) accordingly to a published method [24].

2.5 Proteasome and APEH assays

APEH activity was measured using the substrate, acetyl-A-pNA (Bachem). The reaction mixture (1 mL) containing the appropriate amount of cell extract in 50 mM Tris-HCl buffer, pH 7.5, was preincubated at 37°C for 2 min. Then, 1 mM acetyl-A-pNA was added, and the release of *p*-nitroanilide $\varepsilon 410 = 8800\ M^{-1}\,cm^{-1}$) was measured following the absorbance increase at 410 nm on a Cary 100 SCAN (VARIAN) spectrophotometer equipped with a thermostated cuvette. APEH activity is expressed in IU.

The synthetic fluorescent substrate, *N*-Suc-LLVT-AMC, was used for the measurement of the chymotrypsin-like activity of the 20S proteasome at a final concentration of 80 μM. The reaction mixture (0.9 mL) containing partially purified proteasome was preincubated (as above) in buffer. *N*-Suc-LLVT-AMC was added, and the release of fluorescent product (7AMC: 7-amino 4-methylcoumarin) was monitored for 5 min by a fluorimeter (Perkin–Elmer LS 50B) ($\lambda_{Ex} =$ 380 nm and $\lambda_{Em} = 460$ nm).

Partial purification of the proteasome from Caco-2 and/or individual mouse small intestinal protein extracts (0.7 mg) was carried out by gel filtration chromatography on a Superdex 200 column connected to a SMART system and eluted at 0.1 mL/min in 50 mM Tris-HCl, 0.1 M NaCl, pH 7.5. Active fractions, for both APEH and proteasome, were separately collected and used for further analysis. A typical chromatogram is shown in Supporting Information Fig. 1.

2.6 RNA isolation and quantitative real-time PCR analysis

Total RNA was isolated from the small intestine of DQ8 mice that were fed with GFD or MGFD and with or without the CLA supplement by using the MELT^{TM} Total Nucleic Acid Isolation System (Ambion). Total RNA was then reverse transcribed using the Transcriptor First Strand cDNA Synthesis Kit (Roche). A total of 50 ng of reverse-transcribed complementary DNA was amplified by quantitative real-time PCR (qRT-PCR) on an iCycler iQTM (Bio-Rad) using 300 nM gene-specific primers, iQTM SYBR Green Supermix (Bio-Rad) and the following PCR conditions: 1 cycle at 95°C for 10 min (denaturation), 95°C for 15 s (amplification) and 40 cycles of 60°C for 30 s, and 72°C for 30 s. The $MgCl_2$ concentration used was 3 mM for GAPDH and GCL and 6 mM for NQO1. The expression level of GAPDH was used as an internal control. Raw cycle threshold values (C_t values) obtained for GCL and NQO1 were subtracted from the C_t value obtained for GAPDH transcript levels. The final graphical data were derived from the $2^{-\Delta\Delta Ct}$ formula, where $\Delta\Delta C_t = (C_{t,\ target} - C_{t,\ GAPDH})_{sample} - (C_{t,\ target} - C_{t,\ GAPDH})_{control}$, where "sample" mice are those fed with MGFD with or without CLA or with GFD and CLA, and "control" mice are those fed with GFD. The primers utilized were as follows: GCL, 5′-CAAAGGCAGTCAAATCTGGTG-3′ and 5′-TGGAGCAGCTGTATCAGTGG-3′; NQO1, 5′-TTCTCTGGCCGATTCAGAGT-3′ and 5′-TCTGGTTGTCAGCTGGAATG-3′; and GAPDH, 5′-TAGACTCCACGACATACTCAGCA-3′ and 5′-GTCGGTGTGAACGGATTTG-3′.

2.7 Immunohistochemistry and microscopic evaluation

The preparation of proximal jejunum fragments and the subsequent analysis (morphometrical, immunohistochemical and cell apoptosis determination) were carried out according to the published protocols [7].

2.8 Statistical analysis

Values are presented as the mean ± SD. Statistical analysis was performed with GraphPad Instat 3 software (San Diego, CA, USA). Groups were compared by the Student's *t*-test, and $p < 0.05$ was considered as significant. Correlation analysis was performed using the Statistical Package for Social Sciences (SPSS version 8.0; SPSS, Chicago, IL, USA).

3 Results

3.1 Redox status and detoxifying enzyme activities are influenced by the differentiation status of Caco-2 cells

The majority of in vitro investigations aimed at the estimation of the pro-oxidant activity of gliadin have been carried out using undifferentiated cultures [11]. To investigate the variation of several antioxidant and detoxifying molecules at different stages of cell differentiation, total thiols (GSHtot), glutathione disulfide (GSSG) concentration, phase 2 enzymes (γ-GCL, GST, and NQO1), proteasome, and APEH activities were assayed in Caco-2 cells at different stages of differentiation, as evaluated by following the intestinal alkaline phosphatase (IAP) activity. As expected, significantly higher GST activity ($p<0.005$) was found in differentiated Caco-2 cells as compared with undifferentiated cultures (Supporting Information Fig. 2A). By contrast, intracellular GSHtot, but not GSSG content, progressively declined during differentiation (Supporting Information Fig. 2B). Similarly, a reduction in both NQO1 and GCL activities occurred during this process ($p<0.01$) (Supporting Information Fig. 2C). Proteasome activity exhibited a strong increase during the proliferative phase, with a maximum reached in confluent cultures followed by a progressive reduction thereafter. A similar trend was observed for APEH specific activity, but the maximum was reached 7 days after confluence. Higher specific activity of APEH was found in differentiated cells as compared with undifferentiated ones (Supporting Information Fig. 2D).

3.2 The pro-oxidant activity of gliadin reduces cell viability and detoxifying enzyme activities but not tissue transglutaminase expression

The influence of cell differentiation status on susceptibility to gliadin-induced oxidative stress was investigated. Intracellular GSHtot content was measured in preconfluent (6 days after plating), differentiating and in differentiated cells (14 and 21 days after plating, respectively) that were incubated for 48 h with increasing concentrations of pt-glia. The results showed a dose-dependent decline in intracellular GSHtot in comparison to untreated cells (control) that was independent of the differentiation stage (Fig. 1A).

To determine the effects of pt-glia exposure on differentiated Caco-2 cell viability, caspase-3 activity and the amount of lactate dehydrogenase (LDH) released in the media were measured upon 48 h of incubation with 0.5 or 1 mg/mL of pt-glia. Treatment with the highest concentration produced a significant pro-apoptotic effect when compared with cells exposed to an equal amount of a peptic–tryptic digest of α-lactalbumin (control) ($p<0.01$) (Fig. 1B). Similarly, increased levels of protein-bound carbonyls (PC) and a marked reduction of IAP activity ($p<0.05$) resulted from pt-glia treatment (Fig. 1C). In

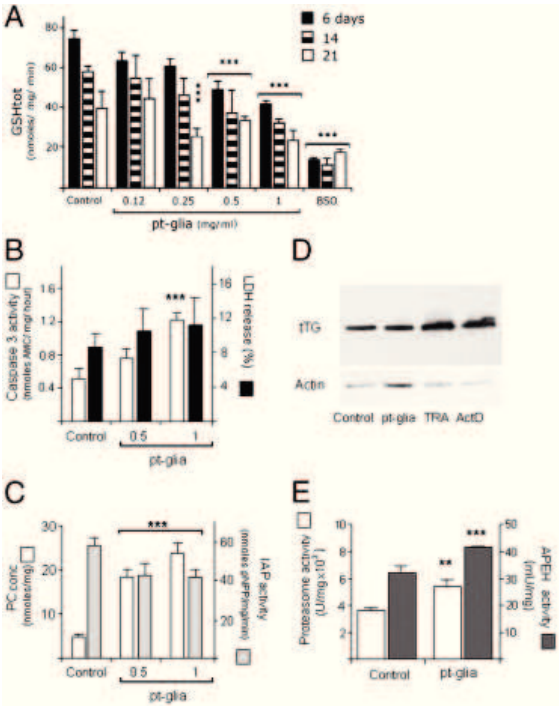

Figure 1. Gliadin exposure enhances apoptosis, PC accumulation, proteasome–APEH activities, and reduces IAP activity in Caco-2 cells (A). Caspase-3 activity and lactate dehydrogenase release were measured in Caco2 cells following 48 h of incubation with gliadin (B). PC levels and IAP activity were measured in differentiated cells exposed to 0.5 or 1 mg/mL of pt-glia (C). Representative Western immunoblot of tTG expression in protein extracts from differentiated Caco-2 cells incubated with 1 mg/mL of gliadin or treated with tTG activators (100 μM transretinoic acid: TRA or 50 μM actinomycin D: ActD) for 24 h. Actin was used as loading control (D). The chymotrypsin-like activity of the proteasome and APEH-specific activities were measured in differentiated cultures incubated with 1 mg/mL of pt-glia (E). Results are expressed as the mean ± SD. ***, **Significantly different ($p<0.005$ or <0.01) from controls.

contrast, no difference in tissue transglutaminase (tTG) expression was noted between cells incubated for 48 h with pt-glia and controls although treatment with known tTG activators produced a noticeable increase in tTG levels (Fig. 1D). Figure 1E shows the effect of pt-glia on proteasome and APEH activities. In agreement with the accumulation of PC proteins, a significant enhancement of both specific activities was observed (from 18.4 ± 0.2 to 27.0 ± 1.9 U/mg $\times 10^3$; $p = 0.002$ and from 32.0 ± 2.8 to 41.0 ± 3.2 mU/mg; $p = 0.012$ for proteasome and APEH activity, respectively).

3.3 Gliadin downregulates Nrf2-activated defenses in Caco-2 cells

GSH synthesis and its export from the cell are the main strategies to control GSH intracellular content [25]. To

examine the mechanism by which gliadin perturbs the redox status GSHtot and GSSG concentrations were measured in the cytoplasm and in the culture media of cells exposed to pt-glia for 48 h. Incubation with pt-glia decreased intracellular GSHtot ($p<0.001$) without affecting GSSG content (Fig. 2A). Moreover, a significant decline in GSHtot and GSSG concentrations was also found in the culture media when compared with the control (from 2.85 ± 0.53 to 1.82 ± 0.14 nmol/mg/min; $p=0.0021$ and from 1.47 ± 0.22 to 0.72 ± 0.42 nmol/mg/min; $p=0.014$, respectively) (Fig. 2B).

To further investigate the mechanism underlying the ability of gliadin to reduce intracellular GSHtot levels, we measured the effect of pt-glia treatment on the activity of GCL, the rate-limiting enzyme in GSH synthesis. As shown in Fig. 2C, a significant reduction in enzyme activity (from 8.15 ± 1.45 to 4.6 ± 1.74 nmol NAD/mg/min; $p<0.005$) was associated with the decrease of Nrf2 levels (57 kDa) in the nuclear extracts and the accumulation of the GCL caspase-cleaved form (60 kDa) in the cytoplasm of pt-glia-treated cells as compared with controls (Fig. 2C, inset). To further confirm the involvement of the Nrf2-ARE pathway, the effects of pt-glia exposure (1 mg/mL for 48 h) on NQO1 and GST activities was also investigated. The observed reduction in the enzymatic activities of both ($p=0.0008$ and 0.0052 for GST and NQO1, respectively) (Fig. 2D) confirms the gliadin ability to downregulate Nrf2-mediated defenses in vitro. The probable role of gliadin-mediated oxidative stress in the reduced activity of IAP was next examined. GSHtot concentration and IAP activity were measured in cells exposed to pt-glia and supplemented with or without buthionine sulfoximine (BSO), a specific inhibitor of GCL or with the antioxidant butylated hydroxyanisole (BHA). Besides the expected decrease in GSHtot and IAP activity produced by gliadin exposure, the two-fold reduction of IAP activity (following buthionine sulfoximine treatment) together with its significant increase in cells incubated with BHA ($p<0.05$) (Supporting Information Fig. 3) indicated the role of intracellular redox status in the regulation of IAP activity.

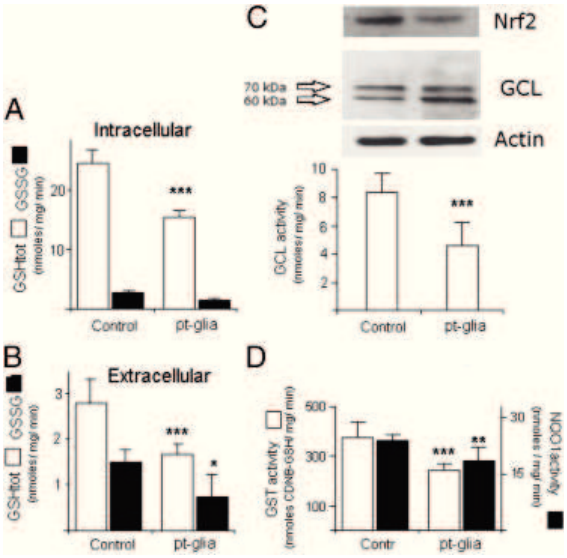

Figure 2. Gliadin exposure reduces intracellular phase 2 enzyme activity in vitro. GSHtot and GSSG concentrations were measured in differentiated Caco-2 cells (A) or in the culture medium following 48 h of incubation with 1 mg/mL of pt-glia, (B) GCL activity and (C) representative Western immunoblot showing GCL expression in differentiated cells following 48 h of exposure to 1 mg/mL of pt-glia. Actin was used as loading control (C, inset). GST and NQO1 activities were evaluated in Caco-2 cells exposed to 1 mg/mL of gliadin for 48 h. (D). Results are expressed as the mean $\pm$ SD. ***, **, *Significantly different ($p<0.005$, <0.01 or <0.05) from controls.

3.4 Gluten intake reduces Nrf2-activated defenses without pathological consequences in DQ8 transgenic mice

To identify possible deleterious effects of gluten intake on animal and intestinal redox status, detoxifying defenses and morphological alterations were examined in DQ8 mice following 3 wk of treatment with StD. The gluten intake did not influenced intestinal tTG expression (Fig. 3A) or caspase-3 activity in the small intestine (Fig. 3B). Similarly, gluten intake only produces minimal alteration of animal redox status as shown by the negligible variation in GSHtot levels (Fig. 3B, lower panel) or PC levels in blood serum sera (data not shown). In contrast, StD intake produced a significant alteration in GST activity and PC content in the intestines of these mice ($p<0.001$) (Fig. 3A). Interestingly, when the GSHtot content of individual mice was plotted against IAP values, a significant positive correlation between these levels was apparent ($r=0.66$; $p=0.036$) (Fig. 3B, upper panel). Notably, the lower intestinal GSHtot content, decreased GSHPx, and IAP activities measured in StD-treated animals compared with mice fed with GFD ($p=0.0004$, 0.025, and 0.0007, respectively) were not associated with some typical pathological alterations of CD (morphological change or increased number of CD3+ lymphocytes) (Table 1).

3.5 Biopsies from CD patients exhibit high oxidative stress conditions

Next, to compare the alterations produced by gluten intake in the small intestine of DQ8 mice to those occurring in CD, tTG expression, PC amount, GST, IAP, and proteasome-APEH specific activities were examined in human biopsies from CD patients. Intestinal biopsies of healthy volunteers were used as controls. Significantly lower GST ($p<0.001$) and proteasome–APEH activities ($p=0.035$ and $=0.023$, respectively) were detected in CD samples as compared with

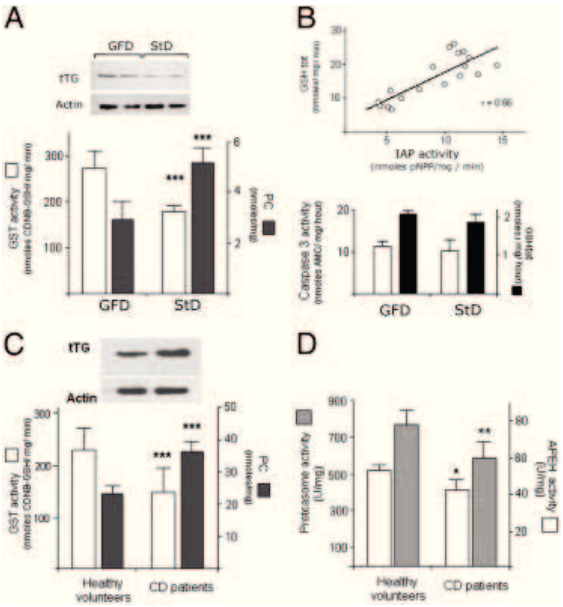

Figure 3. Elevated oxidative stress is observed in CD patient biopsies in comparison to the small intestine of gluten-fed DQ8 transgenic mice. PC accumulation, GST activity (A), and caspase-3 activity were measured in the small intestine of DQ8 mice fed for 3 wk with GFD or StD. (B). Representative Western immunoblot of tTG expression in the intestine of mice receiving different treatments. Actin was used as loading control (A, inset). PC accumulation, GST activity, and (C) proteasome–APEH-specific activities were measured in human biopsies from healthy or CD patients (D). Representative Western immunoblot showing tTG expression in human intestinal proteins. Actin was used as loading control (C, inset). Results are expressed as the mean ± SD from triplicate analyses. ***, **Significantly different ($p < 0.005$ or < 0.01) from GFD-fed mice.

Table 1. The effects of GFD or gluten-containing diet (StD) intake on DQ8 mice intestine

	GFD	StD
GSHtot (nmol/mg/min)	19.2 ± 2.1	9.6 ± 1.1***
GPx (nmol/mg/min)	121.5 ± 31.2	90.4 ± 28.5*
IAP (nmol pNPP/μg/min)	12.5 ± 1.6	8.5 ± 1.3***
Sucrase isomaltase (U/mg/h)	2.0 ± 1.5	2.2 ± 1.0
Height of intestinal villi (μm)	670 ± 23	640 ± 46
$CD3^+$ (cells/mm)	20.5 ± 0.7	20.8 ± 3.5

Results are given as mean ± SD from triplicate analysis.
***,*Significantly different ($p < 0.005$ or < 0.05) from controls.

those from healthy volunteers (Fig. 3C and D). As expected, a marked increase in tTG expression and PC content was found in CD patients when compared with healthy individuals (Fig. 3C) and a conspicuous reduction of IAP activity was also observed in CD patients (data not shown).

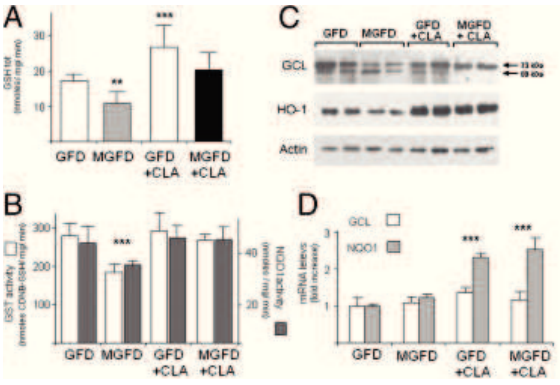

Figure 4. CLA impairs the gluten-mediated decrease in antioxidant/detoxifying defenses in vivo. Small intestine samples from DQ8 mice fed with GFD or MGFD and with or without the CLA supplement were examined for their GSHtot content (A) and GST and NQO1 activities (B). Results are expressed as the mean ± SD from triplicate analyses. ***, **Significantly different ($p < 0.005$ or < 0.01) from GFD-fed mice (C). Representative Western immunoblot of the intestinal expression of GCL and HO-1 from differently treated DQ8 mice. Actin was used as loading control (C). mRNA levels of GCL and NQO1 from the intestines of DQ8 mice receiving different treatments. The housekeeping gene, glyceraldehyde 3-phosphate dehydrogenase (G6PD) was used as control, and results were normalized by taking the mRNA levels of GFD in mice to be 1 (D).

3.6 CLA treatment impairs the gluten-mediated decrease in intestinal defenses

To specifically analyze the effect gluten intake in DQ8 mice, the animals were fed with a diet which differed from GFD only for the addition of wheat proteins (MGFD). Animals receiving GFD were used as controls. Feeding with MGFD reduced intestinal GSHtot content ($p = 0.0012$) (Fig. 4A) and GST and NQO1 activities ($p = 0.0031$ and 0.001, respectively) (Fig. 4B), as well as HO-1 and GCL (full-length form, 70 kDa) expression (Fig. 4C). Remarkably, CLA administration in MGFD mice resulted in a significant enhancement of GSHtot content (Fig. 4A) ($p = 0.0002$) elevated the expression of the HO-1 and GCL proteins (full-length form, 70 kDa) (Fig. 4C) and resulted in increased mRNA levels of GCL and NQO1 (Fig. 4D). As expected, MGFD treatment was associated with significant increases in PC levels ($p = 0.0003$) (Fig. 5A), a two-fold decrease in IAP activity (0.0007) (Fig. 5B) and enhanced proteasome–APEH specific activities when compared with controls ($p = 0.003$ and < 0.001, respectively) (Fig. 5C, 5D). To evaluate the Nrf2 involvement in gluten-mediated toxicity, CLA was used as Nrf2 inducer. Noticeably, CLA administration in MGFD-treated animals restored PC and GSHtot levels (Figs. 4A and 5A) and reinstated intestinal protective enzymes activity that had been perturbed by gluten (Figs. 4B and 5B–D). Finally, when individual average values of proteasome activity were plotted against APEH or PC levels,

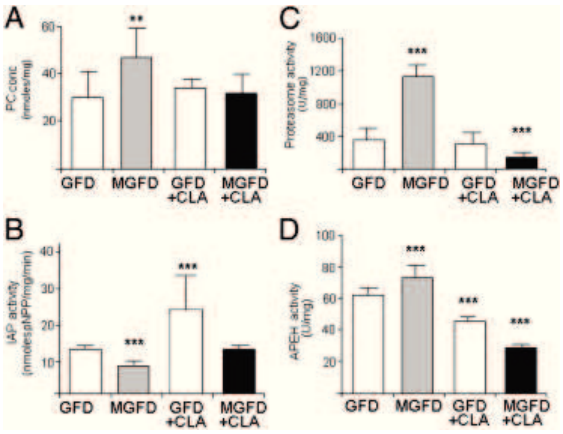

Figure 5. CLA protects against gluten-mediated oxidative stress in vivo. Duodenum samples from DQ8 mice fed with GFD or MGFD and with or without the CLA supplement were examined for (A) their PC concentration and (B) IAP, (C) proteasome and (D) APEH activities, which were measured in the mice receiving different treatments. Results are presented as the mean ± SD from triplicate analyses. ***, **Significantly different ($p < 0.005$ or < 0.01) from controls.

a significant positive correlation was found ($r = 0.935$, $p = 0.0016$ and $r = 0.926$; $p = 0.0001$, respectively).

4 Discussion

The present study confirms the in vitro pro-oxidant activity of gliadin on differentiated Caco-2 cells and demonstrates, for the first time, its in vivo ability to downregulate crucial intestinal defenses. Furthermore, the reported results verify CLA-induced enhancement of the Nrf2 pathway and the central role of this mechanism in the mediation of intestinal protection.

The lower GSHtot content, together with the variation in proteasome–APEH activities during the active metabolic phase, is consistent with a reduced GSH requirement during differentiation and with cellular needs for increased degradation activities during cell proliferation [25]. The decrease of NQO1 activity, which plays a protective effect toward the formation of highly reactive toxic compounds [26], is consistent with the association of cell differentiation with the decline of detoxifying ability [27]. GST enhancement during Caco-2 differentiation is not unexpected and indicates the development of chemoresistance [28].

Gliadin toxicity on redox homeostasis in differentiated Caco-2 cells is consistent with that reported on undifferentiated culture [11] but, in our hands, gliadin treatment only produces a small proapoptotic activity and it is unable to alter tTG expression. This is an ubiquitous intracellular enzyme and its enhanced activity/expression represents an active cellular response to oxidative stress [29]. In particular, the lack of in vitro effect of gliadin on tTG expression is apparently in contrast with the literature data [30, 31] although expression found in biopsies of CD patients is in good accordance with the literature [32]. Bearing in mind that enhanced activity/expression of tTG represents an active cellular response to oxidative stress [29], it is thus likely that chemoresistance development, in differentiated culture might be responsible for the reduced susceptibility to gliadin toxicity. Moreover, the lack of influence of dietary gluten on tTG expression and on the levels of typical pathological markers in mice intestine is consistent with data, indicating that gluten is well tolerated by DQ8 mouse [8]. PC accumulation is a characteristic feature of aging and of a number of pathologies, including inflammatory bowel disease [33] and little is known about the influence of gluten on PC yield. Here, we provide evidence that gliadin raises PC levels in both in vitro and in vivo models and our in vivo data showing that noxious consequences produced by gluten intake are unable to affect the animal redox status are in agreement with the hypothesis that dietary gluten is insufficient to trigger oxidative stress conditions comparable to those found in CD patients [34].

The relevance of Nrf2-mediated defenses in intestinal protection was recently reviewed [14], and among the phase 2 enzymes, GCL has been recognized as the rate-limiting enzyme in GSH synthesis. The alteration of GSH levels may have deleterious effects on both organ homeostasis and disease progression [25]. We confirm the ability of gliadin to decrease intracellular GSHtot content and to block the activity of Nrf2-activated enzymes in vitro [11] and we demonstrate for the first time the ability of gluten to downregulate phase 2 enzyme activity/expression.

The antidifferentiation effect of pt-glia ability was deduced by its ability to affect IAP [35], which was recently demonstrated to play an important role in detoxifying bacterial lipopolysaccharide [36]. The negative correlation between intracellular GSHtot and IAP activity, consistently with data on the inhibitory effect of oxidative stress [37, 38] indicates the modulatory role of Nrf2/ARE pathway on IAP functioning rather than the result of histological injury [39].

Our study demonstrates, for the first time, the in vitro and in vivo ability of gluten to increase the enzymatic activity of the proteasome–APEH system. The marked reduction in proteasome–APEH function detected in intestinal biopsies from untreated CD patients, together with decreased IAP levels, could mirror the severe oxidative stress conditions associated with mucosal lesions in CD; however, further correlation studies on a larger population of CD patients are required.

The ability of CLA to attenuate the oxidative stress cascade has been shown previously [18, 20, 40, 41]. Consequently, to examine the mechanism whereby gluten downregulates intestinal defenses, it was used as an in vivo inducer of Nrf2 pathway. Notably, the association between the increase of cytoprotective defenses with the inhibition of gluten-mediated toxicity in the mouse intestine substantiates the beneficial effects of CLA on the Nrf2 pathway

[20, 40] and supports the relevance of Nrf2 activation against toxic insults in experimental colitis [42]. Taken together, these data indicate the possible use of CLA for the management of intestinal pathologies associated with the depletion of antioxidant/detoxifying defenses. Our results are in good accordance with the previous studies demonstrating the chemo-protective effects of supplementation with mixed CLA isomers on animal [19, 43, 44]. However, since the biological effects of the CLA mixture are likely due to the separate action of its components, further studies are necessary to determine the role of individual isomer in the protective effects against gluten toxicity.

Possible mechanisms by which gluten downregulates intestinal antioxidant/detoxifying may include either indirect modulation of the Nrf2-pathway via the proteasome–APEH system or direct inhibition of Nrf2. However, based on the negligible effects of dietary gluten on intestinal mRNA levels of phase 2 enzymes, the latter hypothesis can be excluded. In addition, bearing in mind that Nrf2 is a known proteasome substrate [45], the hypothesized role played by an increased activity of proteasome–APEH function on the decreased Nrf2-mediated protection upon gluten exposure is supported by data from CLA-supplemented animals. In addition, the ability of CLA to enhance the activity/expression of phase 2 enzymes and to restore proteasome–APEH activity levels is consistent with the reported effects of Nrf2 activation [46, 47]. In fact, it is likely that the release of Nrf2 from Keap1 inhibitor, triggered by CLA, promotes the escape of the Nrf2 protein from proteasomal degradation, thus protecting intestinal cells from gluten-mediated toxicity.

In conclusion, the ability of dietary gluten to produce deleterious effects on several crucial intestinal defense mechanisms, but not the pathological signs associated with CD, is consistent with the hypothesis that gluten exposure may represent only a predisposing factor for further undetermined insults. Moreover, we have identified a novel mechanism by which gluten perturbs several pivotal intestinal defenses and we have discovered the potential therapeutic efficacy of CLA against gluten-mediated toxicity (Supporting Information Fig. 4).

The authors are deeply indebted to Professor Mosè Rossi for the critical reading of this manuscript and insightful comments and express their gratitude to Professor Gaetano Iaquinto, Gastroenterology Unit, Hospital Moscati, Avellino, for supplying human colon biopsies and to Loredana Arciuolo for excellent technical assistance in managing the DQ8 mice colony.

The authors have declared no conflict of interest.

5 References

[1] Fasano, A., Catassi, C., Current approaches to diagnosis and treatment of celiac disease: an evolving spectrum. *Gastroenterology* 2001, *12*, 636–651.

[2] Shan, L., Molberg, O., Parrot, I., Hausch, F. et al., Structural basis for gluten intolerance in celiac sprue. *Science* 2002, *297*, 2275–2279.

[3] Sollid, L. M., Lie, B. A., Celiac disease genetics: current concepts and practical applications. *Clin. Gastroenterol. Hepatol.* 2005, *3*, 843–851.

[4] Sollid, L. M., Coeliac disease: dissecting a complex inflammatory disorder. *Nat. Rev. Immunol.* 2002, *9*, 647–655.

[5] Cheng, S., Baisch, J., Krco, C., Savarirayan, S. et al., Expression and function of HLA-DQ8 (DQA1∗0301/DQB1*0302) genes in transgenic mice. *Eur. J. Immunogenet.* 1996, *1*, 15–20.

[6] Pinier, M., Verdu, E. F., Nasser-Eddine, M., David, C. S. et al., Polymeric binders suppress gliadin-induced toxicity in the intestinal epithelium. *Gastroenterology* 2009, *136*, 136–228.

[7] Senger, S., Maurano, F., Mazzeo, M. F., Gaita, M., et al., Identification of immunodominant epitopes of alpha-gliadin in HLA-DQ8 transgenic mice following oral immunization. *J. Immunol.* 2005, *175*, 8087–8095.

[8] D'Arienzo, R., Stefanile, R., Maurano, F., Luongo, D. et al., A deregulated immune response to gliadin causes a decreased villus height in DQ8 transgenic mice. *Eur. J. Immunol.* 2009, *39*, 3552–3561.

[9] de Kauwe, A. L., Chen, Z., Anderson, R. P., Keech, C. L. et al., Resistance to celiac disease in humanized HLA-DR3-DQ2-transgenic mice expressing specific anti-gliadin CD4+ T cells. *J. Immunol.* 2009, *182*, 7440–7450.

[10] Diosdado, B., van Oort, E., Wijmenga, C., Coelionomics: towards understanding the molecular pathology of coeliac disease. *Clin. Chem. Lab. Med.* 2005, *43*, 685–695.

[11] Elli, L., Dolfini, E., Bardella, M. T., Gliadin cytotoxicity and in vitro cell cultures. *Toxicol. Lett.* 2003, *146*, 1–8.

[12] Aleksunes, L. M., Manatou, J. E., Emerging role of Nrf2 in protecting against hepatic and gastrointestinal disease. *Toxicol. Pathol.* 2007, *35*, 459–473.

[13] Kwak, M. K., Wakabayashi, N., Kensler, T. W., Chemoprevention through the Keap1–Nrf2 signaling pathway by phase 2 enzyme inducers. *Mutation Res.* 2004, *555*, 133–148.

[14] Ciechanover, A., The ubiquitin-proteasome pathway: on protein death and cell life. *EMBO J.* 1998, *17*, 7151–7160.

[15] Jariel-Encontre, I., Bossis, G., Piechaczyk, M., Ubiquitin-independent degradation of proteins by the proteasome. *Biochim. Biophys. Acta* 2008, *1786*, 153–177.

[16] Shimizu, K., Kiuchi, Y., Ando, K., Hayakawa, M., Kikugawa, K., Coordination of oxidized protein hydrolase and the proteasome in the clearance of cytotoxic denatured proteins. *Biochem. Biophys. Res. Commun.* 2004, *324*, 140–146.

[17] Calder, P. C., Polyunsaturated fatty acids, inflammatory processes and inflammatory bowel diseases. *Mol. Nutr. Food Res.* 2008, *52*, 885–897.

[18] Wahle, K. W. J., Heys, S. D., Rotondo, D., Conjugated linoleic acids: are they beneficial or detrimental to health? *Progr. Lipid Res.* 2004, *43*, 553–587.

[19] Bassaganya-Riera, J., Reynolds, K., Martino-Catt, S., Cui, Y. et al., Activation of PPARγ and δ by conjugated linoleic acid

mediates protection from experimental inflammatory bowel disease. *Gastroenterology* 2004, *127*, 777–791.

[20] Bergamo, P., Maurano, F., Rossi, M., Phase 2 enzymes induction by conjugated linoleic acid improves lupus-associated oxidative stress. *Free Radic. Biol. Med.* 2007, *43*, 71–79.

[21] Gianfrani, C., Siciliano, R. A., Facchiano, A. M., Camarca, A. et al., Transamidation of wheat flour inhibits the response to gliadin of intestinal T cells in celiac disease. *Gastroenterology* 2007, *133*, 780–789.

[22] Reagan-Shaw, S., Nihal, M., Ahmad, N., Dose translation from animal to human studies revisited. *FASEB J.* 2008, *22*, 659–661.

[23] Whigham, L. D., Watras, A. C., Schoeller, D. A., Efficacy of conjugated linoleic acid for reducing fat mass: a meta-analysis in humans. *Am. J. Clin. Nutr.* 2007, *85*, 1203–1211.

[24] Shirazi-Beechey, S. P., Davies, A. G., Tebbutt, K., Dyer, J. et al., Preparation and properties of brush-border membrane vesicles from human small intestine. *Gastroenterology* 1990, *98*, 676–685.

[25] Ballatori, N., Krance, S. M., Notenboom, S., Shi, S. et al., Glutathione dysregulation and the etiology and progression of human diseases. *Biol. Chem.* 2009, *390*, 191–214.

[26] Jaiswal, A. K., Regulation of genes encoding NAD(P)H: Quinone oxidoreductases. *Free Radic. Biol. Med.* 2004, *29*, 254–262.

[27] Cornell, J. S., Meister, A., Glutathione and gamma-glutamyl cycle enzymes in crypt and villus tip cells of rat jejunal mucosa. *Proc. Natl. Acad. Sci. USA* 1976, *73*, 420–422.

[28] O'Brien, M. L., Tew, K. D., Glutathione and related enzymes in multidrug resistance. *Eur. J. Cancer* 1996, *32A*, 967–978.

[29] Ientile, R., Caccamo, D., Griffin, M., Tissue transglutaminase and the stress response. *Amino Acids* 2007, *33*, 385–394.

[30] Vincentini, O., Maialetti, F., Gazza, L., Silano, M. et al., Environmental factors of celiac disease: cytotoxicity of hulled wheat species *Triticum monococcum*, *T. turgidum* spp. *dicoccum* and *T. aestivum* spp. *spelta*. *J. Gastroenterol. Hepathol.* 2007, *22*, 1816–1822.

[31] Luciani, A., Villella, V. R., Vasaturo, A., Giardino, I. et al., Lysosomal accumulation of gliadin p31-43 peptide induces oxidative stress and tissue transglutaminase-mediated PPARgamma downregulation in intestinal epithelial cells and coeliac mucosa. *Gut* 2010, *59*, 311–319.

[32] Ciccocioppo, R., Di Sabatino, A., Ara, A., Biagi, F. et al., Gliadin and tissue transglutaminase complexes in normal and coeliac duodenal mucosa. *Clin. Exp. Immunol.* 2003, *134*, 516–524.

[33] Keshavarzian, A., Banan, A., Farhadi, A., Komanduri, S. et al., Increases in free radicals and cytoskeletal protein oxidation and nitration in the colon of patients with inflammatory bowel disease. *Gut* 2003, *52*, 720–728.

[34] Stojiljković, V., Todorović, A., Radlovic, N., Pejić, S. et al., Antioxidant enzymes, glutathione and lipid peroxidation in peripheral blood of children affected by coeliac disease. *Ann. Clin. Biochem.* 2007, *44*, 537–543.

[35] Giovannini, C., Maiuri, L., De Vincenzi, M., Cytotoxic effect of prolamin-derived peptides on in vitro cultures of cell line Caco-2: implications for coeliac disease. *Toxicol. In Vitro* 1995, *9*, 251–255.

[36] Dudeja, P. K., Brasitus, T. A., Inactivation of rat small intestinal brush-border membrane alkaline phosphatase by oxygen free radicals. *Gastroenterology* 1993, *105*, 357–366.

[37] Marchionatti, A., Alisio, A., Dỳaz, G., de Barboza, V. et al., DL-buthionine-S,R-sulfoximine affects intestinal alkaline phosphatase activity. *Comp. Biochem. Physiol. C Toxicol. Pharmacol.* 2001, *129*, 85–91.

[38] Geddes, K., Philpott, D. J., New role for intestinal alkaline phosphatase in gut barrier maintenance. *Gastroenterology* 2008, *135*, 8–12.

[39] Prasad, K. K., Thapa, B. R., Nain, C. K., Sharma, A. K., Singh, K., Brush border enzyme activities in relation to histological lesion in pediatric celiac disease. *J. Gastroenterol. Hepatol.* 2008, *8*, 348–352.

[40] Bergamo, P., Maurano, F., D'Arienzo, R., David, C., Rossi, M., Association between activation of phase 2 enzymes and down-regulation of dendritic cell maturation by 9c,11t – conjugated linoleic acid. *Immunol. Lett.* 2008, *117*, 181–190.

[41] Bergamo, P., Luongo, D., Maurano, F., Mazzarella, G. et al., Conjugated linoleic acid enhances glutathione synthesis and attenuates pathological signs in MRL/MpJ-Fas lpr mice. *J. Lipid Res.* 2006, *47*, 2382–2391.

[42] Theiss, A. L., Vijay-Kumar, M., Obertone, T. S., Jones, D. P. et al., Prohibitin is a novel regulator of antioxidant response that attenuates colonic inflammation in mice. *Gastroenterology* 2009, *137*, 199–208.

[43] Bassaganya-Riera, J., Hontecillas, R., CLA and n-3PUFA differentially modulate clinical activity and colonic PPAR-responsive gene expression in a pig model of experimental IBD. *Clin. Nutr.* 2006, *25*, 454–465.

[44] Evans, N. P., Misyak, S. A., Schmelz, E. M., Guri, A. J. et al., Conjugated linoleic acid ameliorates inflammation-induced colorectal cancer in mice through activation of PPAR-gamma. *J. Nutr.* 2010, *140*: 515–521.

[45] Stewart, D., Killeen, E., Naquin, R., Alam, S., Alam, J., Degradation of transcription factor Nrf2 via the ubiquitin-proteasome pathway and stabilization by cadmium. *J. Biol. Chem.* 2003, *278*, 2396–2402.

[46] McMahon, M., Itoh, K., Yamamoto, M., Hayes, J. D., Keap1-dependent proteasomal degradation of transcription factor Nrf2 contributes to the negative regulation of antioxidant response element-driven gene expression. *J. Biol. Chem.* 2003, *278*, 21592–21600.

[47] Nguyen, T., Sherratt, P. J., Huang, H-C., Yang, C. S., Pickett, C. B., Increased protein stability as a mechanism that enhances Nrf2-mediated transcriptional activation of the antioxidant response element. *J. Biol. Chem.* 2003, *278*, 4536–4541.

